CENTRE FOR ORE DEPOSIT AND EXPLORATION STUDIES

STRUCTURE AND MINERALISATION OF WESTERN TASMANIA

AMIRA PROJECT P.291A
Final Report
March 1997

UNIVERSITY OF TASMANIA

CODES Special Research Centre
Geology Department
University of Tasmania GPO Box 252-79
Hobart Tasmania Australia 7001

another Pongratz Production 1997

Contents

Executive Summary

Ron Berry

The principal aim of this project was to test the models of the Cambrian fault structure in western Tasmania which were developed in P291 and to refine these models where appropriate. This was always going to be difficult given the complexity of Cambrian tectonics. It was not sufficient to identify a structure as Cambrian in age but rather to see the Cambrian as five separate structural events. The extensional faulting which has been clearly identified near VHMS deposits is a very short lived event which is restricted to part of the Middle Cambrian (?Undillan). The extension project P291A was proposed to test the model at appropriate locations and test extensions of the model wherever possible.

Project 1 The Mt Cripps Fault as a Middle Cambrian transfer structure

Detail provenance and facies studies indicate the Mt Cripps Fault was present during the deposition of the Southwell Subgroup but no evidence was found for activity on this fault during the deposition of the Animal Creek Greywacke. The Mt Cripps Fault was a relatively small feature during the late stage of the Yolande Cycle with an offset less than the thickness of the Southwell Subgroup, but sufficient to lift the southern block into a subaerial position.

Project 2 Cambrian structure of the western basin margin Pieman-Rosebery-Dundas.

There are fundamental differences between Middle and Late Cambrian strata close to the western limits of the Dundas ìtroughî in the area near Rosebery which require a complex basin margin geometry. The transfer fault system proposed in P291 is compatible with these geometric requirements but other solutions are possible.

Project 3 Henty Fault/Red Hills-Selina transfer system

The southern extension of a Cambrian fault in the Moxons Saddle area and an E-W transfer zone south of Red Hills were present during Tyndall Group deposition and subsequent erosion from a subaerial northeastern fault block. A normal, west dipping fault orientation is preferred. The ìMoxon Faultî was inverted, probably in the Late Cambrian and, in the Devonian.

Project 4 Linda Zone-Firewood Siding Fault

A near complete section of Middle to Upper Cambrian strata is exposed north of the Firewood Siding Fault. This succession records a prolonged period of below wave base sedimentation sourced primarily from basement. During the upper part of the Middle Cambrian, a change in basin geometry is heralded by the influx of medium to coarse-grained detritus and the development of a slope fan system. No structural or stratigraphic evidence was found that the Firewood Siding Fault existed during the Middle Cambrian. The primary evidence remains that this structure existed as a Late Cambrian transfer zone during the N-S folding.

Project 5 Lithostratigraphic correlations

The Cambrian rocks of western Tasmania were subdivided into three ìcyclesî based on pre-Tyndall Group (Yolande Cycle), Tyndall and post-Tyndall Group (Denison Cycle) sequences, using bio-stratigraphic constraints where possible. The Tyndall Cycle, although occupying only a very short time span (1-2 Myr?) at the end of the Middle Cambrian acts as a marker unit that allows this subdivision to be extended across the Cambrian rocks of western Tasmania. A map of this distribution was developed.

Cycle 1 opens with deep water sedimentation and dacitic volcanism. Towards the top of Cycle 1 the basin becomes more complex with increased basaltic volcanism and active extensional faulting. This major change in basin geometry occurs at the stratigraphic interval that hosts the major massive sulphide deposits, perhaps reflecting a thermal maximum that also correlates with maximum basaltic volcanism. Cycle 2 was initiated in many areas by explosive basaltic volcanism with a mild but distinct tholeiitic character. This widespread volcanic event formed at many small centres unrelated to the major centres of Cycle 1 volcanism. Cycle 3 is dominated by clastic sedimentation and is synchronous with east–west compression and basin inversion.

The heavy mineral assemblages in sandstones provided source signatures for all the basement units of western Tasmania. These sources contributed to units at all stratigraphic levels and, while their relative importance varied, no new ?exotic source appeared during the depositional history.

Project 6 Professor Range to Tyndall Range section

A restorable section was drawn along 535000mN. The strong out-of-section movement at the Henty Bridge prevents a meaningful reconstruction across this zone, so the restoration is in two sections. This section matches the style of sections to the south, with only moderate total shortening of 14 km. The level of erosion is such that a very good separation of this shortening between Cambrian and Devonian deformation with Late Cambrian folding producing a third of the total shortening in the section. The Rosebery section remains a major problem because of the large shortening required by the Rosebery and Mt Black thrusts for which no equivalent has been found on other sections.

Project 7 2D Geophysical modelling

Four structural sections across the Mt Read Volcanics were tested by 2D modelling of the gravity and magnetic fields. The structural models are consistent with the geophysical data within the constraints of the publicly available physical properties database. Regionally averaged physical properties determined along the line of the each section are required to improve the stringency of this test of the structural models.

Project 8 Cleavages associated with the Rosebery Fault

There is a close spatial relationship between the Rosebery Fault and a late N-striking cleavage (S_2). An earlier cleavage was not visible in the most intense zones of S_2 cleavage development but overprinting was found on the edge of the zone of S_2 development. The earlier cleavage has a composite origin including both a NNW striking Devonian cleavage and a N striking cleavage of Devonian or Cambrian age. We could not find any way to resolve whether the N-striking cleavage was Cambrian in age.

Project 9 Chemical fingerprints for Cambrian Faults

Growth faults are dynamic structures in a fluid history sense. Where these faults have been examined in detail, their isotopic composition is very variable, and this is accounted for by a complex retainment pattern of the isotopic signature of multiple fluid batches passing through each fault. Only sulfur isotope values >18‰ and <-5‰ are diagnostic of Cambrian fluids in the Mount Read Volcanic Belt, because of overlaps with the isotopic range of Devonian magmatic and metamorphogenic fluids. Values less than -5‰ have only been identified in background oxidised Cambrian aquifers, particularly

associated with albitisation. It is likely that this fluid facies was widespread, but poorly preserved, in early Cambrian faults. Cambrian signatures >18‰ have been recorded from the ìMoxons Faultî and the western boundary fault of the Dundas ìtroughî in the Pieman Gorge supporting the growth fault interpretation.

The nature of Middle and Late Cambrian deformation is complex in both time and place. The whole of the Cambrian was a period of very active tectonics in western Tasmania. This can be characterised by a number of stages. A period of extension in the Middle Cambrian reached a thermal and structural maximum in the Undillan and Boomerangian stages of the Middle Cambrian. The major phase of VHMS mineralisation occurred at this time. The transition from a simple deep water basin associated with dacite dominated volcanism to a complex basin with large ranges in water depth and substantial andesitic to basaltic volcanism occurs during the Undillan. Cambrian extensional faults (Henty-Moxons-Cripps zone, Pieman-Rosebery-Husskisson zone) are recognisable at this time but not before. The basin was inverted in the Late Cambrian with active erosion of the older volcanics.

While the Late Cambrian and Devonian deformation have obscured much of the basin geometry during the extensional phase, a few of the larger structures can still be recognised. There is no evidence for wholesale dismemberment of the basin geometry.

Abstracts

Heavy minerals, provenance and lithostratigraphy
R.F. Berry, S. Meffre, G. Jenner and R. Fulton

The Mt Read Volcanics have been subdivided into three depositional cycles each with a distinct basin geometry and history. Samples of sandstones have been collected from each of these cycles. The heavy mineral assemblages provide signatures for a range of sources these sandstones. The recycled metasedimentary source is characterised by rounded zircon and tourmaline. The only difference between the Tyennan (eastern) and Rocky Cape block (western) recycled sediments was in the age of zircons. The Rocky Cape block has a larger range in zircon ages than the metasediments of the Tyennan block. The MUC (mafic/ultramafic complex) source is characterised by low-Ti chromites. The Crimson Creek Formation source contains high-Ti chromite, euhedral zircon and minor recycled metasedimentary components. The Cambrian felsic volcanism contributes euhedral zircon. All the basaltic sources (Crimson Creek Formation, MUC, Henty dyke swarm) are capable of producing high oxide components in unaltered immature sandstones and volcaniclastic units.

The older part Yolande Cycle sandstones are dominated by a well mixed component of MUC and recycled metasediments (including at least some Rocky Cape block) and locally a felsic volcanic component, interpreted here as CVC derived. No local fluctuations in provenance were found over the 150 km of strike length investigated except the influx of local volcanic components. The implication is that this is a large deep basin with no local basin margins. Towards the top of the Yolande Cycle, the MUC component becomes less significant in the south. By the top of the Yolande Cycle the basin is complex with many local variations in provenance. The Crimson Creek Formation becomes dominant in the provenance of the Dundas area. These provenance changes reflect similar changes in the sedimentology. The older part of the Yolande Cycle is a deep water turbidite sequence with a well mixed composition while the younger part of the Yolande Cycle is shallower with many facies variations

A new volcanic phase dominated parts of the basin east of the Rosebery Fault through the Tyndall Cycle but west of the Rosebery fault the stratigraphy was dominated by a western source through this biostratigraphic interval. The Denison Cycle syn-orogenic sediments also show very rapid facies variation with local sources dominant.

It is significant that the major change in basin geometry during the Yolande Cycle occurs close to the stratigraphic interval that hosts the major massive sulphide deposits. The major basaltic elements of the Mount Read Volcanics are also concentrated in the upper Yolande Cycle and lower Tyndall Cycle, perhaps reflecting the thermal maximum in the area.

Lithogeochemistry
R.F. Berry, D. Selley, M.J. White and S. Meffre

The Mt Read Volcanics have been subdivided into three depositional cycles primarily on the bases of bio- and litho-stratigraphic techniques (Corbett et al., this report). In addition to these techniques, the whole rock chemistry of the sedimentary rocks of the Mt Read Volcanics can be employed as an effective tool in resolving some of the more difficult lithostratigraphic problems as well as discriminating between the various sources terrains which were actively supply detritus during basin development. Examination of temporal and spatial variations in source characteristics provided insight into basin geometry and evolution.

The investigation demonstrated that whole rock chemistry is very useful in distinguishing the Tyndall Group volcaniclastics. The basaltic component of source is well defined in the less mature sandstones but this signal is lost in the mature sandstones. Both immature sandstones and mudstones provide evidence of the changing nature of the basin and of the difference between the western margin and more central parts of the basin.

Stratigraphic correlation and basin analysis
K.D. Corbett, R.F. Berry and D. Selley

Subdivision of the Cambrian rocks of western Tasmania into three "cycles" based on pre-Tyndall (Yolande Cycle), Tyndall and post-Tyndall (Denison Cycle) sequences, using biostratigraphic constraints where possible, provides a practical framework for considering basin geometry and geological evolution. The Tyndall Cycle, although occupying only a very short time span (1–2 My?) at the end of the Middle Cambrian, is important because it was initiated by a distinctive phase of transitionally tholeiitic volcanism. This compositional signature has been used to correlate the Lynchford member of the Tyndall Group with the Henty Fault wedge basalts and dykes, Native Track Tier volcaniclastics, Lobster Creek intrusives and the lower King River basalts. The distribution of these units supports a widespread volcanic event which occurred after the main CVC style volcanism and formed at discrete small centres unrelated to the major centres of CVC volcanism. Together these units act as a marker allowing the application of our three-fold subdivision across all the Cambrian sequences of western Tasmania.

Cycle 1 opens with deep water sedimentation and dacitic volcanism. Towards the top of Cycle 1 the basin becomes more complex with increased basaltic volcanism and active extensional faulting. The Tyndall Cycle was initiated in many areas by explosive basaltic volcanism with a mild but distinct tholeiitic character. Cycle 3 is dominated by clastic sedimentation and is synchronous with east–west compression and basin inversion.

Mt Cripps Fault: Evidence for Cambrian movement
Ron Berry, Keith Corbett and Stuart Bull

Detailed investigation of the Mt Cripps Fault was used to test the model that it was a transfer fault in the Middle Cambrian. Sedimentological studies targeted the Murrays Road Greywacke and the Animal Creek Greywacke. The variation in provenance and facies variations indicate the Mt Cripps Fault was present during the deposition of the Southwell Subgroup but no evidence was found for activity on this fault during the deposition of the Animal Creek Greywacke. The structural interpretation suggests that the Mt Cripps Fault was a relatively small feature durin the late stage of the Yolande Cycle with an offset less than the thickness of the Southwell Subgroup, but sufficient to lift the southern block into a subaerial position.

Structure and sedimentology of Middle and Upper Cambrian strata adjacent to the Firewood Siding Fault

David Selley and Sebastien Meffre

A near complete section of Middle to Upper Cambrian strata is exposed north of the Firewood Siding Fault. This succession records a prolonged period of below wave base sedimentation sourced primarily from extrabasinal basement sources, but with a locally significant volcanogenic and intra-basinally-derived component particularly towards the base. During the upper part of the Yolande Cycle, a change in basin geometry is heralded by the influx of medium to coarse-grained detritus and the development of a slope fan system. Significant basin activity also occurs in the upper part of the Denison Cycle with dominantly coarse-grained debris accumulating in narrow, laterally restricted depo-centres which potential mark the onset of Late Cambrian folding in the area.

The structural geometry of the region north of the Firewood Siding Fault reflects the interaction of Cambrian and Devonian structures. N- to NNE-trending Cambrian structures were tightened and rotated during the main Devonian folding episode. Sinistral movement on the Firewood Siding Fault occurred coevally with Devonian folding and has resulted in a complex fold interference pattern that is not evident north of this major fault.

Sedimentological evidence for Cambrian growth faults on the eastern side of the Dundas Trough, western Tasmania

Matt White, edited by Ron Berry

Four areas on the eastern side of the Dundas Trough were studied to test the model for Middle Cambrian extension proposed in AMIRA project P291. Three areas were along a proposed precursor to the Henty Fault. These areas were the Moxon Saddle–Henty area, the Northern Anthony Road–Murchison Gorge area, and the Hanging Rock area. Another probable Cambrian growth fault structure, to the east of Moxon Saddle, in the Anthony River–Mount Selina area was also studied to test a smaller growth fault.

In the Moxon Saddle area, Tyndall Group rhyolites were probably originally deposited on both sides of the fault, and were subsequently eroded off the northeastern fault block across a fault scarp. In the Henty area, provenance of volcaniclastic units of the upper part of the Tyndall Group, were probably derived from the CVC to the east, being consistent with a west-block-down fault configuration. A normal, west dipping fault orientation is preferred. This fault was active during or after Tyndall deposition. We found no evidence that indicated a pre-Tyndall Group fault in this area. In the Murchison and Hanging Rock areas no new evidence was found for Cambrian movement along the palaeo-Henty Fault. In the Anthony River area, the geometry of the surviving sedimentary package is most consistent with active extensional faulting during Tyndall Group deposition with basin inversion during the Denison Cycle.

Middle and early Late Cambrian growth structures along the western margin of the Dundas Trough

Stuart Bull and David Selley

In Project P291, the "Rosebery transfer system" was proposed as a link between a N-S striking growth fault which coincided with the western limits of Dundas Group sedimentation at the southern end of the Huskisson Syncline, and second N-S trending structure to the northeast which terminated just west of Rosebery or along the eastern margin of the "Dundas inlier". The lithological variation between the Denison Cycle correlates contained in the Huskisson River section and those positioned immediately west of Rosebery reflect fundamental differences in the drainage patterns for each region. The Huskisson River section was derived from Precambrian siliciclastics and Crimson Creek Formation correlates located immediately north from the "Rosebery transfer system" and accumulated on or near a topographically uplifted transfer ramp. In contrast, the Stitt Quartzite has a more distal provenance, with sediment pathways probably occupying a basin-axial position. The principal function of N-S trending growth faults in terms of

sediment dispersal patterns was to provide a corridor for major drainage systems rather than to actively supply and direct detritus into the basin. There are fundamental differences between strata positioned close to the western limits of the Dundas Tough and in the area near Rosebery. These differences are interpreted to reflect contrasts in sediment dispersal patterns and basin geometry between these regions. A model of a lateral ramp between overlapping synthetic normal faults may be more applicable to this zone than a discrete transfer fault.

The sulfur isotope signature of Cambrian faults in the Mt Read Volcanic Belt, and their implications for sulfur enrichment in submarine volcano-sedimentary rift basins

Garry J. Davidson and Paul Kitto

Sulfur isotopic results from Cambrian growth faults in the Mount Read Volcanics can in some circumstances constrain their timing. Those containing base-metal sulfides, with S- and Pb-isotope values similar to the large Mount Read Volcanic Belt VHMS deposits ($\delta^{34}S$ 5–18‰), are likely to represent fault-controlled upflow zones in Cambrian hydrothermal cells. Unmineralised faults with normal or strike-slip fault offsets, can contain pockets of heavy sulfur isotope values ($\delta^{34}S > \sim 18$‰), as finely disseminated pyrite, within 50 m of the recognisable fault trace. The same range of heavy values is recognised at the margins of large base metal deposits, such as Rosebery and Hellyer, where it is interpreted to represent shallow sub-surface reduction of Cambrian seawater sulfate. The heavy values in the faults are interpreted to have been emplaced into fault traces either by sulfate reduction of fault anhydrite during the evolution of the fault, or by mixing of seawater sulfate with reduced hot porewaters on the fault margins during initial fluid recharge. The mechanism of continuous anhydrite burial on growth fault hangingwalls is regarded as a fundamental mechanism of delivery of seawater sulfate-derived sulfur into hydrothermal reservoirs, and may account for the strong sulfur enrichment of altered back-arc basin crust compared to its mid-ocean ridge counterpart.

Growth faults are dynamic structures. As time passes, every portion of the downthrown fault trace experiences the full range of fluid and thermal conditions available on the fault, because each segment initiates at surface and is progressively buried by deposition and fault movement. It is consequently expected that a wide range of sulfur isotope signaures should be recorded in growth faults, and this is added to if the fault has a complex later history. Where faults have been examined in detail in this study, their isotopic composition is very variable, and this is accounted for by a complex retainment pattern of the isotopic signature of multiple fluid batches passing through each fault, rather than by isotopic heterogeneity in a single event.

However, only sulfur isotope values >18‰ and <~–5‰ are diagnostic of Cambrian fluids in the Mount Read Volcanic Belt (MRVB), because of overlaps with the isotopic range of Devonian magmatic and deformational fluids. Values less than –5‰ have only been identified in background oxidised Cambrian aquifers to date—particularly associated with albitisation—but it is very likely that this fluid facies was widespread, but possibly poorly preserved, in early Cambrian faults. Background rocks in the MRVB contain a very wide isotopic range with no definite mode, including the very light values of oxidised aquifers (0 to –14.5‰), light to intermediate values consistent with an original igneous signature (0 to ~6‰), and intermediate values overlapping the range of Cambrian massive sulfide deposits (5–18‰), which are interpreted as products of low W/R reaction with high temperature hydrothermal fluids during the Cambrian.

The recommended strategy to determine fault parentage is to sample at <20 m spacing across fault traces and their margins, incorporating all alteration styles and sulfide generations, and analysing using wholerock sulfur isotope methods. The near-surface history of growth faults is likely to be preserved on their margins, because of greater lateral permeability, and proliferation of small fault traces, whereas the isotopic record of the deep history of the same fault is likely to be preserved in focussed thin zones of movement. Sampling strategies should take account of this.

Geophysical data as a control on geological sections
Ron Berry and Michael Roach

Four structural sections across the Mt Read Volcanics were tested by 2D modelling of the gravity and magnetic fields. The structural models are broadly consistent with the geophysical data within the constraints of the publicly available physical properties database. The geophysical data requires addition of Cambrian and Devonian granites for which there is no surface evidence. Some large magnetic anomalies also require addition of ultramafic bodies but these lie below the level of the original sections. Regionally averaged physical properties determined along the line of the each section are required to improve the stringency of this test of the structural models.

Trace Element Investigation of Pyrite: a possible discriminator for Cambrian and Devonian fault structures
Paul Kitto

A new multi-trace element ratio Pyrite Discriminator Index (PDI), base on electron microprobe analyses of pyrite (Co, Ni, Cu, Zn, Pb, As, Se, Ag, Au), provided for the first time a low cost method to differentiate between Cambrian VHMS mineralisation and Devonian granite related hydrothermal mineralisation. The PDI was based on the ratio of trace elements most common to Cambrian pyrite mineralisation (i.e. Co, Zn, As, Se, and Pb) compared to those elements more commonly associated with Devonian granite related pyrite mineralisation (i.e. Ni, Cu, Ag, and Au). Based on the available pyrite trace element data, a PDI value greater than 50 was indicative of a Cambrian VHMS style of mineralisation, and a PDI value less than 50 was indicative of a Devonian granite related style of mineralisation.

The breakdown of the Cameca SX-50 microprobe for a number of months since the last AMIRA meeting has delayed data collection for this project, and this has been exacerbated by the very long analysis times that have been used do far. The microprobe count times required to obtain low detection limits have been a major concern. Low detection limits are critical to the success of this technique but a trade off between limited data acquisition at over 1 hour per analysis must be considered. The solution being trialed is to lower analysis time to 10 minutes. This means discarding Au as an indicator element and increasing other detection limits to 50 ppm. This may allow a substantial database to be provided by the final meeting. The final results from this investigation will be presented as a supplementary report at the final AMIRA meeting.

Heavy minerals, provenance and lithostratigraphy

R.F. Berry, S. Meffre, G. Jenner and R. Fulton
CODES Special Research Centre, Geology Department, University of Tasmania

Abstract

The Mt Read Volcanics have been subdivided into three depositional cycles each with a distinct basin geometry and history. Samples of sandstones have been collected from each of these cycles. The heavy mineral assemblages provide signatures for a range of sources these sandstones. The recycled metasedimentary source is characterised by rounded zircon and tourmaline. The only difference between the Tyennan (eastern) and Rocky Cape block (western) recycled sediments was in the age of zircons. The Rocky Cape block has a larger range in zircon ages than the metasediments of the Tyennan block. The MUC (mafic/ultramafic complex) source is characterised by low-Ti chromites. The Crimson Creek Formation source contains high-Ti chromite, euhedral zircon and minor recycled metasedimentary components. The Cambrian felsic volcanism contributes euhedral zircon. All the basaltic sources (Crimson Creek Formation, MUC, Henty dyke swarm) are capable of producing high oxide components in unaltered immature sandstones and volcaniclastic units.

The older part Yolande Cycle sandstones are dominated by a well mixed component of MUC and recycled metasediments (including at least some Rocky Cape block) and locally a felsic volcanic component, interpreted here as CVC derived. No local fluctuations in provenance were found over the 150 km of strike length investigated except the influx of local volcanic components. The implication is that this is a large deep basin with no local basin margins. Towards the top of the Yolande Cycle, the MUC component becomes less significant in the south. By the top of the Yolande Cycle the basin is complex with many local variations in provenance. The Crimson Creek Formation becomes dominant in the provenance of the Dundas area. These provenance changes reflect similar changes in the sedimentology. The older part of the Yolande Cycle is a deep water turbidite sequence with a well mixed composition while the younger part of the Yolande Cycle is shallower with many facies variations

A new volcanic phase dominated parts of the basin east of the Rosebery Fault through the Tyndall Cycle but west of the Rosebery fault the stratigraphy was dominated by a western source through this biostratigraphic interval. The Denison Cycle syn-orogenic sediments also show very rapid facies variation with local sources dominant.

It is significant that the major change in basin geometry during the Yolande Cycle occurs close to the stratigraphic interval that hosts the major massive sulphide deposits. The major basaltic elements of the Mount Read Volcanics are also concentrated in the upper Yolande Cycle and lower Tyndall Cycle, perhaps reflecting the thermal maximum in the area.

Introduction

A major aim of the combined ARC-AMIRA project is to define the basin geometry for the Mount Read Volcanics. A structural model was put forward in P291 which is being used as a template for this analysis. The project described here looks at the heavy mineral suite as a guide to what sources are available to the basin at each stage in its genesis.

The threefold classification of the Mount Read volcanics has been used to constrain the analysis of the heavy mineral provenance study.

CYCLE 3
Denison Group biostratigraphic correlates
All the units which are Mindyallen or younger.

CYCLE 2
Tyndall Cycle of deposition
Boomerangian

CYCLE 1
Yolande Cycle of deposition
Undillian (pre- to syn- granite intrusions).

Heavy minerals are a good test of the provenance of sandstones. They potentially survive minor alteration and deformation. The phases are characteristic of their source. The distribution of heavy minerals place constraints on the basin architecture. In addition, if certain sources only become available during the history of the belt a separation of the stratigraphy should be possible. For example the existing problem with the definition of the Tyndall Group. At present the recognition of granitic clasts are required to recognise this group as distinct from the Eastern Quartz-phyric sequence. Sandstones from all cycles and scattered across the belt have been included but the sampling has concentrated on the Yolande Cycle sandstones as the distribution of these sediments reflect conditions close to the time of massive sulphide formation

Thirty-seven samples were collected for the first phase and an additional 47 samples have been added to this original collection. The second group included some Precambrian units to provide information on the nature of the potential source material. They have been crushed gently as recommended by Henningsen (1967). The fine sand fraction (63–125 mm) from these rocks was extracted by sieving, washed and then separated by heavy liquids. The samples in the second series 96/?? were acid-washed to reduce the amount of goethite. This also removes the apatite and strongly corrodes monazite. For a few samples pan concentrates of chromite was obtained with no regard to the other phases. These are indicated in Table 1. The heavy mineral grains were mounted on polished thin sections. Detailed point counting has been carried out on these samples and many have been checked by microprobe analysis. The major aim of microprobe analysis has been to determine the type of chromite present as this was found to be the most useful in the preliminary studies. An additional separate of zircon was prepared and analysed by LAMS-ICP-MS to define discrete metasedimentary sources.

Provenance and stratigraphic correlation

The heavy mineral contents are summarised in Table 1. The results of this analysis are shown below. The weight of heavy minerals varies from 0.001 to 1.55 gm despite the small range in amount of sandstone used (20–30 gm). Even on total heavy minerals alone the Denison and Tyndall Cycle sandstones are distinct from the Yolande Cycle sandstones and volcaniclastics. This difference reflects the large amount of oxides in Tyndall Cycle sandstones and along the western flank of the Dundas trough in Yolande Cycle sandstones.

Statistical analysis

The variability of the heavy minerals is very large. In order to put some order on this data the total data set was processed in a multivariate statistical package (MVSP). The most distinctive analysis of provenance is obtained if sulphides, chlorite and goethite are excluded as these may reflect diagenetic and alteration processes. The major correlations between detrital minerals are

1. magnetite-hematite-ilmenite (-apatite)
2. TiO_2 - euhedral zircon (-rounded zircon)
3. rounded zircon-tourmaline
4. chromite (-tourmaline)

These components can be understood in terms of the source and level of maturity of the sandstone. The first group reflect a basaltic source and a low level of maturity. This component is high in Smithton Basalt, Crimson Creek Formation and the Tyndall Group and Denison Cycle sandstones derived from the western margin of the basin. The second component is dominated by euhedral zircon which is the main indicator of a felsic volcanic source. The weak correlation with rounded zircon and TiO_2 suggests it is enriched in the more mature sandstones. Rounded zircon-tourmaline is the recycled sandstone

Table 1. Heavy mineral populations in sandstones from western Tasmania

	Stichl		Range		Formation			Animal		Creek		Greywacke		Northern Sector				
												Farrell Sl	Farrell Sl	Boco Rd	Boco Rd	Boco Rd	Southwell SG	Southwell Sbgp
sample no.	94/42	SR19	SR90	B197	B272	B275	J180	V109	94/11	94/12	94/14	94/15	94/1	94/2	94/3	94/8	94/9	94/19	96-26
easting	3883	3887	3886	3883	3879	3879	4052	4052	3811	3844	3853	3910	3877	3874	3784	3793	3792	3947	3948
northing	53699	53540	53538	52755	52779	52784	53917	53917	53853	53897	53903	53985	53833	53831	53850	53853	53853	53986	53986
									<----------micaceous sst----------							volcanicl	WS correl	sst	sst
treatment																			at
pyrite	52	2		1			6						39	61	36	148		4	
magnetite	4														1	19		2	
hematite	2			2				14		4		1	1	4	5	3	1	17	
ilmenite	2	1						2		7		3			1	6	2	19	
tourmaline	9	40	75	10	88	20		10	32	18	93	25	3	6		2	1	4	2
zircon (euh)	2	54	14	1	6		4	1	5	3	11	18	6		1		25	1	11
zircon (round	28	45	16	43	22	9	4	5	8	19	20	16	7	12		4	2		1
apatite	11			2					3	38	2	18	10	10	2		7	10	
chromite		1				1			48	146	147	105	46	15		4		20	32
TiO2	61	94	81	151	54	52	36	21	54	55	40	50	22	17	44		94	10	200
goethite	7	8		12	20	109	151	170	2		27	2	2	3	13		151		
pyroxene																			
chlorite	3						31		6	1	3	1	13	1	1	6		1	
epidote																			
monazite		11																	
garnet							1												
quartz		17	4	3	10	6		16											
lithic fragment					28		34												
barite																			
other	34		6	1			26		3		2	2	7	8			5		
total	215	273	196	226	228	197	293	239	161	291	345	241	156	137	104	192	288	88	246
weight sam	27.91	11.86	11.89	11.03	9.66	6.17	4.76	12.47	27.8	29.16	25.9			29.11	28.59	22.47	23.54		8
heavies	0.045	0.016	0.016	0.017	0.033	0.009	0.002	0.061	0.06	0.03	0.03	0.05		0.07	0.1	0.03	0.02		0.051

	Southern sector									Husskisson Group				
	CVC	CVC	YolRG	YolRG	YolRG	YolRG	YolRG	YolRG	Murch. V	Merton Rd	Pieman Rd	Ehm	Ehm	Colebrook
sample no.	94/34	94/35	94/27	94/26	94/28	94/29	94/32	94/33	94/21	94/23	96-31	96-45	96-46	96-47
easting	3804	3823	3756	3753	3765	3789	3780	3795	3873	3677	3683	3730	3739	3747
northing	53302	53315	53475	53496	53467	53430	53338	53310	53755	53794	53789	53723	53724	53726
	volc sst	volcanicl	mica sst	volc sst	volc sst	volcanicl	volcanicl	sst	volcanicl	sst	felds sst	volc sst	volc sst	sst
treatment											at	at	at	at
pyrite		8			2	6	100		42	35		2		
magnetite	1		1						38					
hematite		25		23	5									10
ilmenite	1	6										21	190	97
tourmaline	13		36			1	2			1	2	1		7
zircon (euh)	60	27	4	1	47	210	2	171	13	2	7	1	13	11
zircon (round	20		20	1	4	8		5			2	1	3	1
apatite	1	8	16		1	2	48	2	19	7				
chromite	11		108							3	19	6	9	2
TiO2	106	23	35	8	68	1		39	40	10	161	135	4	95
goethite	19	79	3	169	116	8	2	4	3	122		107	32	5
pyroxene														
chlorite		2	2			3		3	81		17	1	54	1
epidote														34
monazite													r	
garnet														
quartz											11		21	3
lithic fragment												5		
barite														
other	16	81			8		74			9	7			1
total	248	259	225	202	251	239	228	224	236	189	226	280	326	267
weight sam	42.14	26.13			19.15	21.31	18.16	31.25	24.48	19.59	12.84	9.06	pan	12
heavies	0.02	0.01		0.08	0.01	0.02	0.09	0.001	0.912	0.04	0.039	0.01	conc	0.063

CODES: AMIRA Project P.291A — Structure and Mineralisation of Western Tasmania. March 1997

Table 1. cont.

	Tyndall				Cycle				Denison					Cycle			
	LynchfordM	LynchfordM	Tyndall	MtCripps	MtCripps	Tyndall Gp	Jukes C		Strahan rd	Strahan Rd	Stitt Qte	StittCorr	Westcott	Westcott	Higgins Ck	Higgins Ck	Higgins Ck
sample no.	94/31	94/30	94/36	94/18	94/17	94/37	94/20		94/38	94/39	SQ-1	94/4	94/22	96-28	94/7	94/6	94/5
east	3789	3790	3838	3957	3967	3846	3863		3684	3662		3768	3758	3767	3761	3759	3753
northing	53378	53374	53306	53987	53987	53303	53761		53297	53328		53846	53785	53786	53861	53844	53844
					sst	pebbly sst			sst	volc sst	sst	sst	fine sst	sst	fine sst	fine sst	sst
treatment														at			
pyrite				1						1	7	30	2	4		31	
magnetite	101		8	49	15					3	4		1			1	18
hematite	3	3	2	72	13	108	3			3	26	1	3		3		93
ilmenite		2		5	23		207			9	4		2			37	30
tourmaline	**1**	**1**								**2**	**48**	**23**		**7**		**1**	**4**
zircon (euh)	**1**	**15**	**9**			**7**	**6**		**4**		**3**	**12**		**11**	**1**	**6**	
zircon (round	**1**		**1**		**2**		**1**		**2**	**2**	**47**	**12**		**9**	**2**		
apatite	2			9	76		3		1	11	8	21				2	2
chromite				**0**					**15**	**5**	**12**		**3**	**71**	**2**	**8**	**1**
TiO2	60	265	59	4		12	5		65	79	9	61	115	108	9	18	27
goethite	7	15	152		63	87	1		1	30		11	15		202	44	67
pyroxene																	
chlorite	9								1	3		17	119		1		
epidote																	
monazite														7			
garnet																	
quartz														11			
poly min														26			
barite																	
other						15			4	9		4	30	7		57	
total	**185**	**301**	**231**	**140**	**192**	**229**	**226**		**93**	**157**	**168**	**192**	**290**	**261**	**220**	**205**	**242**
weight sam	26.54	27.11	24.85	27.88	22.23	23.91	20.86		23.57		23.54	25.37	21.63	7.66	13.82	17.58	32.95
heavies	0.39	0.02	0.11	0.47	0.71	0.12	0.52		0.36	0.01	0.06	0.01	0.23	0.005	0.05	0.006	1.53

	Dial	Range		and	Fossey	Mountain	trough		Woolnorth		and	Smithton	
	Gog corr	Gog corr	Gog corr	Gog Grwk	Gog Grwk	Gog Grwk	Cateena M	Sprent Fmn	Esc	Es	Esc	ic-older faus	c-older fauna
sample no.	96-1	96-2	96-3	96-4	96-5	96-24	96-25	96-22	96-23	96-12	96-13	96-14	96-15	96-16
east	4732	4762	4742	4640	4486	4212	4298	4278	4233	3294	3334	3271	3313	3313
northing	53941	53934	53976	54005	54126	54311	54217	54367	54328	54875	54809	54775	54678	54678
	mica sst	greywacke	coarse sst	pebbly sst	grywk	greywacke	coarse sst	mica sst	coarse sst	mica sst	fine sst	med sst	fine sst	fine sst
treatment	at	at	at	at	at	at	at	at	at	at	at	at	at	at
pyrite	1													
magnetite					1			10						
hematite						4					3			
ilmenite				2		2	1	20	198			10	1	
tourmaline	**24**		**34**	**23**	**8**	**1**	**18**		**7**	**22**		**12**		
zircon (euh)	**1**		**3**	**2**	**3**	**1**	**6**	**2**	**1**	**1**	**6**	**3**		
zircon (round	**9**		**8**	**44**	**4**		**12**	**2**		**6**		**4**	**1**	
apatite											**7**			
chromite	**1**	**r**	**27**	**33**	**2**	**r**	**161**	**6**	**r**	**40**	**6**	**25**	**r**	**8**
TiO2	202		195	118	127	13	46	106	19	220		151		6
goethite	30		7	3	29	112	67	85	18	3	103	2	210	
pyroxene									2		1			
chlorite		15	3		7				5	1			2	
epidote		201				r								
monazite	8		6	7			2				5			
garnet							4							
quartz	8		21	3	9			1		4	79	2	14	3
poly min	7	7	5	11	75	199	3		4				9	
barite														
other														280
total	**291**	**223**	**309**	**246**	**265**	**332**	**320**	**232**	**254**	**297**	**210**	**209**	**237**	**297**
weight sam	24.6	13.05	14.71	21.37	18.65	12.36	17.65	14.56	7.27	16.9	5.57	28.33	pan	9
heavies	0.013	1.55	0.229	0.046	0.053	0.027	0.02	0.342	0.005	0.037	0.014	0.19	conc	0.01

Table 1. cont.

	Kununnah Subgroup			Crimson Creek Formation							Success Creek Gp		Oonah Formation	
	Forest Cg	Es	Es											
sample no.	96-10	96-11	96-17	94/24	96-29	96-30	96-32	96-33	96-34	96-35	96-36	96-37	96-38	96-39
east	3573	3422	3420	3634	3753	3740	3644	3638	3625	3617	3598	3594	3576	3525
northing	54767	54782	54753	53813	53787	53789	53813	53809	53804	53800	53803	53804	53813	53793
	orthoqtzt	greywacke	sst		wthred sst	wthred sst	sst	arkosic sst	sst	sst	fine sst	fine sst	sst	sst
treatment	at	at	at		at	at	at	at	at	at	at	at	at	at
pyrite	10		12	2						4			203	r
magnetite			3	6						13				
hematite				3						4				
ilmenite	6	44		69			1	2	42	28		1		
tourmaline	**25**			**3**			**7**	**2**			**6**	**25**		**16**
zircon (euh)	**1**	**1**		**7**		**2**	**4**	**1**	**4**		**1**	**2**		
zircon (round)	**12**			**2**					**1**		**8**	**3**		**5**
apatite														
chromite		**24**	**4**	**8**	**17**	**5**	**1**	**12**	**8**	**140**		**r**		
TiO2	130	226		57	248	54	64	254	24		85	125	3	47
goethite	6	5	135	22	23	217	158	1	78	60	68	92	4	14
pyroxene			30						9	9		15		
chlorite			1	33					3		2			
epidote								1	2		1		1	
monazite	1									r	3	r		159
garnet		2												
quartz	22	2					2	2	37	11	1	6	2	5
poly min	1		34				2				6		3	
barite														
other			15	7		2								
total	**214**	**304**	**234**	**219**	**288**	**280**	**239**	**275**	**208**	**269**	**181**	**269**	**216**	**246**
weight sam	15.15	18.09	8.22		8.92	7.44	11.74	12.45	10.23	pan	17.56	26	12	15.6
heavies	0.015	1.23	0.109	0.23	0.113	0.272	0.012	0.258	0.194	conc	0.001	0.013	0.376	0.001

	SthComet	Cuni		<——Port Sorell sequence——>				<——Penguin to Ulverstone——>				
	??ccf	Etl	Ecc		Epe	Epc?	Epc?	Beecrft Mb	Teetree Mb	Barrington	WestbankC	Bowery Fm
sample no.	96-41	96-43	96-44	96-6	96-7	96-8	96-9	96-18	96-19	96-20	96-21	96-40
east	3574	3664	3721	4658	4670	4663	4660	4240	4243	4265	4278	3445
northing	53599	53657	53723	54332	54423	54432	54431	54476	54476	54467	54453	53788
	fine sst	fine sst	sst	fine sst	felds wacke	fine sst	fine sst	bltic sst	green sst	fine sst	green sst	qtz phyllite
treatment	at	at	at	at	at	at	at	at	at	at	at	at
pyrite			3			23			195		235	r
magnetite	2								2			
hematite	64				2							
ilmenite	1			2		1	9	217				
tourmaline		**2**		**9**	**6**				**r**		**1**	**27**
zircon (euh)		**1**	**10**	**6**	**8**	**1**			**3**		**1**	**r**
zircon (round)			**1**	**10**	**7**							**r**
apatite												
chromite	**50**	**4**	**12**		**1**	**2**	**1**		**2**		**15**	**r**
TiO2	6	80	263	244	92	31	8	28	20			74
goethite	89	209	10	30	1	4	56	28	23	120		166
pyroxene				1		8		2	3			
chlorite	5						3		1			
epidote	55					1	9					
monazite				1								
garnet							1					
quartz	3	4	9		4	5	106	8	10			10
poly min	11	2		3	92	165	8	17	3			
barite					56							
other						1		1				5
total	**286**	**302**	**308**	**306**	**269**	**242**	**201**	**301**	**262**	**120**	**252**	**282**
weight sam	10.37	14.97	17.35	8.14	13.4	7.02	5.82	13.73	10.07	9.15	5.45	pan
heavies	0.036	0.005	0.06	0.013	0.022	0.001	0.001	0.033	0.003	0.587	0.026	conc

signature derived from metasediments. The chromite indicates a basaltic to ultramafic component but it is swamped by oxides in immature sandstone and only becomes a major component in more mature sandstones. Thus it is negatively correlated with these oxides.

The data set has very high variability as a result of the large range of rocks considered, the level of maturity, the level of weathering and also to some extent the method of processing. However, if we concentrate on the most robust components and compare their relative abundance in a triangular plot the components can be summarised successfully (Fig. 1). The samples from the Dundas Trough include volcaniclastics which are dominated by euhedral zircon and sandstone with a variable mix of basement sources. The Sticht Range Formation have very low chromite and reflect a direct mix between the euhedral and rounded zircon. In Figure 1b. the slight dominance of tourmaline over rounded zircon of this source is plain. In contrast the Animal Creek Greywacke is dominated by detrital chromite indicating a high mafic to ultramafic component. Samples that have this chromite signature are: Animal Creek Greywacke 94/11, 94/12, 94/14, 94/15; Farrell Slate 94/1, 94/2; Yolande River Group 94/38, 94/39, 94/27; Rosebery Group 96-28 and Southwell Subgroup 94/19, 96-26. These are all micaceous sandstones from the Yolande Cycle. Other Yolande Cycle sandstones (CVC sandstone 94/34, Boco Road 94/8, 94/9), and basal Denison Cycle (Stitt Quartzite SQ-1, 94/4) have low chromite to rounded zircon ratio which is interpreted here as a smaller component of mafic/ultramafic unit (MUC) source. They are more like the Sticht Range Formation. These sandstones may reflect an increasing influence of eastern source towards the top of the Yolande cycle but this is not supported by the zircon age structure (see below). Alternatively this transition could be interpreted as the erosional unroofing of the Rocky Cape block as the MUC is stripped from it.

The erosion of an uplifted eastern source is supported by an unconformity at the base of the Tyndall Cycle in the east which is not found in the west. Tyndall Cycle sandstones (94/31, 94/30, 94/36, 94/18, 94/17, 94/37, 94/20) are also low in chromite but Denison Cycle sandstones from close to the western margin such as the Higgins Creek section (94/5, 94/6, 94/7) are again rich in chromite reflecting an increasing of a local component of the western basement source (see chromite section below).

A few samples have been collected in the northern Cambrian sequences. The samples from the Dial and Fossey Troughs concentrated on micaceous sandstones of the Gog Greywacke. These have a very similar content of chromite, rounded zircon and tourmaline to the lower Yolande Cycle sandstones. The other samples were from the Cateena Mudstone which matched the Gog Greywacke, and from the Sprent Formation which is volcanogenic and plots near to the euhedral zircon corner of Fig 1c. This latter sample is anomalous in that it is dominated by ilmenite. The composition and stratigraphic position of the Sprent Formation suggests correlation with the Lynchford Member as the base of the Tyndall Cycle (see lithogeochemistry this volume).

Samples from the Smithton area were collected from the Denison and Yolande Cycles based on biostratigraphy and all samples are high in chromite/rounded zircon ratio. The Denison Cycle sandstone (Scopus 96-13) has the highest euhedral zircon component. The Denison Cycle sandstone (96-12) from Stoney Head and the ?Yolande Cycle sandstone (96-14) from Barcoo Road are very high in detrital chromite and tourmaline. However the Barcoo Road chromites are from tholeiitic rather than MUC sources (see chromites section below).

In order to constrain the source of heavy minerals some of the possible source rocks were sampled. It is assumed here that the Sticht Range Formation is a good model for a Tyennan source component and no direct sampling of this material was carried out. For comparison sample were taken of the late Precambrian from the Smithton area, including the Forest Conglomerate (96-10) and in the greywackes at Smithton, Kanunnah Subgroup (96-11, 96-17), of the Crimson Creek Formation, Success Creek Group and Oonah Formation along the Lower Pieman Road, and of the Port Sorell sequence. The Kanunnah Subgroup and Crimson Creek Formation are dominated by volcanogenic sandstones with high chromite and high oxide contents. The exception is one Crimson Creek Formation sample (96-32) which does not have this signature. The Forest Conglomerate, Success Creek Group, Oonah

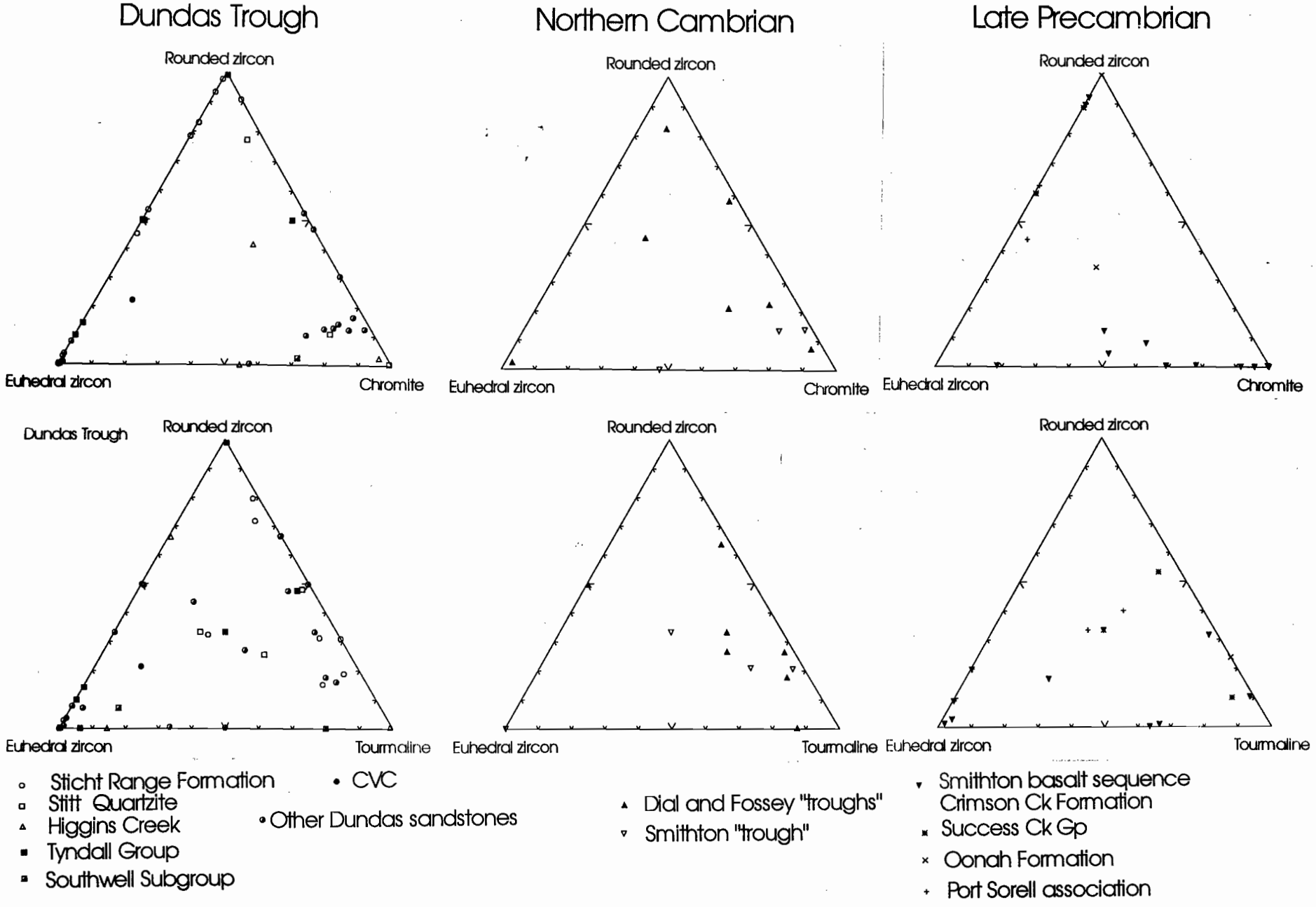

Figure 1 Heavy minerals in sandstones from western Tasmania. Dundas "trough" a. zircon-chromite, b. zircon-tourmaline. Northern Cambrian province c. zircon-chromite, d. zircon-tourmaline. Precambrian rocks e. zircon-chromite, f. zircon-tourmaline.

Formation and Port Sorell association samples are similar to the Sticht Range Formation indicating these sources cannot be distinguished from a Tyennan source (except from zircon age structure). An important feature of the Crimson Creek Formation is the high component of euhedral zircon suggesting there is a felsic volcanic component to the Late Precambrian volcanism that has not been recognised.

Some samples are dominated by specific minerals. Rocks which are high in magnetite are:

Eastern Quartz-phyric sequence (Murchison Volcanics) 94/21

Tyndall Group (94/31, 94/18).

Those which are high in ilmenite are:

Tyndall Group (94/20)

Sprent Formation (96-23)

Smithton sequence (96-11)

Crimson Creek Formation (94/24, 96-34)

Husskisson Group 96-46, 96-47)

Beecraft Megabreccia (96-18).

These samples reflect a low level of maturity and a large basaltic component in the source. Some other samples may also have this source signature but it has been altered by weathering to goethite and TiO_2 so that the maturity is obscured. Goethite could also be formed from mafic minerals and pyrite. TiO_2 is stable in the transport mechanism and may be a detrital mineral or can be formed from oxidation of Ti-bearing oxides.

Minerals

Chromite

Chromite represents one of the most distinctive minerals within the heavy mineral suite. The data presented above suggests this material comes from the west and is sourced out of the Crimson Creek Formation and the mafic/ultramafic complexes (MUC). The MUC contain rocks which have a very refractory composition and have chromites with a very high Cr# (100 * Cr/(Cr+Al)). The chromite in the Crimson Creek Formation is largely from basalt and the conventional view is that this will have a Cr# < 70. In order to properly define this source composition, chromite from both the Kanunnah Subgroup and Crimson Creek Formation were sampled (Fig. 2). The TiO_2 vs Cr# shows a very large range with TiO_2 reaching 5% and Cr# reaching a maximum of 80 at around 1.5% TiO_2 (Fig. 2a) and 10% Fe_2O_3 (Fig. 2b) representing evolved tholeiitic sources. The very low TiO_2 in 96-11 probably indicates a picritic source. In the 180 analyses shown here only five grains have an extreme refractory chromite composition. We assume that these grains are sourced from xenoliths within the basalts. This contrasts with the expected pattern from ophiolite sources in Tasmania (MUC). The Bowery Formation at Reece Dam also has a tholeiitic source signature (Fig. 3).

Six samples of Animal Creek Greywacke and Farrell Slate (94/11, 94/12, 94/14, 94/15, 94/1, 94/2) have been tested for chromite composition (Fig. 4). These all show a large range in Cr# from 20 to 90 but at very low TiO_2. About 20% of grains lie in the very high Cr# range characteristic of MUC. The lower Cr# below 50 may reflect an evolved gabbroic source. There is no evidence in this analysis of any tholeiitic sources for the chromite. The Farrell Slate samples has a similar range of chromite compositions to the Animal Creek Greywacke. These samples all support a chromite source in the MUC.

The micaceous sandstone samples from the Yolande River Group (Yolande Cycle 94/27, ?Denison Cycle 94/38, 94/39) have a similar range in Cr# to the Animal Creek Greywacke (Fig. 5). Again no definite tholeiitic spinels were detected but one grain from Sample 94/39 has a high TiO_2. The other sandstone from the southern Dundas region is sample 94/34 which comes from within the CVC along the Jukes Road. The grains from this sample have a very high Cr# but are associated with low Mg# and high magnetite component suggesting they have been modified from the normal trends during metamorphism. They do not match the normal tholeiite trend and are probably modified MUC chromites.

Chromites are rare in the Sticht Range Formation but some examples were analysed from SR19 (Lake Dora) and B275 (D'Aigular Range). These grains (Fig. 6) match typical MUC source material except for two grains that are more compatible with a tholeiitic source. Samples of the Southwell Subgroup (Fig. 7) come from the Cradle Mountain Link Road. These samples all have very low TiO_2 and include a trend to high Cr# typical of an MUC source.

Samples from west of the Rosebery Fault show mixed pattern (Fig. 8). Chromites from the Stitt

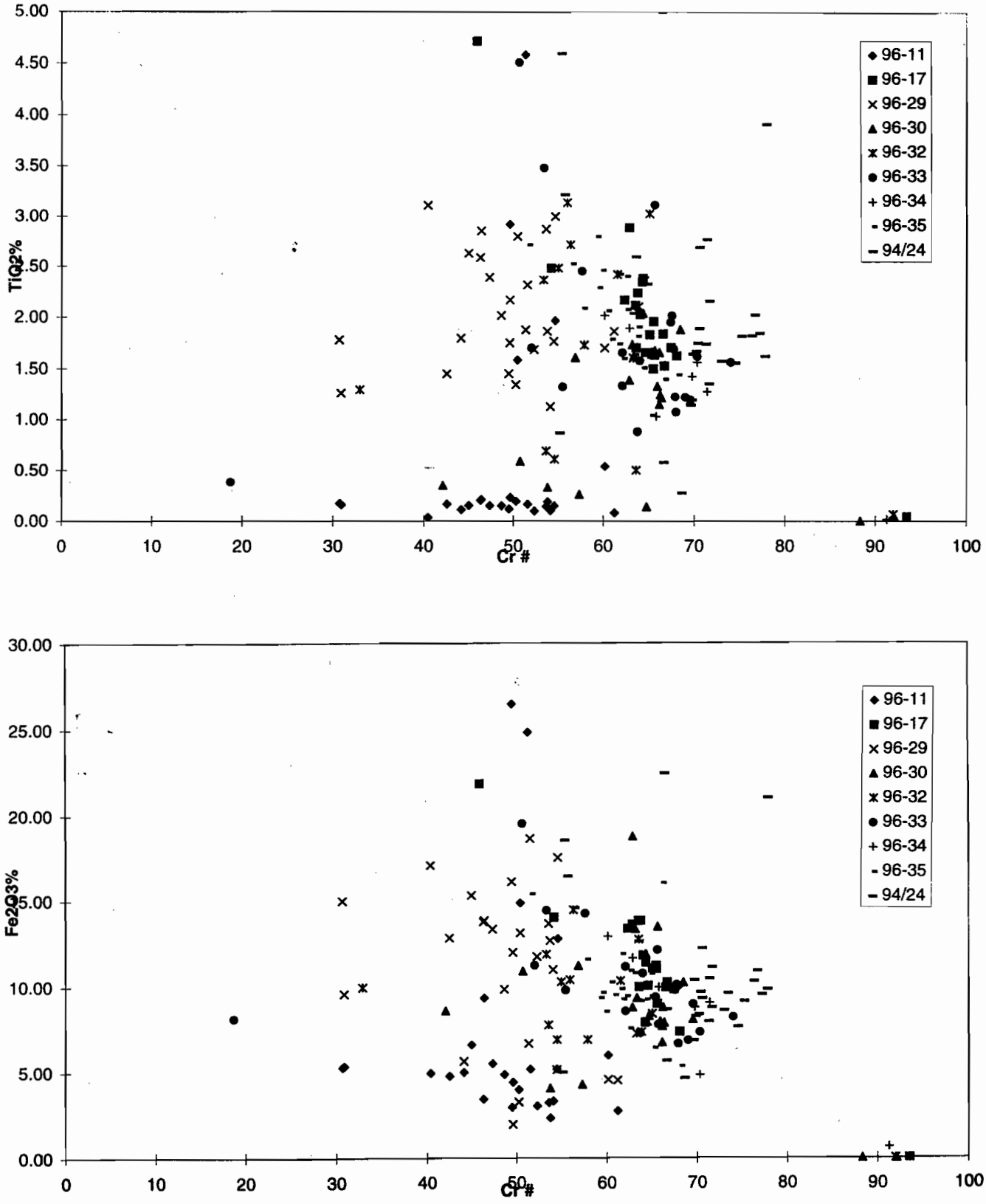

Figure 2. Chromites from Kanunnah Subgroup and Crimson Creek Formation. (a) TiO_2 vs Cr#, (b) Fe_2O_3 vs Cr#.

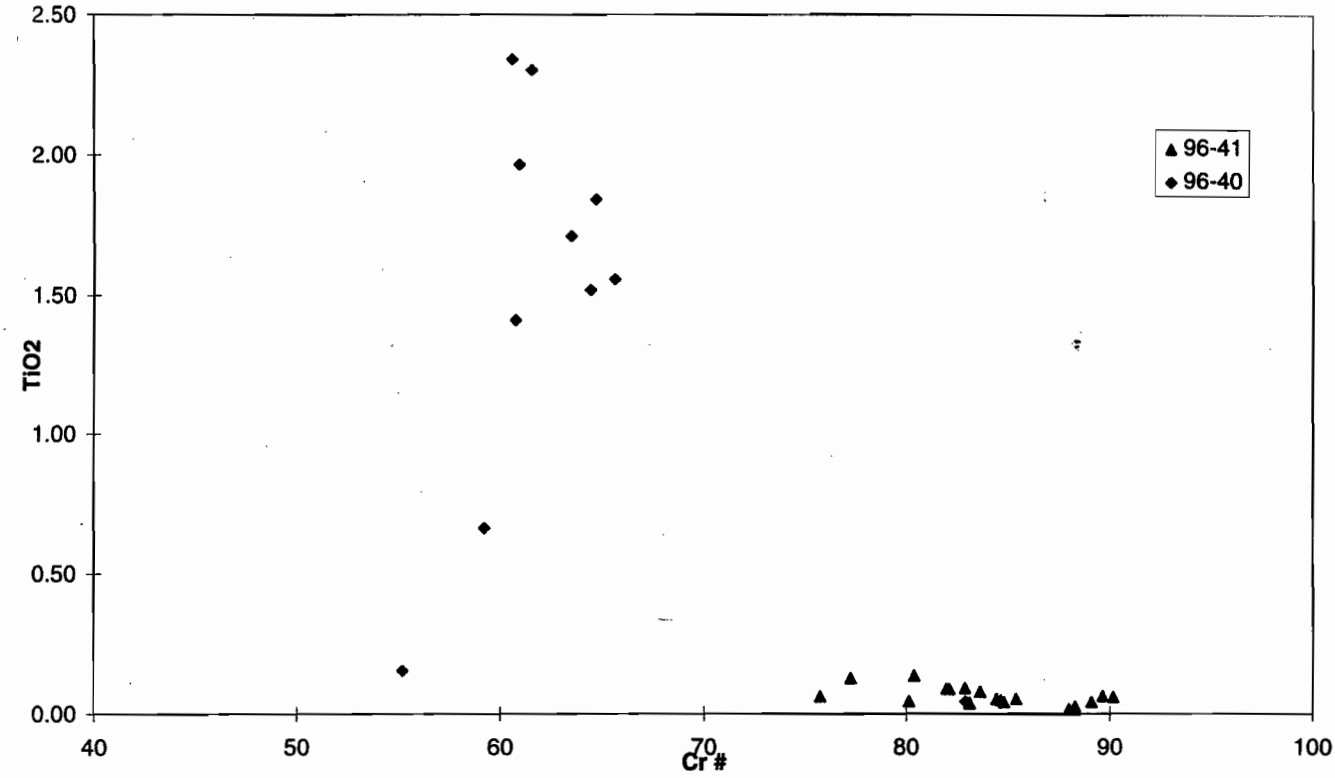

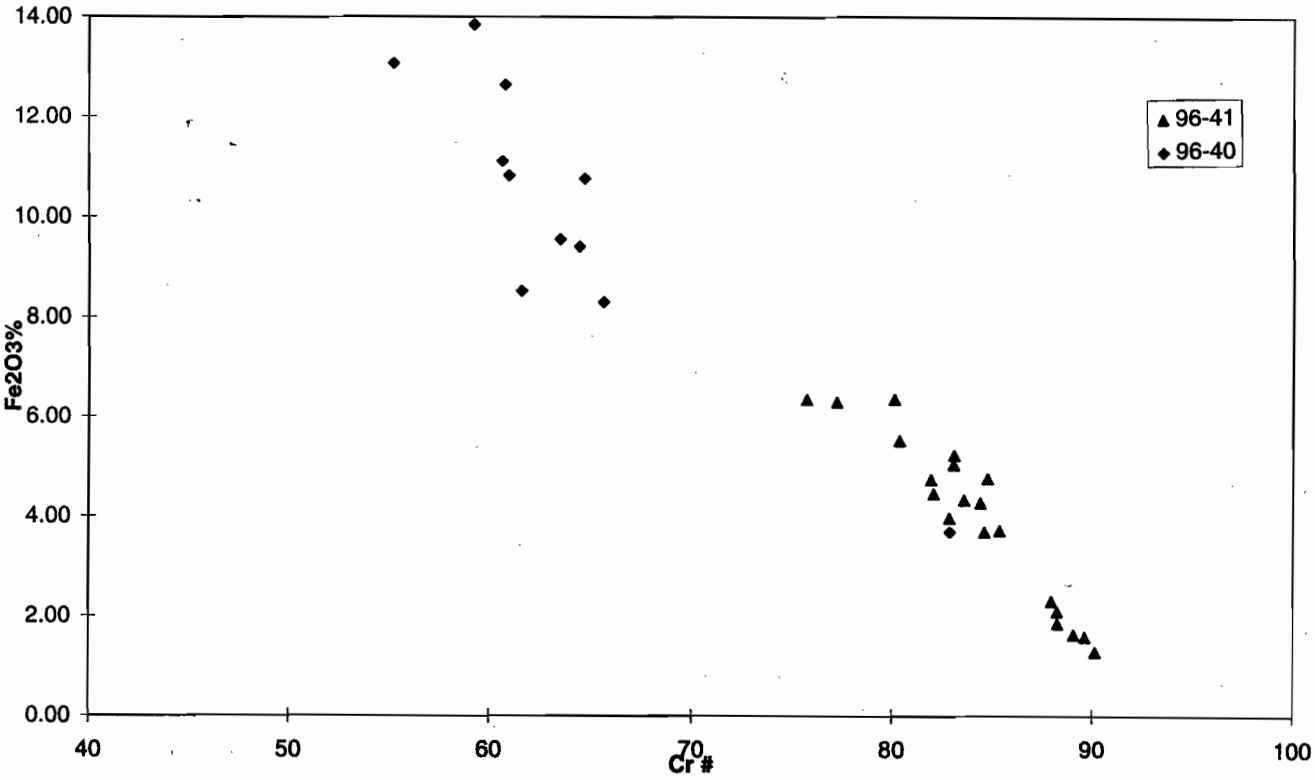

Figure 3. Chromites from Bowery Formation and South Comet. (a) TiO_2 vs Cr#, (b) Fe_2O_3 vs Cr#.

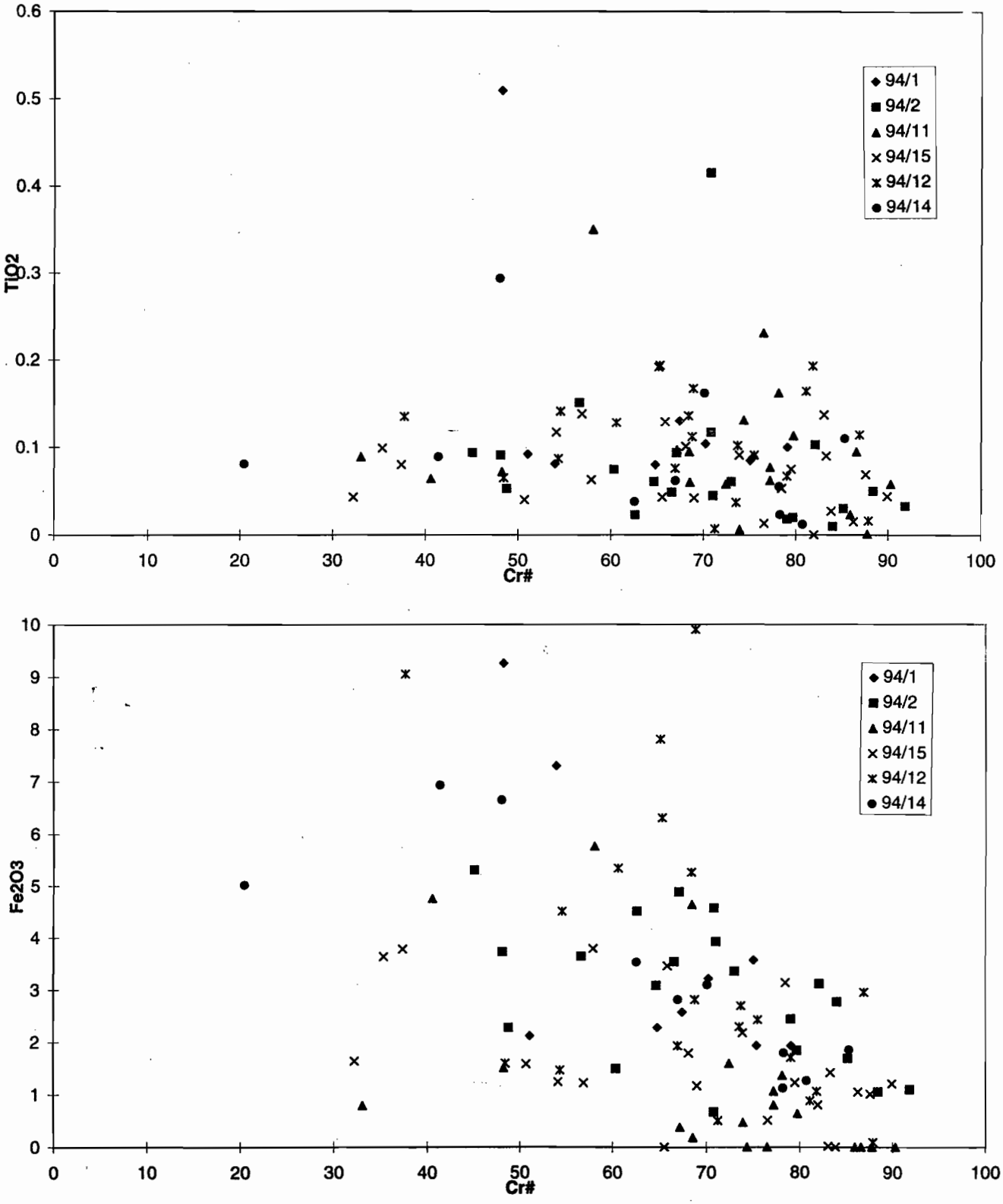

Figure 4. Chromites from Animal Creek Greywacke and Farrell Slate. (a) TiO_2 vs Cr#, (b) Fe_2O_3 vs Cr#.

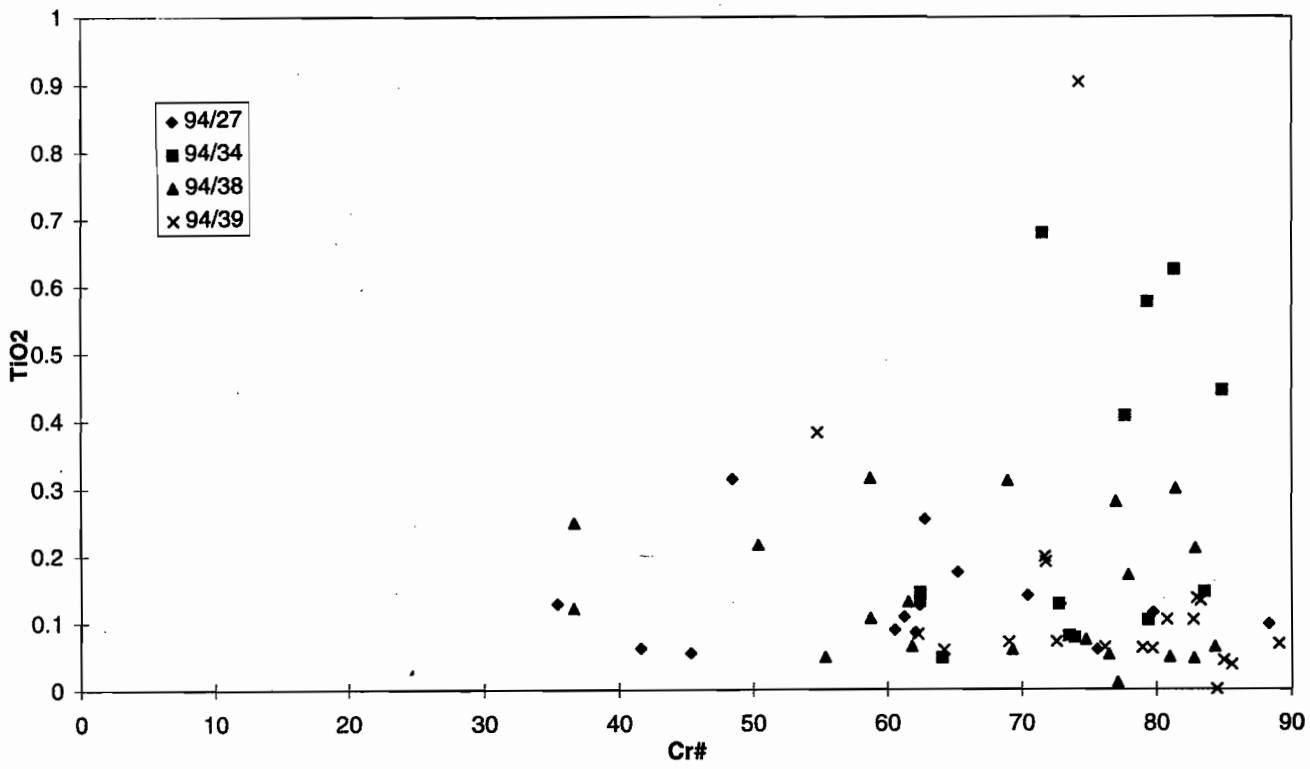

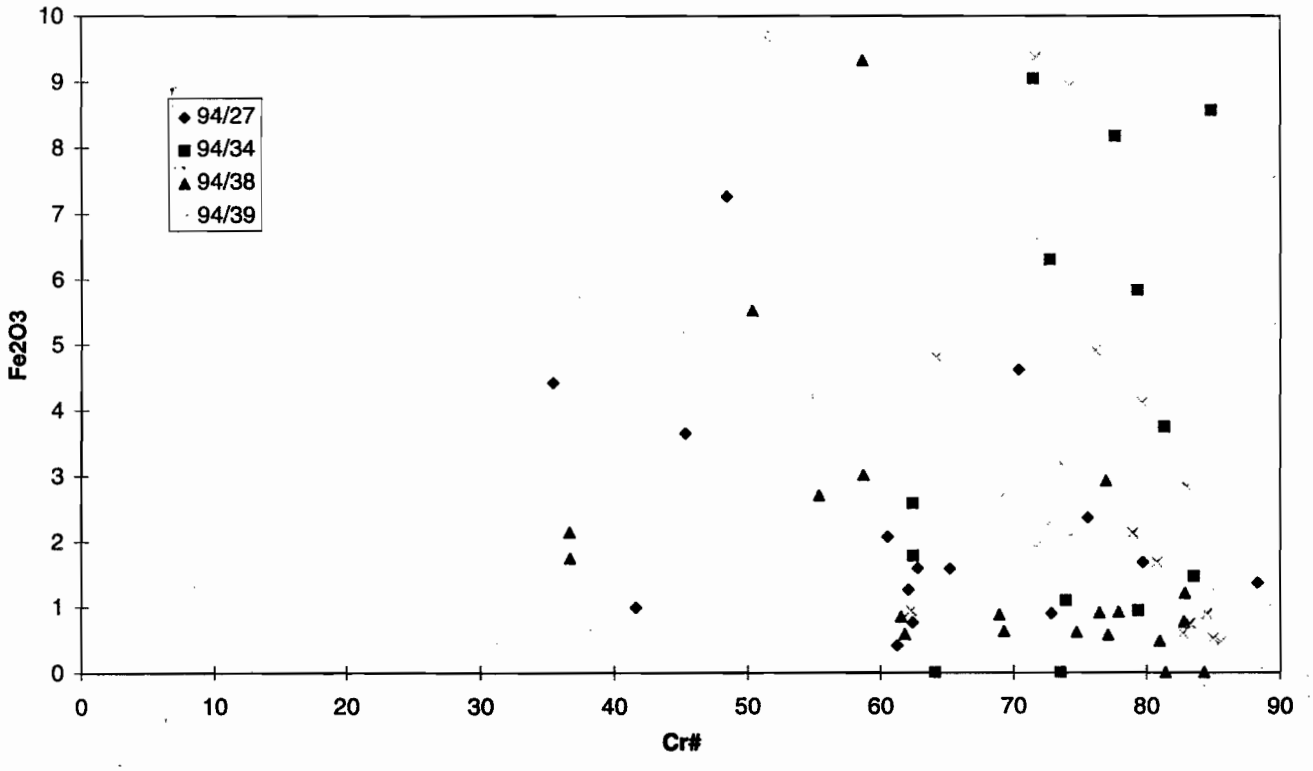

Figure 5. Chromites from southern Dundas "trough". (a) TiO_2 vs Cr#, (b) Fe_2O_3 vs Cr#.

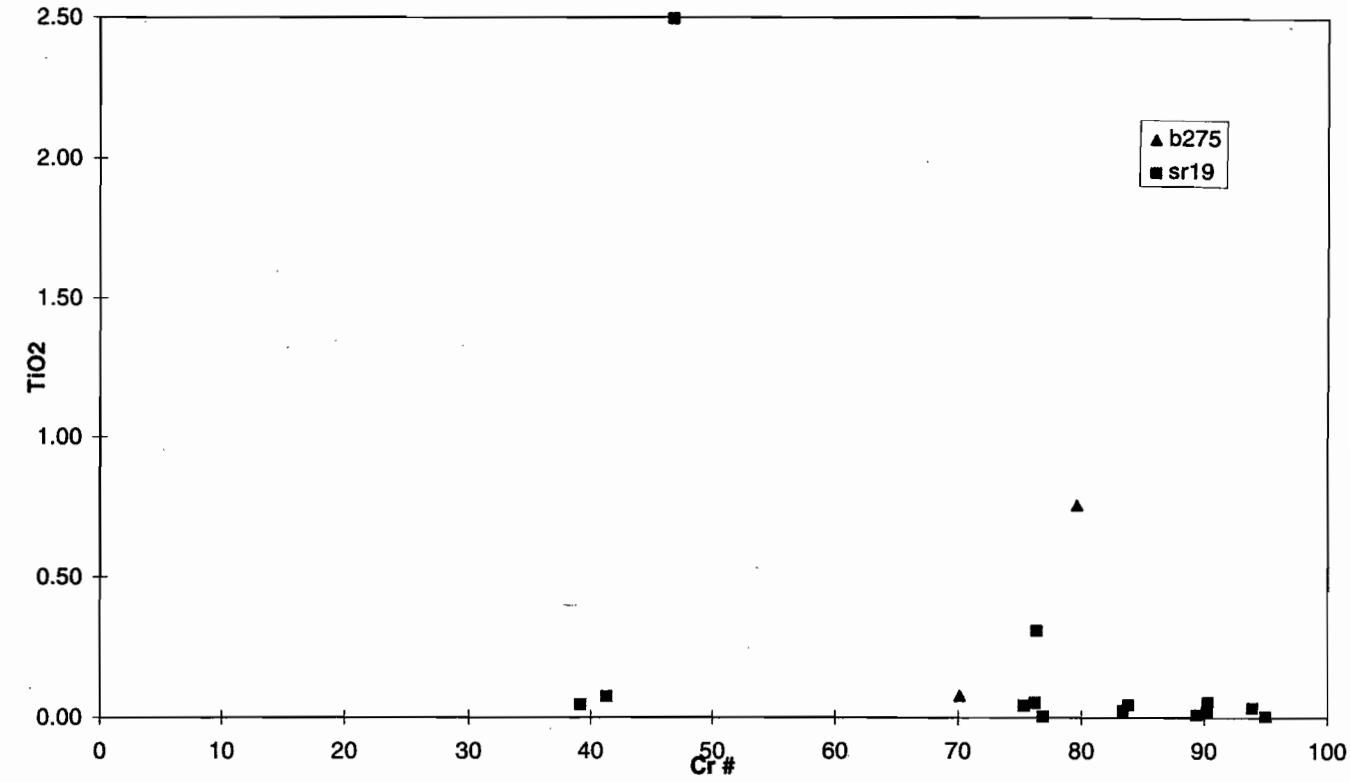

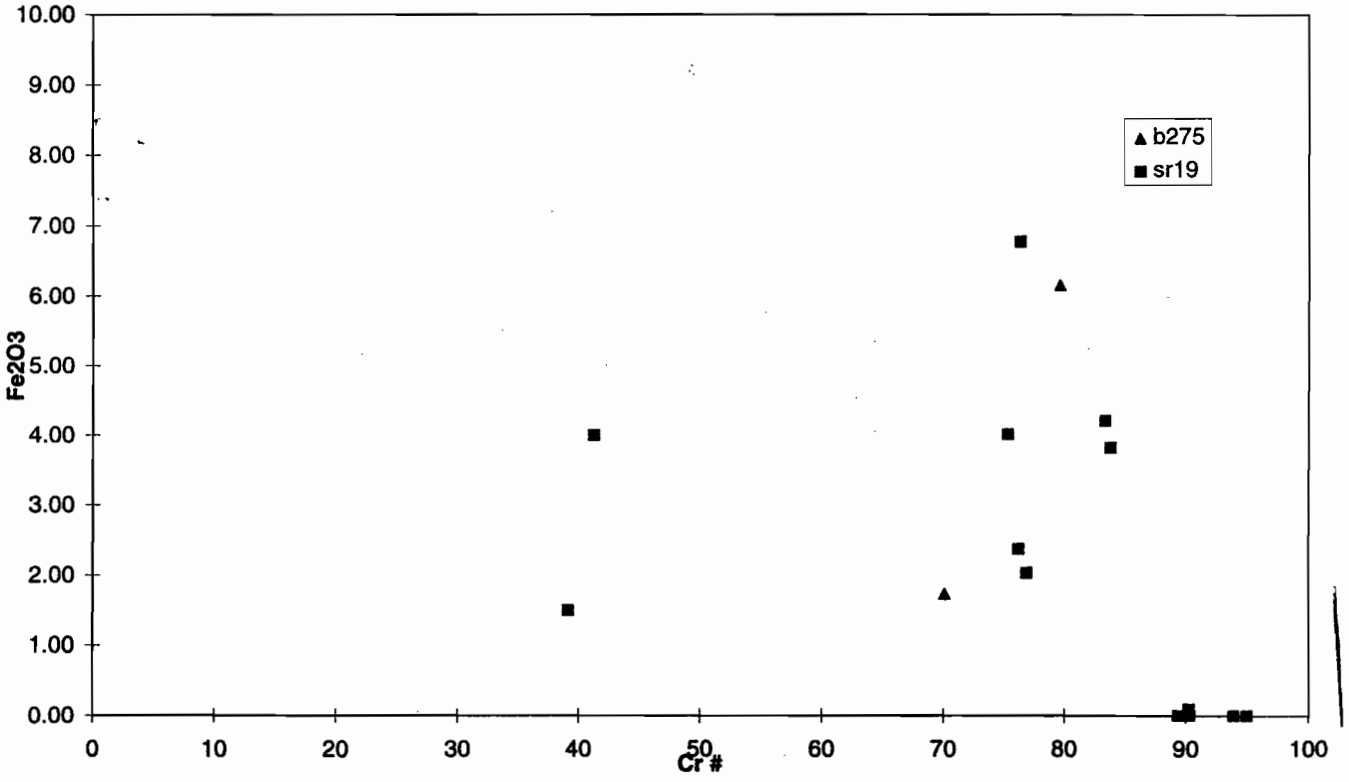

Figure 6. Chromites from Sticht Range Formation. (a) TiO_2 vs Cr#, (b) Fe_2O_3 vs Cr#.

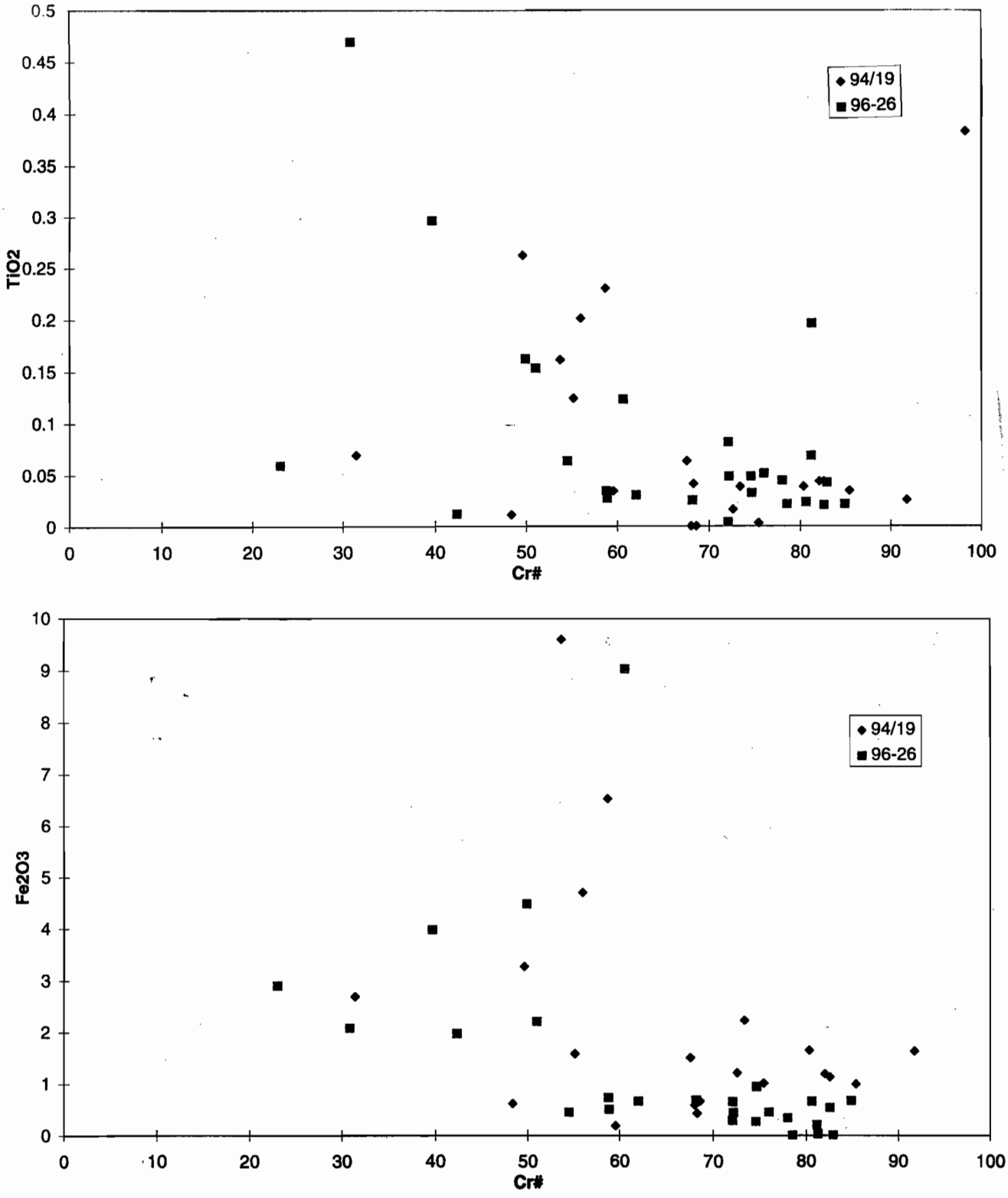

Figure 7. Chromites from Southwell Subgroup. (a) TiO_2 vs Cr#, (b) Fe_2O_3 vs Cr#.

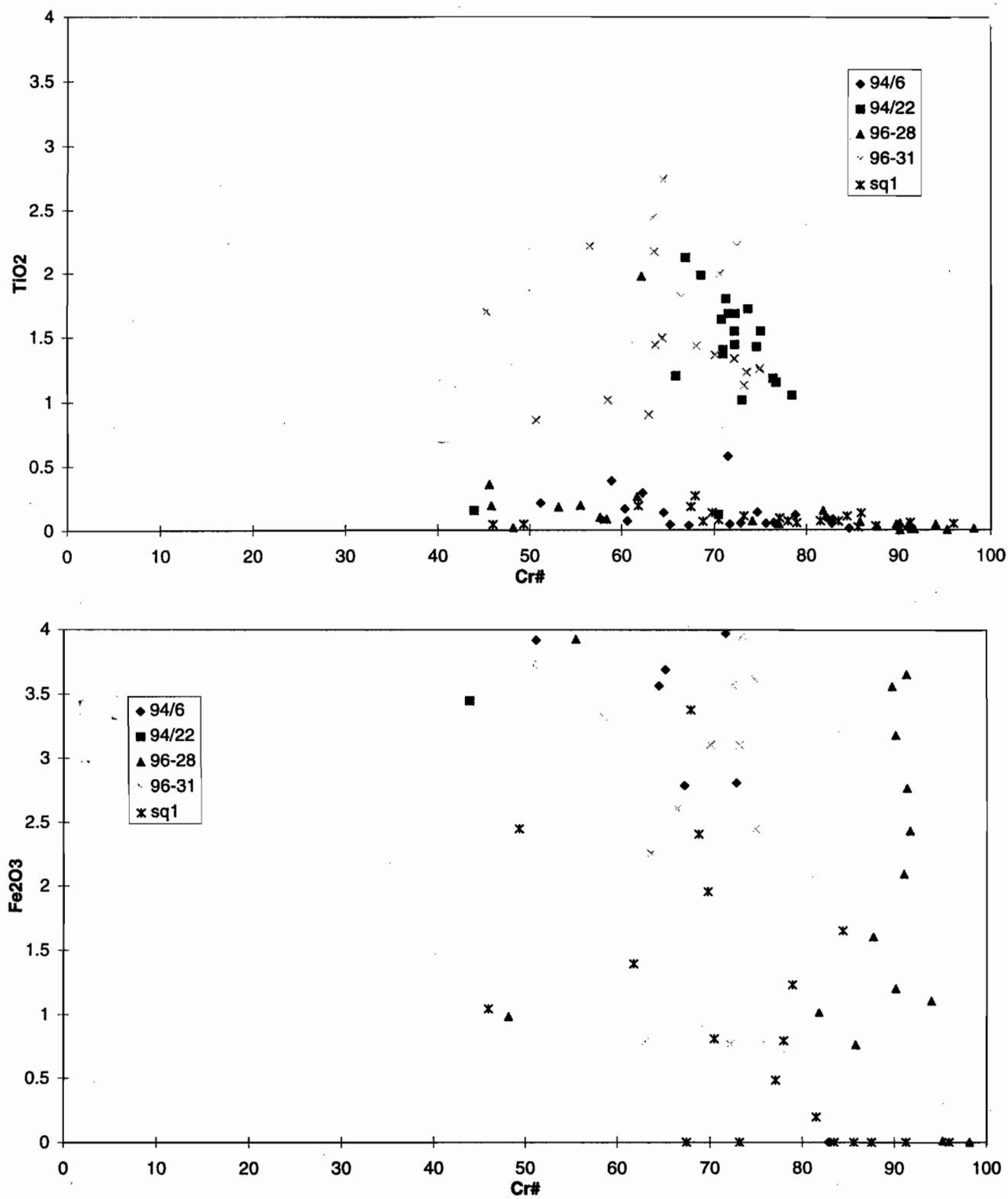

Figure 8. Chromites from west of the Rosebery Fault. (a) TiO_2 vs Cr#, (b) Fe_2O_3 vs Cr#.

Quartzite (SQ1), Westcott Argillite (96-28) and Higgins Creek (94/6) have MUC derived chromite with only one high TiO_2 grain detected. In contrast samples 94-22 is from very close to 96-28 but is dominated by tholeiitic chromites. Sample 94-22 was collected less than 100 m from the mapped edge of the Westcott Argillite and the possibility exist that the mapping (Corbett & McNeill, 1988) is slightly incorrect and that this sample is from within the Crimson Creek Formation. Alternatively it may indicate a proximal facies to the marginal fault. Selley (1997) has recognised high components of Crimson Creek Formation in the upper section of the Dundas Group in the Dundas area.

The Huskisson Group (Dundas correlate, sample 96-31) is also dominated by tholeiitic chromite. This is very surprising considering this sample sits very close to the serpentinites of the Wilson River MUC.

The chromites from Cambrian sandstones in northern Tasmania contrast with this pattern (Fig. 9). Samples from the micaceous sandstones (Gog Greywacke) are dominated by MUC chromite. These samples (96-01, 96-02, 96-03, 96-05, 96-23, 96-24, 96-25) are identical to the micaceous sandstones of the Animal Creek Greywacke and Yolande River Group. Almost all the analyses cluster at low TiO_2 (<0.5%) and there is a continuous trend towards high Cr# at low TiO_2. In contrast, the chromites from north-western Tasmania have more tholeiitic components. The sample from Stoney Head (96-12, Denison correlate), has a mixed signature suggesting both tholeiitic and MUC sources. Sample 96-13 (Scopus–Denison cycle) has one grain from the 20 convincingly sourced from tholeiitic basalts. For Tyndall cycle correlates (Christmas Hills), sample 96-15 has chromites largely derived from the Kanunnah Subgroup and sample 96-16 has a mixture of MUC and tholeiitic chromite. Sample 96-14 (Barcoo Road Yolande Cycle) has mainly tholeiitic chromites. The transition to deeper water recorded at Christmas Hills by Jago (1971) lies at the transition from a local chromite source to a MUC source which dominates the younger rocks.

Only one sample from the Dial Range "trough", sample 96-22 from Isandula Road, has chromites largely derived from a tholeiitic source.

The distribution of chromite between different samples above suggest that detrital chromite populations could be used to test some stratigraphic and mapping problems in Western Tasmania. Most samples of Middle Cambrian sandstones from the Dundas "trough" have a MUC dominated chromite population which has not been recognised in the Crimson Creek Formation.

Example 1

The first application attempted was the distinction between Crimson Creek Formation and Dundas Group around the Renison area. Samples were collected in the area from Cuni (96-43) and along the main road from Renison to Rosebery (96-44, 96-45, 96-46, 96-47). These samples have been mapped as listed in the table below.

Sample 96-43 contains a suite of tholeiitic chromites (Fig. 10) compatible with the original interpretation of Brown (1986) that these are Crimson Creek Formation correlates and not supporting correlation with the Dundas Group. Greenhill (1995) found a similar population of chromites in this area.

Samples 96-44, 96-45 and 96-46 are also tholeiitic and do not support a correlation of this area with the Dundas Group. The original Zeehan map sheet

	Zeehan Sheet (Brown et al 1994)	Mt Read Project Corbett & McNeill(1986)	Brown (1986)
96-43	Etl Dundas correlate		Ecc Crimson Ck Fm
96-44	Ecc	Ecc	Ecc
96-45	Ehm	Ed	Emu
96-46	Ehm	Ed	Eh
96-47	Ehm	Ecc	Eh

(Blissett & Gulline, 1962) identified this area as Crimson Creek Formation and this interpretation needs to be considered again. Alternatively the data here merely indicate the Husskisson Group is derived from Crimson Creek Formation. The sample 96-47 from the Colebrook area has typical MUC sourced chromite and cannot be a Crimson Creek Formation correlate.

Example 2

The area south of and probably beneath the Tenth Legion thrust at South Comet has substantial significance for the age of thrusting along this zone. Brown et al. (1994) mapped this area as Ets and correlated the area with the Dundas Group. Chromites from sample 96-41 are from this area. The chromites area high Cr# and low TiO_2 (Fig. 3) supporting the correlation of this unit with the Dundas Group.

Example 3

The foreshore from Penguin has been an area of major contention for many years. Originally all the basalts and sediments here were considered to be Cambrian (Burns, 1964) but more recently (e.g. Brown 1989) the Motton spilite and Barrington Chert have been reinterpreted as Precambrian (correlates of the Crimson Creek Formation/Success Creek Group) and thrust over the Cambrian sequence in the Dial Range "trough". However the associated sequences, Beecraft Megabreccia, Teatree megabreccia, Westbank Chaos are less certain. Seymour & Calver (1995) in there latest review, placed these units at the top of the Cambrian section despite their close spatial correlation with the Motton spilite and Barrington chert. Chromites from these sequences (Fig. 11) are typical of a tholeiitic source and no MUC chromites were detected. Most of this data comes from the Westbank Chaos and the other two units were poorly tested. The detrital chromite provide no support for the interpretation of Seymour & Calver (1995). Note, however, that Sproule (1994) reports MUC chromites from the Beecraft megabreccia.

A similar test was attempted for the Port Sorell sequence. However only four chromites were analysed (Fig. 11), not enough to adequately test the provenance.

Apatite

Most apatites show fractured or euhedral shapes. No well rounded apatites were recognised. The compositions are mostly F-rich Cl-poor suggesting a magmatic origin, and combined with the textures, a proximal source from local magmatic activity is proposed.

Three samples contain a distinctly different apatite form. These apatites are broken grains and are full of fine grained inclusions. The apatites from these samples have higher Cl content than the magmatic apatites from other samples (Fig. 12a) and are probably formed by alteration. They were recognised from the Mt Cripps Subgroup on the Cradle Mountain Link Road (94/17), a volcaniclastic sandstone in the Yolande River sequence south of Lynchford (94/32) and the Tyndall Group (94/41). The alteration apatites also have marginally lower FeO and Sr than the clear apatites.

One sample (94/6, Higgins Creek) has been found with a population of apatites with much higher Cl contents(Fig. 12b). These samples contain 2% Cl and require a different source from the apatites found in other rocks in the area.

Zircon

Zircons have been found in most rocks. There is very little variation in composition. The ratio of rounded to euhedral zircons reflects the proportion of extrabasinal sediment represented in the sandstones. Some of the rounded zircons (especially in the Sticht Range Formation) are slightly metamict but the euhedral zircons are all clear and unaltered. This is consistent with detrital zircons including some very old grains. Eleven samples of rounded zircon were analysed by LAMS-ICPMS. This technique has been described by Scott & Gauthier (1996). The method uses Pb isotope ratios to determine an "age" for each spot. The LAMS-ICPMS technique uses a slightly larger spot than ion probe dating and has a poorer precision but is adequate for the purpose of determining the age profile of detrital zircons. The analysis here includes mainly the rounded grains as previous work on the euhedral zircons of the Mount Read Volcanics (Perkins & Walshe 1993) has given a tight cluster around 500 Ma.

Histograms showing the distribution of zircon Pb^{207}/Pb^{206} ages are shown in Fig 12. The Sticht Range

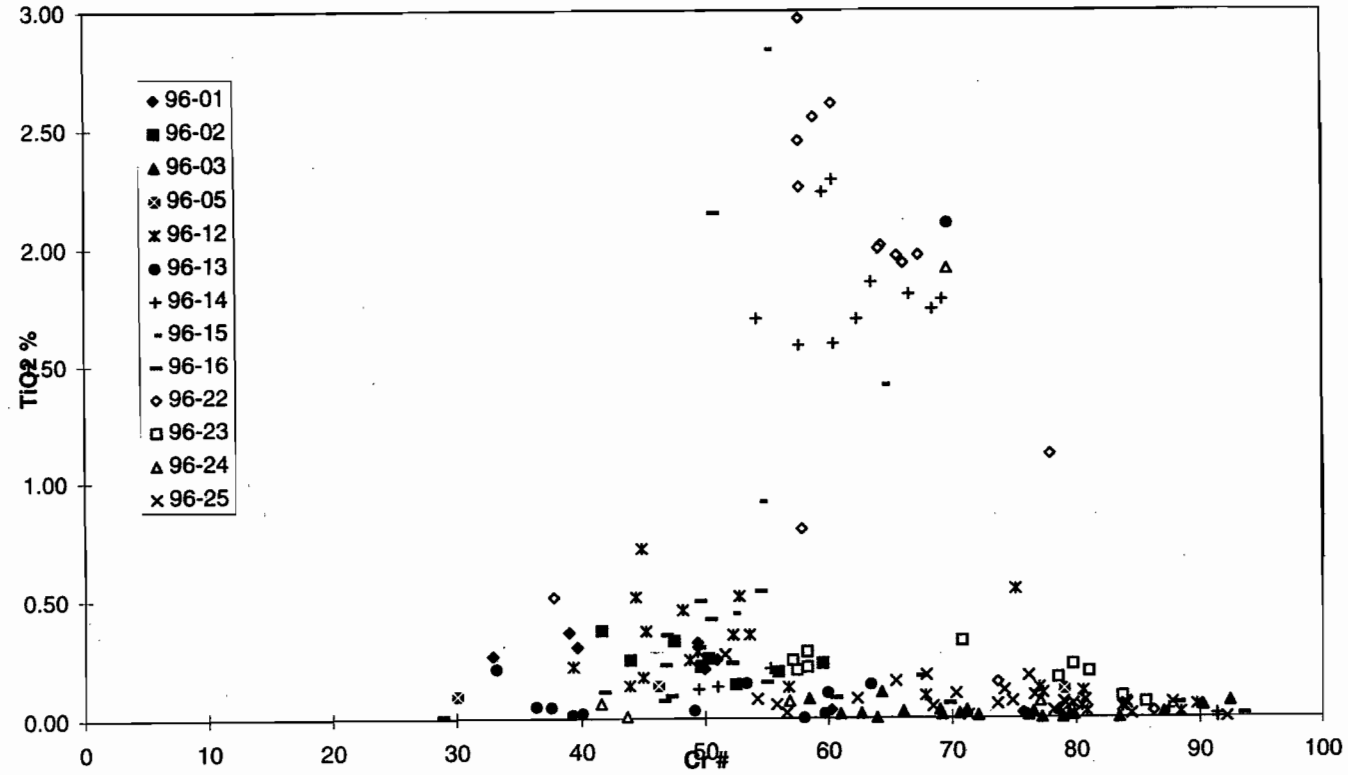

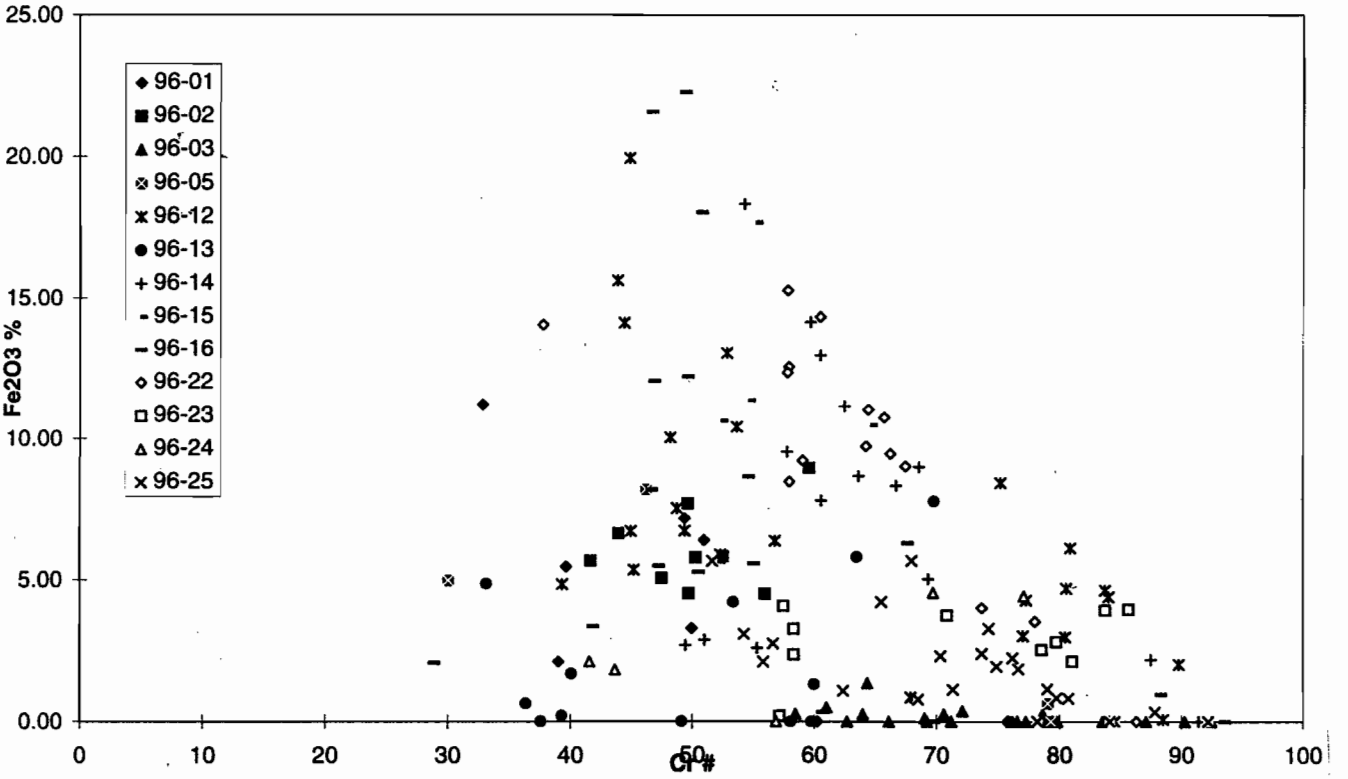

Figure 9. Chromites from Cambrian rocks in northern Tasmania. (a) TiO_2 vs Cr#, (b) Fe_2O_3 vs Cr#.

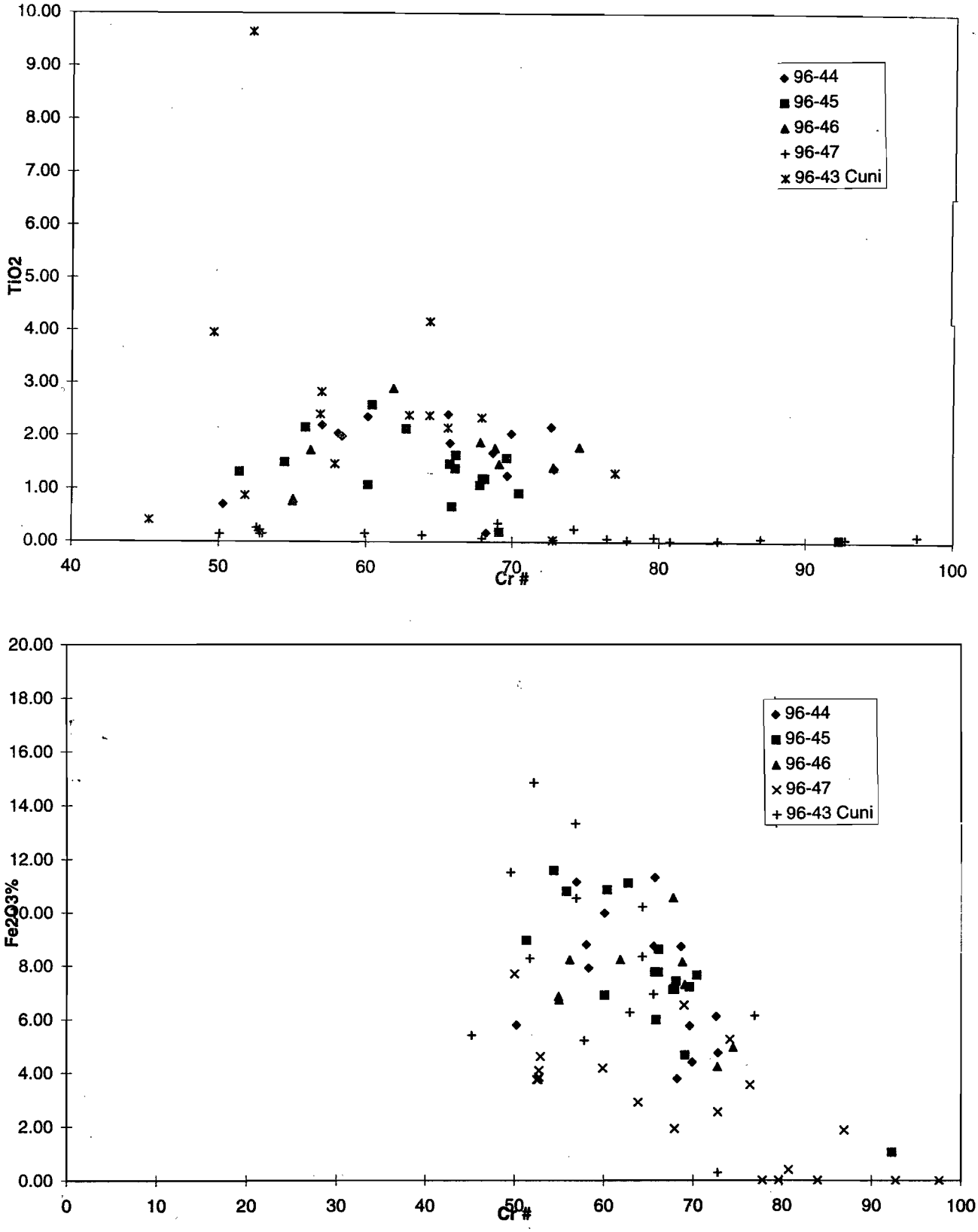

Figure 10. Chromites from Renison area. (a) TiO_2 vs Cr#, (b) Fe_2O_3 vs Cr#.

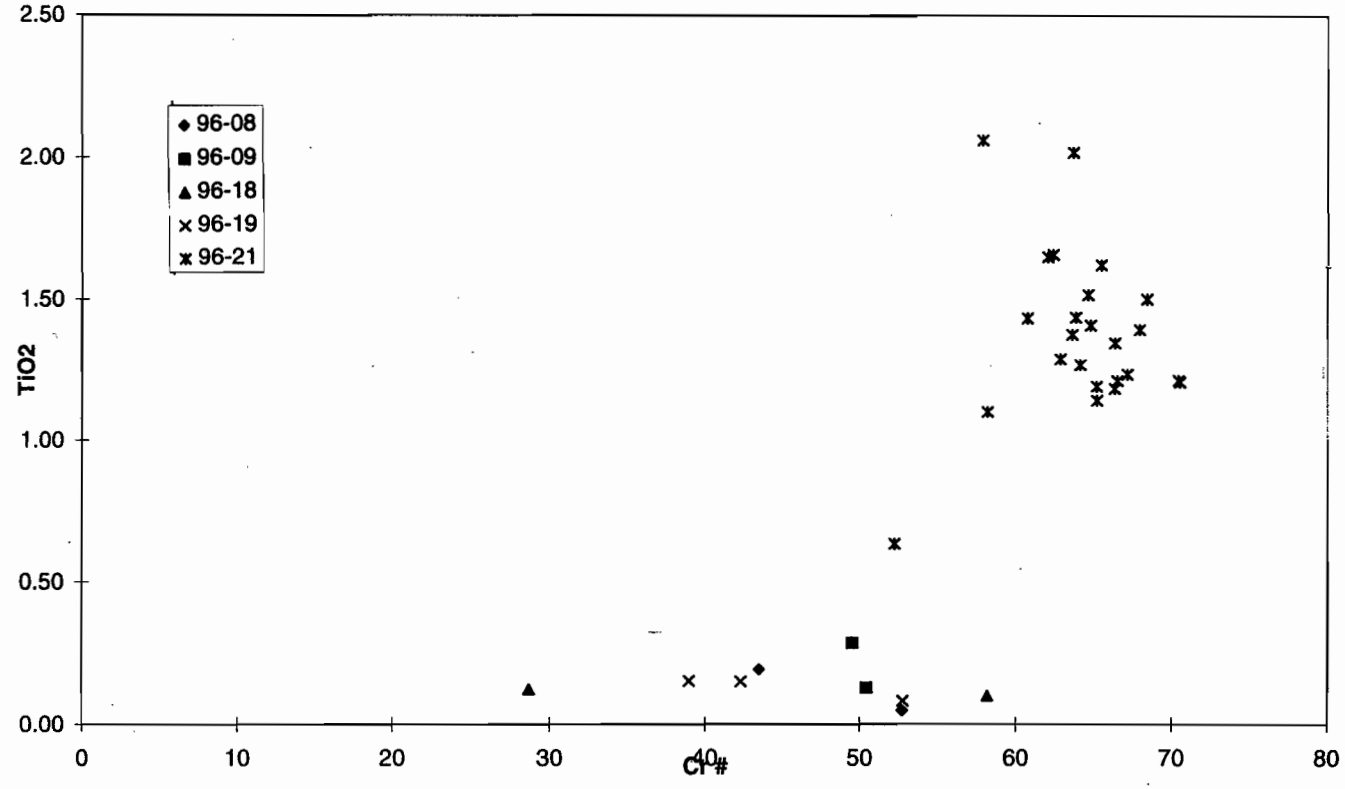

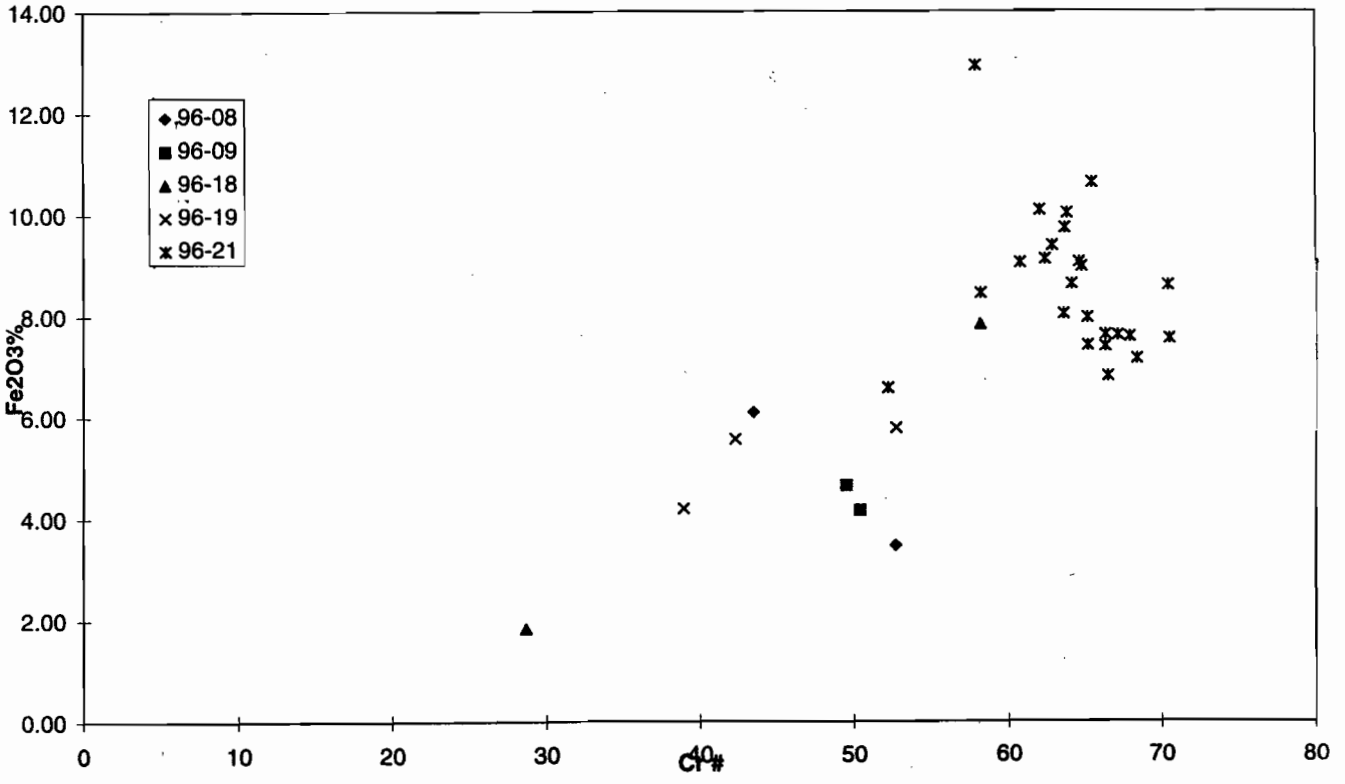

Figure 11. Chromites from possible Precambrian in northern Tasmania. (a) TiO_2 vs Cr#, (b) Fe_2O_3 vs Cr#.

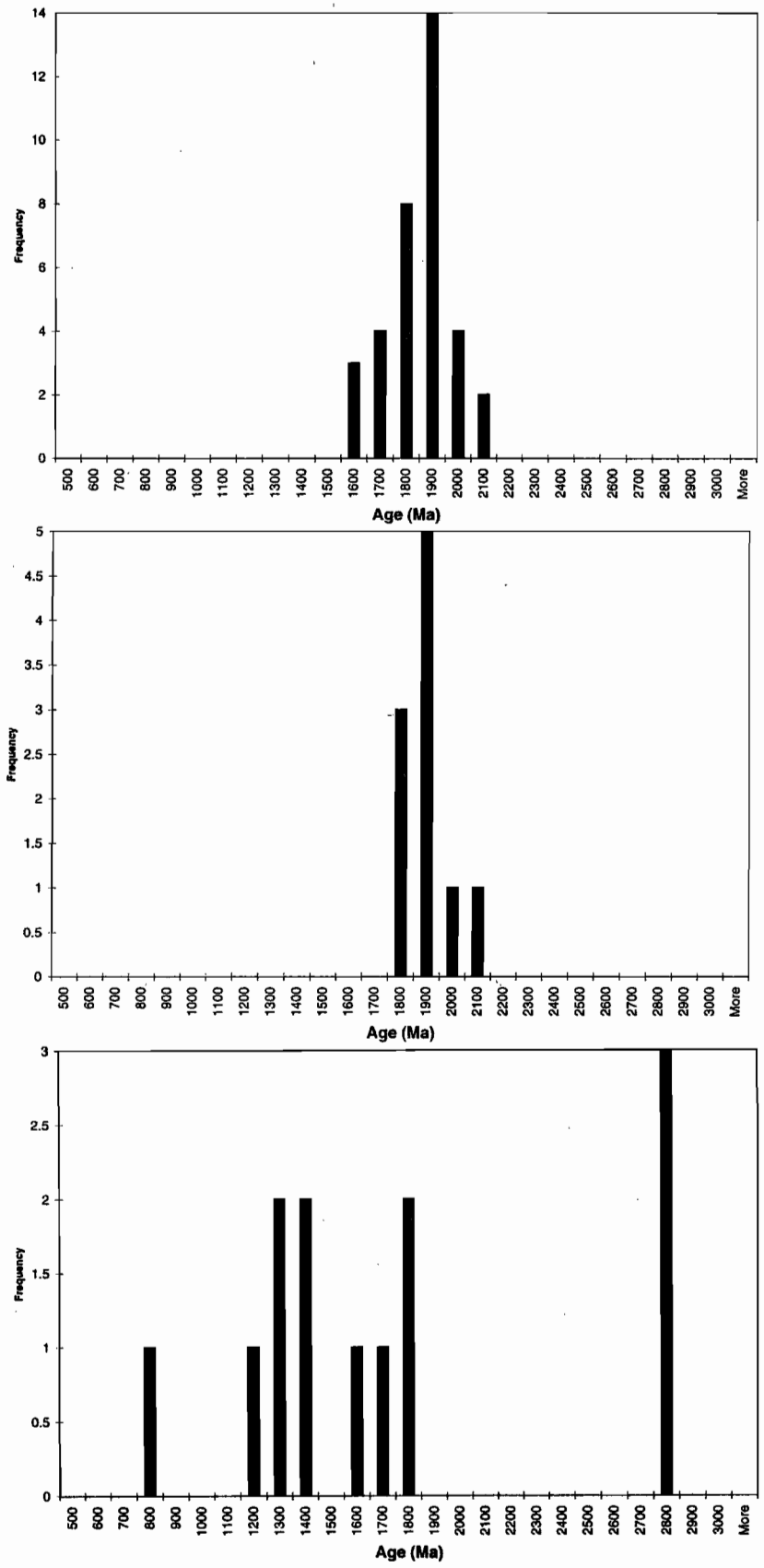

Figure 12. Histograms of zircons age distributions from western Tasmanian sandstones.
a) Sticht Range Formation SR19
b) Sticht Range Formation V109
c) Animal Creek Formation 94/12

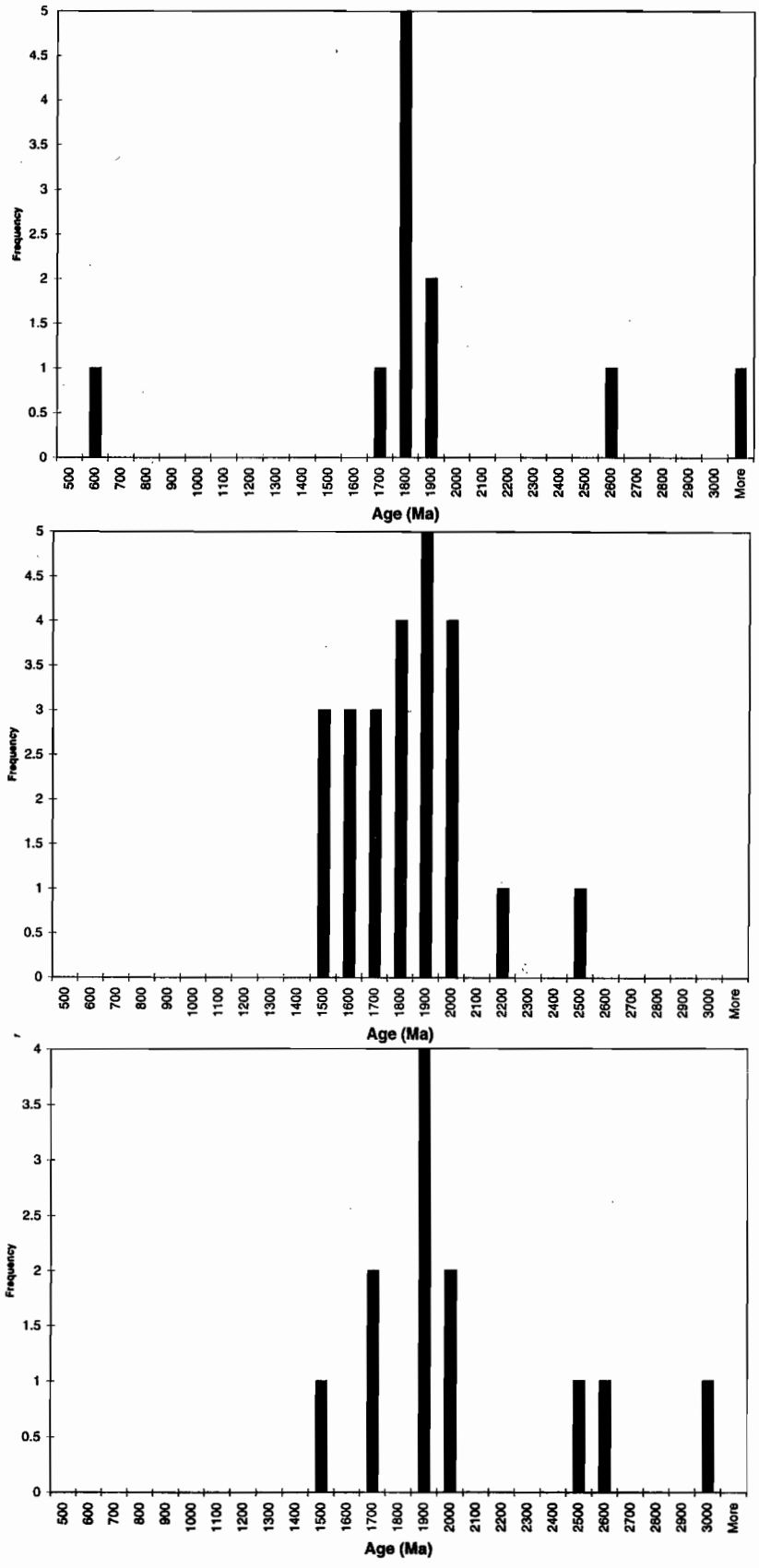

Figure 12. Histograms of zircons age distributions from western Tasmanian sandstones.
d) Animal Creek formation 94/14
e) Stitt Quartzite SQ1
f) Stitt Quartzite 94-4

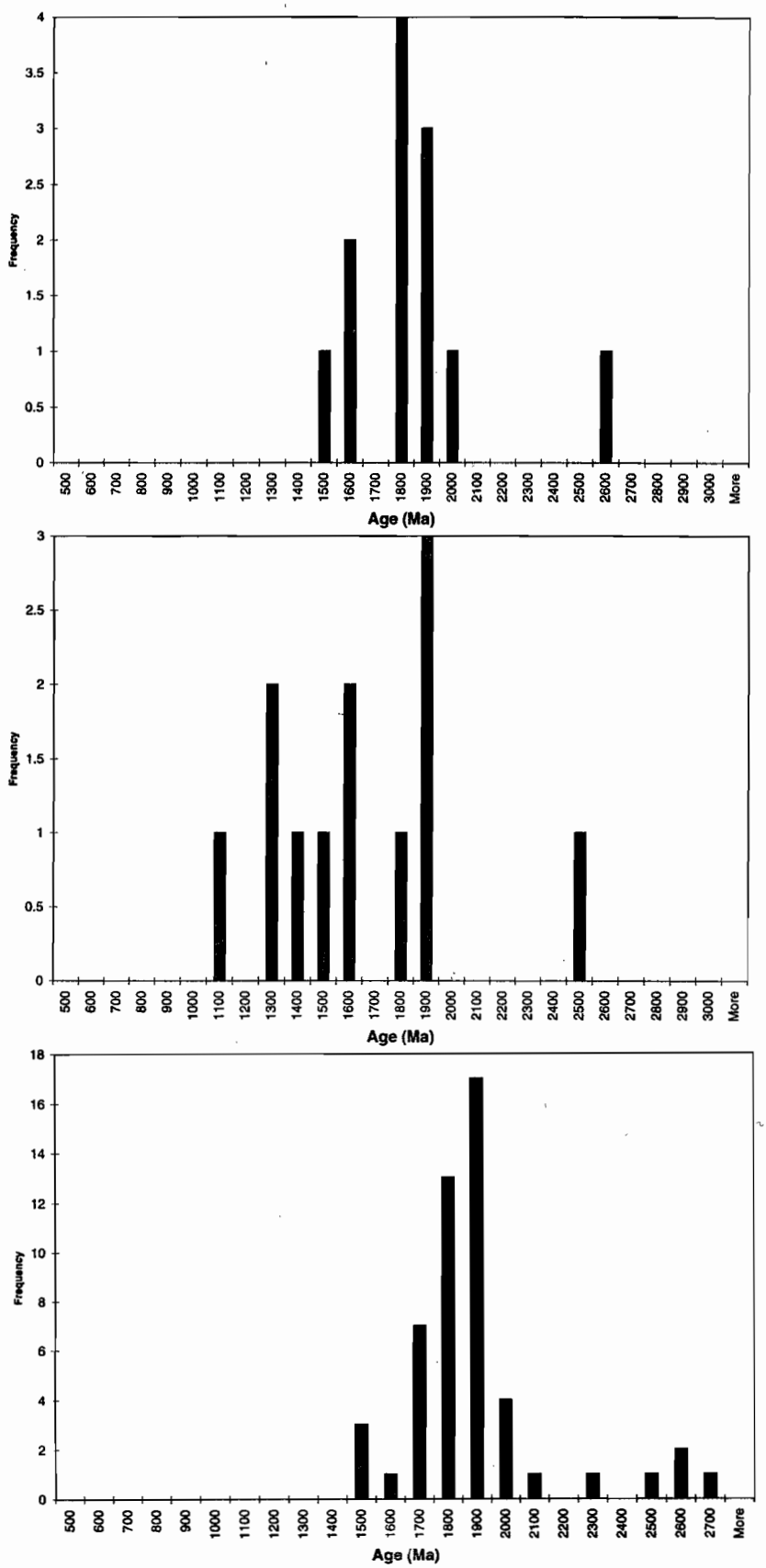

Figure 12. Histograms of zircons age distributions from western Tasmanian sandstones.

g) Gog Greywacke 96-4

h) Gog Greywacke 96-25

i) Forest Conglomerate 96-10 (Precambrian sandstone at the base of the Smithton sequence)

Formation samples (SR19, V109) have a unimodal zircon population centred on 1800 Ma. This 1800 Ma peak is recognisable in all other samples analysed including the Forest Conglomerate. The Forest Conglomerate also has a peak at 2600 Ma and a few grains of this age are also recognised in the Animal Creek Greywacke (94-12, 94-14), Gog Greywacke (96-4, 94-25) and Stitt Quartzite (SQ1, 94-4). The implication is that these signature comes from the Rocky Cape block and does not occur in the Tyennan block. A few rocks have a tail of zircon ages down to 1400 Ma. This trend is strongest in 94-12 and 96-25 (both Middle Cambrian micaceous sandstones) but is present in some others (96-4, SQ1). Finally the recently reported age of the King Island Granite (Black, 1994) suggests there should be some 700 Ma zircons but these are rare (two grains total and both in the Animal Creek Greywacke). We may have biased the result against such grains by selecting only rounded grains for dating.

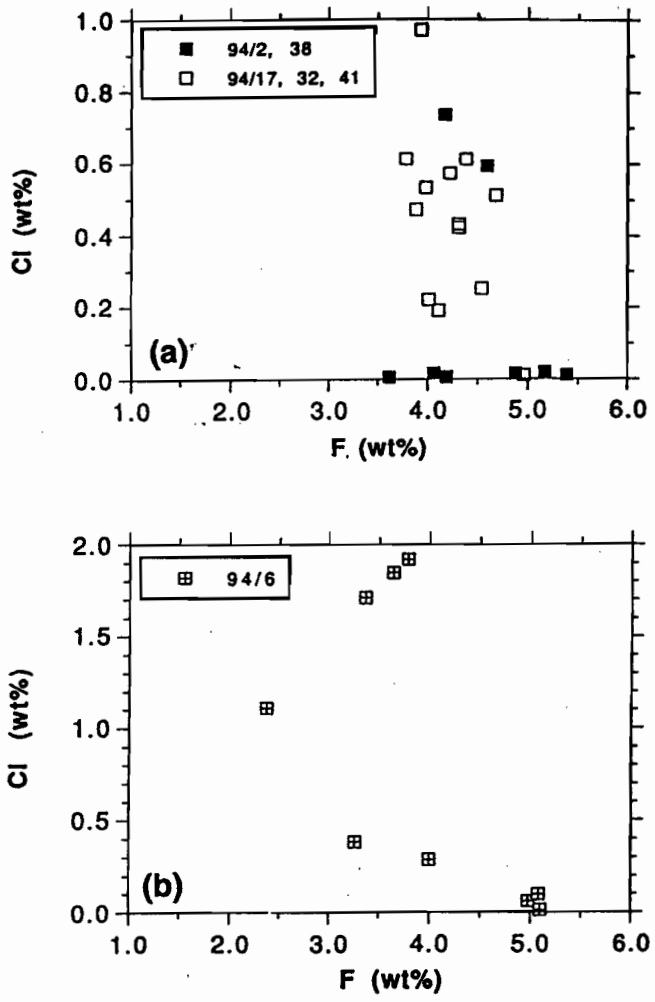

Figure 13. Apatite compositions. a) Magmatic grain - 94/2, 94/38, alteration - 94/17, 94/32, 94/41; b) 94/6.

Extensive work on zircon provenance has been carried out around the Gondwana margin (e.g. Williams et al., 1991; Muir et al., 1994; Ireland et al., 1995). The Kanmantoo and Lachlan fold belts show a very similar zircon inheritance pattern with major peaks at 500–600 Ma and 1000–1200 Ma with a scatter of ages back to >2000 Ma. In contrast, the Adelaidean sediments have a major peak at 1750–2000 Ma and a few grains up to 2800 Ma.

The detailed investigation here link the source region of the basement of Tasmania to an Adelaidean sedimentation history. This correlation is best for Sticht Range Formation which is directly sourced from the Tyennan block. The Animal Creek Greywacke and Stitt Quartzite which have more ophiolite in the source and also have another age component in their zircon pattern. These rocks all contain a few grains with ages of 1200–1400 Ma zircons.

The strong Adelaidean signature of the Sticht Range Formation makes the interpretation of an exotic origin for the Tyennan block very unlikely. The inheritance pattern of the Sticht Range Formation is also very similar to the pattern recognised in the Cooee dolerite, assumed to be from the Burnie Formation (Black, 1994). The Animal Creek Greywacke (94/12) has a complex zircon pattern very similar to the sum of all inherited grains recorded by Black (1994).

Tourmaline

Tourmalines are largely euhedral or broken. No evidence was noted for rounded tourmaline. Some tourmalines have visible zoning in colour but this has not been investigated in detail. The compositions range in Mg#, with MgO varying from 4.4–11.3% but other elements are not very variable. Tourmaline is very common in the Animal Creek Greywacke, and forms part of the diagnostic mineralogy for this assemblage, but is rare in the Tyndall Group and youngest rocks (e.g. Higgins Creek). The tourmaline analyses of samples from Animal Creek Greywacke, Farrell Slate and Stitt Quartzite are shown in Figure 14. All the points plot in the fields 4, 5 and 6 of the Al, Mg and Fe diagram from Henry & Guidotti (1985). These fields are meta-pelites, meta-psammites,

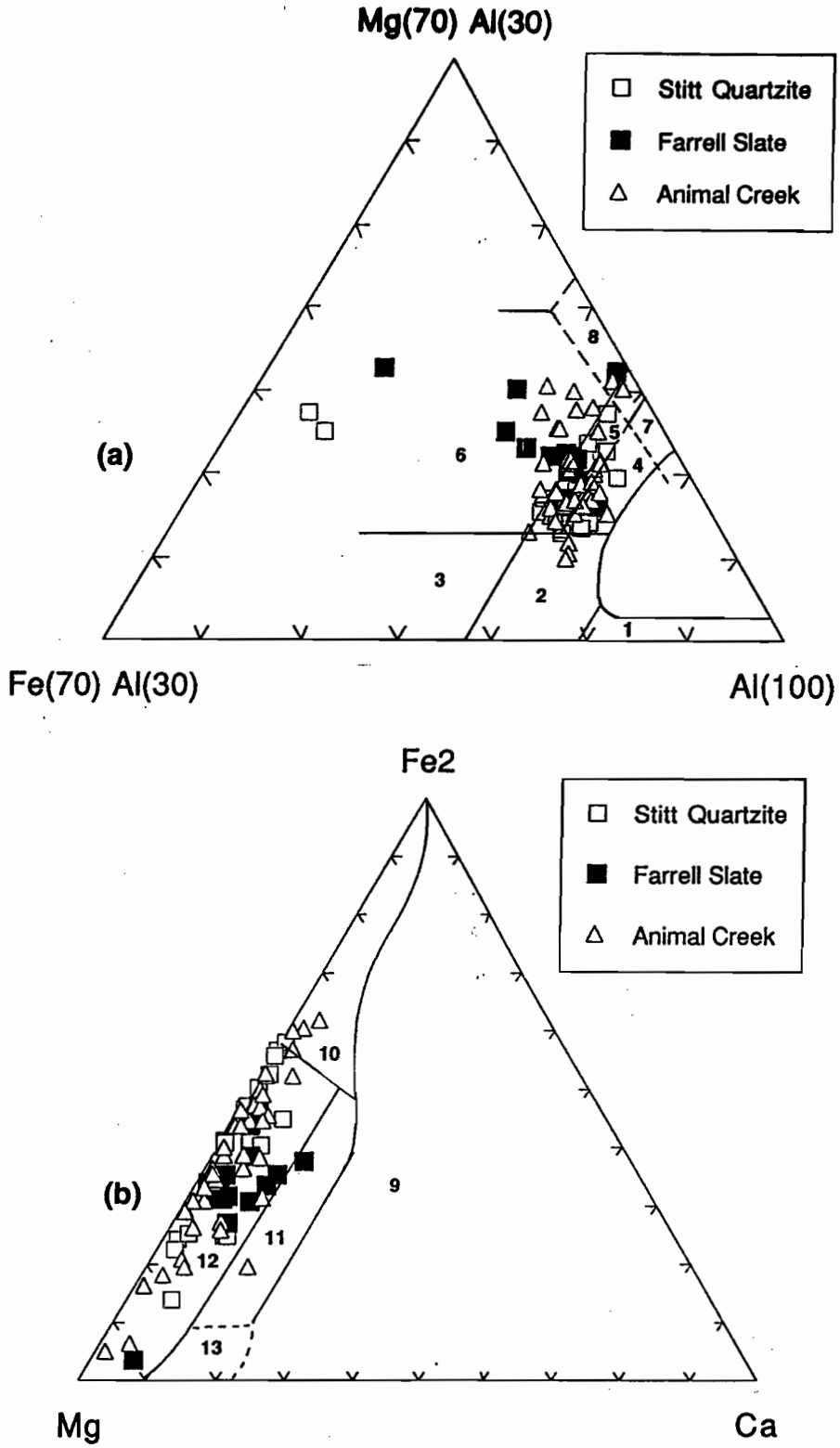

Figure 14. Tourmaline compositions a) Mg-Fe-Al, b) Mg-Fe-Ca. Interpreted fields are from Henry & Guidotti, 1985. Types are 1- Li-rich granitoid pegmatites and aplites, 2- Li-poor granitoids, 3- Fe3+ qtz tourmaline rocks (altered granites), 4- Metapelites and metapsammites with coexisting Al-saturating phase, 5- Metapelites and metapsammites without coexisting Al-saturating phase, 6- Fe3+ rich quartz-tourmaline rocks, calc-silicates and metapelites, 7- Low Ca meta-ultramafics and Cr, V metasediments, 8- Metacarbonates and meta-pyroxenites.(7 and 8 overlap 4 and 5). 9- Li-rich granitoid pegmatites and aplites, 10- Li-poor granitoids, 11- Ca rich metapelites, metapsammites and calc-silicates, 12- Ca poor metapelites, meta-psammites and quartz-tourmaline rocks, 13- Metacarbonates.

and quartz-tourmaline rocks. The Ca-Mg-Fe diagrams shows that these tourmalines are from a low Ca precursor. There is no evidence in this data for a granitic source. Taylor & Slack (1984) demonstrated that tourmalines from massive sulphide bodies have a very similar range in composition to the samples reported here.

Magnetite

Magnetite grains are all heavily altered with hematite rims and replacement. In many rocks there are only a few flecks of magnetite left. After coating for the microprobe it is difficult to distinguish the magnetite cores from the hematite and most of the oxide analyses have low totals indicating that they are largely hematite. TiO_2 is fairly low. The presence of ilmenite exsolution lamellae in hematised magnetite suggests titano-magnetite original compositions.

Fe oxides in the Farrell Slate(94/2) and Stitt Quartzite (SQ-1) are all hematite with very low TiO_2. Sample 94/41 (Tyndall Group) has a spread in Ti and Fe (Fig. 15) which reflects a titano-magnetite component and an ilmenite component. The spread in Ti among the "ilmenite" is unrealistic given the possible range of Ti at magmatic conditions and is interpreted here as the result of analysing edges of small exsolution patches of ilmenite associated with hematised titano-magnetite. The Mt Cripps sample (94/18) shows similar problems with a large and unrealistic spread in TiO_2 contents, suggesting that oxidised titano-magnetite is the major component (Fig. 16). The freshest Higgins Creek sample (94/5) has two distinct oxide populations (Fig.17), ilmenite and magnetite with scatter between them. These are compatible with a primary detrital grain population of ilmenite and magnetite which is partially hematised.

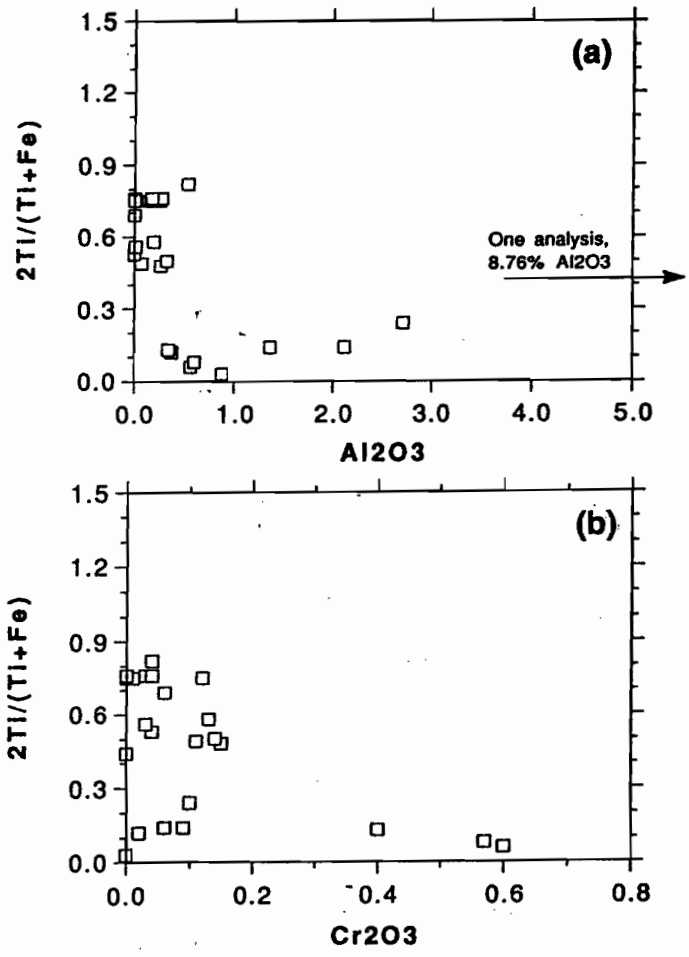

Figure 15 Oxide compositions from sample 94/41 (Tyndall Group) The y axis is a measure of the ilmenite component in an oxide.

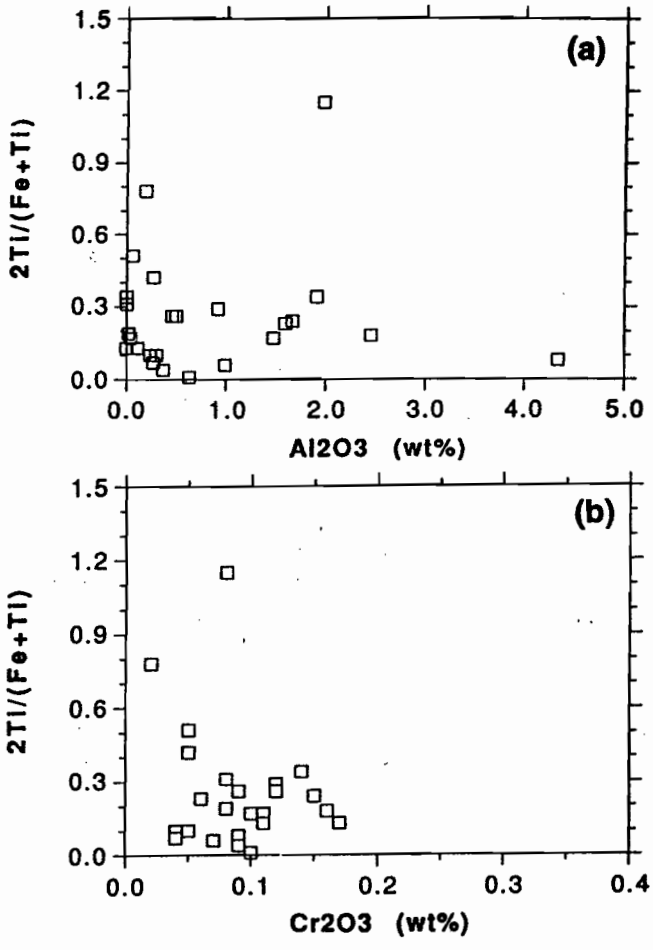

Figure 16 Oxide compositions from sample 94/18 (Mt Cripps Subgroup) The y axis is a measure of the ilmenite component in an oxide.

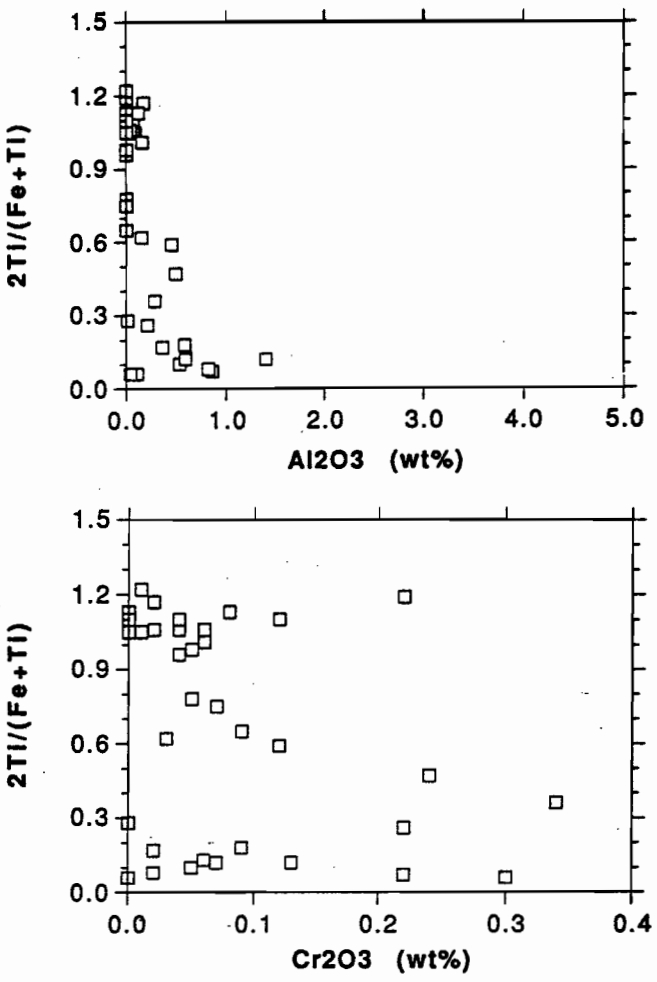

Figure 17 Oxide compositions from sample 94/5 (Higgins Creek) The y axis is a measure of the ilmenite component in an oxide.

The observations of oxides in this project have direct implications for magnetic interpretation within the Mt Read Volcanics. Very high magnetite are found in both Tyndall Group rocks (up to 0.8%) and in rocks sourced directly from the Crimson Creek (up to 0.35%). However in many cases these magnetites are extensively hematised and other samples have no relict magnetite. At least for the Tyndall Group rocks this variation appears to be alteration rather than weathering. The very high magnetic signal over the eastern edge of the Mt Read Volcanics has often been linked to Cambrian granite but some of this signature may be the magnetic parts of the Tyndall Group. With variable alteration this can produce highly variable magnetic responses.

Hematite

The irregular form of hematite grains is interpreted here to indicate the hematite is not a primary detrital mineral but replaces the magnetite and possibly ilmenite.

Ilmenite

Some ilmenite grains are rounded and are detrital. They are weathered with alteration to TiO_2. The analyses are mainly too low in TiO_2 for ilmenite suggesting there is extensive hematisation of the ilmenites. In many rocks the fine grained patchy hematisation is visible in reflected light.

High ilmenite has been detected in the Crimson Creek Formation, Smithton sequence, Jukes correlate from the Murchison Gorge, Sprent Formation, Beecraft Megabreccia and Higgins Creek. It is not typical of the Tyndall Group where ilmenite is largely found as a minor component due to exsolution and oxidation of original titano-magnetite. Much of this ilmenite could be attributed to the western source (Crimson Creek Formation) but the Jukes correlate (94/20) and Sprent Formation are anomalous.

Rutile, anatase

TiO_2 is a common component in most rocks. Much of this especially in the Tyndall Group, is the result of weathering ilmenite and magnetite. In some samples, rutile is apparently a primary detrital phase. The Animal Creek Greywacke is the best example of this form of TiO_2. The dominance of TiO_2 over FeO in these rocks is best explained by preconcentration of TiO_2 in a weathering profile before erosion. In contrast Tyndall Group and Denison Cycle sandstones show evidence of oxidation after transport.

Garnet

Surprisingly, garnet has not been recognised as major contributor to the heavy mineral suite. It has been found in the Smithton sequence (96-11), Crimson Creek Formation (94/24, 96-35), Yolande River sequence (94/38), Browns River sequence and Dundas Group near Pinnacles (94/3, 94/8), Higgins Creek area (94/6) and the Sprent Formation (96-23). Garnet has previously been reported from the Radfords Creek Group (Sproule 1994). Thus it has been recovered over a large area in the late Precambrian section and in all cycles of the Cambrian

section but not in the core of the Mt Read Volcanics. The later omission probably reflects the level of alteration and metamorphism in the core of the volcanics. Most of the garnet from all sources is typical of metamorphic almandine with moderate pyrope and low grossular content. However in some samples there is a trend to higher Ca and higher Mg reflecting more intense metamorphic conditions.

Sproule (1994) showed the Radfords Creek Group garnets matched the range of garnets in the Forth Metamorphic Complex very closely. Two of the garnets from the Sprent Formation reported here fall in the same area but two others are grossular spessartine garnets typical of a skarn source.

The two samples of from the Strahan Highway have trace garnet. Sample 94/38 garnets have high MgO and low CaO, and are most probably sourced from granulites (Fig. 18), but are on the margin of the range of garnets from Nye Bay (McNeill, 1985). This unusual, high-MgO-garnet composition has also been found in the Denison Cycle sandstone (94/6) and Yolande Cycle sandstone at Boco Road (94/3). One grain from the Crimson Creek Formation (96-35) also has a high-Mg almandine composition.

The remaining garnets are typical of amphibolite facies pelites (94/24, 96-11, 94/8) except two grains from 94/8 which are probably from amphibolites.

According to recent interpretations of Turner et al (1994) all the garnet-rich rocks in the Tyennan area formed in the Cambrian and cannot be sources for the garnets in the late Precambrian section. The King Island granite has some metamorphic garnet (Blackney, 1982) but this has higher Mn and lower Ca than the almandine reported here. Berry et al. (in prep) have reported high Mg garnets from Precambrian rocks dredged from the South Tasman Rise. These may be a source for the granulite facies garnets reported here. Alternatively, Antarctica occupied a position west of Tasmania in the Cambrian and may be the source for garnets in the Smithton, Crimson Creek Formation, Higgins Creek area and in Yolande River Group.

Pyroxene

Igneous clinopyroxene has been recognised in a number of different units mainly peripheral to the Mt Read Volcanics core area. The Smithton basalt and Crimson Creek Formation (96-17, 96-33, 96-34,

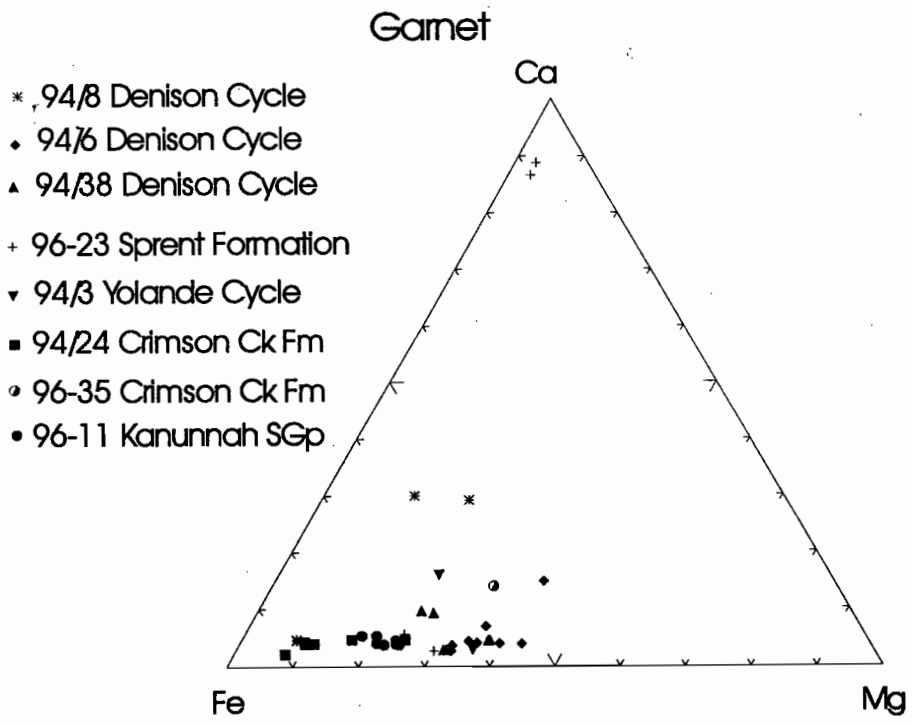

Figure 18. Octahedral components in pyralspite garnet.

96-35) have a large number of clinopyroxene grains. Using the classification diagrams of Leterrier et al. (1982) these are shown in Fig. 19 a,b,c. On the Ti vs Ca+Na diagram (Fig. 19a) these samples plot below the alkali basalt field. On the Ti+Cr vs Ca diagram (Fig. 19b) these samples plot in the field for non-orogenic tholeiites in keeping with there origin.

Clinopyroxene was also recovered from the Success Creek Group (96-36, 96-37). These samples have much lower Ti (Fig. 19a). The clinopyroxene from 96-37 plots in the orogenic basalt but is still tholeiitic in composition (Fig. 19).

The Beecraft megabreccia and Teatree megabreccia (96-18, 96-19) contains clinopyroxene with a composition similar to alkali basalt. The high Ti content of these clinopyroxene grains is unexpected and requires further investigation. Previous investigations in this area have not shown any component of alkali basalt (Hashimoto et al., 1981; Sproule, 1994). The only known potential source is the pillow basalts within the Burnie Formation. The other sample from the Penguin area was from the Barrington Chert on Lodders Point with non-orogenic tholeiites consistent with a source in the Motton Spilite.

The Sprent Formation (96-23) and Gog Greywacke (96-24) have very low Ti clinopyroxene consistent with formation in an orogenic tholeiite (Fig. 19a,b,c). These are similar in composition to grains found in the Success Creek Group but unlike most Crimson Creek Formation clinopyroxene. Sproule (1994) suggested a Motton Spilite source for the Sprent Formation basalt clasts but Berry et al. (Lithogeochemistry, this volume) suggest the Kerrison Volcanics may be the source for this material.

Orthopyroxene grains were recognised in the heavy mineral fraction of samples from the Crimson Creek Formation (96-34, 96-35, 96-44), Success Creek Group (96-37) and the Port Sorell area (96-8).

Pyrite

Pyrite is a common heavy mineral. Most of the pyrite is euhedral but a minor proportion is in framboids. The more weathered samples may contain goethite after pyrite (e.g. Higgins Creek 94/7) and this blurs the distinction between Tyndall Cycle and Denison Cycle sandstones.

A few samples contain chalcopyrite and/or other sulphides.

Discussion

The heavy mineral assemblages reported here have been used to characterise a range of sources for sandstones in the Mt Read Volcanics. The recycled metasedimentary source is characterised by rounded zircon and tourmaline. No evidence was found that the Tyennan (eastern) and Rocky Cape Group (western) recycled sediments have a different signature. The MUC source is characterised by low-Ti chromites. The Crimson Creek Formation source contains high-Ti Chromite, euhedral zircon and minor recycled metasedimentary components. The Cambrian felsic volcanism contribute euhedral zircon. All the basaltic sources are capable of producing high oxide components to the heavy mineral suite but these are only recognisable in unaltered immature sandstones and volcaniclastic units.

Yolande Cycle sandstones are dominated by a well mixed component of MUC and recycled metasediments. They have high MUC chromite, high rounded zircon content and high tourmaline. The Yolande Cycle sandstones are locally mixed in variable proportion with a felsic volcanic component, interpreted here as CVC derived. Towards the top of the Yolande Cycle, the MUC component becomes less significant in the south (Sticht Range Formation, Mt Jukes Road, Boco Road but not Southwell Subgroup). At this level the recycled meta-sedimentary component is dominant except in the Huskisson area where there is a major influx of chromite from the Crimson Creek Formation.

The Tyndall Group and correlates (Tyndall Cycle) continue this trend with no evidence of a contribution from MUC and the sediments dominated by a oxide rich source interpreted here as the result of active tholeiitic volcanism related to the Henty Dyke Swarm. During the Denison Cycle, along the western margin, Selley (1997) recognised an increasing contribution from a local western source (Crimson Creek Formation, Success Creek Group and MUC). The perfect example of this is the sample of Westcott Argillite taken from the Pieman Road very close to the boundary fault. This sample (94/22) lies very

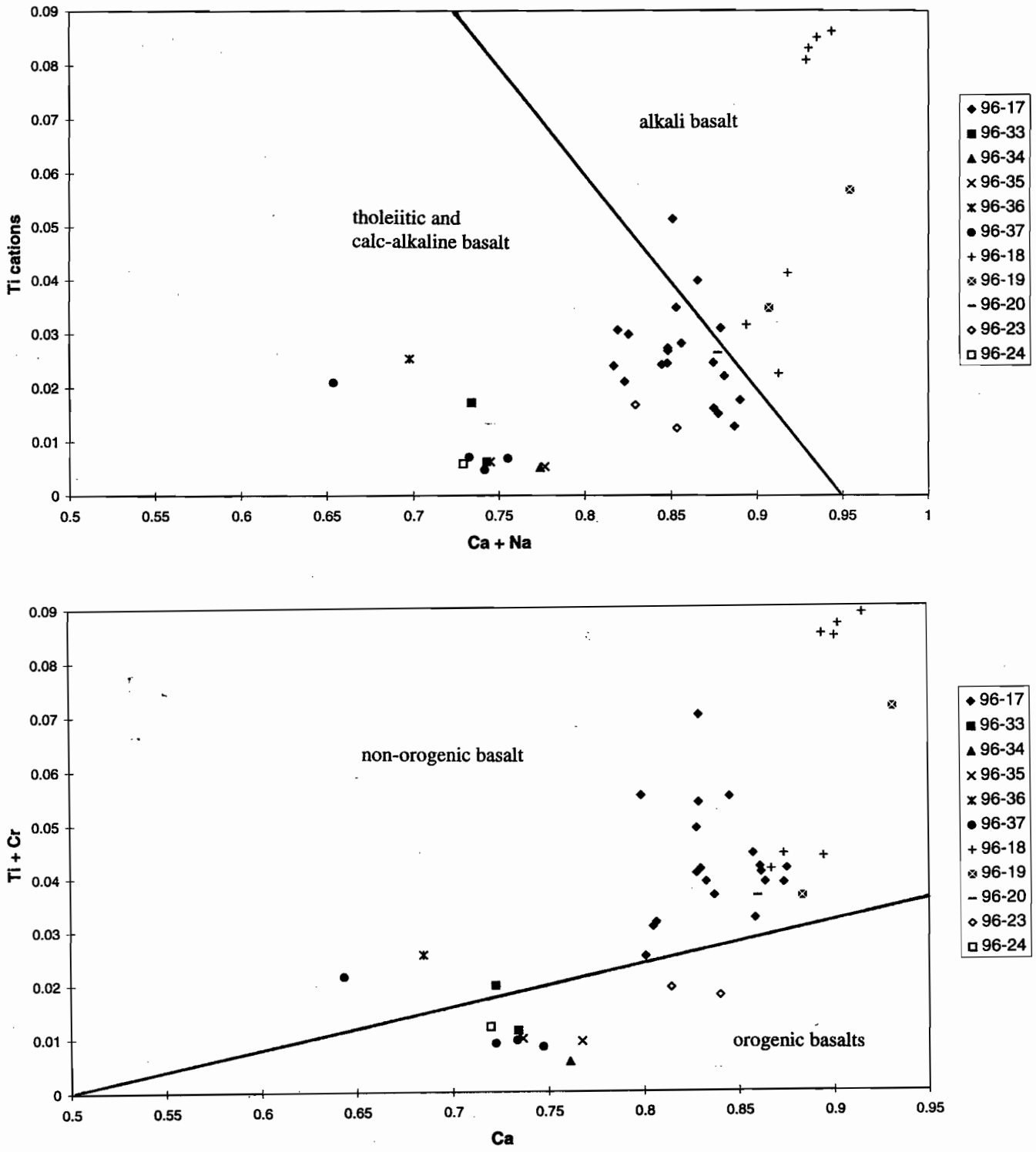

Figure 19. Clinopyroxene compositions. Fields for tectonic interpretations are from Leterier et al. (1982)

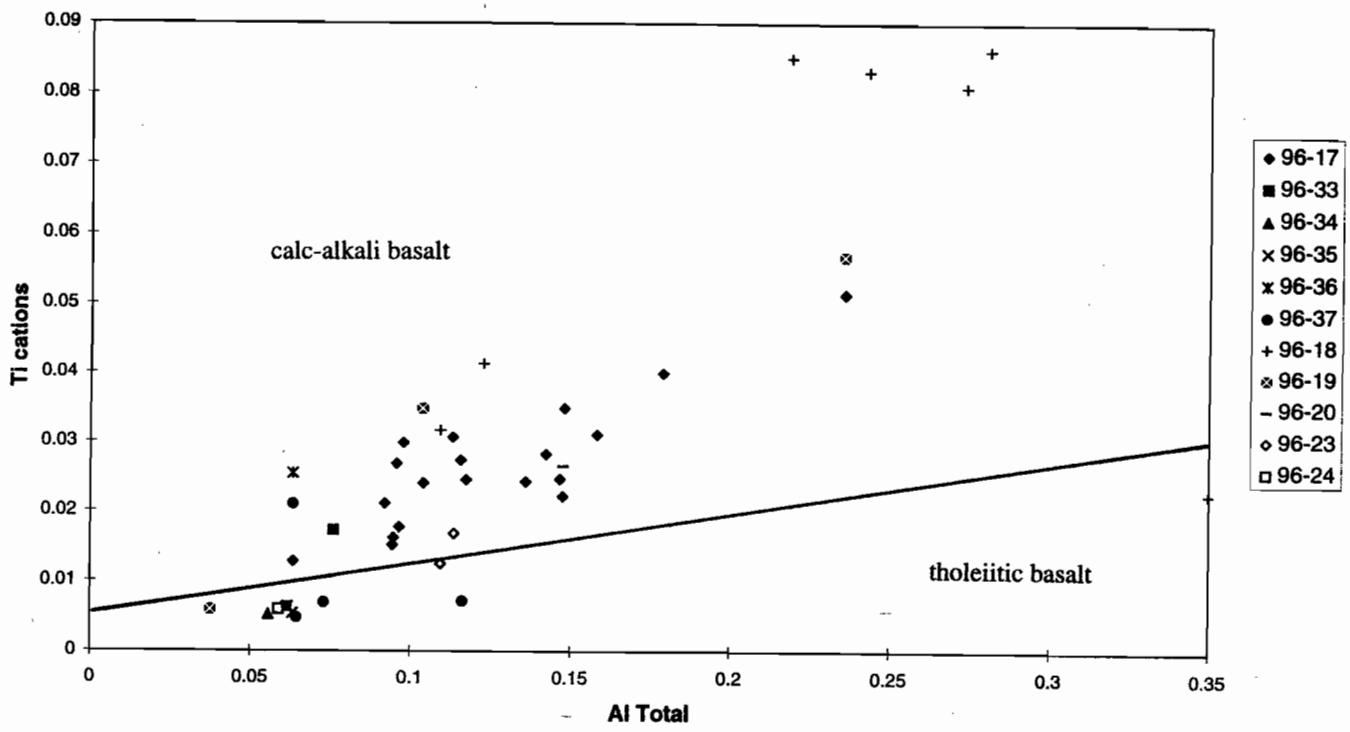

Figure 19 cont. Clinopyroxene compositions. Fields for tectonic interpretations are from Leterier et al. (1982)

close to the Crimson Creek sample (94/24) in most plots. It has very high TiO_2 and low chromite with minor FeTi oxides.

The provenance changes outlined here reflect similar changes in the sedimentology (Bull & Selley this volume). The older part of the Yolande Cycle is a deep water turbidite sequence with a well mixed composition. No local fluctuations are recorded over the 150 km of strike length investigated here (includes the Fossey "trough") except the influx of local volcanic components. The implication is that this is a large deep basin with no local basin margins. This well mixed sedimentary assemblage did not extend as far as Christmas Hills in the northwest where only tholeiitic sources were available.

In contrast towards the top of Yolande Cycle there is evidence of rapid variations in source type, for example Husskisson Group, Sticht Range Formation and Southwell Subgroup.

A new volcanic cycle dominated parts of the basin east of the Rosebery Fault through the Tyndall Cycle but west of the Rosebery fault this biostratigraphic interval is missing or perhaps represented by black shales.

The complex local variations continue in the Denison Cycle with a contrast between an axial fan facies, Stitt Quartzite dominated by a recycled metasedimentary rocks, and locally derived mass flows from a western margin (conglomerates in the Dundas area and Westcott Argillite).

It is significant that the major change in basin geometry during the Yolande Cycle occurs close to the stratigraphic interval that hosts the major massive sulphide deposits. The major basaltic elements of the Mount Read Volcanics are also concentrated in upper Yolande Cycle and lower Tyndall Cycle, perhaps reflecting the thermal maximum in the area.

Acknowledgements

This project could not have proceeded without the heavy mineral separations carried out by Nilah Hliang. Andrew McNeill, Nathan Duhig and Rohan

Hine have contributed extensively to the point counting and microprobe analyses. Their help, often at critical times, was much appreciated. The microprobe analyses were carried out with the help of Wis Jablonski using the Cameca SX-50 in the Central Science Laboratory, University of Tasmania.

References

Black LP 1994. The significance of current and proposed SHRIMP dating. MRT report 1994/16, 20pp.

Blackney PCJ 1982. The petrology and conditions of metamorphism of the Fitzmaurice Bay to Stokes Point area, King Island. BSc (Hons) Univ. Tas. (unpubl.)

Blissett & Gulline (1962). Zeehan geological atlas, 1:63,360 series, Tasmanian Dept Mines

Brown AV, 1986. Geology of Dundas-Mt Lindsay-Mt Youngbuck Region. Geol. Surv. Tasm. Bulletin 62.

Brown AV 1989. Eo-Cambrian-Cambrian. in Burrett CF & Martin EL (eds). Geology and Mineral resources of Tasmania. Special Publication Geological Society of Australia 15, 47-83.

Brown AV, Findlay RH, Goscombe BD, McClenaghan MP & Seymour DB 1994. Zeehan geological atlas, 1:50,000 series, Tasmanian Dept Mines.

Burns KL 1964. Devonport Tasmania. Tasm Dept Mines Geol. Atlas 1;63,360 Explanatory Report, 266p.

Corbett KD & McNeill AW 1986. Mt Read Project. Map 2. Geology of Rosebery -Mt Block area. 1:25,000. Dept. Mines Tasm.

Greenhill P 1995.The geological setting and mineralisation of the Cuni Cu/Ni deposits. BSc Hons. Univ.Tas. thesis (unpubl.).

Hashimoto M, Saito Y & Kashima N 1981. Relic clinopyroxenes and metamorphism of the Leven Hills district, Tasmania. Pap. Proc. Royal Soc Tasmania 115, 173-180.

Henningsen D 1967. Crushing of sedimentary rock samples and its effect on shape and number of heavy minerals. Sedimentology 8, 253-255.

Henty D J & Guidotti C V 1985. Tourmaline as a petrogenetic indicator-mineral: an example from the staurolite grade metapelites of NW Maine. Am. Mineral.

Ireland TR, Fanning CM, Flottman T, Weaver SD, Bradshaw JD & Adams C 1995. Continental structure of the Pacific margin of Gondwana: detrital zircon ages from the Lachlan Fold Belt, Kanmantoo Group and Adelaide Fold Belt of Australia, and Victoria Land correlatives. VII International Symposium on Antarctic Earth Sciences Siena Abstracts p202.

Jago JB 1971. An abrupt Upper Middle Cambrian faunal change, Christmas Hills, Tasmania, Australia. Pap. Proc Roy Soc Tasm 105, 83-85.

Leterier J, Maury RC, Thonon P, Girard D & Marschal M 1982. Clinopyroxene composition as a method of identification of the magmatic affinities of paleo-volcanic series. Earth Planetary Sc. Letters 59, 139-154.

McKibben J A J 1993. The geology and geochemistry of the North Pinnacles Ridge, western Tasmania. BSc Hons. Thesis Uni. Tas. (unpubl.).

McNeill AW 1986. BSc Hons. Thesis Uni. Tas. (unpubl.).

Muir RJ, Ireland TR, Weaver SD & Bradshaw JD 1994. Ion microprobe U-Pb zircon geochronology og granitic magmatism in the Western Province of the South Island, New Zealand. Chemical geology (isotope geoscience section) 113, 171-189.

Perkins C & Walshe JL 1993. Geochronology of the Mount Read Volcanics, Tasmania, Australia. Economic Geology 88, 1176-1197.

Selley D 1997. Structure and sedimentology of the Dundas area, western Tasmania. PhD Thesis Uni. Tas. (unpubl.).

Seymour DB & Calver CR 1995. Explanatory notes for the time-space diagram and stratotectonic elements map of Tasmania. Tasmania Geological Survey Record 1995/01.

Scott DJ & Gauthier G 1996. Comparison of TIMS(U-Pb) and laser ablation microprobe ICP-MS(Pb) techniques for age determination of detrital zircons from the Paleoproterozoic metasedimentary rocks from northeastern Laurentia, Canada, with tectonic implications. Chemical Geology 131, 127-142.

Sproule RA 1994. Stratigraphy and geochemistry of the Dial Range Trough, NW Tasmania. BSc Hons. Thesis Uni. Tas. (unpubl.).

Taylor B E & Slack J F 1984. Tourmalines from Appalachian-Caledonian massive sulfide deposits: Textural, chemical and isotopic relationships. Economic Geology 79, 1703-1726.

Turner N.J., Black L.P. and Kamperman M. 1995. Pre-Middle Cambrian stratigraphy, orogenesis and geochronology in western Tasmania. Geol Soc Aust Abstr 39, 51-56.

Lithogeochemistry

R.F. Berry, D. Selley, M.J. White and S. Meffre
CODES Special Research Centre, Geology Department, University of Tasmania

Abstract

The Mt Read Volcanics have been subdivided into three depositional cycles primarily on the bases of bio- and litho-stratigraphic techniques (Corbett et al., this report). In addition to these techniques, the whole rock chemistry of the sedimentary rocks of the Mt Read Volcanics can be employed as an effective tool in resolving some of the more difficult lithostratigraphic problems as well as discriminating between the various sources terrains which were actively supply detritus during basin development. Examination of temporal and spatial variations in source characteristics provided insight into basin geometry and evolution.

The investigation demonstrated that whole rock chemistry is very useful in distinguishing the Tyndall Group volcaniclastics. The basaltic component of source is well defined in the less mature sandstones but this signal is lost in the mature sandstones. Both immature sandstones and mudstones provide evidence of the changing nature of the basin and of the difference between the western margin and more central parts of the basin.

Introduction

A major aim of the combined ARC-AMIRA project is to define the basin geometry for the Mount Read Volcanics. A structural model was put forward in P291 which is being used as a template for this analysis. The project has looked at whole rock chemistry as a guide to what sources are available to the basin at each stage in its genesis.

The results discussed below are heavily dependent on work that is formally outside the AMIRA project but made available to the AMIRA sponsors in a pre-publication form. The geochemistry of the Tyndall Group reported here is from White (1996) and outside the AMIRA project. The geochemistry of rocks from the Dundas area (Dundas Group and correlates, Crimson Creek Formation and the probable Precambrian rocks of the "Dundas inlier"), Stitt Quartzite and Oonah Formation samples, and arguments about the distinction of the Crimson Creek Formation from Dundas Group sedimentary rocks, are from Selley (1996) which was formally outside the AMIRA project. Analyses from the Que River Shale, Eastern Quartz-phyric sequence and many volcanic rocks were made available to us on the basis that rights of first publication were retained by the people concerned. Many of the ideas summarised here were developed in extensive discussion with Joe Stolz and Tony Crawford. The results here could not have been achieved without this discussion. The AMIRA project has generated the data from the Animal Creek greywacke, CVC sandstones, Yolande River Group, Tyndall correlates and northern Dundas Group. The major contribution of the P291a is to bring the diverse data sources together to achieve a basin-wide view of the sedimentary rock geochemistry. Seventy rocks were analysed specifically for this project.

In the following sections groups of samples are discussed in terms the proposed three-fold stratigraphic sub-division of the Mt Read volcanics: ie. Yolande Cycle, Tyndall Cycle and Denison Cycle. Within each cycle samples are separated on the bases of grainsize (ie. sandstone and mudstone chemistries

will be discussed separately) and whether or not sedimentary rocks were deposited from coevally erupted volcanic debris or reworked from pre-existing volcanic packages. In other words, texturally mature volcanogenic sedimentary rocks are distinguished from immature, rapidly (re-) deposited volcaniclastic units.

The analysis of mudstones has not been a part of the AMIRA project. However it is useful to report on work being carried on by graduate students at CODES. This is principally the work of David Selley but includes analyses from other graduate student theses (White 1996, Sinclair 1994) and a few samples from Stolz (pers. comm.). A total of 90 mudstone analyses were available for consideration.

The work of Selley (1996) demonstrated that spider diagrams can usefully be applied to the understanding of sandstones in western Tasmania. Following his example we will discuss all the coarse-grained rocks here in these terms. The normalisation factors that are used here are the average Post Archaean Australia Shale (PAAS) of Taylor & McClennan (1985). These factors have a weak calc-alkaline signature compared to commonly used MORB normalisation factors. Thus tholeiites have positive Ti, P and Nb anomalies on these diagrams. It should also be noted that PAAS represents an average granodioritic composition and as such, spider diagram patterns which have a positive slope to the right (ie. towards relatively enriched compatible element abundances) grossly reflect samples with mafic characteristics, whereas those which have a negative slope to the right are indicative of more felsic compositions.

Yolande Cycle

Sandstones

Sticht Range Formation (SRF) — The SRF comprises the eastern-most exposures of Yolande Cycle siliciclastics in the Dundas Trough. It involves a narrow belt of rocks which flank the western margin of the Tyennan nucleus and extends northward from near the Lyell Highway to Lake Mackingtosh.

The high degree of compositional maturity characterised by these sandstones and their consequential elevated SiO_2 values (average SiO2 87%) results in an overall depletion of trace element abundances relative to PAAS (Fig. 1). Trace elements are housed predominantly in heavy minerals, with concentrations of ultrastable minerals such as zircon providing the principal control on the shape of the patterns. Troughs at P, Ti and low absolute concentrations of ferromagnesian elements are highlighted by relative enrichment of light rare earth elements (LREE), Zr and Y, all of which are likely to be contained in zircon grains. Although chromite grains (derived from an MUC source) have been identified in heavy mineral separates of SRF sandstones, their low abundance relative to zircon and quartz means that any positive Cr-signature is masked.

On the basis of whole rock chemistry, SRF is very difficult to distinguish from other compositionally mature sandstones such as those from the Precambrian Oonah Formation and their probable correlates contained in the "Dundas inlier" (Fig. 2). The only visible difference is the lower Ba in the latter rocks. A remarkable similarity is also shown between SRF and Stitt Quartzite sandstones (Fig. 22), a feature which will be discussed further below. The extremely close similarity between the chemical signature of SRF sandstones and those of the Oonah Formation and correlates is considered to reflect a lack of basaltic or felsic volcanic source component and a predominance of detrital input from compositionally mature "basement" sources.

Animal Creek Greywacke (ACG) — Samples of Animal Creek Greywacke (including the Farrell slates) were collected from various localities in the Que–Hellyer region between the type section near the Murchison Highway and the Cradle Mountain link road. Samples are micaceous quartz sandstones, which are distinguished petrographically from SRF sandstones by a lower degree of compositional maturity and an abundance of "matrix" (much of which is probably diagenetic) and lithic fragments. Additional sandstone samples from the Farrell Slates, collected north of Tullah at the Mackingtosh Dam spillway, are also discussed here.

PAAS normalised patterns for ACG sandstones are considerably less 'spiky' compared to SRF, with lower Zr, Y and weaker negative, or in some cases, no P and Nb anomalies (Fig. 3). This change in pattern reflects in part, at least, the increased "matrix" and/or lithic component relative to zircon in ACG

sandstones. A broader range of trace elements can therefore be incorporated within ACG compared to SRF, not just those which are preferentially housed in zircon grains. Of the compatible elements, Sc, Ni and Cr are markedly enriched in ACG relative to SRF, indicating a significant detrital input from a basaltic source. Note also that Cr/Zr values are greatly elevated in ACG sandstones, a feature which is interpreted to reflect the increased contribution from the basaltic source relative to a compositionally mature basement precursor. The trough at Ti and to some extent Nb, coupled with the elevated absolute abundances of Ni and Cr indicate an arc-type signature for the basaltic precursor. This chemistry is consistent with derivation from the mafic-ultramafic complexes (MUC), an interpretation which is supported by detrital chromite compositions (see Berry et al, this report). The source region of this rock type is substantially different from the Sticht Range Formation.

Other Yolande Cycle micaceous sandstones

Other Yolande Cycle micaceous sandstones are shown in Fig. 4. Those samples from Yolande River Sequence (YRS) were collected west of the Murchison Highway. The remainding samples occupy stratigraphic positions which are demonstrably younger than the ACG. The Merton Road sample was collected west of the Huskisson River, whereas Murrays Road Greywacke and Southwell Subgroup samples were collected from the Que–Hellyer region.

YRS sandstones and the sample from the Southwell Subgroup display comparable chemical signatures with ACG sandstones, suggesting a similar provenance. Diagnostic features of this signature include the trough at Ti coupled with elevated Ni and Cr, which indicate detrital input from the MUC.

The Murrays Road Greywacke (MRG) samples show an overall positive slope towards the right of the pattern, consistent with mixing of quartz-mica-rich and basaltic sources. Note however that the lack of a strong Zr spike implies that a compositionally mature basement-derived component is becoming less significant in these rocks. The very high Sc and V values (in excess of PAAS) supports the interpretation of basaltic input. The patterns can be distinguished from that characterised by ACG sandstones however, via higher P concentration relative to Zr and LREE, the trough at Zr and the moderate Ni and Cr abundances. As MUC-derived chromite grains have been identified within this package of rocks however (Berry et al., this report), an MUC signature should still be apparent. The MRG pattern cannot solely be attributable to masking of an MUC signature through dilution from a felsic volcanic and/or compositionally mature basement source as Sc and V concentration are still very high, whereas more compatible element abundances such as Th, LREE and Zr are lower than, or comparable with those of ACG sandstones. One interpretation of this signature is mixing of an MUC and tholeiitic (ie. P-, Nb- and Ti-enriched) volcanic source. This would explain the lack of negative Nb, P and strongly negative Ti anomalies displayed by most other Yolande Cycle micaceous sandstones. Tholeiitic detritus derived from the Crimson Creek Formation is the most plausible origin for this additional mafic component.

An alternative explanation for the 'basaltic signature' might be an additional detrital component sourced from a P- and Ti-enriched (relative to MUC) intermediate to mafic volcanic source such as the Que–Hellyer Volcanics. The low incompatible element abundances indicate that the LREE-enriched shoshonitic magmatic suite (eg. Que–Hellyer hangingwall basalts: Crawford et al., 1992) is inconsistent with this conclusion. Possible source rocks could include the more mafic members of Suite I of Crawford et al. (op cit.) (eg. Que–Hellyer footwall andesites and basalts). The appearance of a basaltic signature in MRG sandstones which is not easily attributable to a single "basement" source (eg. MUC) may imply intrabasinal reworking of Cambrian strata.

The Merton Road sample has higher abundances of compatible elements (ie. Th, LREE) and lower abundances of ferromagnesian elements relative to ACG and the remaining Yolande Cycle micaceous sandstones. This pattern is interpreted to indicate that a basaltic component is either lacking or very weak in the Merton road sample. Furthermore, detrital chromite grains were not identified in this Merton Road sample (Berry et al., this report), providing support for this interpretation.

Halls Rivulet Canal sandstones — The sandstones from the Halls Rivulet Canal (Nunn 1995), sampled immediately north of the North Henty Fault near Howards Road, have a range of spider patterns (Fig.

5). At one end of the spectrum, patterns have a 'spiky' character with marked troughs at P and Ti, elevated LREE and depleted ferromagnesian elements (eg. 131358 and 131387). The chemical signature of these sandstones compares best with those of the SRF and compositionally mature "basement" units. The enrichment of incompatible elements (notably Th) with respect to Zr in the more "felsic" Halls Rivulet Canal samples is the main distinguishing feature from "compositionally mature" sandstones and can be explained either by a greater lithic fragment/primary clay component or an additional felsic volcanic component in the former. A pronounced trough at Nb (relative to Th and LREE) may be considered as evidence for an arc-type felsic volcanic input. Patterns of the remaining samples are interpreted to reflect various degrees of mixing with a basaltic source as indicated by progressively increasing Ti and ferromagnesian element concentrations coupled with lower abundances of Th and LREE. Sample 131376 has a smooth positive slope to the right and probably contains the largest component of basaltic detritus. This pattern compares most favourably with those of the Murrays Road Greywacke, although P/Ti is noticeably higher in the latter. Although MUC chromites have been identified in the Halls Rivulet Canal sandstones (Nunn 1995), the progressive increase of Ti with ferromagnesian elements tends to suggest that MUC detritus cannot account entirely for the basaltic signature. Low P/Ti values coupled with a very slight enrichment of Nb relative to LREE indicate that the Crimson Creek Formation tholeiitic volcanics have provided some detrital input.

'Lower' Dundas Group sandstones — 'Lower' Dundas Group sandstones were all collected from the Dundas region and represent the western-most exposed units from the Yolande Cycle. Samples 835 and 839 represent lithologies contained in the type section along the Dundas River, whereas D94, RL1 and 958 were collected from units situated along the eastern and southern flanks of the Serpentine Hill MUC. Sample 858 represents the eastern-most Yolande Cycle lithologies in the Dundas region and was collected from the Ring River approximately 1km west of Bonnie Dundee Mine.

Samples 835, 839 and 858 are biostratigraphic equivalents of the Southwell Subgroup (thus also Murrays Road Greywacke). Samples D94, RL1 and 958 represent an older part of the sequence (correlates of the Red Lead Conglomerate) and predate deposition of the Que River Shale in the Que–Hellyer region. These latter sandstones are biostratigraphic correlates of the ?upper part of the Animal Creek Greywacke.

PAAS normalised spider diagrams display relatively smooth patterns, with subtle to moderate positive slopes to the right and only minor variation between samples (Fig. 6). This signature is akin to the Murrays Road Greywacke and the most basaltic end-member of the Halls Rivulet Canal sandstones. As discussed in the preceding sections, this signature is characteristic of a mixed basaltic-mature "basement" and/or felsic volcanic source. The presence of MUC-derived detritus has been identified in each of the lithological units represented in the form of low-Ti chromites (Selley, 1996). In terms of rock whole geochemistry, the MUC signature is only subtly shown via slightly depleted Zr, Ti and elevated Sc, Ni and Cr. The stratigraphically youngest group of samples generally have the highest abundances of compatible elements, Zr and lowest Sc and reflect the greatest contamination of the MUC signature by compositionally mature "basement" and/or felsic volcanic sources. Of particular interest is the one sample from the oldest portion of the Dundas Group (958) which shows marked peaks at Nb, P, Ti and Sc. This signature is diagnostic of input from the Crimson Creek Formation tholeiitic rocks and has completely masked evidence of MUC derivation. It should be noted that no other Yolande Cycle sandstone included in this data-base records a dominant contribution from the Crimson Creek Formation.

Mudstones

'Lower' Dundas Group mudstones — 'Lower' Dundas Group mudstone samples all come from the Dundas region and range in age from Undillan to Boomerangian. They represent biostratigraphic equivalents of the Que River Shale and Southwell Subgroup from the Que–Hellyer region. No biostratigraphic equivalents of older strata such as the Animal Creek Greywacke have been analysed.

As expected for mudstones which have accumulated slowly (compared to turbiditic sandstones) and include a significant detrital component derived from hemipelagic fall out, chemical signatures are

relatively flat (Fig. 7) and indicative of thorough source mixing (ie. of 'felsic' and 'mafic' sources). A subtle positive slope to the right indicates the presence of a mafic component, however the lack of distinctive trace element anomalies hampers confident identification of a particular source. Comparison with Yolande Cycle sandstones reveals a tightest correlation with the Murrays Road Greywacke (Fig. 4) which as mentioned above occupy a similar stratigraphic position. A small positive anomaly at P represents the most diagnostic feature of each of these two groups of rocks. Curiously, a fit with most 'lower' Dundas Group sandstones is not as close (Fig. 6). Very weak Nb and Ti peaks which accompany the stronger P peak in the mudstone tends to suggest that some of the mafic input at least is from a tholeiitic source. A similar pattern is shown by sample 958 from the 'lower' Dundas Group sandstones, which was interpreted above to indicate dilution of a dominant MUC component by detritus from the Crimson Creek Formation. Although the peak at P and moderate P/Ti values shown by some mudstones could be interpreted to indicate contribution from a P-enriched intrabasinal volcanic source (as was presented as an alternative explanation for the patterns shown by the Murrays Road Greywacke), the clear mixing of a tholeiitic and MUC source in the 'lower' Dundas Group sandstone sample 958 leads us to conclude that the latter explanation is more convincing.

Que River Shale — PAAS-normalised spider diagrams for the Que River Shale (Fig. 8) show a slightly more flat pattern than 'lower' Dundas Group mudstones, with a subtle sag in the middle of the pattern rather than a positive slope to the right. Slightly depleted Ti values are most likely attributable to an arc-type volcanic source rather than a compositionally mature basement source as P abundances are not also diminished (compare with Fig. 9). However, as Th, Nb and most LREE analyses are lacking, is it very difficult to accurately determine the nature of the volcanic component.

Volcaniclastic rocks

The volcaniclastic rocks of the Yolande Cycle are variable in composition but no link between stratigraphic position and chemical composition have been determined. The Suite I volcanic signature of Crawford et al. (1992) occurs in rocks throughout this subdivision. On a PAAS normalised diagram (Fig. 10) these rocks have strong negative anomalies for Ti and P and a weaker anomaly for Nb. All samples show high Th/Nb and a low Sc/Y, distinct from the Lynchford Member pattern (Tyndall Cycle: see below). A few samples show a very LREE depleted signature which we assume is related to crystal concentration during eruption and deposition. The compositions shown in Fig. 10 are from the CVC but similar patterns have been found in EQPS, White Spur Formation and Southwell Subgroup. If there is a chemical distinction between these units, it is subtle. The other compositions that are recorded within the Yolande Cycle are Suite III and Suite II lavas (Figs. 13 and 14 respectively) with their high P and LREE contents. The data shown here are from Crawford et al. (op cit.) and are from lavas, but these signatures are also recorded in related volcaniclastic rocks. Suite II and Suite III signatures are a feature of middle to upper Yolande Cycle.

Tyndall Cycle

We have no data for micaceous sandstones or "background" mudstones from the Tyndall Cycle. The sandstones from this unit are all immature volcaniclastic deposits , hence their chemistries provide information about their parental magmas rather than sedimentological mixing processes and source areas.

Tyndall Group volcaniclastic sandstones — The Tyndall Group includes a contribution from a distinct mafic source not recognised in other parts of the Mt Read stratigraphy. This component was most easily recognised in the Ti/Th ratio which was much higher than in any other unit. This component was best reflected in the Lynchford Member from the base of the Tyndall Group. All analyses of Tyndall Group samples are shown on normalised (to PAAS) diagrams in Figs. 11a and 11b. Samples of the Lynchford Member represent the stratigraphically lowest portion of the Tyndall Group and show an overall incompatible element depleted signature (positive slope to the right) indicating a mafic

signature (Fig. 11a). There is no negative Nb, P or Ti anomaly in contrast to most volcaniclastic rocks in the Mt Read Volcanics. In addition there are two other unusual features. The Th is very low, less than Nb in normalised terms and the Sc is extremely high. These features overall form a very distinctive signature for lower Tyndall Group rocks. The extreme Ti/Th values reported for Lynchford Member in the previous report reflects the very low Th combined with the lack of a negative Ti anomaly. The pattern revealed here is typical of a tholeiitic to weakly calc-alkaline basaltic source. The sample 78300-JM, from the magnetic sandstone package north and west of Pinnacles, fits very closely with the Lynchford Member samples supporting the correlation of this package with the Tyndall Group (McKibben 1993).

This signature is not as strong in younger Tyndall Group rocks which have been sourced from more felsic magmas. These rocks still have a distinctive positive slope to the right in the PAAS normalised spidergram (Fig. 11b) and lack a Nb depletion. Some of the samples, 4 of 15, have a low Th (<Nb in normalised terms) and the Sc/Y is fairly high for felsic rocks. However the signature is not as distinctive as the Lynchford Member. Troughs at P and Ti highlighted by the peak developed at Zr, coupled with the progressive depletion in ferro-magnesian elements results in a pattern which resembles those of Yolande Cycle volcaniclastic rocks.

The distinctive composition of the Lynchford Member indicates a discrete new source of basaltic material with a transitional tholeiitic signature. A likely composition in age terms is the high Ti tholeiitic basaltic andesites from the Henty Fault wedge analysed by Poltock (1992) . These are shown in Fig 12a. Other Suite IV volcanics (Henty dykes) have been reported by Crawford et al 1992 (Fig 12b). The Suite IV Henty dykes and related Henty Fault wedge volcanics are the most likely source for the Lynchford Member.

Other volcaniclastic units of the Tyndall Cycle — There is large database of volcanic and volcaniclastic rocks from the Mt Read Volcanics. We considered several hundred analyses of CVC, Yolande River Group, Eastern Quartz -phyric volcanics and White Spur Formation. These rocks do not have the signature reported above for the Tyndall Group (compare Fig. 10). The Suite III and Suite II lavas of Crawford et al (1992) are distinctive from the suite I compositions. The Que–Hellyer hangingwall volcanics have the distinctive high P and LREE Suite III signature (Fig. 13) while andesites from the Anthony Road (Suite II) have a weaker signature but of a similar type (Fig. 14). This chemical signature is common in upper Yolande Cycle volcanic rocks and appears to be a precursor to the Tyndall "event". The chemical variation reported from Sock Creek (Crawford et al 1992) is apparently the start of the transition to tholeiitic composition of which the Tyndall Group represents a further step.

Since the Tyndall Group can be distinguished from other volcanic rocks in the Mt Read Volcanics, samples were collected from potential Tyndall Group correlates and the chemistry was compared with the signature defined above. The other volcanic horizons tested were:

1. The Native Track Tier is a biostratigraphic correlate of Tyndall Group. Andesitic volcaniclastics were sampled from near to the fossil locations on which this correlation is based. The samples from this area show the normal Tyndall Group signature supporting the biostratigraphic correlation (Fig. 15)
2. The Winterbrook area was mapped as Tyndall Group by Pemberton & Vicary (1989). In this area are a number of basic volcanic units. Samples from this area also show a typical Tyndall Group signature (Fig. 16)
3. The latest Mines Department 1:250,000 map has indicated that Tyndall Group is exposed along the Yolande River west of the Murchison Highway. Samples from this area were collected and also show compositions typical of the Lynchford member at the base of the Tyndall Group (Fig. 17).
4. The Radford Creek Formation is a biostratigraphic correlate of the Tyndall Group. The Kerrison Volcanics is slightly lower in the stratigraphy but previous analyses by Sproule (1994) indicated that this area also had the positive slope to the right trace element pattern of the Tyndall Group (Figure 18).

The Sprent Formation occurs within the Tyndall Cycle but is more texturally mature than typical Tyndall Group volcaniclastics. It contains

reworked volcanic detritus and hence may not accurately reflect the composition of coeval magmatism. The PAAS-normalised spider diagram in Figure 18 shows the Sprent Formation sample as having marked positive P and Ti anomalies as well as elevated abundances of Ni and Cr. This pattern is suggestive of a more tholeiitic source than typical of Tyndall Group volcaniclastics but is compatible with the Crimson Creek Formation source signature identified in Denison Cycle siliciclastics from the Dundas Trough (see next section). Thus in the Dial Range Trough the swing to more tholeiitic compositions apparently occurred slightly earlier than in the Dundas Trough.

5. The Lobster Creek intrusives in the Dial Range, intrude the Cateena Group. Sproule (1994) argued these intrusives were comagmatic with the Radford Creek Group. The composition of these intrusives is a very close match to the Lynchford Member (Fig. 19) and supports a lithological correlation.
6. The volcaniclastic sequence east of Strahan has basalt-andesite association for which no analyses are published. The petrography of these rocks was described by Stephen Cox in Baillie & Corbett (1985). Samples of the described rocks were made available by the Tasmanian Department of Mines. The analyses of these rocks and the spider diagram (Fig. 20) are in many respects similar to Lynchford Member compositions. They are unlike typical Suite I, II or III compositions. The weak negative Nb and zero Ti and P anomalies in PAAS normalised diagram are diagnostic. However, Th abundances are higher than the typically 'depleted' signature of the Lynchford Member and as such correlation is not as tight as other Tyndall Cycle rocks. Ni and Cr are higher than typical for other Tyndall Cycle correlates reflecting the relatively basaltic composition of these rocks.
7. The Dundas region has always been anomalous because of the absence of clearly definable Tyndall Group correlates despite fossil evidence that the sequence spans the correct age range for Tyndall Cycle. There are a number of discrete volcaniclastic units in the Dundas Group in the Dundas region. Amongst the samples analysed from this area, only samples 982 and D158 (both from the eastern part of the Dundas region) have any of the features of the Lynchford Member (Fig. 21). Sample 982 has a strong positive slope to the right, high Sc/Y and lacks a negative Ti anomaly. P, however, is very high, as are LREE abundances and there is a weak negative Nb anomaly. These features indicate a composition which is transitional between the shoshonitic association of Suite III and the parental magma of Lynchford Member. Sample D158 has a strong positive slope to the right, lacks a Nb or P anomaly, has a weak negative Ti anomaly but Sc/Y is low. This sample is like some Tyndall Cycle rocks. The similarity provides some support for considering this rock a Tyndall Cycle correlate.

Denison Cycle

We have not undertaken a basin-wide analysis of sedimentary rocks contained in the Denison Cycle. The majority of the data presented below involves that collected as part of David Selley's PhD program and are representative of lithologies from the western portions of the Dundas Trough. Two lithostratigraphic elements are considered here: the Stitt Quartzite and the 'upper' Dundas Group succession.

Sandstones

Stitt Quartzite — Four sandstone samples were collected at widely-spaced intervals from the belt of Stitt Quartzite which extends northward from the Farrell Rivulet to the Boco Road. These rocks represent the eastern-most samples analysed from the Denison Cycle. In terms of their lithology, the samples can be described as compositionally mature quartzose sandstones and as such are very difficult to distinguish on chemical basis from older mature sandstones such as the Sticht Range and Oonah Formations.

PAAS-normalised spider diagrams for the Stitt Quartzite are shown in Figure 22 and clearly display marked the troughs at P and Ti as well as depleted ferromagnesian trace element abundances relative to PAAS. As discussed in the Yolande Cycle section, this signature characterises sandstones of which the

principal detrital input is from a compositional mature basement source whereas contribution from basaltic or felsic volcanic sources is lacking. Comparison with Figs. 1 and 2 reveals the extremely close similarity of this signature with those of older compositionally mature sandstones. The only distinction of Stitt Quartzite from Sticht Range Formation that we have found is the larger component of chromite in the former. This greater contribution from an MUC source is not obvious from the trace element chemistries of the two units, primarily due to the dilution effects of quartz which results in very low absolute abundances of most trace elements (the exception being those elements preferentially housed in zircon).

'upper' Dundas Group sandstones — Sandstones analysed from the Dundas region range in age from Mindyallan to Idamean. Stratigraphically younger samples were collected in the Que River from a belt of rocks which we consider to lie within the footwall of the northern projection of the Rosebery Fault. These younger sandstones were interpreted by Selley (1996) to be correlates of the fossiliferous Higgins Creek strata and were tentatively included within the Iverian stage.

The chemistries of 'upper' Dundas sandstones from the Dundas region show little resemblance to those collected from the Stitt Quartzite to the east (Figs. 23a and 23b). Patterns show an overall positive slope to the right, which is punctuated in all but one sample by peaks at Nb and Ti. A marked positive anomaly is also shown for P in sandstones from the Dundas Group type section in the western part of the Dundas region (Fig. 23a). This signature is consistent with a significant contribution from a tholeiitic basaltic source and contrasts with moderately to strongly Ti-Nb-P-depleted signature of MUC-derived siliciclastics such as the Animal Creek Greywacke (compare with Fig. 3). Furthermore, most 'upper' Dundas Group sandstones do not have a distinct change in slope at V as seen in the Animal Creek Greywacke. Only one sample from the eastern part of the Dundas Group displays this latter pattern (Fig. 23b). It also has the lowest values of Ti, Nb and P, implying that tholeiitic input is volumetrically subordinate to an MUC-derived component. Microprobe analyses of detrital chromites contained in this sample confirms an MUC source component. It is noteworthy that this anomalous sample is the eastern-most 'upper' Dundas Group sandstone analysed from the Dundas region and that an MUC source signature is not recognisable from whole rock geochemistry in strata further to the west.

There are some similarities between the tholeiitic signature and Yolande Cycle sandstones from the Murrays Road Greywacke (compare Fig. 4), however Ti is not as 'enriched' and values of Ti/P and Ti/Sc are lower in the latter. Comparison with the geochemical patterns of potential tholeiitic source rocks reveals a strong correlation with the Crimson Creek Formation. PAAS-normalised spider diagrams for greywacke and mudstone correlates of the Crimson Creek Formation (Figs. 24a and 24b respectively: note the change in scale for Crimson Creek Formation sandstones) display a very uniform pattern characterised by strong peaks at Nb, Ti and a moderate peak at P. Although basalts from the Henty Fault wedge have a similar tholeiitic signature (Fig. 12), they lack the ubiquitous strong Nb peak which is present in 'upper' Dundas Group sandstones. Those 'upper' Dundas Group samples with elevated incompatible trace element abundances (Th, LREE) and Zr probably record a greater contribution from a compositionally mature basement and/or felsic volcanic source.

'Upper' Dundas Group sandstones from the Que River are chemically distinct from most further to the south in that they show evidence of contribution from both the Crimson Creek Formation and the MUC (Fig. 25: note the change in scale). Although they have the strong Nb and Ti peaks which characterise Crimson Creek Formation detritus, they also have the distinctive kink at V which results from markedly elevated Ni and Cr abundances. As demonstrated earlier, this latter pattern is distinctive of MUC input and is supported by the identification of MUC-derived chromites in these sandstones (Selley, 1996).

Mudstones

'Upper' Dundas Group mudstones — 'Upper' Dundas Group mudstones have fossil ages ranging up to Iverian and are all situated in the Dundas region.

Fossil ages for the oldest mudstones are not precisely constrained (upper Boomerangian to lower Mindyallan: Brown, 1986) and straddle the Tyndall Cycle–Denison Cycle boundary as defined by Corbett et al. (this report). If the older upper Boomerangian limit of the fossil age is accepted, two samples from the Dundas Group type section fall within the biostratigraphic range of the Tyndall Cycle. Although it is conceded that this may be the case, there is no chemical distinction between these mudstones and immediately overlying samples which are unequivocally of lower Denison Cycle age. In view of the age discrepancy of the oldest fossil and the chemical homogeneity of lower Denison Cycle mudstones from the type section, all 'upper' Dundas Group mudstones are discussed together below.

On the basis of their whole rock geochemistry mudstones can be broadly separated into two groups: a high Nb-P-Ti group (Fig. 26a) and another group that is somewhat depleted in these trace elements (Figs. 26b and 26c). Absolute Ti values are the most effective means of discriminating between these two groups of samples, whereas there is a degree of gradation (but no over-lap) in terms of Nb and P.

The high-Ti suite includes all "pre"-Iverian mudstones from the western portion of the Dundas region. Spider diagram patterns for these samples correlate strongly with 'upper' Dundas Group sandstones of similar age and geographic distribution. This tholeiitic chemical signature is consistent with significant detrital input from a Crimson Creek Formation source (compare with Fig. 24).

Mudstones included in the low-Ti suite represent Mindyallan to Idamean strata from central and eastern portions of the Dundas region (Fig. 26b) and Iverian strata from the type section in the west (Fig. 26c). Thus, in terms of geochemistry, it is not possible to correlate latest Middle and earliest Upper Cambrian mudstones from the western portions of the Dundas region with those to the east. This apparent inability to construct a coherent chemostratigraphy across the Dundas region during Denison Cycle times supports the similar conclusion based on 'upper' Dundas Group sandstone chemistry. Two of the mudstones from the eastern Dundas region have a slight trough at Ti and considerably higher Cr abundances than the high-Ti suite, indicating dilution of the Crimson Creek signature by MUC derived detritus.

Iverian mudstones stratigraphically overlie the high-Ti suite in the Dundas Group type section and reflect a transition from dominant Crimson Creek Formation input to that of a compositionally mature "basement" source. This is indicated by the zero to negative anomalies at P and Ti coupled with the trend towards lower of ferromagnesian trace element abundances.

Conclusions

Contribution of detritus from compositionally mature "basement" and/or felsic volcanic sources is evident from the chemistries of many Yolande Cycle rocks (particularly lower parts of this cycle) with elevated Zr abundances with respect to P and Ti. This component is dominant in sandstones of the Sticht Range Formation which have a geochemical signature that is indistinguishable from compositionally mature "basement" rocks. A simple monogenetic provenance is lacking throughout the central and western parts of the Dundas Trough however, where various degrees of mixing with one or more basaltic sources becomes important. In lower Yolande Cycle sandstones from the central parts of the Dundas Trough (Animal Creek Greywacke and ?Yolande River Sequence), this basaltic component is largely indicative of an MUC source signature characterised by depleted Ti, Nb and markedly elevated Ni and Cr. This signature locally extends up into biostratigraphic correlates of the Southwell Subgroup, however rocks of this age generally show a more complex mixed basaltic provenance. P-enriched sandstones from the Murrays Road Greywacke have chemistries suggestive of input from either a tholeiitic basaltic source or intrabasinally-derived Mt Read volcanic source. Source mixing is most pronounced in 'lower' Dundas Group sandstones and mudstones from the western margin of the Dundas Trough which have flatter PAAS-normalised patterns and localised enrichment of Nb, P and Ti indicative of dominant input from the Crimson Creek Formation.

The Tyndall Group has a distinctive source composition which has contributed to the magnetic susceptibility of this unit. This composition is best reflected in the Lynchford Member and reflects an andesitic character with a tholeiitic incompatible element pattern. The closest match to this pattern in

western Tasmania is the Henty dykes and the basalts of the Henty Fault wedge. The major contribution of whole rock geochemistry to this project has been the recognition of a distinctive Tyndall Group chemistry in the volcaniclastic rocks which has aided the lithostratigraphic correlation across the basin.

Although the geographic distribution of Denison Cycle data is limited to western parts of the Dundas Trough, considerable variation in provenance characteristics have been recognised. The compositionally mature signature of the Stitt Quartzite is completely absent in rocks from the type section of the Dundas Group. This lack of lateral chemostratigraphic correlation in Denison Cycle times provides support for the conclusion of Bull (1995) that the Stitt Quartzite represents an axial graben facies and has no direct lithostratigraphic correlate to the west. Furthermore, variation in the composition of 'upper' Dundas Group rocks indicates provenance contrasts between those contained within the type section and biostratigraphic correlates immediately to the east. Specifically, Idamean and younger Denison Cycle rocks from the Dundas Group type section have a very significant contribution from the Crimson Creek Formation, whereas rocks to the east show various degrees of contamination from MUC sources. The Crimson Creek Formation signature of the Dundas Group extends down to Yolande Cycle times and is characteristic of western Dundas Trough strata at least until the lower Iverian. Iverian sandstones from the Que River maintain a mixed Crimson Creek-MUC signature, however biostratigraphic correlates from the Dundas region have progressively higher contributions from a compositionally mature "basement" source. This latter signature heralds the rapid influx of "basement" derived detritus which constitutes much of the Late Cambrian–early Ordovician Misery Hill and Zeehan Conglomerates.

References

Baillie PW & Corbett KD 1985. Geological Survey explanatory report Strahan 1:50,000 sheet. Department of Mines, Tasmania 76 pp.

Brown AV 1986. Geology of the Dundas–Mt Lindsay–Mt Youngbuck region. Geological Survey Bulletin 62. Department of Mines, Tasmania 221pp.

Bull SW 1995. Second report: Sedimentology of the Dundas Group and correlates with reference to a possible syn-depositional growth fault west of Rosebery. AMIRA Project P.291A Third Report 35–44.

Crawford AJ, Corbett KD & Everard JL 1992. Geochemistry of Cambrian volcanic-hosted massive-sulfide-rich Mount Read Volcanics, Tasmania, and some tectonic implications. Econ Geol. 87, 597–619.

McKibben J A J 1993. The geology and geochemistry of the North Pinnacles Ridge, western Tasmania. BSc Hons. thesis (unpubl.).

Nunn T 1995. Geology of the Hall Rivulet Canal, western Tasmania. BSc Hons. thesis Univ Tas (Unpubl.)

Pemberton J & Vicary MJ 1989. Geology of the Winterbrook Moina area. Mt Read Project 1:25000 map 9. Tasmania Dept Mines, Hobart

Poltock R 1992. Geology of the Henty Fault wedge, western Tasmania. M Econ Geol Thesis, Univ Tasm (unpubl.) 76pp.

Selley D 1996. Structure and sedimentology of the Dundas Group, western Tasmania. PhD, Univ. Tas. (unpubl.).

Sinclair BJ 1994. Geology and geochemistry of the Que River Shale, western Tasmania. Hons Thesis University of Tasmania (unpubl).

Sproule RA 1994. Stratigraphy and geochemistry of the Dial Range Trough, NW Tasmania. BSc Hons. Thesis Uni. Tas. (unpubl.).

Taylor SR & McClennan SM 1985. The continental crust: its composition and evolution. Blackwell Sci. Pub. Oxford 312pp.

White M.J. 1996. Volcanic facies analysis of the Cambrian Tyndall Group, Mount Read volcanics, western Tasmania. PhD, Univ. Tas. (unpubl.).

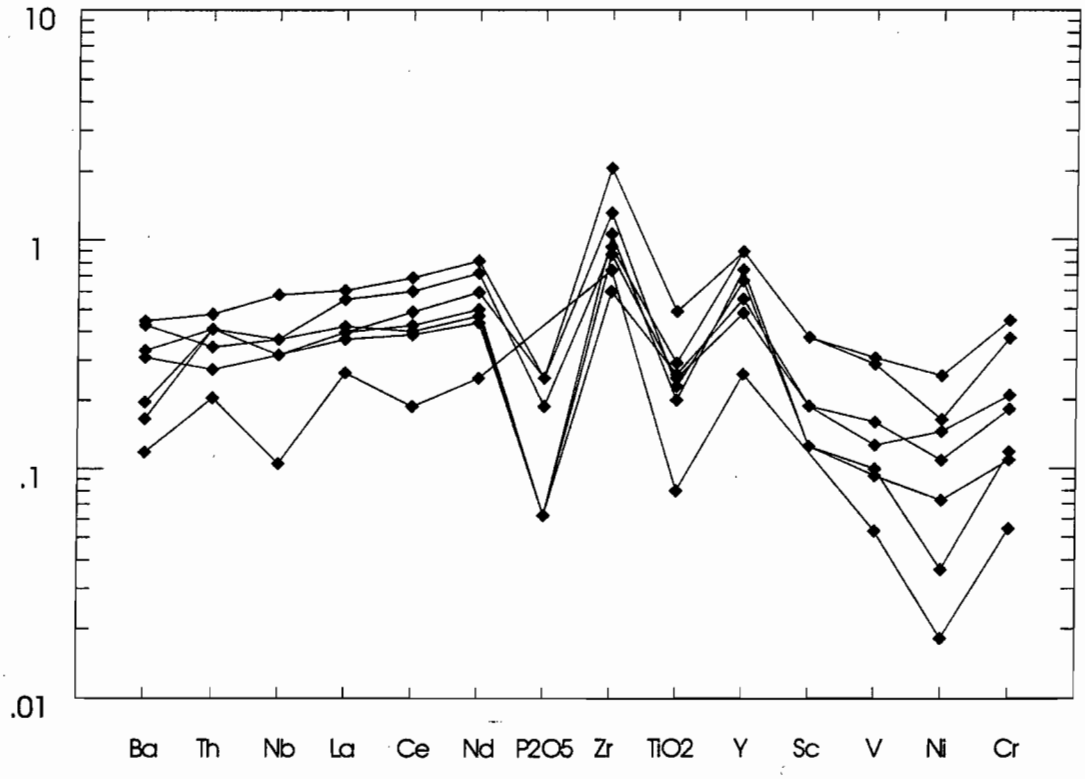

Fig. 1. Spidergrams normalised to Post-Archean Australia shales (PAAS, Taylor & McClennan 1985). Sticht Range Formation sandstone.

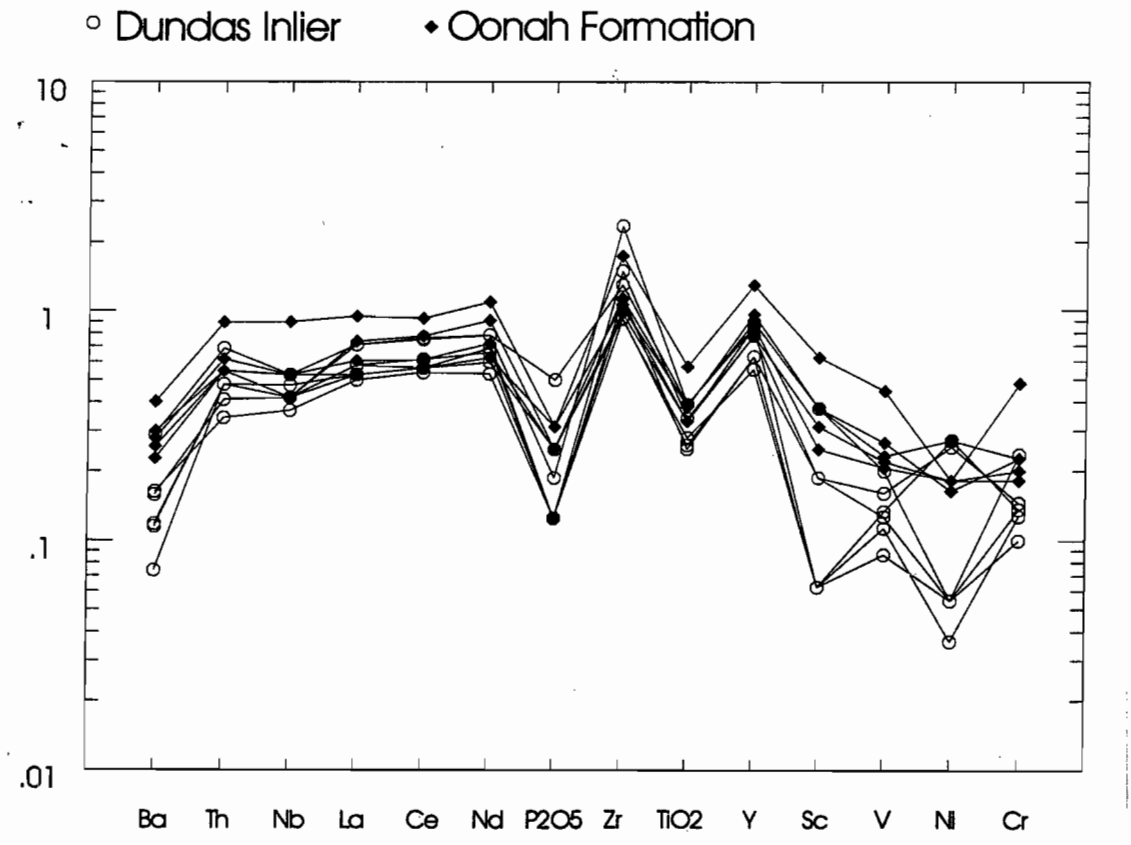

Fig. 2. Spidergram normalised to Post-Archean Australia shales (PAAS, Taylor & McClennan 1985). Oonah Formation and Dundas inlier sandstone.

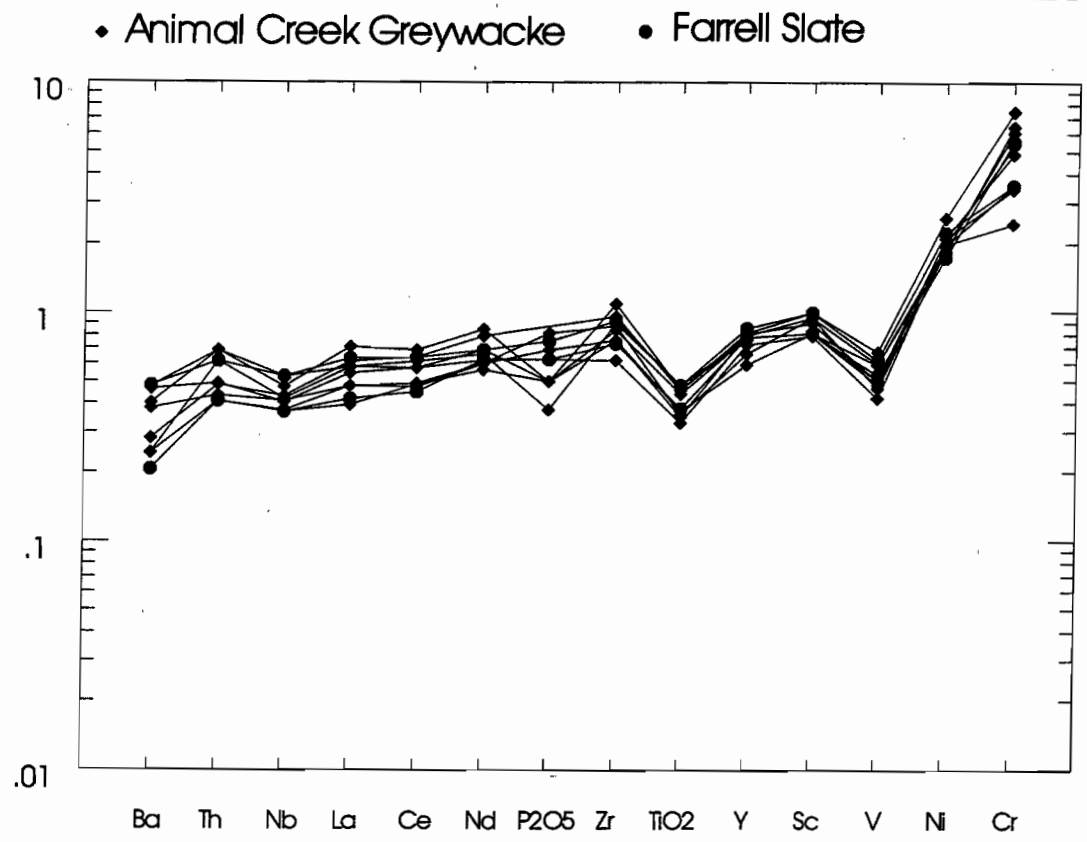

Fig. 3. Spidergram normalised to Post-Archean Australia shales (PAAS, Taylor & McClennan 1985). Animal Creek Greywacke and Farrell Slates.

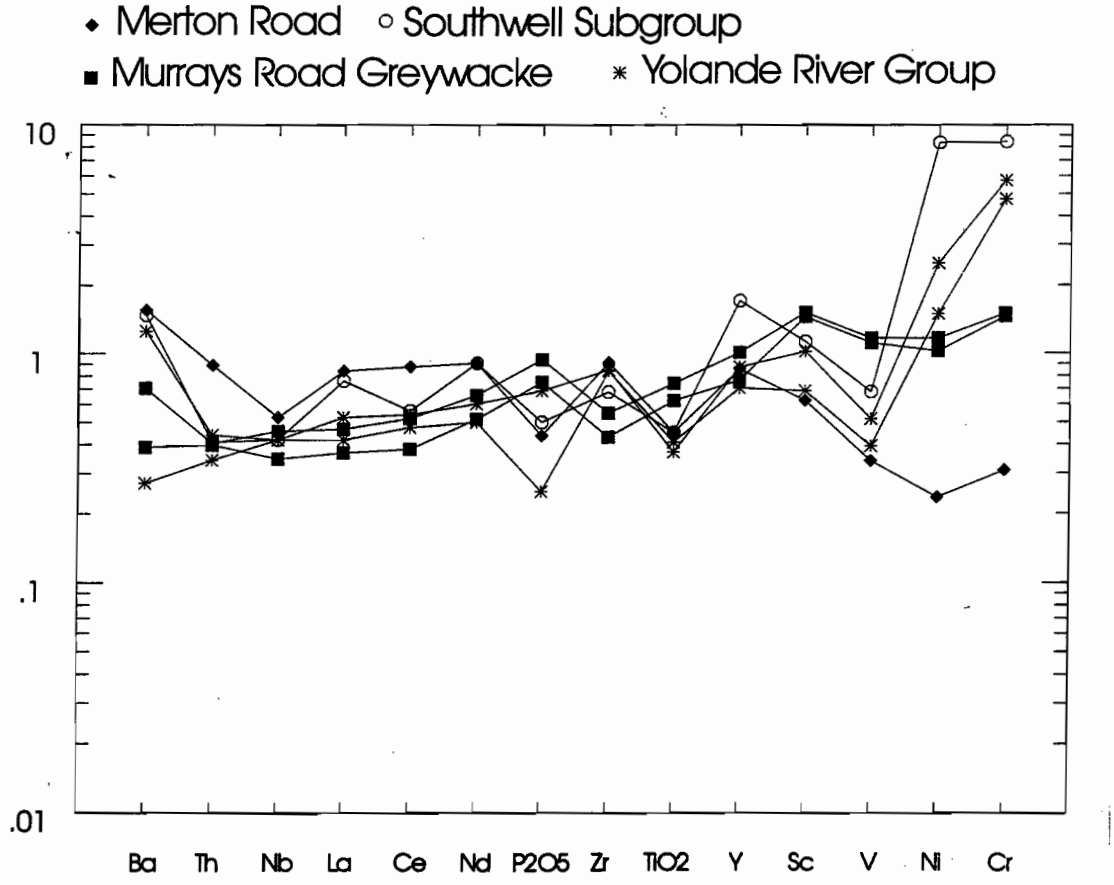

Fig. 4. Spidergram normalised to Post-Archean Australia shales (PAAS, Taylor & McClennan 1985). Yolande River Sequence, Southwell Subgroup, Murrays Road Greywacke and Merton Road.

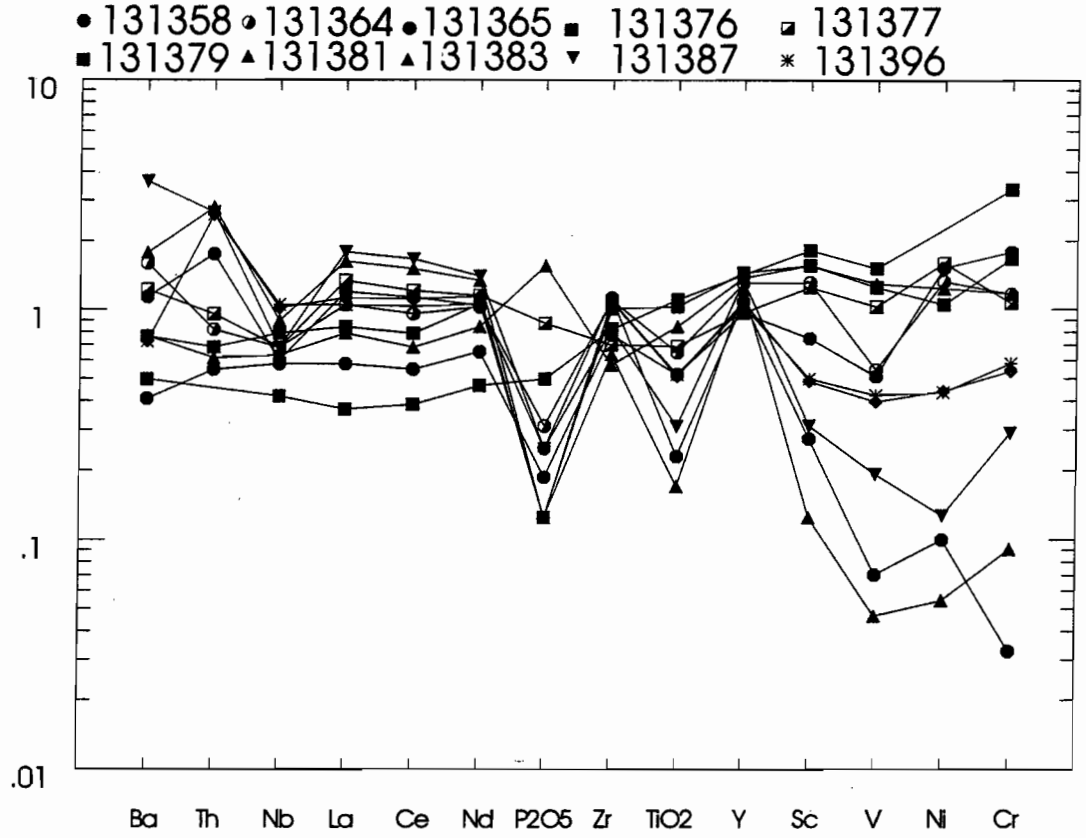

Fig. 5. Spidergram normalised to Post-Archean Australia shales (PAAS, Taylor & McClennan 1985). White Spur sandstone from Halls Rivulet Canal (Nunn 1995).

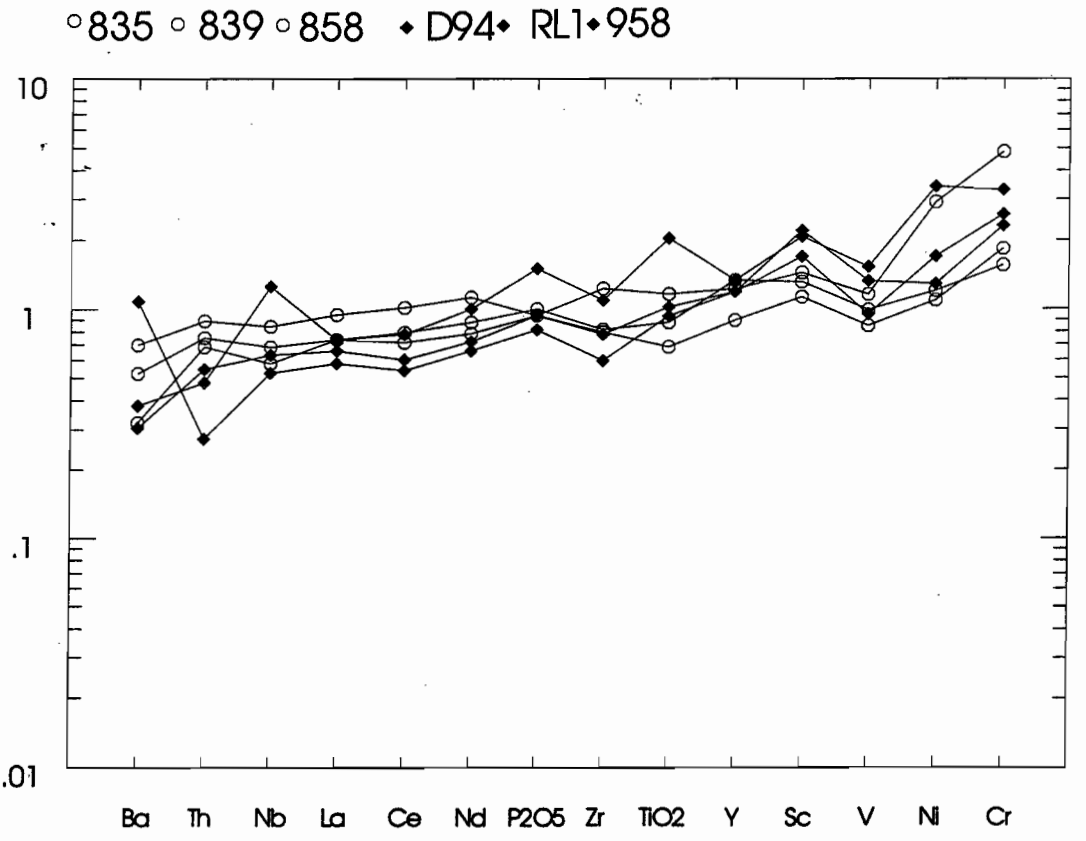

Fig. 6. Spidergram normalised to Post-Archean Australia shales (PAAS, Taylor & McClennan 1985). "Lower" Dundas Group sandstone from the Dundas region.

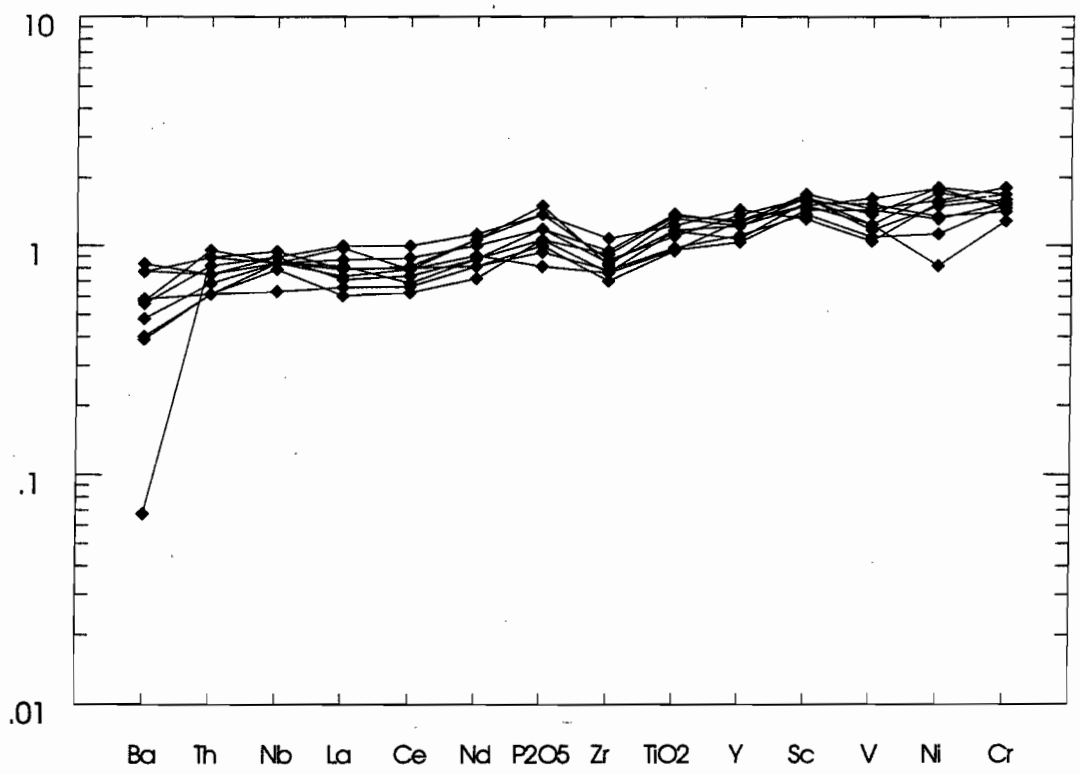

Fig. 7. Spidergram normalised to Post-Archean Australia shales (PAAS, Taylor & McClennan 1985). "Lower" Dundas Group mudstone from the Dundas region.

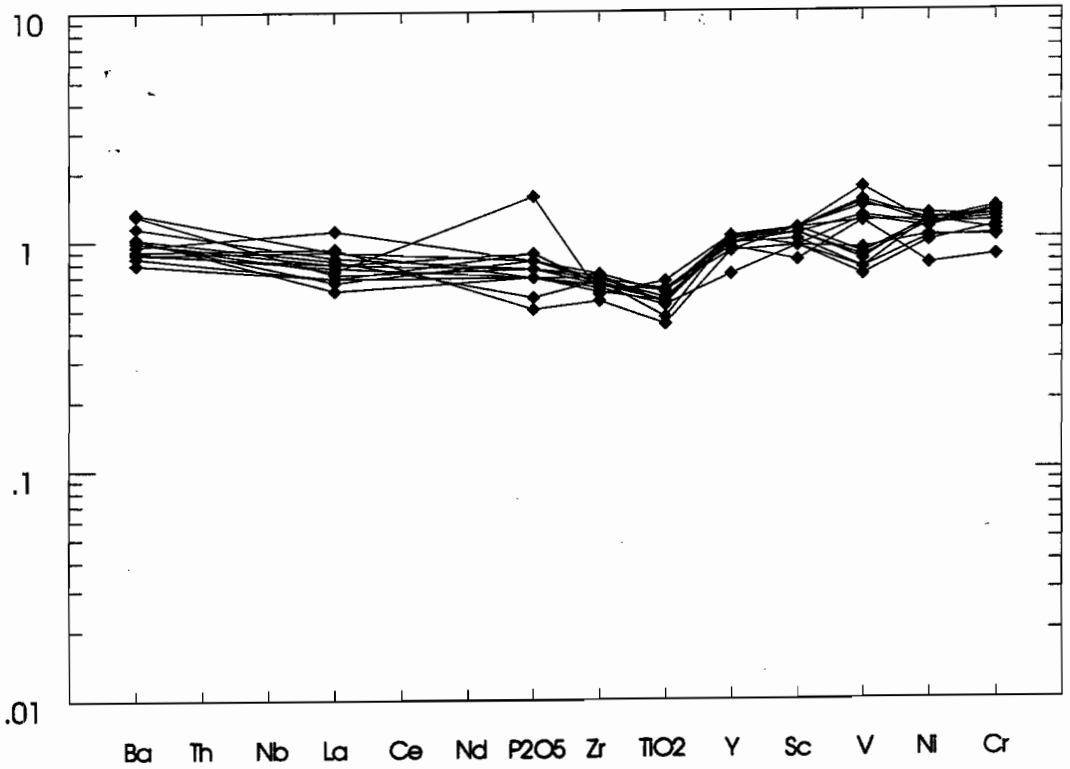

Fig. 8. Spidergram normalised to Post-Archean Australia shales (PAAS, Taylor & McClennan 1985). Que River Shale (Sinclair 1994)..

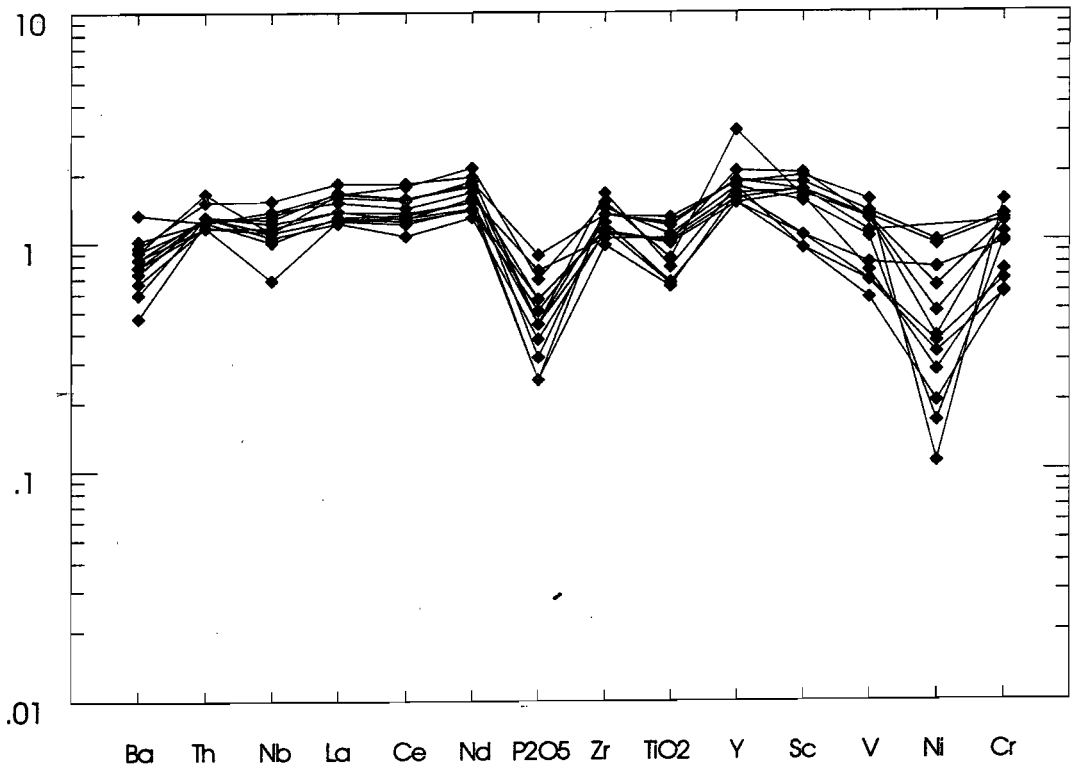

Fig. 9. Spidergram normalised to Post-Archean Australia shales (PAAS, Taylor & McClennan 1985). Dundas inlier mudstones.

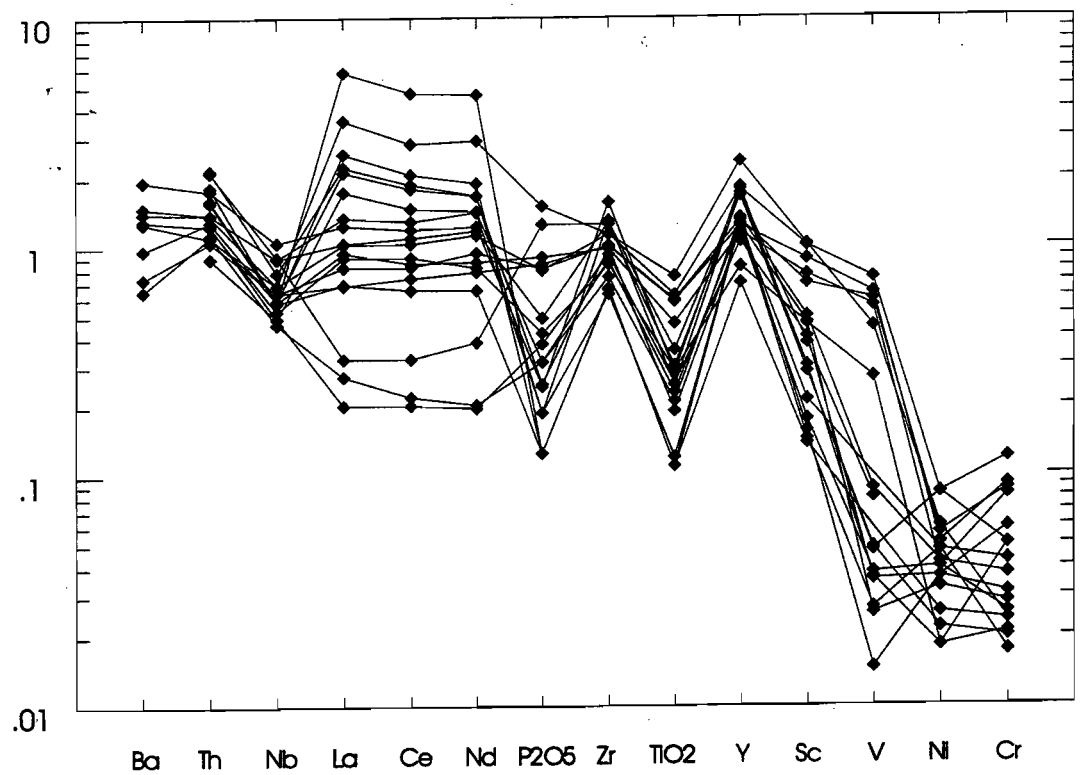

Fig. 10. Spidergram normalised to Post-Archean Australia shales (PAAS, Taylor & McClennan 1985). Representative volcaniclastic sandstones from the CVC.

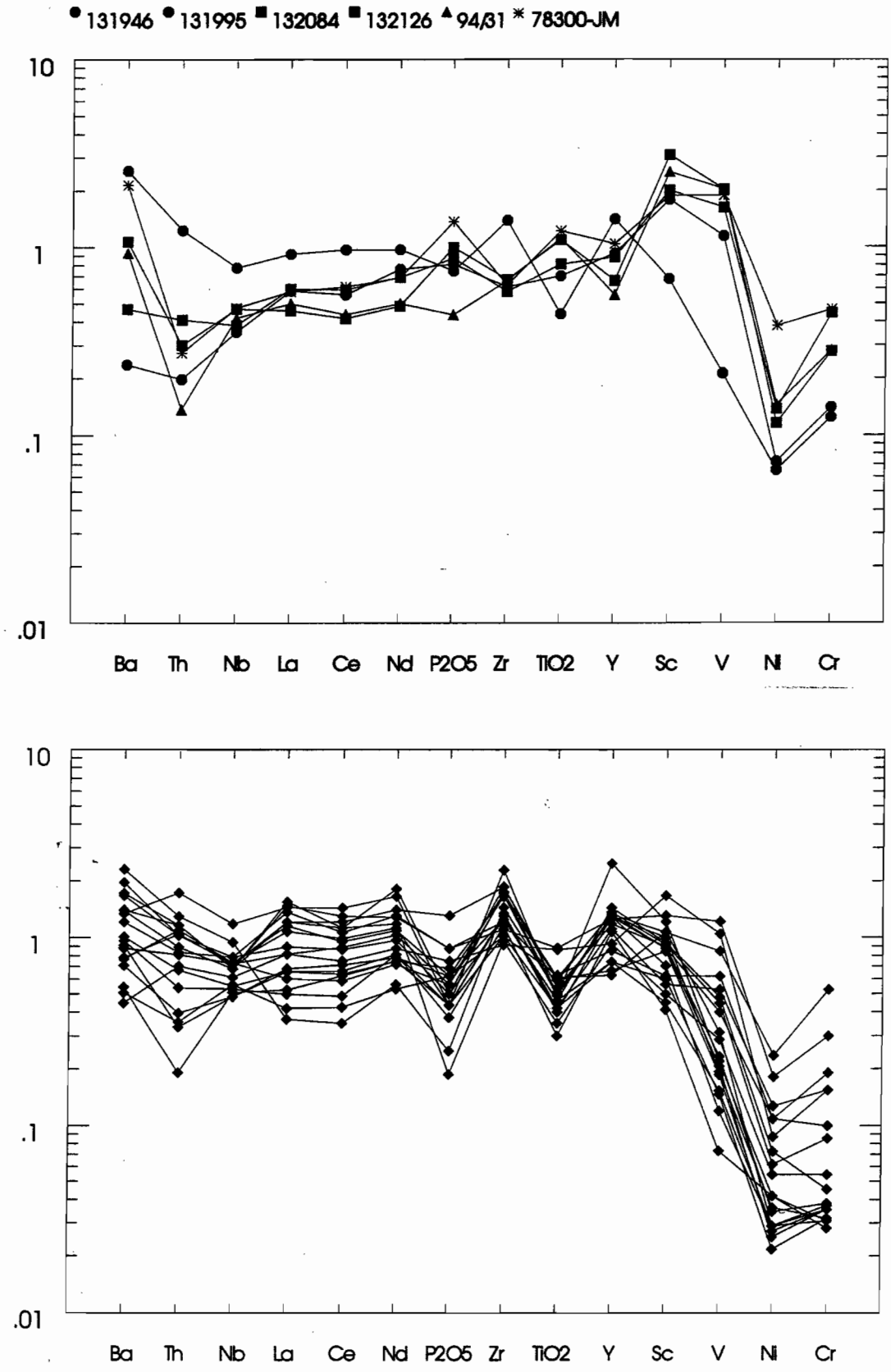

Fig. 11. Spidergrams normalised to Post-Archean Australia shales (PAAS, Taylor & McClennan 1985). a) Lynchford Member b) Younger Tyndall Group

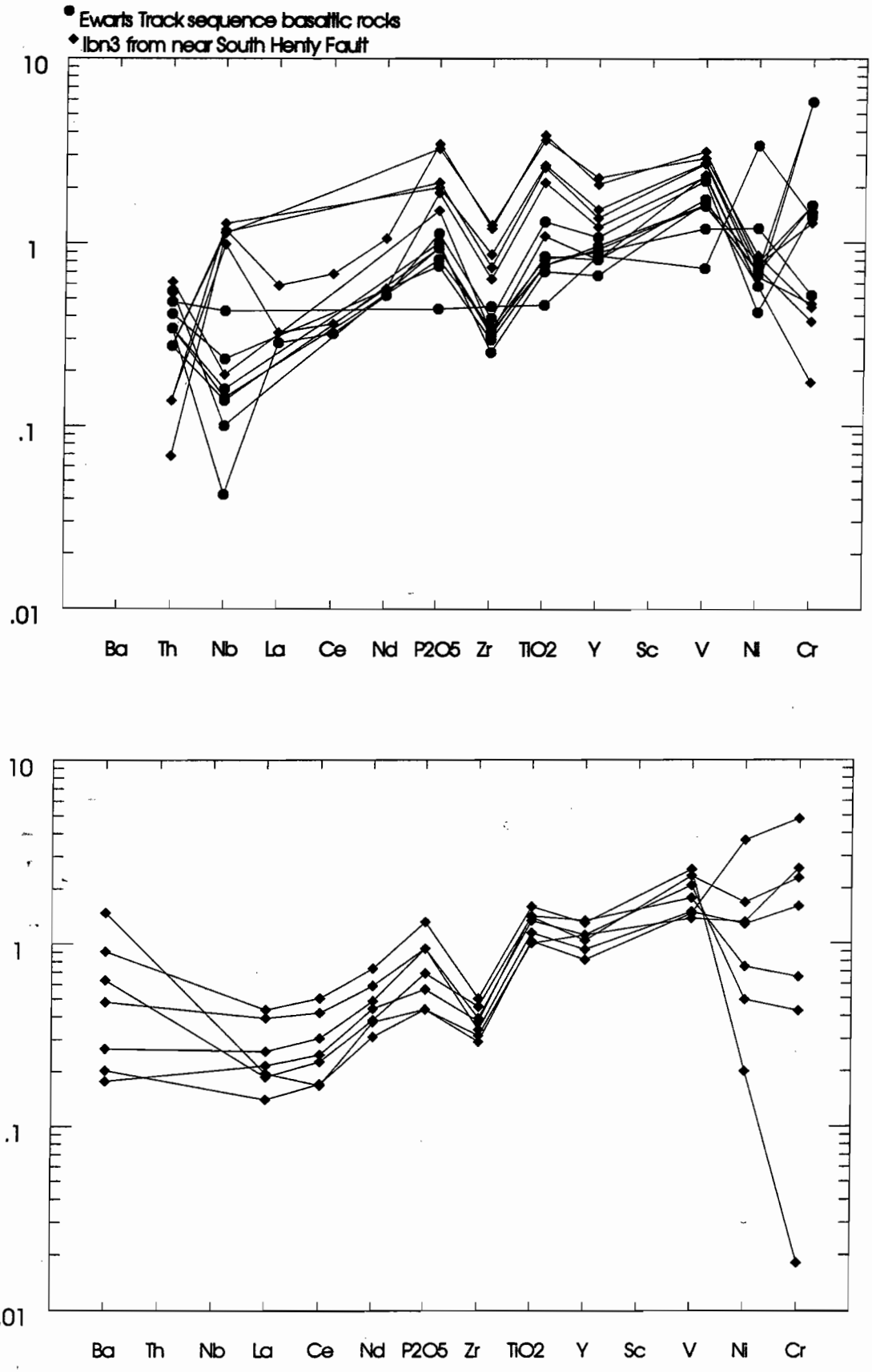

Fig. 12. Spidergrams normalised to Post-Archean Australia shales (PAAS, Taylor & McClennan 1985). a) Henty Fault Wedge basalts (Poltock 1992), b) Henty dykes (Crawford et al 1992),

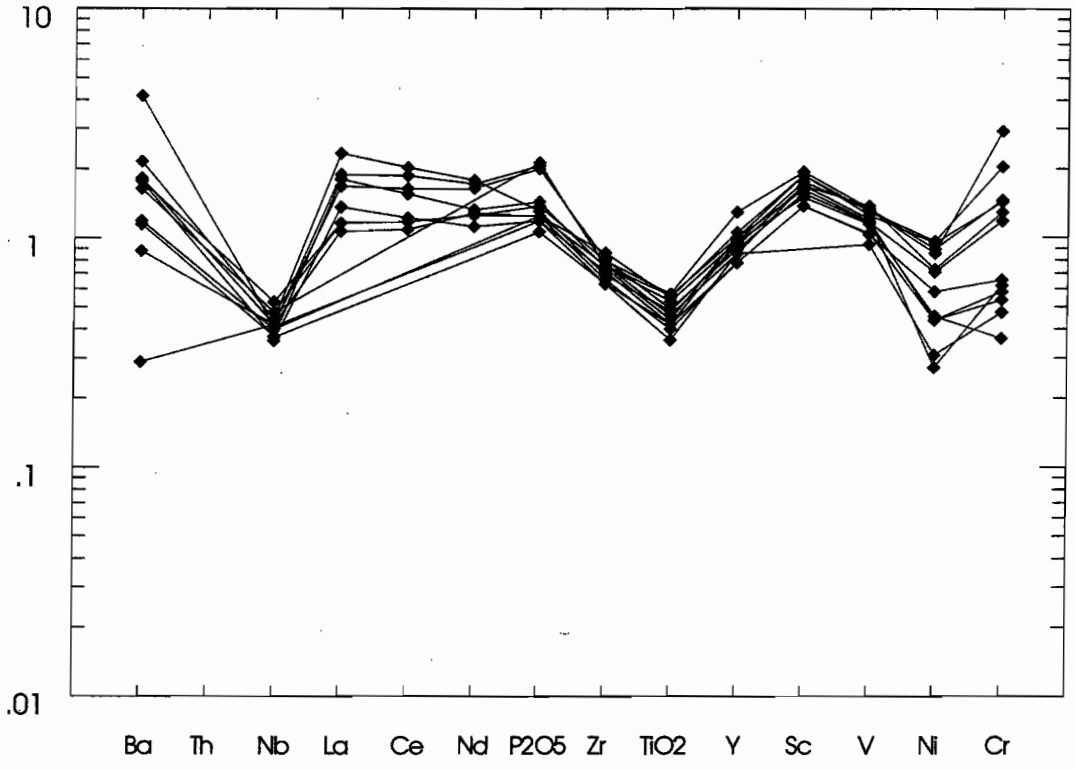

Fig. 13. Spidergrams normalised to Post-Archean Australia shales (PAAS, Taylor & McClennan 1985). Suite III basalts (Crawford et al 1992).

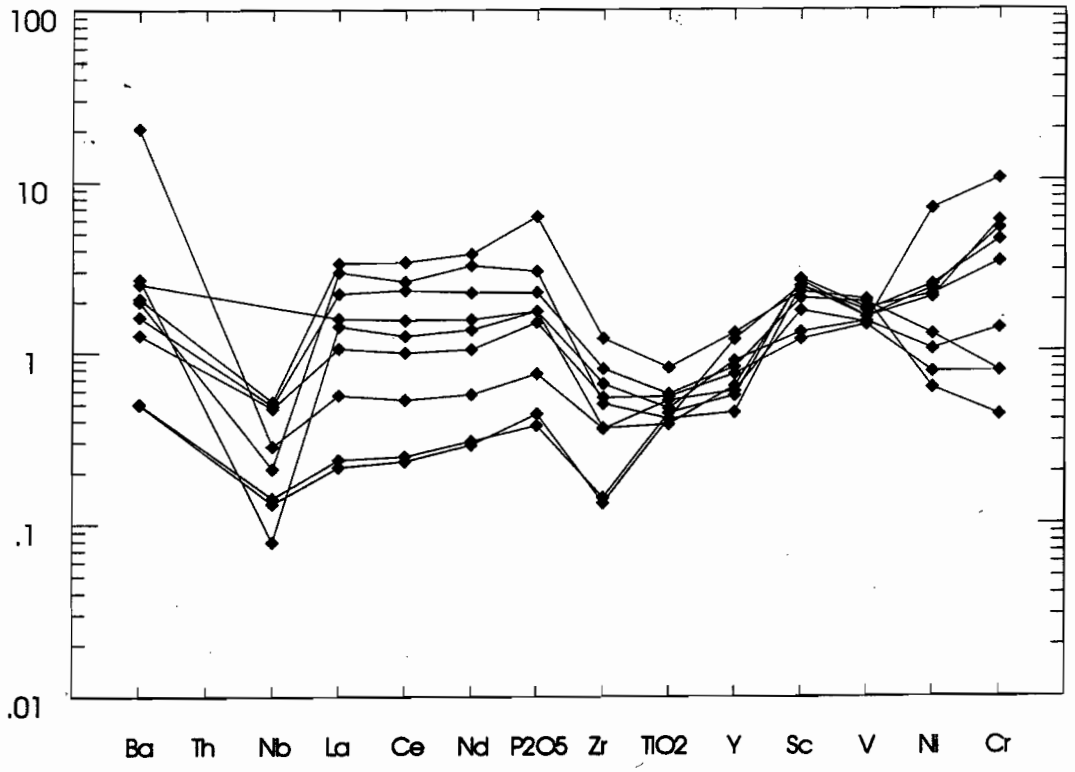

Fig. 14. Spidergrams normalised to Post-Archean Australia shales (PAAS, Taylor & McClennan 1985). Suite II andesites (Crawford et al 1992).

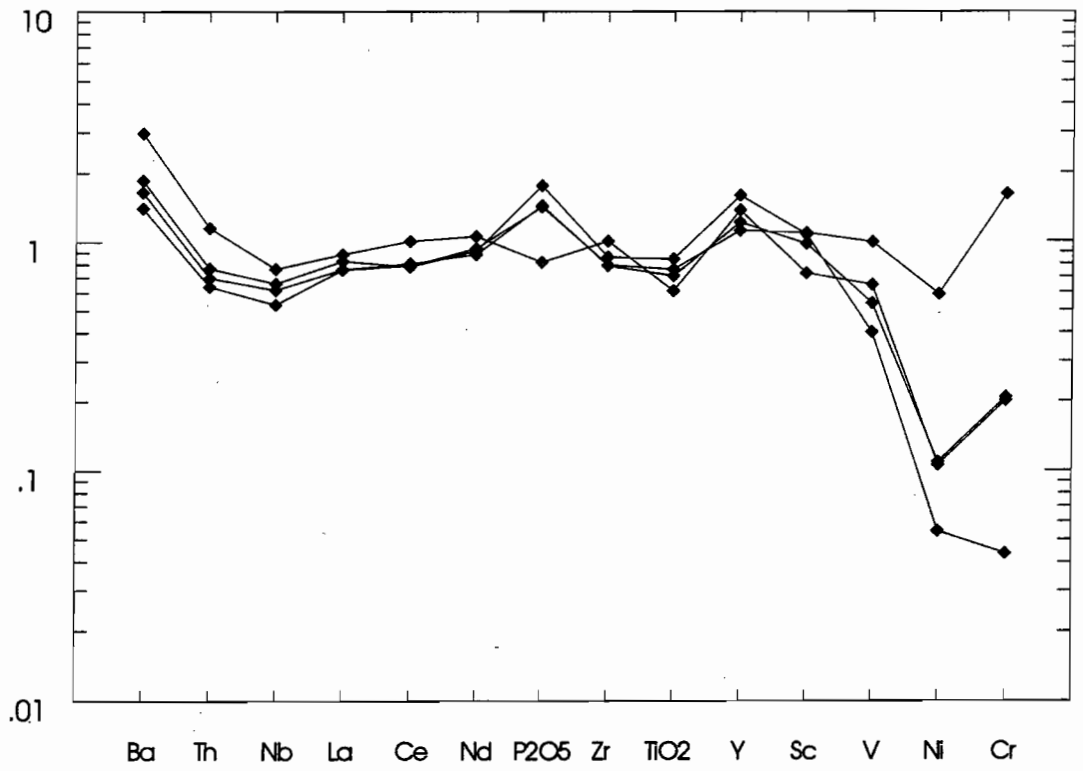

Fig. 15. Spidergram normalised to Post-Archean Australia shales (PAAS, Taylor & McClennan 1985). Tyndall correlates from Native track tier.

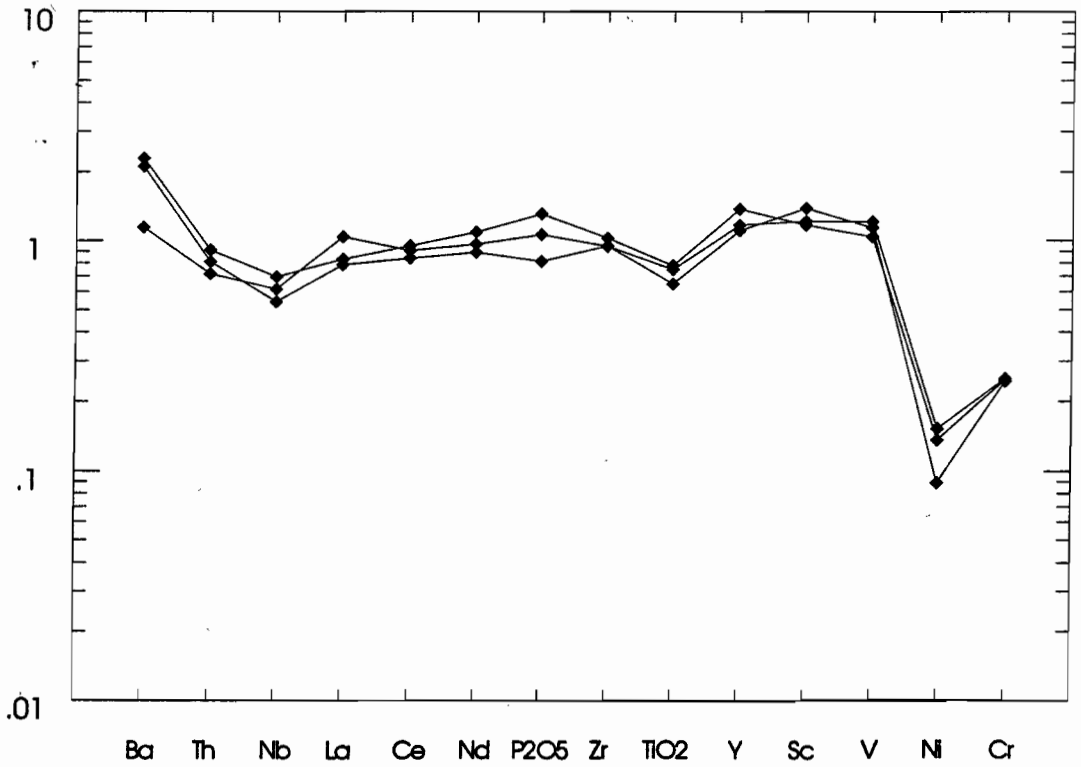

Fig. 16. Spidergram normalised to Post-Archean Australia shales (PAAS, Taylor & McClennan 1985). Tyndall correlates from Winterbrook and the Smith Plains.

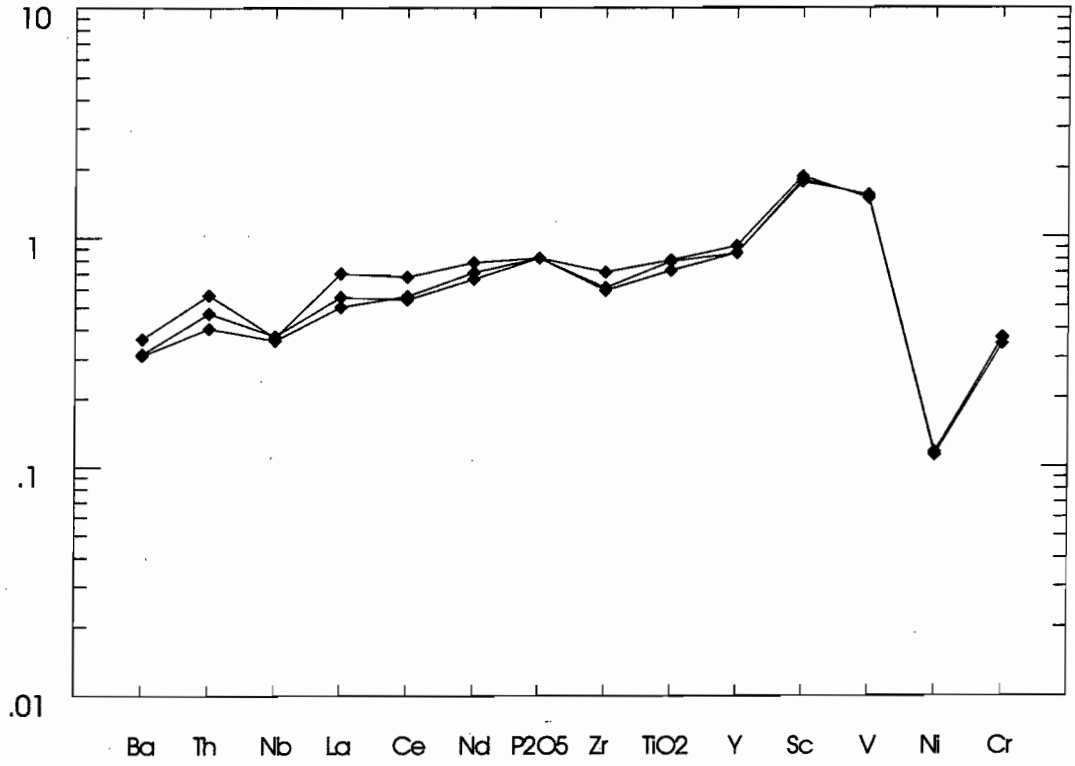

Fig. 17. Spidergram normalised to Post-Archean Australia shales (PAAS, Taylor & McClennan 1985). Tyndall correlates from the Yolande River.

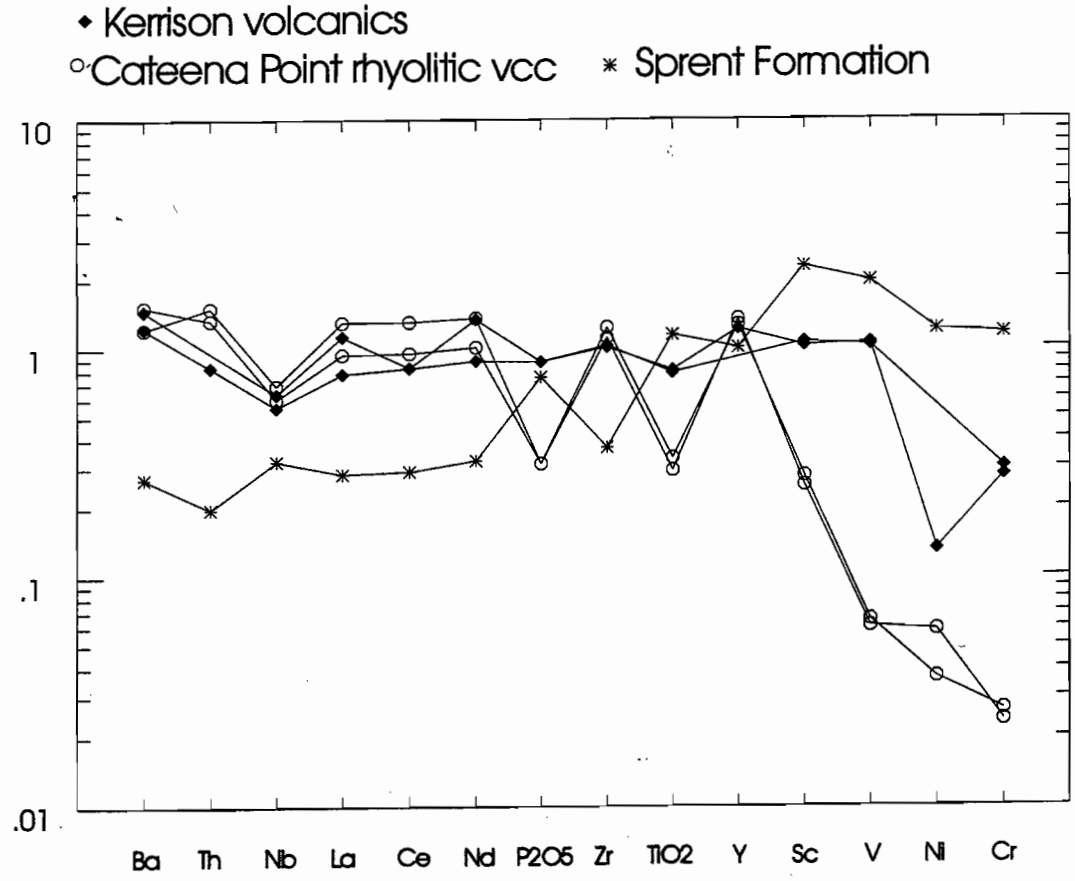

Fig. 18. Spidergram normalised to Post-Archean Australia shales (PAAS, Taylor & McClennan 1985). Kerrison Volcanics and the Sprent Formation (Sproule 1994).

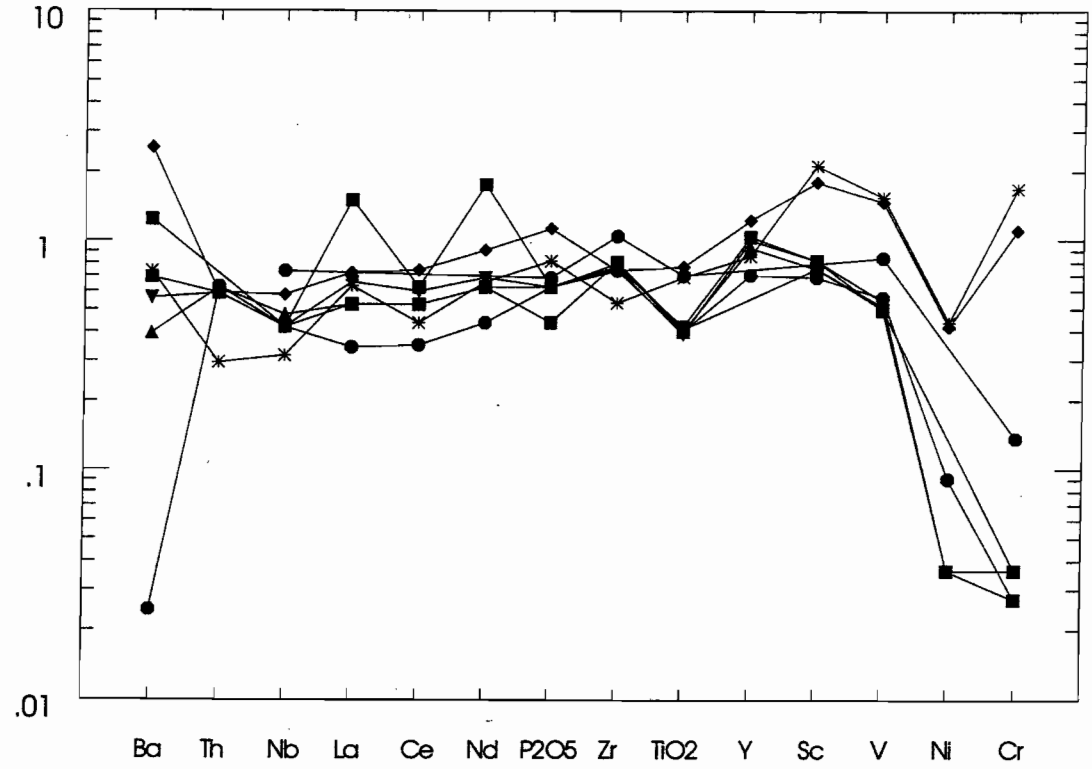

Fig. 19. Spidergram normalised to Post-Archean Australia shales (PAAS, Taylor & McClennan 1985). Lobster Creek Intrusives (Sproule 1994).

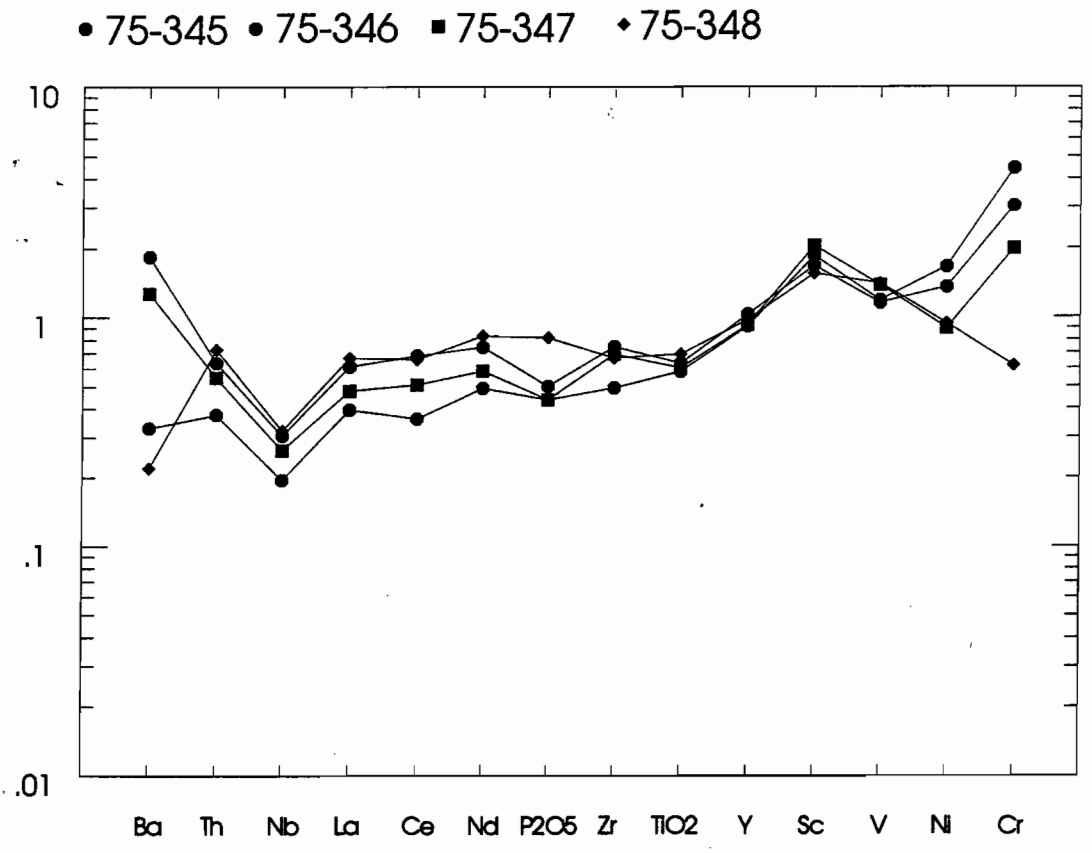

Fig. 20. Spidergram normalised to Post-Archean Australia shales (PAAS, Taylor & McClennan 1985). Lower King River (samples from Cox in Baillie & Corbett 1985).

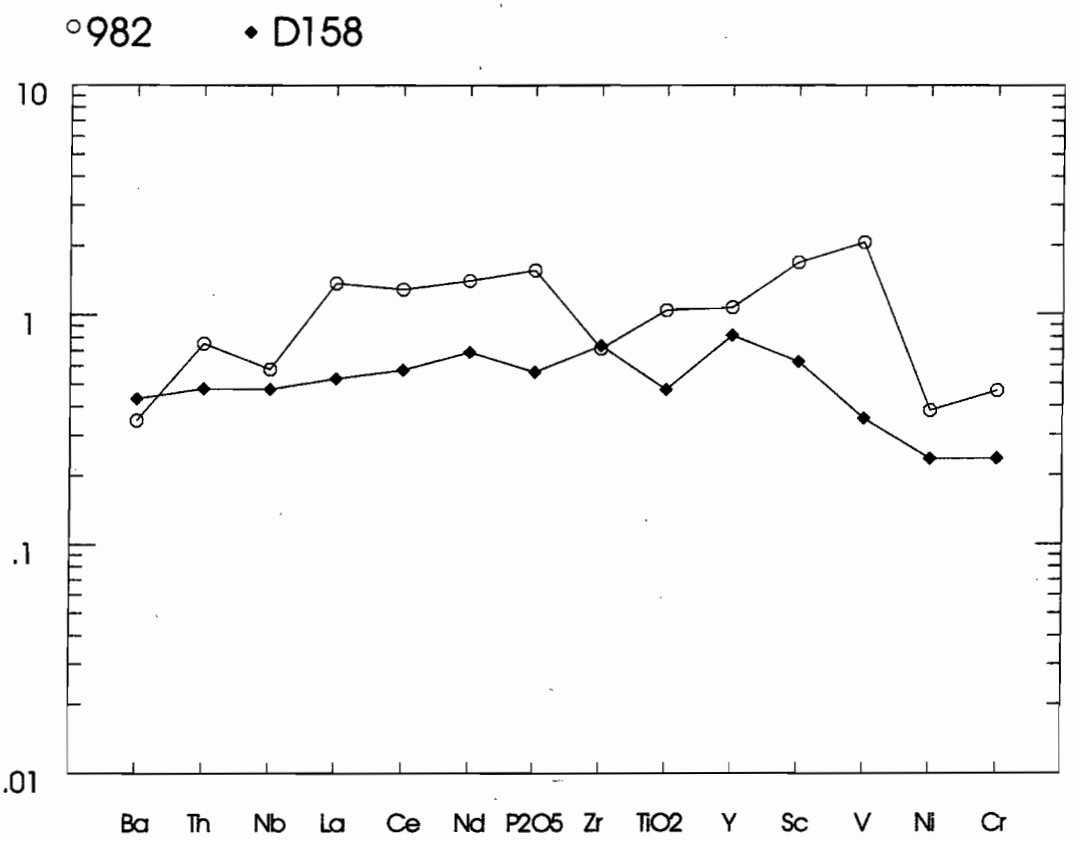

Fig. 21. Spidergram normalised to Post-Archean Australia shales (PAAS, Taylor & McClennan 1985). Possible Tyndall Group correlates from the Dundas area.

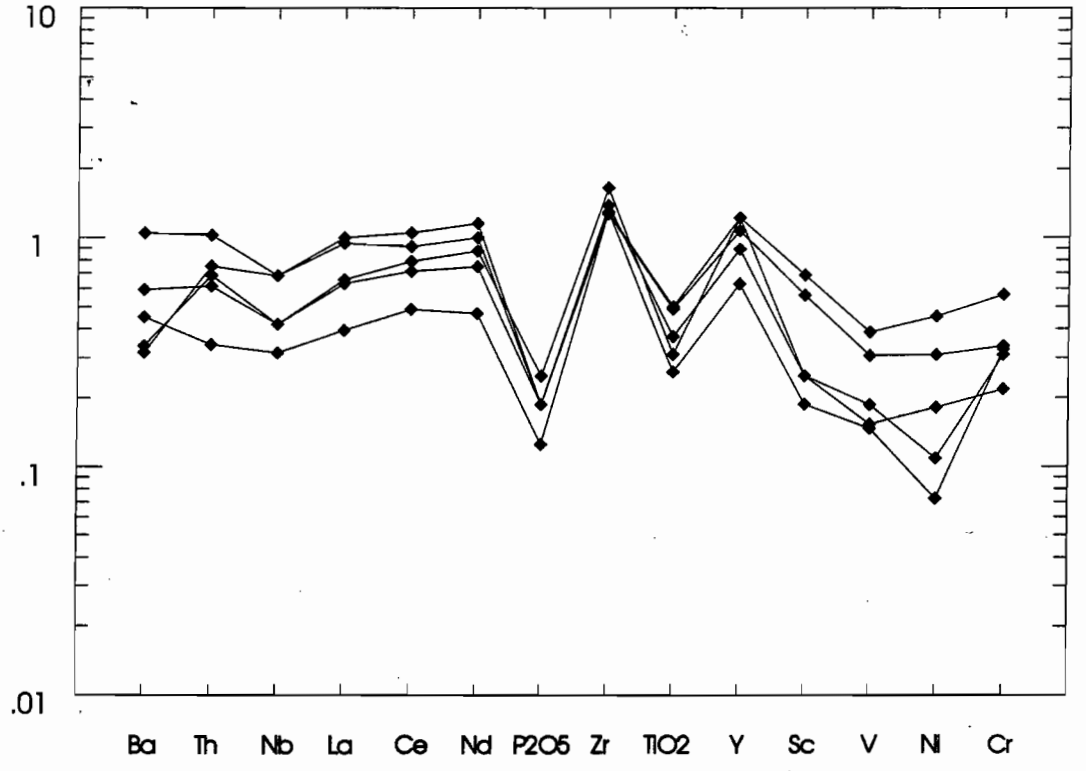

Fig. 22. Spidergram normalised to Post-Archean Australia shales (PAAS, Taylor & McClennan 1985). Stitt Quartzite sandstones.

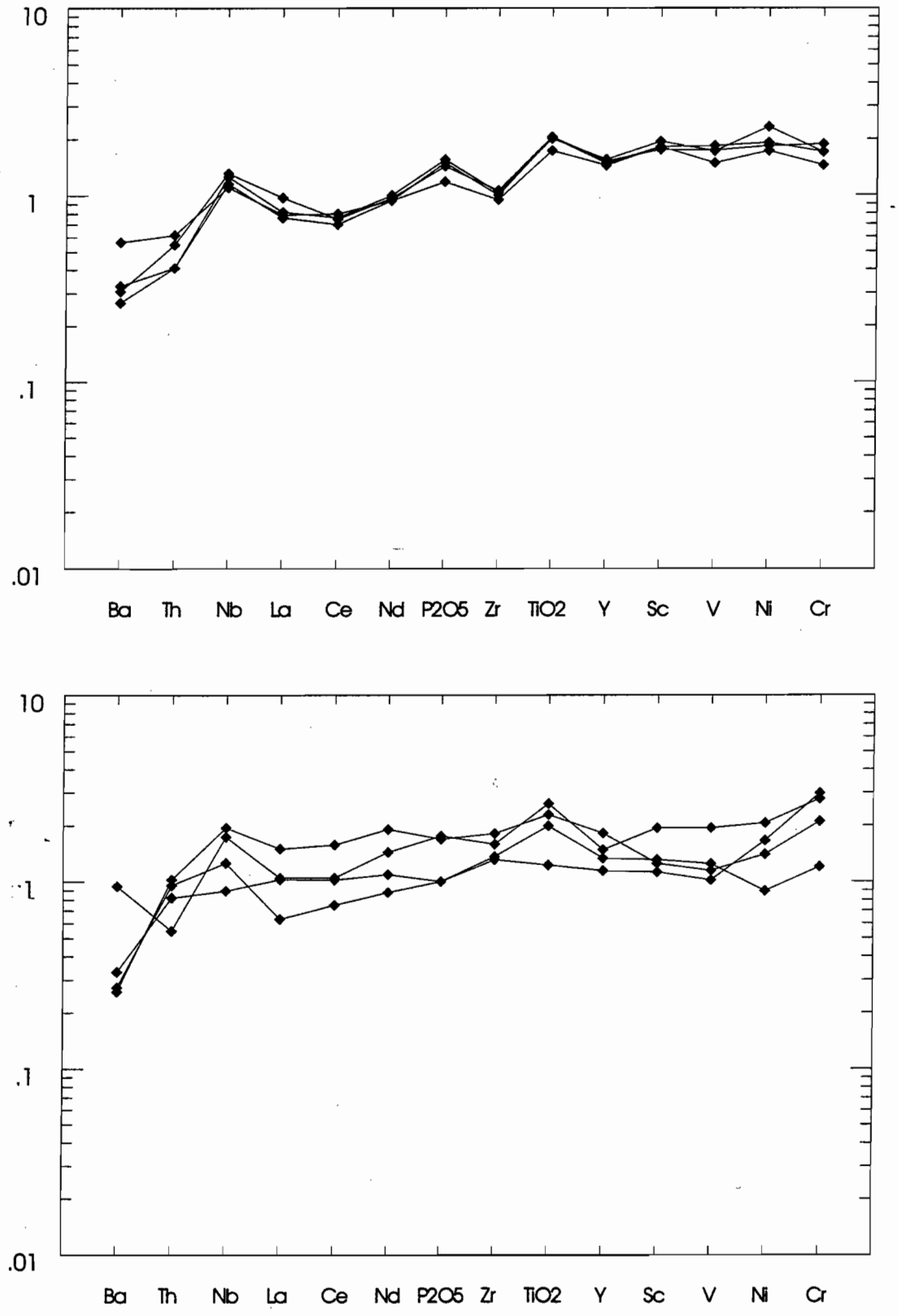

Fig. 23. Spidergram normalised to Post-Archean Australia shales (PAAS, Taylor & McClennan 1985). (a) "Upper" Dundas Group sandstones from the Dundas Group type section, (b) 'Upper" Dundas Group sandstones from western and eastern parts of the Dundas region.

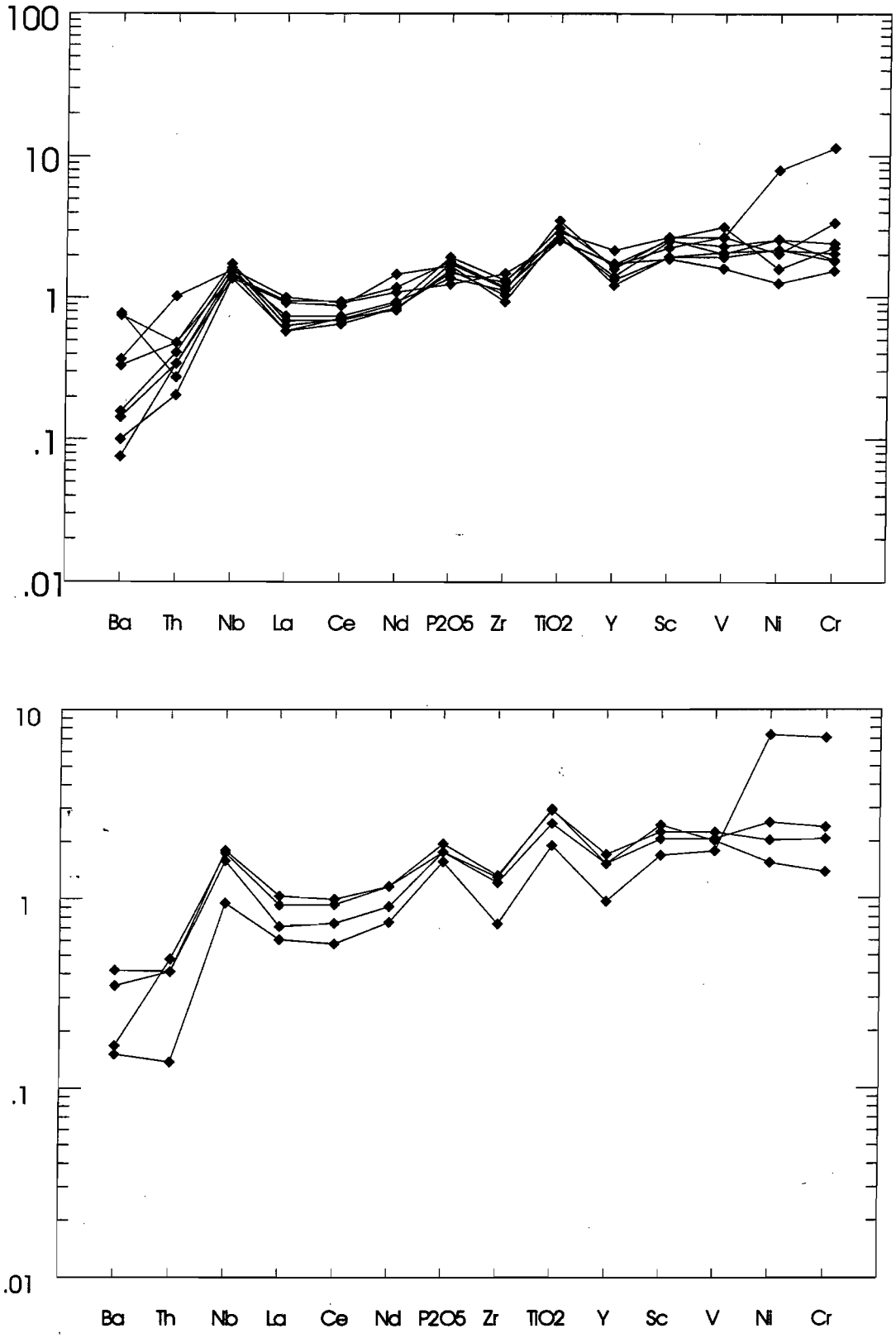

Fig. 24. Spidergram normalised to Post-Archean Australia shales (PAAS, Taylor & McClennan 1985). (a) Crimson Creek Formation sandstones, (b) Crimson Creek Formation mudstones.

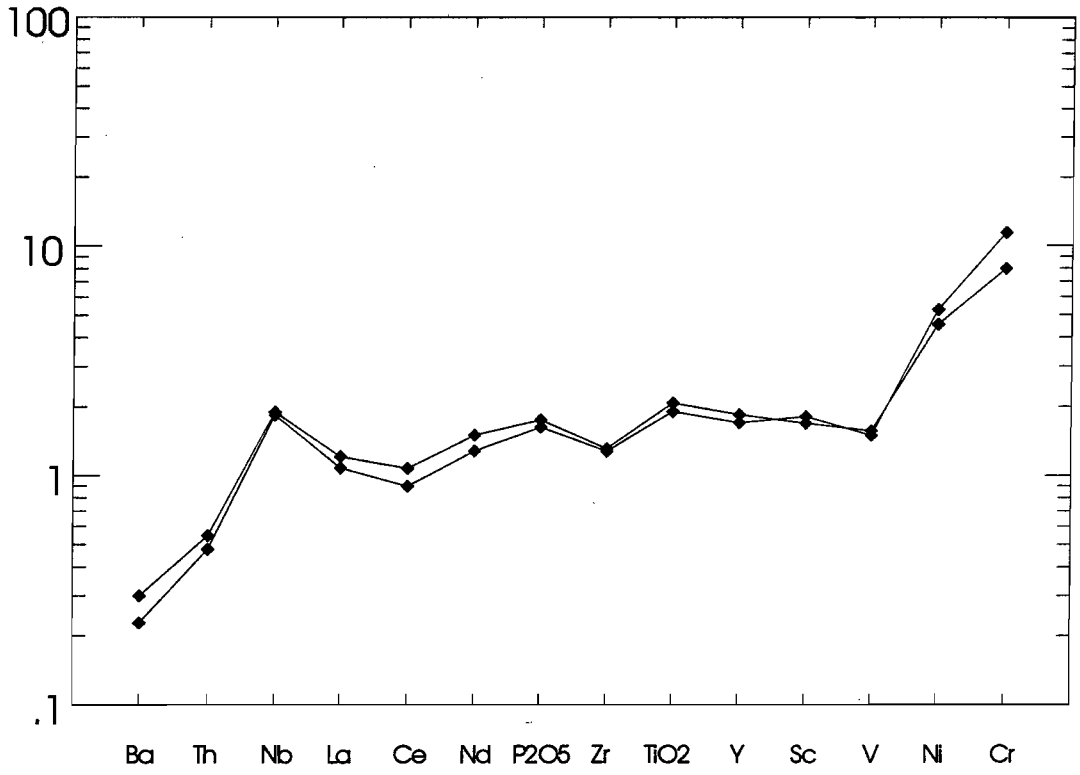

Fig. 25. Spidergram normalised to Post-Archean Australia shales (PAAS, Taylor & McClennan 1985). "Upper" Dundas Group sandstones from the Que River.

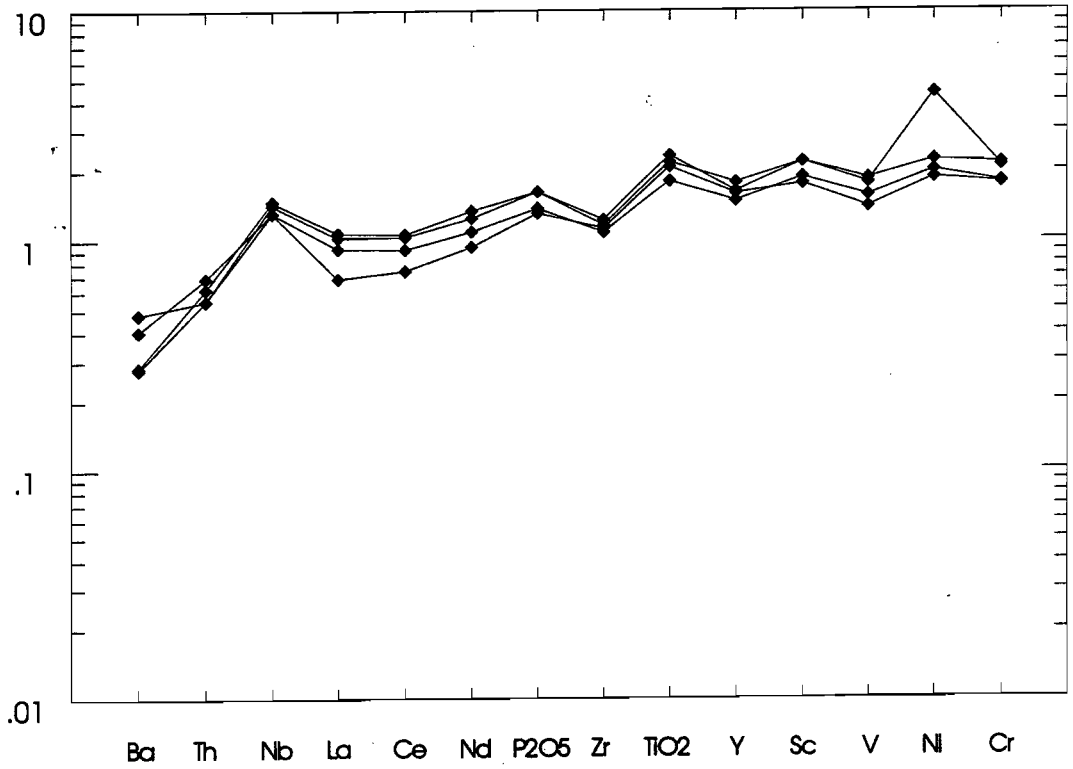

Fig. 26. Spidergram normalised to Post-Archean Australia shales (PAAS, Taylor & McClennan 1985). (a) Idamean and older 'upper' Dundas Group mudstones from the Dundas Group type section.

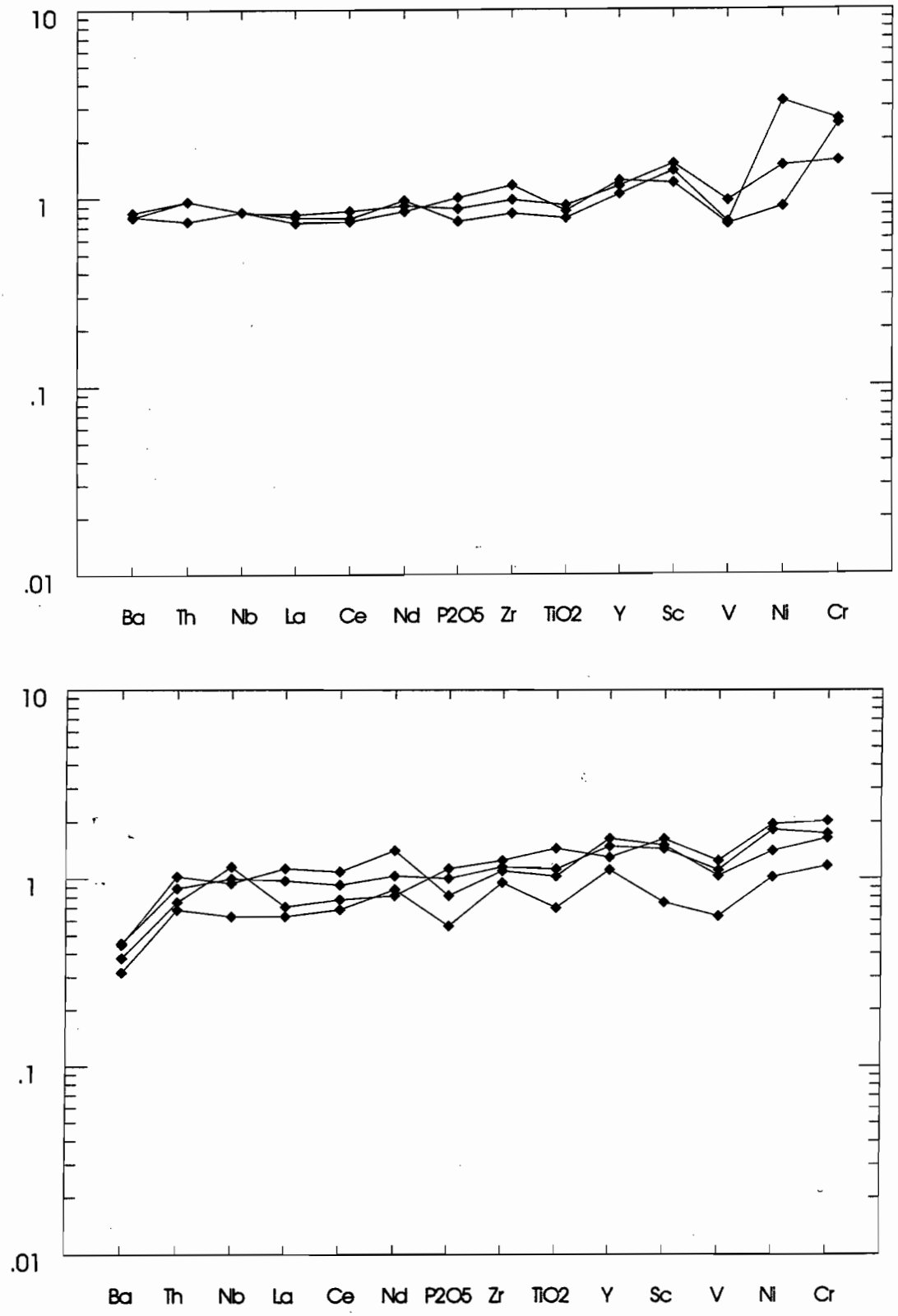

Fig. 26 cont . Spidergram normalised to Post-Archean Australia shales (PAAS, Taylor & McClennan 1985). (b) Mindyallan to Idamean 'upper' Dundas Group mudstones from central and eastern parts of the Dundas region, (c) Iverian 'upper' Dundas Group mudstones from the Dundas Group type section.

Stratigraphic correlation and basin analysis

K.D. Corbett, R.F. Berry & D. Selley
CODES Special Research Centre, Geology Department, University of Tasmania

Abstract

Subdivision of the Cambrian rocks of western Tasmania into three "cycles" based on pre-Tyndall(Yolande Cycle), Tyndall and post-Tyndall (Denison Cycle) sequences, using biostratigraphic constraints where possible, provides a practical framework for considering basin geometry and geological evolution. The Tyndall Cycle, although occupying only a very short time span (1–2 Myrs?) at the end of the Middle Cambrian, is important because it was initiated by a distinctive phase of transitionally tholeiitic volcanism. This compositional signature has been used to correlate the Lynchford member of the Tyndall Group with the Henty Fault wedge basalts and dykes, Native Track Tier volcaniclastics, Lobster Creek intrusives and the lower King River basalts. The distribution of these units supports a widespread volcanic event which occurred after the main CVC style volcanism and formed at discrete small centres unrelated to the major centres of CVC volcanism. Together these units act as a marker allowing the application of our three-fold subdivision across all the Cambrian sequences of western Tasmania.

Cycle 1 opens with deep water sedimentation and dacitic volcanism. Towards the top of Cycle 1 the basin becomes more complex with increased basaltic volcanism and active extensional faulting. The Tyndall Cycle was initiated in many areas by explosive basaltic volcanism with a mild but distinct tholeiitic character. Cycle 3 is dominated by clastic sedimentation and is synchronous with east–west compression and basin inversion.

Introduction

A major aim of the project has been to enhance lithostratigraphic correlation within the Dundas Group and between sections of the Mt Read Volcanics generally. The rationale for this was to tighten up the structural interpretations in the existing regional sections and to provide a framework for basin analysis.

Biostratigraphy remains the cornerstone for correlations in the Tasmanian Cambrian, and refinement of the ages of the known fossil faunas continues (Laurie et al., 1995). New fossil localities at Cradle Mountain Link Road (Pemberton et al., 1991), Southwell Subgroup drill core (Jago and McNeill, in press), Native Track Tier (Seymour et al., 1989) and Paradise (Laurie et al., 1995) have aided correlations in the northern part of the Mt Read belt, as have lithostratigraphic studies such as those of McKibben (1993) and Pemberton and Corbett (1992). McPhie and Allen (1992) have suggested alternative correlations for the Hellyer–Rosebery area based on volcanic facies analysis. The most recent correlations are summarised in the correlation chart (Fig. 1).

Stratigraphic correlation remains difficult in the area southeast of the Henty Fault despite a large amount of work, mainly because of the paucity of fossil localities. The problem of distinguishing Tyndall Group rocks from Eastern Quartz-phyric Sequence remains to be resolved (eg. Corbett et al., 1993).

Most recently, the Geological Survey has published a revised series of 1:250,000 maps of the state in which much of the post-Crimson Creek Cambrian stratigraphy has been simplified into two major groups (Middle Cambrian volcaniclastic

sequences, late Cambrian siliciclastic sequences). The Tyndall Group has also been distinguished in some areas as a subdivision of the volcaniclastic sequence. The two-fold format has been applied to a generalised 1:500,000 map of strato-tectonic elements and accompanying explanatory notes (Seymour and Calver, 1995a, b). This simple system clarifies much of the confusion arising from use of groups terms (such as Dundas Group) which spanned both sequences, but is rather coarse in scale for basin analysis.

Using all these sources and the results from our geochemical and provenance studies, and applying strict biostratigraphic constraints, we have produced a refined three-fold stratigraphic subdivision and a preliminary map and basin analysis based on it. The Geological Survey's digital version of the 1:250,000 map has been modified to show the three cycles at 1:250,000 scale (Fig. 2) and 1:100,000 scale (Figss 3, 4)

Three-cycle stratigraphic system

We believe there is sufficient stratigraphic information now available to attempt basin analysis based on three Cambrian groups: a Late Cambrian siliciclastic unit, a late Middle Cambrian unit based on the Tyndall Group and correlates, and the pre-Tyndall sequences. Major attributes of the cycles are listed below, and the basis of the correlations is shown on the correlation chart (Fig. 1).

Cycle 1: The Yolande cycle

Age: Middle Cambrian up to possibly lower Boomerangian

Includes: Most of the Yolande River Sequence, Central Volcanic Complex (N and S), Anthony Road Andesites and correlates, Animal Creek Greywacke, Black Harry Beds, Que-Hellyer Volcanics, Que River Shale, Southwell Subgroup (most if not all), Sticht Range Beds, Eastern Quartz-phyric Sequence (most if not all).

Geochemical character: The volcanic chemistry of these units has been well described by Crawford et al (1992). The Suite 1 volcanics occupy much of this cycle but Suites 2 and 3 are typical of upper Yolande Cycle sequences.

Cycle 2: the Tyndall cycle

Age: Lower Boomerangian–upper Boomerangian. The Comstock limestone fossil age is not well constrained (Undillan–Boomerangian, J.B. Jago, pers. comm., 1997), but the Mt Cripps and Southwell Subgroup faunas, and those from other areas (Fig. 1) strongly suggest that the Tyndall Group is limited to the Boomerangian.

Includes: Tyndall Group (comprising Lynchford Member, Mt Julia Member — previously Comstock Tuff, Zig Zag Hill Formation), Mt Cripps Subgroup, Radfords Creek Group, Native Track Tier fossiliferous sequence, St Valentines Peak sequence, western part of Yolande River sequence, western part of Henty Fault Wedge sequence (Ewart Creek sequence of Poltock, 1992), Trial Ridge Beds.

Geochemical character:

The distinctive chemical character from the basal part of this cycle has been defined from the Lynchford member and extended to many other areas as reported in the Lithogeochemistry section (this volume). They are largely andesitic rocks very similar to Suite 4 (Henty dykes) of Crawford et al (1992) and a few very evolved rhyolites.

Cycle 3: the Denison cycle

Age: Early Mindyallan through Late Cambrian, possibly into early Ordovician.

Includes: Upper Dundas Group from Upper Brewery Junction Formation; Owen Group (comprising Jukes Conglomerate, Lower Owen Conglomerate, Newton Creek Sandstone, Middle Owen Conglomerate, Upper Owen sandstone) but ***not*** including Pioneer Beds; upper Huskisson Group including black shale near base with *G. reticulatus*; Farrell Rivulet sandstone-conglomerate sequence and overlying Tom Creek sequence; the Stitt Quartzite and overlying

	Stage	Zone	Dundas	Rosebery-Farrell Rivulet	Queenstown-Henty Area	Hellyer-Que River	Huskisson River	Fossey Mtns & other areas		Dial Range Trough	Smithton Basin	Adamsfield Trough
ORD.	WARENDAN											Squirrel Creek Formation
490	DATSONIAN				?							
LATE CAMBRIAN	PAYNTONIAN	*M. perplexa* *N. quasibilobus-S. nomas* *S. impages*	Sandstone-siltstone at Misery Hill ?		Upper Owen Sandstone			Birch Inlet faunas				
	IVERIAN	*R. clarki maximus-R. papilio* *R. bifax-N. denticulatus* *R. clarki prolatus-C. sectatrix* *R. clarki patulus-C. sqamosa* *P. tertia-R. quarta* *R. secunda-R. glabella* *W. iota-R. apsis* *I. tropica*	Misery Congl Climie Fmn Fernflow Fmn	Higgins Creek Sequence	Middle Owen Conglomerate Newton Creek Sandstone	OWEN GROUP	Higgins Creek ?	Professor Range				Reeds Congl Great Dome Sandstone DENISON GROUP
495	IDAMEAN	*S. diloma* *E. sentum* *P. cryptica* *G. reticulatus*	Comet Fmn Fernfields Fmn	Westcott Argillite ?	Lower Owen Conglomerate		Conglomerate& sandstone Black shale		CYCLE 3		Scopus fauna	Singing Creek Formation
MIDDLE CAMBRIAN	MINDYALLAN	*G. stolidotus* *C. quasivespa* *E. eretes*	Upper Brewery Junction Fmn	Tom Creek Stitt Qtzite ?	'Jukes Congl'		Conglomerate & sandstone	Native Track Tier St. Valentines Paradise faunas		Riana fauna		
	BOOMERANGIAN	*L. laevigata* *D. torosa-A. janitrix* *H. arepo* *P. Agra* *P. cassis*	Lr Brewery Jn Fmn Razorback Cgl Hodge Slate	Chamberlain Shale ? White Spur Formation CVC	TYNDALL GROUP Comstock lst Granites Andesites CVC Yolande River Sequence	Mt Cripps Subgroup Southwell Subgroup Que River Shale Que-Hellyer Volcanics Animal Ck Gwacke Black Harry Beds CVC	Merton Road volcaniclastic sequence ?		CYCLE 2 CYCLE 1	Radfords Creek Group Cateena Point fauna	Christmas Hills fauna	Trial Ridge Beds & Island Road Fmn
500	UNDILLAN	*G.(G.) nathorsti* *D. deltoides* *P. punctuosus*										
505	LATE TEMPLETONIAN-FLORAN	*E. opimus* *A. atavus* *T. gibbus*	Red Lead Congl ? 'Judith Fmn'							Isandula Road faunas		
	ORDIAN-EARLY TEMPLETONIAN	*X. templetonensis-R. chinensis*	? ?									
510	EARLY CAMBRIAN											

UPPER DUNDAS GROUP

LOWER DUNDAS GROUP

HUSKISSON GROUP

Figure 1. Correlation chart for the Cambrian of western Tasmania (based on Laurie et al, 1995)

units (Natone Volcanics, Salisbury Conglomerate, Westcott Argillite) of 'Rosebery Group'; most of the sequence in the Professor Range–Sisters area.

Geochemical character: Volcanic rocks of this age are rare and low in volume eg. Natone volcanics.

Comments and modifications to the map

1. The 'Rosebery Group' problem

The correlation of the 'Rosebery Group' sequence, and its probable extension into the Farrell Rivulet area to the south, is problematic because of the lack of fossil control. At Farrell Rivulet, a distinctive sequence of siliciclastic conglomerate and sandstone, with interbedded grey siltstone, is a correlate of the Stitt Quartzite of the Rosebery area, and is apparently overlain by fossiliferous beds at Tom Creek containing an early Late Cambrian (upper Mindyallan) fauna. This fauna lies above the Tyndall Cycle and by implication places the Farrell Rivulet sequence and Stitt Quartzite at the base of the Denison cycle. As a consequence, the higher units of the 'Rosebery Group' — Natone Volcanics (a fairly local lens of felsic volcanics at Rosebery), Salisbury Conglomerate, Westcott Argillite — are also included in this cycle. The upper part of this sequence is apparently represented by the unit of interbedded sandstone, siltstone and siliceous conglomerate in the Higgins Creek–Boco Road area containing a rich Iverian fauna (Jell et al., 1991).

If the Stitt Quartzite is regarded as the base of the Owen-Denison cycle, then it seems likely that some of the underlying rocks will be Tyndall Group equivalents. We have tentatively included the upper part of the White Spur Formation at Farrell Rivulet in the Tyndall cycle, and its equivalent in the Rosebery area, known as the Chamberlain Shale. This interpretation is compatible with the suggestion of McPhie and Allen (1992) that the lower part of the White Spur Formation at Hercules could be equivalent to the Southwell Subgroup.

2. Tyndall Group sequences in axial part of Dundas "trough"

Although the distribution of Tyndall Group sequences along the main Mt Read belt is reasonably well known from the Mt Read Project mapping, the nature and distribution of Tyndall equivalents to the west of the volcanic belt is less well understood. Company aeromagnetic surveys in the Yolande River area have picked up a probable Tyndall Group sequence in the vicinity of the Pearl Creek-Yolande River junction, and this has been confirmed by lithogeochemistry in this project. This zone has been extended northwards to include the western part of the Henty Fault Wedge sequence (Ewarts Track sequence of Poltock, 1992), based on strong lithogeochemical similarities of the basalts in that area to the Lynchford Member of the Tyndall Group at Queenstown (see Lithogeochemistry, this volume).

There appears to be a significant change across the position of the North Henty Fault, indicated by the disappearance of the Henty Fault Wedge basaltic sequence and an apparent 'shrinking' of the Tyndall Group so that it becomes difficult to recognise. We have tentatively assumed it to be represented by siltstones in the upper part of the White Spur Formation at Farrell Rivulet and Rosebery (Chamberlain Shale). At Dundas there appears to be little or no sequence preserved in the appropriate time range (Selley 1997).

In the Pinnacles–Silver Falls area, an equivalent of the lower Tyndall Group has been recognised from its magnetic signature and composition (McKibben, 1993), and this has been supported by geochemical work for this project. We have tentatively extrapolated this zone northwards into the Que–Hatfield area based on the distribution of the strongly magnetic zone, although it is recognised that the rocks in the western part of the zone include siliceous conglomerates of probable Owen type.

Further north, the anticlinal sequence beneath the Owen correlates (Denison Cycle) at St Valentines Peak contains Tyndall-age fossils and includes a probable welded ignimbrite within contact-metamorphosed sandstones and siltstones (Seymour et al., 1989; Jago et al., 1975). East of this, the volcaniclastic sequence at Native Track Tier also contains Tyndall-age fossils (Seymour et al., 1989), and the Tyndall correlation is supported by geochemistry (this volume). The southern part of the Native Track Tier area may be of different age, based on informal comments from industry personnel. The boundary position and relations are poorly constrained.

In the southern part of the Dundas "trough", the volcaniclastic sequence along the lower King River

has no biostratigraphic control, but contains basalts (Baillie et al., 1985) which have a geochemical signature suggesting affinities with the lower Tyndall (this volume). The sequence is tentatively correlated here with the Tyndall Group, and the overlying siliciclastic-micaceous sequence to the east with the Denison Cycle.

3. Tyndall Group equivalents in the Fossey Mountains and Dial Range "troughs"

The volcaniclastic sequence in the Winterbrook area, east of Black Bluff, has not yielded fossils but was tentatively correlated with the Tyndall Group by Pemberton and Vicary (1989) on the basis of general lithology and stratigraphic position. Our geochemical studies (this volume) support this correlation. The Winterbrook Tyndall sequence seems to be replaced eastwards by older rocks in the Bell Mountain area, but may reappear further east. Fossils collected by KDC at Paradise just northeast of Mt Roland, during mapping by Aberfoyle, are of probable Tyndall age (J.B. Jago, pers. comm., 1989; Laurie et al., 1995), and occur within siltstone lenses in an east-facing felsic volcaniclastic sequence. This occurrence raises the possibility that Tyndall equivalents may be widespread in this area.

In the Dial Range "trough", the Radfords Creek Group is a biostratigraphic equivalent of the Tyndall Group, and our geochemical studies support this. The large intrusive mass of the Lobster Creek porphyry has been correlated with volcanics in the Radfords Creek Group by Sproule (1995), and has a Tyndall-type geochemical signature (this volume). Correlation of this large intrusive complex with the Tyndall Group, as well as the other volcanic/intrusive units mentioned, raises the possibility of a widespread phase of intrusive-volcanic activity which is chemically, spatially and temporally different from the main Yolande Cycle volcanic activity, i.e. from most of the Mt read Volcanics.

4. General comment on Fossey Mountains "trough" stratigraphy

Very little biostratigraphic control is available for the complex sequences of the Fossey Mountains "trough", and most mapping is either too old or too fragmentary to allow useful integration. The Paradise fossils indicate that Tyndall Group equivalents are present in the Mt Roland area, and the Winterbrook geology suggests that these could be fairly extensive. The similarity of the 'Beulah Granite' to the Lobster Creek porphyry (KDC's observations) suggests that this phase of distinctive early Tyndall magmatism is also represented in the Fossey Mountains area.

Two localities of Late Cambrian fossils are known from the Fossey Mountains area. A loose block from the Mersey River near Weegeena (east of Beulah) is thought to have come from the 'Gog Range Greywacke' upstream (Jennings, 1979), and the second locality from near Lower Barrington (Banks, 1982) is also mapped as this formation. Thus the 'Gog Range Greywacke' is at least partly Denison Cycle, but the name appears to have been used as a basket term for all sandstone-siltstone sequences in the area, and is therefore likely to include equivalents of all three cycles.

5. Basin geometry

Cycle 1

This cycle encompasses the bulk of the Cambrian volcanic and volcaniclastic sequences, and reflects the time period between the emplacement of the nappes of ultramafics and associated rocks in about the early Middle Cambrian, and the consequent destabilising of the Tasmanian crust, and the Tyndall period near the close of Mt Read volcanism towards the end of the Middle Cambrian. Despite the complex history, the total time may only have been only 5–6 million years (Fig. 1).

Some of the earliest events are represented in the northern CVC-Black Harry Beds-Animal Creek Greywacke association. The early volcanic components have a strong calc-alkaline signature (negative TiO_2, P_2O_5, Nb anomalies) and are dominated by dacitic volcanics and volcaniclastics. The sedimentary sequences appear to have been deposited in deep water (below storm wave base) and with no obvious local sources. No sedimentological evidence was found for within-basin structural controls at this stage.

Towards the upper part of Cycle 1 the basin appears to have become much more locally variable. In the Que–Hellyer area, a discrete andesitic-basaltic volcanic centre developed with a new shoshonitic association. Other smaller centres with this affinity are scattered throughout the basin at upper Cycle 1

positions. The overlying Southwell Subgroup contains some relatively shallower water facies, and indications of some local derivation from intra-basinal faults (e.g. Murrays Road Greywacke and Mt Cripps Fault).

East of the Henty Fault, the Eastern Quartz-phyric Sequence sits directly on basement, and indicates that an eastern basin margin was well established at this time. Similarly, in the Dundas–Huskisson area, the westernmost exposures of the upper Cycle 1 sedimentary rocks were receiving mass-flow conglomerates from a western source, indicating that they were near to a margin of the basin. The Red Lead and Razorback Conglomerates possibly occupy a similar position to the Sticht Range Formation. Most of the northern CVC appears to have been buried by this time beneath the Southwell Subgroup, with some late activity indicated by the lava 'nose' at Burns Pinnacles.

The southern CVC partly overlies, and partly interfingers with, the Yolande River Sequence, and may be largely of upper Cycle 1 age. Considerable erosion of this unit occurred before the Tyndall cycle, suggesting there was a shallow water to emergent volcanic setting in parts of this area towards the top of Cycle 1. This erosional period seems to have followed a major phase of intrusive activity at or near the close of Cycle 1, marked by shallow emplacements of granites (Darwin, Murchison, etc.) and large porphyry bodies (e.g. Bonds Range Porphyry).

We have been unable to demonstrate that the Linda/Firewood Siding Fault system was active at this time, although emplacement of basaltic intrusives in the Pearl Creek area may indicate a structural control.

Most of the major VHMS deposits lie towards the top of the Cycle 1 stratigraphy well after the basin had become dominated by local effects. Evidence from the VHMS environments indicates an extensional tectonic regime, and we therefore interpret the basin complexity as being due to a phase of extensional faulting. The increasing basaltic magmatism evident towards the top of Cycle 1 probably reflects this extension and an increase in related thermal gradients. Granite intrusion may also have contributed to the thermal gradients.

Cycle 2

The Tyndall cycle was initiated in some areas by explosive basaltic volcanism and associated magmatic activity with a mild but distinct tholeiitic character, in contrast to the previous calc-alkaline igneous activity. The volcanic products are particularly evident as the basaltic detritus in the Lynchford Member around Queenstown, and possibly in the Sprent Formation of the Dial Range "trough" (although the Motton Spilites are a possible source for the latter). The Henty Fault Wedge basalts and associated dykes have the appropriate geochemical character to have been the source of the Lynchford detritus, and it appears that the western part of the Wedge may have been a major volcanic source for the early Tyndall cycle. Other possible sources identified in our preliminary study are the Lobster Creek porphyry (and its probable correlate, the Beulah "granite"), and the lower King River basalts. Another possibility are the metadolerites which intrude Southwell Subgroup and Tyndall Group rocks in the Mt Tor area (Pemberton and Vicary, 1988), but there are insufficient data to confirm this.

The volcanism appears to have introduced a large amount of magnetite into the environment, to the extent that the early Tyndall sandstones produce a distinct magnetic anomaly in many areas.

As the maps show, the Tyndall Group appears to have been deposited in a series of separate and partly separate basins along the Mt Read belt, many of which were overlapped and buried by Cycle 3 siliciclastics. Much of the material was derived from weathering of pre-existing volcanics, with sub-volcanic granites unroofed and eroded at Mt Darwin and probably Mt Murchison. Contacts between Cycle 1 and Cycle 2 vary from erosional and unconformable (e.g. at Mt Darwin) to gradational and interbedded (e.g. at Comstock near Mt Lyell, where andesite lavas are interbedded within the lower Tyndall sequence (KDC observation). In the Murchison–Selina area, the Tyndall group appears to be represented only by isolated basins of volcaniclastic conglomerate, and no Tyndall Cycle rocks have been recognised between here and the southern part of the Black Bluff Range. Detailed studies such as at Red Hills (White, this volume) suggest the absence of Tyndall Group from this area is a result of erosion rather than non-deposition.

A dramatic change is evident across the position of the North Henty Fault in the Farrell Rivulet area, where the Tyndall Group becomes difficult to recognise and appears to be represented only by a siltstone-mudstone unit below the Stitt Quartzite correlate. The Cycle is even less obvious in the Dundas section. This lack of development suggests either that the area was somewhat emergent (but why no input from the Henty Fault Wedge volcanoes, from which detritus easily reached a greater distance to Lynchford?), or that it was a local restricted basin with no access to the south, or that it was much further away than it is now.

The Tyndall Cycle re-appears 'in strength' in the Pinnacles area (where the typical magnetic signature is well developed), and also to the east at Mt Cripps. No obvious magmatic sources for these areas have yet been recognised. The extensive areas of Tyndall equivalents at St Valentines Peak and Native Track Tier may be a continuation of the axial basin evident at the Pinnacles, and there is probably continuity into the Dial Range "trough". The fault marking the southeastern limit of the Native Track Tier sequence appears to be an important structure, and could possibly be a continuation of the Henty Fault system.

The Winterbrook area appears to represent a deep basin of Tyndall Group rocks exposed within an anticlinal core of Cycle 3 siliciclastics. The presence within the sequence of probable welded ignimbrites, and of abundant conglomerates, suggests relatively shallow water to emergent conditions. The strip of volcaniclastic conglomerates overlying Southwell Subgroup rocks in the Mt Cattley–Mt Tor area probably represents the western margin of this basin. The eastern margin probably lies close to the Bonds Range Porphyry. Ignimbritic rocks seen in 'windows' on the Black Bluff Range (Vicary and Pemberton, 1988) are mostly probably Tyndall correlates. Similar large basins of Tyndall age rocks are likely to be present in the Mt Roland–Gog Range area.

Cycle 3

Accepting a strict biostratigraphic definition for Cycle 3 has resulted in much more of the map being given over to Owen-Denison correlates than was previously apparent. While the Denison Cycle sedimentary rocks are very widespread the upper Denison Cycle coarse conglomerates (classic Owen/Roland Conglomerate) are thickest in distinct zones such as Mt Strahan-Professor Range-Mt Zeehan, West Coast Range, Black Bluff, Mt Roland.

Sedimentation related to contemporaneous folding (Professor Range, Berry 1996) and fault inversion (Henty Fault, Great Lyell Fault) was a feature of Cycle 3. Very active erosion of the eastern (Tyennan) margins dominates a large part of the basin, but a significant input from the west and from intra-basinal sources (particularly cherts) is also apparent.

Most of the Cycle appears to be coincident with east–west compression and basin inversion, but it is not clear how early the folding begins. For example, the lower half of the sequence on the Professor Range section dips at 30¡ by the end of the cycle, and we could not detect any angular difference in folding between lower Cycle 3 and Cycle 2 in this section (Berry 1996). Major fold amplification (limb dips over 10∞) is apparently delayed until after Iverian (Newton Creek and Professor Range faunas) in most places.

Summary

The three fold stratigraphy proposed for the Cambrian stratigraphy of western Tasmania has been adjusted to fit more recent results and also the suggestions of the Seymour & Calver (1995b). This subdivision has been applied to the Dundas, Dial Range and Fossey Mountain "troughs". The cycles are biostratigraphic in concept but additionally litho- and chemo-stratigraphic criteria have been used to produce the distribution map. The classification separates the stratigraphy into Late Cambrian, late Middle Cambrian and middle Middle Cambrian.

The Dundas "trough" has the largest database and while fossil control is much less than we would prefer there is a reasonable basis for classifying each substantial block into one of the three cycles. The most difficult task was defining a base for Cycle 3 in the area of Dundas and the Rosebery group where Cycle 2 is missing, or lacks defining characteristics. In the Dial Range "trough", biostratigraphic and geochemical data provide a reasonable basis for the subdivision of Middle to Late Cambrian rocks along the same lines as in the Dundas "trough". Very little biostratigraphic control is available for the complex sequences of the Fossey Mountains "trough" and our extension of the three stratigraphic cycles into this area is speculative.

The oldest part of Cycle 1 is the northern CVC-Black Harry Beds-Animal Creek Greywacke association. These sedimentary sequences appear to have been deposited in deep water. No sedimentological evidence was found for within-basin structural controls at this stage. Towards the upper part of Cycle 1 the basin contains more variable styles of deposition and a discrete eastern and western basin margin is recognisable. Most of the major VHMS deposits lie towards the top of the Cycle 1. We interpret the basin complexity at this stage, and the increased basaltic volcanism, as results of active extensional faulting.

Contacts between Cycle 1 and Cycle 2 vary from erosional and unconformable (in the southeast) to continuous deposition. Cycle 2 is recognisable as a distinctive unit everywhere except the far west (Dundas/Husskisson/Rosebery area).

The Tyndall Cycle was initiated in some areas by explosive basaltic volcanism and associated magmatic activity with a mild but distinct tholeiitic character. The volcanism appears to have introduced a large amount of magnetite into the environment, to the extent that the early Tyndall sandstones have an associated distinct magnetic anomaly in many areas.

The base of Cycle 3 lies on an angular unconformity east of the Henty Fault but continuous sedimentation is inferred over most of the basin. The Cycle appears to be coincident with east–west compression and basin inversion, with the major fold amplification delayed until after the Iverian.

References

Baillie PW & Corbett KD 1985. Geological Survey Explanatory Report Strahan 1:50,000 sheet. Department of Mines, Tasmania 76 pp.

Banks MR 1982. Cambrian fossils and fossil localities in Tasmania - a catalogue and a range chart. University of Tasmania, Hobart, 48 pp.

Berry RF 1996. A structural cross-section of the Mt Read Volcanics at 535000N. AMIRA project 291A. Report 5, 1–11.

Corbett KD, Pemberton J & Vicary MJ 1993. Geology of the Mt Jukes-Mt Darwin area. Mt Read Volcanics Project Map 13. Mineral resources Tasmania.

Crawford AJ, Corbett KD & Everard JL 1992. Geochemistry of Cambrian volcanic-hosted massive-sulfide-rich Mount Read Volcanics, Tasmania, and some tectonic implications. Econ Geol. 87, 597–619.

Jago J B 1979. Tasmanian Cambrian biostratigraphy - a preliminary report. J Geol. Soc. Aust. 26, 223–230.

Jago JB, Pike GP & Mills D, 1975. Cambrian stratigraphy of the St Valentines area, northwest Tasmania. Pap. Proc. R Soc Tasm 109, 85–90.

Jell PA, Hughes NC & Brown AV, 1991. Late Cambrian (Post-Idamean) trilobites from the Higgins Creek area, western Tasmania. Memoirs of the Queensland Museum, 30 (3), 455–485.

Jennings IB, 1979. Sheffield. Geological Survey Explan Report. Tasm. Department Mines.

LaurieJR, Jago JB & Bao J-S, 1995. Review of Cambrian biostratigraphy. AGSO Record 1995/69

McKibben J A J 1993. The geology and geochemistry of the North Pinnacles Ridge, western Tasmania. BSc Hons. thesis (unpubl.).

McPhie J & Allen RL 1992. Facies architecture of mineralized submarine volcanic sequences: Cambrian Mt Read Volcanics, western Tasmania. Econ Geol 87, 587–596.

Pemberton J & Corbett K D 1992. Stratigraphic-facies associations and their relationship to mineralisation in the Mt Read Volcanics. Bull. Geological Survey Tasmania. 70, 167–176.

Pemberton J & Vicary MJ 1988. Geology of the Mt Cattley-Mt Tor area. Mt Read Volcanics Project Map 8. Geological Survey Tasmania.

Pemberton J & Vicary MJ 1989. Geology of the Winterbrook Moina area. Mt Read Volcanics Project 1:25000 Map 9. Tasmania Dept Mines, Hobart

Pemberton J, Vicary MJ & Corbett KD, 1991. Geology of the Cradle Mountain Link Road–Mt Tor area. Geological Report Mt Read Volcanics Project Tasmania, 4

Poltock R 1992. Geology of the Henty Fault wedge, western Tasmania. M Econ Geol Thesis, Univ Tasm (unpubl.) 76pp.

Selley D 1997. Structure and sedimentology of the Dundas Group, western Tasmania. PhD, Univ. Tas. (unpubl.).

Seymour DB et al., 1989. Geological atlas 1:50,000 series St Valentines. Explanatory Report. Geological Survey Tasmania.

Seymour DB & Calver CR 1995a. Stratotectonic elements map of Tasmania.. Geological Survey Tasmania.

Seymour DB & Calver CR 1995b. Explanatory notes for the time-space diagram and stratotectonic elements map of Tasmania. Tasmania Geological Survey Record 1995/01.

Sproule RA 1994. Stratigraphy and geochemistry of the Dial Range Trough, NW Tasmania. BSc Hons. Thesis Uni. Tas. (unpubl.).

Vicary MJ & Pemberton J, 1988. Geology of the Back Peak– Cradle Mountain area. Mt Read Volcanics Project Map 7: Dept Mines, Tasmania.

Appended maps (map pocket)

Figure 2. Map at 1:250,000 scale showing distribution of three stratigraphic cycles of the Cambrian in the Dundas "trough" north of Macquarie Harbour. (Based on the Mines Department of Tasmania 1:250,000 digital geology map. Changes as indicated in the text.)

Figure 3. Map at 1:100,000 scale distribution of three stratigraphic cycles of the Cambrian in the Dundas "trough". (Based on the Mines Department of Tasmania 1:250,000 digital geology map. Changes as indicated in the text.)

Figure 4. Map at 1:100,000 scale distribution of three stratigraphic cycles of the Cambrian in the Fossey Mountain "trough" and Dial Range "trough". (Based on the Mines Department of Tasmania 1:250,000 digital geology map. Changes as indicated in the text.)

Mt Cripps Fault: Evidence for Cambrian movement

Ron Berry, Keith Corbett & Stuart Bull
CODES Special Research Centre, Geology Department, University of Tasmania

Abstract

Detailed investigation of the Mt Cripps Fault was used to test the model that it was a transfer fault in the Middle Cambrian. Sedimentological studies targeted the Murrays Road Greywacke and the Animal Creek Greywacke. The variation in provenance and facies variations indicate the Mt Cripps Fault was present during the deposition of the Southwell Subgroup but no evidence was found for activity on this fault during the deposition of the Animal Creek Greywacke. The structural interpretation suggests that the Mt Cripps Fault was a relatively small feature during the late stage of the Yolande Cycle with an offset less than the thickness of the Southwell Subgroup, but sufficient to lift the southern block into a subaerial position.

Introduction

The Mt Cripps Fault was identified as a major Cambrian transfer fault in the final report of the AMIRA project P291. The evidence for this was largely based on differences between structure and stratigraphy north and south of this fault. The model proposed suggested a major Cambrian normal fault roughly in the position of the Henty Fault was offset along this structure and this offset was not entirely a result of Late Cambrian and Devonian compressional tectonics. The aim here is to consider sedimentological evidence in the context of an improved structural assessment of the immediate environment.

In order to clarify the structure in this area, new cross-sections were drawn north (5396000mN) and south (5392000mN) of the Mt Cripps Fault. These sections include detailed information from the Que River and Hellyer Mine Leases made available by Aberfoyle Ltd.

The most suitable sedimentological target for the recognition of growth faulting on the Mt Cripps Fault is the Murrays Road Greywacke, a sandstone/granule-pebble conglomerate unit within the Southwell Subgroup extending from north of the Cradle Mountain Link Road to the Mt Cripps Fault (Vicary & Pemberton, 1988; Komyshan, 1986).

The Murrays Road Greywacke is stratigraphically much higher than the Hellyer and Que River deposits. In order to test that the Mt Cripps Fault was active during the mineralising phase we should be looking much lower in the stratigraphy. However there are no suitable clastic rocks exposed along the Mt Cripps Fault that represent this stratigraphic level. The Animal Creek Greywacke is exposed near the Henty Fault between the Que River mine and the Sharks Fin. At this point the Henty Fault is terminated or offset by the Mt Cripps Fault and the proposed activity on the Mt Cripps Fault is linked in the original interpretation to normal faulting on the Henty Fault. As the Animal Creek Greywacke is stratigraphically below the Hellyer deposit, we have investigated these exposures to bracket the relevant age. Near the Sharks Fin the Animal Creek Greywacke is exposed within a few hundred metres of the Henty Fault. No examples of Animal Creek greywacke are known immediately east of the Henty Fault. The provenance and sedimentology of this area are discussed below.

Murrays Road Greywacke

The Murrays Road Greywacke (Corbett & Komyshan, 1989; Pemberton et al., 1991) is a 200 m thick sequence of interbedded sandstone, siltstone and granule-pebble conglomerate within the Southwell Subgroup. The unit extends from the Mt Cripps Fault northwards along the eastern side of the Southwell River to the Cradle Mountain Link Road, where it disappears under Tertiary basalt (Fig. 1). The unit dips and faces east, and is underlain and probably intruded by a sill-like body of felsic porphyry. The aim was to examine the sequence to determine if there were recognisable changes in composition and/or grainsize which could be related to movement on the Mt Cripps Fault during sedimentation. The exposures proved inadequate for normal facies studies, but sufficient material was available for general consideration of grain size variations and the sampling of coarser-grained units to look at provenance.

Initial sampling of the unit was done by R.F. Berry in the area adjacent to the Mt Cripps Fault (as reported in Report 5), and petrological examination was carried out by K. Corbett. The three main localities were at distances of 100 m, 150 m, and 300 m from the fault (Fig. 1), with a fourth locality at about 800 m from the fault. Subsequent sampling was done on the Cradle Mountain Link Road, 4 km north of the fault, by K. Corbett. Six samples suitable for thin sectioning were obtained, mostly from float boulders since the road section outcrops were too weathered.

The sequence at the Cradle Mountain Link Road, as exposed immediately west of the Murrays Road intersection, is of the order of 100 m thick, of which the lower 50 m is predominantly grey siltstone, followed by 10–15 m of sandstone, followed by 20 m of conglomeratic beds, followed by 20 m or so of mainly sandstone. The upper part of the unit, east of the Murrays Road, is poorly exposed but appears to be mainly volcaniclastic sandstone. The samples are all from the conglomeratic section, with MRG1–MRG4 being from a bulldozed track north of the road, MRG5 from a loose block on the south side of the road, and MRG6 from a cutting on a branch road 100 m south of the highway.

The conglomeratic units are up to pebble grade (clasts to 30 mm), and typically form beds up to 2 m thick which are graded from pebble-granule conglomerate at the base to sandstone at the top. The sequence generally appears to be of proximal to distal turbidite type.

Grainsize variations

The southernmost locality, nearest the Mt Cripps Fault, consisted of float boulders with a high ratio (>50%) of conglomeratic material. The next locality, at 150 m distance, comprised discontinuous outcrops over 50 m, of which about 30% was conglomeratic. The locality at 300 m distance comprised some 30 m of nearly continuous exposure, in which only one bed was conglomeratic. Although the available outcrop at the localities was insufficient to establish any grainsize variations with certainty, within the unit as a whole, the observations were clearly suggestive of a rapid decrease in the proportion of coarse material away from the fault. The fourth locality, 800 m from the fault, showed about 10% of the exposed stratigraphy to be conglomeratic.

The sampling from the Cradle Mountain Link Road indicates that about 20% of the main part of the section is conglomeratic, and that actual grainsize of the coarser material is at least as coarse as that from the samples close to the fault (i.e. pebbles to 3 cm). There was some indication from the Link Road area that the conglomeratic material was forming a larger proportion of the float boulders than it represented in outcrop, possibly because of its more massive nature initially.

Thus it cannot be argued that there is an overall increase in clasts size towards the Mt Cripps Fault. In terms of the proportion of conglomeratic material present, it seems highly likely that this will vary along strike according to where the main depositional lobes (fans) are located, and this will be largely controlled by depositional conditions between the sampled area and the main source area — presumably a Tyennan-type metamorphic terrain, since the overwhelming majority of clasts are of metamorphic derivation. However, lobe-fan formation could be influenced by local faulting, and the apparent increase in proportion of coarse material noted near the Mt Cripps Fault could reflect contemporaneous movements on that structure.

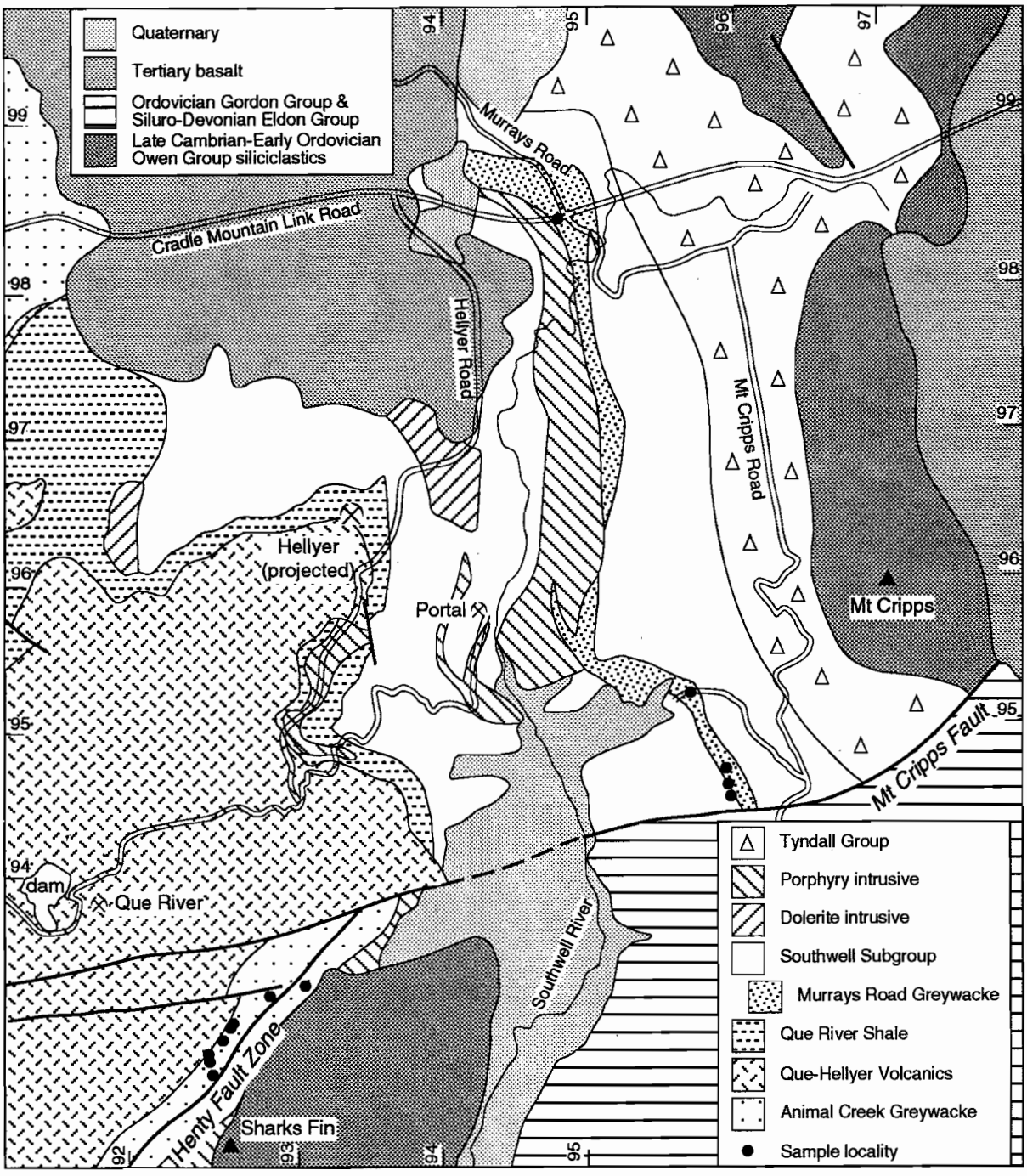

Fig. 1 Location map for samples of Animal Creek Greywacke along the Henty Fault. The outline of the Henty Fault and the distribution of the Animal Creek Greywacke is from Komyshan (1986).

Provenance

The four relevant samples from the locality nearest the fault (MC3/1, 2, 4, 5) show a consistent detrital composition as follows: @60% metamorphic clasts (quartzite, quartz-mica phyllite, phyllite); @20% chert (fine-grained, 'muddy' appearance with very fine sericite in some cases, rarely with internal quartz-±hematite veining, usually structureless, probably of Cambrian age); @10% felsic volcanics/intrusives, including feldspar–quartz ± biotite porphyry; @2–5% mafic volcanics/intrusives, usually chlorite-altered; minor amounts of sedimentary clasts (sandstone, siltstone, dark mudstone), quartz and feldspar grains of probable igneous (granitic?) origin, and various indeterminate clasts.

Two samples from the next locality out (MC2/1, 2) are dominated by metamorphic (quartzite) detritus, with little obvious volcanic material, and only one small chert clast each. The one sample from the 300 m locality (MC1/1) is also dominated by metamorphic detritus, with no identifiable volcanic clasts and only one small chert clast. The one sample from the 800 m locality (MC4) is a medium-grained sandstone lacking coarse material, and is therefore difficult to compare with the conglomeratic samples. It is rich in small clasts of quartzite and chert, and has some possible igneous/volcanic quartz grains.

The Cradle Mountain Link Road samples (MRG1–MRG6) are fairly consistent in their clast composition. All are dominated by metamorphic material (quartzite, quartz-mica phyllite, phyllite, schist) which constitutes about 90% of the clasts. Other clast types present are chloritised amphibolite (?), felsic porphyry (particularly an altered feldspar–quartz ± biotite porphyry), altered mafic rock (ranging from basaltic to gabbroic in texture), chert, coarse-grained feldspar (granitic?), and yellowish 'amorphous' to poorly crystalline material of uncertain origin.

The only notable change in clast composition along strike appears to relate to the high ***chert*** component in the samples closest to the fault. The four relevant samples here each have several dozen chert clasts (about 50 in MC3/1, a similar number in MC3/2, about 40 in MC3/4 and about 25 in MC3/5), whereas none of the comparable coarse samples from the other localities has anything approaching this abundance. The two samples from the 150 m locality contain only one small chert clast each, as does the granule-grade sample from the 300 m locality. Of the Cradle Mountain Link Road samples, MRG1 has 4–5 chert clasts, and the other five samples have one each plus several 'cherty-altered porphyry' clasts. The latter represent a felsic porphyry with small quartz and feldspar phenocrysts and a groundmass which has largely been altered to fine cherty silica. Patches or clasts of similar cherty-altered porphyry can be seen in sample MC3/3 from close to the Mt Cripps Fault. This sample appears to represent a primary volcaniclastic rock (i.e. locally derived from a volcanic source) formed by breakdown of a porphyry body similar to that which directly underlies (and probably intrudes) the Murrays Road Greywacke along much of its length. However, the bulk of the chert clasts in the other MC3 samples are uniformly fine-grained and lacking phenocrysts, and may have a different origin.

The sample from the 800 m locality (MC4) also contains abundant small grains of similar chert to that in the MC3 samples, and possibly represents a more distal part of one of the conglomeratic mass-flows occurring close to the fault.

Further, more rigorous sampling would be required to compare chert compositions through the full thickness of Murrays Road Greywacke at sufficient sites to demonstrate any real variations related to the Mt Cripps Fault. However, the preliminary data suggest that the fault could have been responsible for exposing a source of chert clasts which were concentrated in mass-flows close to the fault.

At drill hole MXRD-1, a further 5 km to the north, there is 40 m of section of Murrays Road Greywacke in the core but there are no granule conglomerates present. The coarsest unit examined was a coarse sandstone, beds of which are up to 15 cm thick and have a mass flow character. The largest fragments present are of black shale and there is no evidence for coarse quartz grains (all less than 2 mm). The ambient facies at this locality comprises approximately 80 % of the section and consists of laminated/thinly interbedded fine-grained sandstone, siltstone and mudstone. In some areas intervals of climbing/amalgamated ripples in silt and/or fine-grained sandstone clearly infill scours. This indicates agitated bottom water conditions and, in contrast to the situation described below for the Animal Creek

Greywacke intersections, suggests the unit accumulated in relatively shallow water depths (i.e. < 100 m). A similar ambient facies has been described in an earlier report from the Stitt Quartzite in the Rosebery area (Report 1: 11–14).

Animal Creek Greywacke

The Animal Creek Greywacke was examined in two drill core intersections, one from the Middlesex Road area (MXRD1; 601.5 m to EOH) and one from the Black Harry Road area (BLHY1; 121–203 m). The Middlesex Road intersection is constrained by overlying units to be the uppermost part of the unit, however, the Black Harry intersection is stratigraphically unconstrained. The ambient facies in each case was delicately laminated/interbedded siltstone and mudstone with no significant evidence of current reworking. This indicates that the host environment for both localities was a quiet, reduced, sub-wave base setting that probably represented considerable water depths (i.e. hundreds of metres).

Interbedded mass flows in both areas consist of both volcaniclastic and micaceous sandstone beds. The former comprise the bulk of the mass flow part of the Black Harry intersection, but are only a minor component in the Middlesex Road intersection. At both localities they tend to be a few metres (maximum 8 m) thick, variably pumiceous and feldspar-phyric. Some quartz was also present in units from the Black Harry area. The variable proportions of volcaniclastic material present may relate to the stratigraphic position of the sections. A tuffaceous sequence is present beneath the greywacke-dominated Animal Creek Greywacke in the area that was originally considered as the lower part of the unit (Pemberton et al., 1991). The Black Harry intersection in which the mass flows are predominantly volcaniclastic, and which is stratigraphically unconstrained, may be low in the Animal Creek Greywacke unit and close to this underlying tuffaceous sequence.

The micaceous sandstone beds vary markedly in character between the two localities. In the Middlesex Road area, where mass flows comprise about 70 % of the section, the micaceous sandstone units are are the dominant unit present. Beds are relatively thick (i.e. up to at least 2 m), often amalgamated and commonly have basal mudstone intraclasts. This type of facies association suggests channelised deposition close to the feeder axis for the mass flows. In terms of submarine fan models for turbidite systems (e.g. Report 1: 12; Figure 6), it would correspond to a middle fan (i.e. relatively proximal) setting. In the Black Harry area, where mass flows comprise only about 30–40 % of the section, they are relatively thin (less than 15 cm) and are only a minor mass flow component relative to the thicker and more abundant volcaniclastic units. This would clearly correspond to a lower fan/basin plain (i.e. relatively distal) setting. The fact that apparently distal (i.e. Black Harry area) and proximal (i.e. Middlesex Road area) fan elements both occur within the same ambient quiet water mudstone facies, provides further evidence for considerable water depths at Animal Creek Greywacke time.

Samples of sandstone from the Animal Creek Greywacke in these drill holes described above (MXRD1 at 625.6m, 684.8m and 742.7m) were compared to samples of sandstone from along the Henty Fault south east of Que River (Fig. 1). The sandstones in MXRD1 have angular fragments of quartz, metamorphic rock fragments and minor chromite in a recrystallised micritic matrix. The sandstones exposed south east of Que River have the same even grained sandstone texture found throughout the Animal Creek Greywacke. No coarser facies was found. Thin sections of seven samples from this area were studied and these are identical to the more distal Animal Creek Greywacke except that the carbonate has been removed by weathering. Despite the fact that this area is within 500 m of the Henty Fault no effect on the sedimentology or sedimentary petrography was detected at the stratigraphic level of the Animal Creek Greywacke.

Structural sections

Two new structural sections (Figs 2, 3) were drawn to compare the structure north and south of the Mt Cripps Fault. The basic dataset for this interpretation is the Mt Read Project maps 1 (Komyshan, 1986), 2 (Corbett & McNeill, 1986) and 7 (Vicary & Pemberton, 1988), the Mackintosh 1:63,360 sheet (Barton et al., 1966) and the Tullah 1:50,000 compilation (Green &

Bamford, 1986). The new sections draw on the original sections and data in P291 Reports 1 and 5. The western end of these sections is drawn directly from the section given in the P291 Final Report. The dips of structures are shallower because these lines are now drawn E–W to facilitate application of geophysical modelling and match the orientation of proposed Cambrian structures. The previous versions were drawn perpendicular to Devonian fold axes. The area over the Que–Hellyer region has been improved by reference to Aberfoyle confidential data. The sections here are drawn at a smaller scale than the data made available so some of the smaller structures recognised by Aberfoyle geologists could not be shown. The Black Harry beds are shown here as continuing to thicken to the east as a distal apron to a thinning CVC. This is taken as a mirror of the relation of the Yolande River Group to the southern CVC. The truncation of the Que Hellyer Volcanics against the Southwell Subgroup is based on Aberfoyle data. This would require a steep topographic surface on this side of the volcanic edifice (~10°).

The eastern section is much clearer because the sections does not cross the Mt Cripps fault obliquely as was the case in previous versions. The structure along the line 5396000mN is relatively well constrained by the surface geology and follows the sub-surface interpretation of Pemberton et al. (1991). The dip of the Henty Fault extension is taken as parallel to dips measured to the south. The deeper structure with growth faults are projected from south of the section.

South of the Mt Cripps Fault the whole section east of the Henty Fault is covered in Owen Conglomerate or younger units. The surface structure is simple. In the far west against the Henty Fault the underlying material is based on Aberfoyle mapping south of the Sharks Fin. The central section is poorly constrained. The provenance data from the Murrays Road Greywacke above suggests that there is a source for basement, porphyry and especially chert in this section. The interpretation here is that this indicates a thin cover of Southwell Subgroup over basement, and the Bond Range Porphyry does not extend this far west. This interpretation is consistent with the structure north of the Mt Cripps Fault and suggests that this fault was a relatively small feature at the time of deposition of the Southwell Subgroup, having an offset in this position of less than the thickness of the Southwell Subgroup, but sufficient to lift the southern block into a subaerial position.

Conclusions

Detailed investigations along the Mt Cripps Fault have provided supporting evidence that the fault was present during the deposition of the Southwell Subgroup. No additional evidence has been found for the existence of this structure during the earlier part of the Mt Read depositional cycle.

References

Barton, C.M. et al., 1966. Geological atlas one mile series Sheet 44 (8014N) Mackintosh. Dept Mines Tasmania.

Corbett, K.D. & Komyshan P., 1989. Geology of the Hellyer–Mt Charter area.. Mt Read Volc. Project Tasm. Geol. Rep. 1 Dept Mines Tasm..

Corbett, K.D. & McNeill, A.W., 1986. Mt Read Project. Map 2. Geology of Rosebery–Mt Block area. 1:25,000. Dept. Mines Tasm.

Green, G.R. & Bamford, A.L., 1986 Mt Read Volcanics Project, 1:50,000 Metallic mineral deposit map series: Tullah. Dept Mines Tasm.

Komyshan, P., 1986. Mt Read Project. Map 1. Geology of the Mt Charter–Hellyer area. 1:25,000. Dept. Mines Tasm.

Pemberton, J., Vicary, M.J. & Corbett, K.D., 1991. Geology of the Cradle Mountain Link Road–Mt Tor area (Maps 7 and 8). Mt Read Volc. Project Tasm. Geol. Rep. 4. Dept Mines Tasm.

Vicary, M.J. & Pemberton, J., 1988. Mt Read Project. Map 7. The geology of the Back Peak–Cradle Mountain Link Road area. 1:25,000. Dept. Mines Tasm.

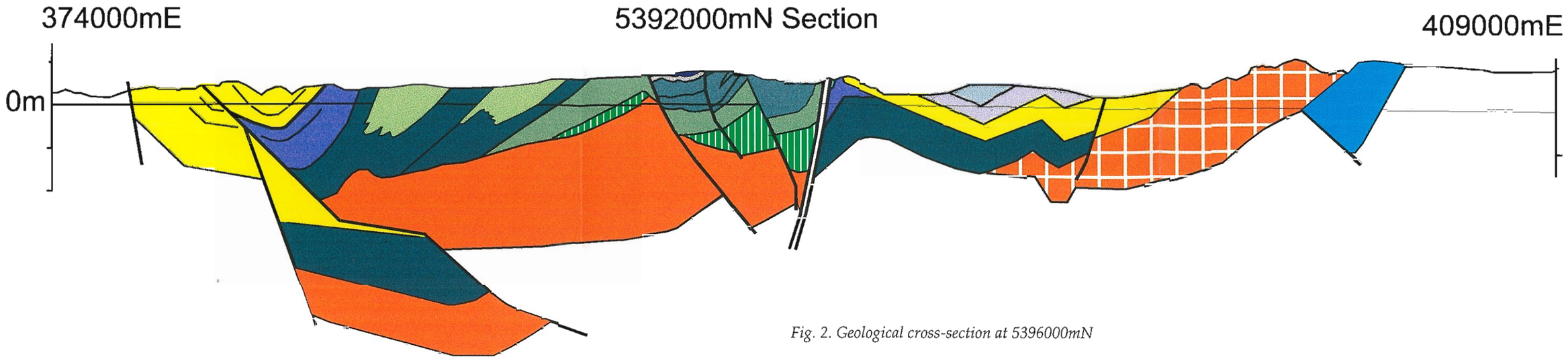

Fig. 2. Geological cross-section at 5396000mN

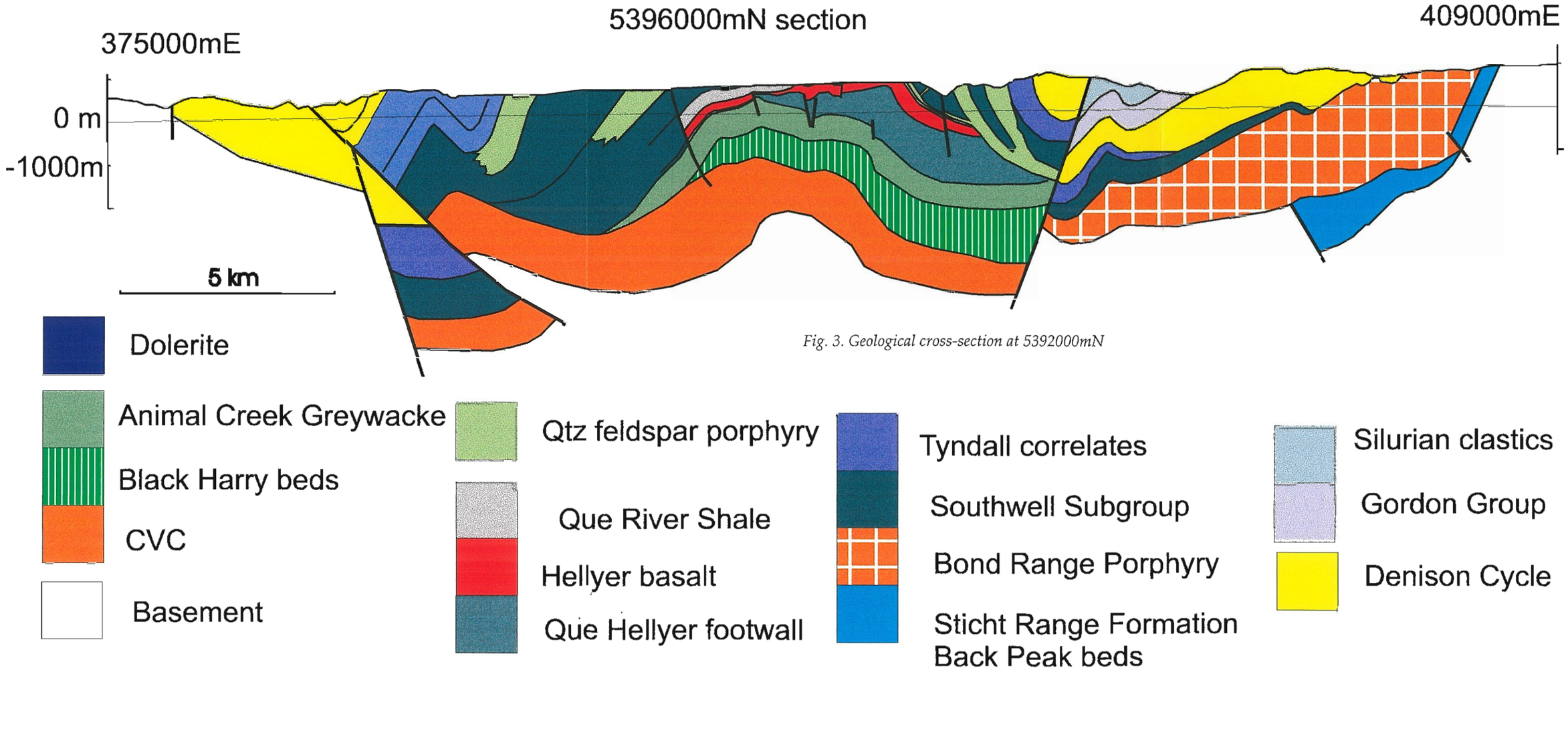

Fig. 3. Geological cross-section at 5392000mN

Structure and sedimentology of Middle and Upper Cambrian strata adjacent to the Firewood Siding Fault

David Selley and Sebastien Meffre
CODES Key Centre, Geology Department, University of Tasmania

Abstract

A near complete section of Middle to Upper Cambrian strata is exposed north of the Firewood Siding Fault. This succession records a prolonged period of below wave base sedimentation sourced primarily from extrabasinal basement sources, but with a locally significant volcanogenic and intrabasinally-derived component particularly towards the base. During the upper part of the Yolande Cycle, a change in basin geometry is heralded by the influx of medium to coarse-grained detritus and the development of a slope fan system. Significant basin activity also occurs in the upper part of the Denison Cycle with dominantly coarse-grained debris accumulating in narrow, laterally restricted depocentres which potential mark the onset of Late Cambrian folding in the area.

The structural geometry of the region north of the Firewood Siding Fault reflects the interaction of Cambrian and Devonian structures. N- to NNE-trending Cambrian structures were tightened and rotated during the main Devonian folding episode. Sinistral movement on the Firewood Siding Fault occurred coevally with Devonian folding and has resulted in a complex fold interference pattern that is not evident north of this major fault.

Introduction

This report presents the results from three traverses through Middle to Late Cambrian strata positioned immediately north of the Firewood Siding Fault (FSF). It forms one of a series of studies undertaken as a part of the AMIRA P.291A project which utilise sedimentological and structural techniques to establish basin geometries during the Cambrian. Most of the data presented was collected during field work for this study, however interpretations draw together significant contributions from previous and contemporary P.291 and P.291A studies (Berry and Keele, 1993; Bull, 1994; 1995; Keele, 1995; Berry, 1996).

Although there is widely accepted evidence for Late Cambrian tectonism in the region north of the FSF as demonstrated by the unconformity at the base of the Pioneer Sandstone (Baillie and Corbett, 1985), there is little stratigraphic evidence for extensional basin activity during the Middle Cambrian, in particular at the time of massive sulphide mineralisation. The main priority of this study was to investigate the Middle Cambrian sedimentary record in order to test the model proposed by Berry and Keele (1993) that the FSF was active as a major transfer structure during this period. In addition, I aimed to evaluate the significance of the local Cambrian fold geometries interpreted by Keele (1995) and Berry (1996), in terms of their implications for Late Cambrian basin development and their geometric control over Devonian fold generations.

Stratigraphy and sedimentology

The pre-Pioneer Sandstone stratigraphy north of the FSF includes litho- and bio-stratigraphic correlates of Yolande, Tyndall and Denison Cycles. This stratigraphy has a minimum thickness of 3 km and although closely to tightly folded, youngs mainly towards the west.

Yolande Cycle correlates

The most complete section of Yolande Cycle strata is situated east of the Henty Fault (Fig. 1). This sequence of rocks is formally known as the Yolande River Sequence (Corbett, 1992). Rocks young and dip steeply westward for the most part, but are folded about a major synclinal closure adjacent to the Henty Fault. It comprises at least 1900 m of intercalated shard- and pumice-rich volcaniclastic rocks, micaceous quartz-dominated greywacke, conglomerate, mudstone and minor felsic and basic volcanic rocks. A smaller fault-bounded sliver of volcanogenic sandstones and mudstones in the region of the Queensbury Mine have been interpreted as Tyndall Cycle by Corbett et al. (this report).

Two traverses through Yolande Cycle correlates were mapped as a part of this project: (1) the section along Pearl Creek between Madam Howards and the FSF (near 376200E–5344875N), and (2) the Yolande River section west of the Murchison Highway bridge to the base of the Tyndall Cycle correlates near 374675E–5344675N. The Pearl Creek section closely follows the trace of the FSF and was chosen due to its proximity to the proposed Cambrian transfer fault. It was hoped that if locally derived material had been shed northward of this structure during the Middle Cambrian, evidence in the form of slumped strata or texturally immature sedimentary breccias would be contained in the immediately adjacent strata. Further potential evidence for growth fault activity could be identified through comparison of this section with the Yolande River traverse 4km to the north. Lateral facies variation or the identification of erosional surfaces between these two sections would be expected in a tectonically active sedimentary environment. Exposure along both sections was sufficient to construct a coherent stratigraphy.

On the basis of this mapping, a broad two-fold stratigraphy is proposed: 'lower' and 'upper' Yolande Cycle. The boundary between the two packages occurs at 375500E–5345850N in the Yolande River and is defined by an abrupt change in the strike of bedding and lithofacies (Fig. 1). Only the lower part of this stratigraphy occurs in the Pearl Creek section.

'Lower' Yolande Cycle

The stratigraphy of the 'lower' Yolande Cycle is shown in Figure 2. In general, there is good correlation of lithofacies between the Pearl Creek and Yolande River sections and no significant variation in the thicknesses of individual rock packages is discernible. The diagrams show an gross upward transition from fine-grained, felsic vitriclastic sandstone and background mudstone to a slightly coarser-grained division comprising micaceous sandstone, pumice breccia and subordinate mudstone. Influx of medium- to coarse-grained sandstones with mixed volcanogenic-sedimentary provenance occurs approximately 700 m above the base of the Pearl Creek section. The percentage of volcanic detritus in these sandstones decreases progressively up section. Geochemical and petrographic analysis of a micaceous sandstone unit from the upper part of the Pearl Creek section reveals a dominant source component derived from metamorphosed Precambrian rocks as well as a conspicuous contribution from the mafic-ultramafic complexes (see Berry et al., this volume). Thick to very thick units of pumice breccia (up to 80 m thick) occur throughout the package, but become volumetrically significant towards the top. In addition to pumiceous detritus, they also contain crystal and lithic components which vary in both abundance and composition. The dominant crystal component is quartz in basal sandstones, but becomes increasingly feldspar-rich up section, implying a transition from felsic to more intermediate magmatism with time.

At the top of the Pearl Creek section is a thick, clinopyroxene + plagioclase–porphyritic basaltic andesite unit. The upper contact of this unit was not mapped making it difficult to unequivocally establish its mode of emplacement. The basal margin does not appear to transgress bedding however and peperitic textures were recognised along the contact with host rocks, implying interaction of hot magma and wet sediment. In view of these relationships, emplacement as a shallow level sill or emergent body is probable. This unit is not present in the Yolande River section, where a thick feldspathic pumice breccia unit occupies a similar stratigraphic position.

The geochemical signature of the Pearl Creek basaltic andesite and other Mt Read andesites and basalts are shown in Figure 3. The MORB-normalised spider diagram (Fig. 3a) shows calc-alkaline affinities for the Pearl Creek unit, with enriched P, strongly enriched incompatible elements (notably Th and Ce) and depleted Ti. This signature has affinities with both Suite II and Suite III andesites and basalts of

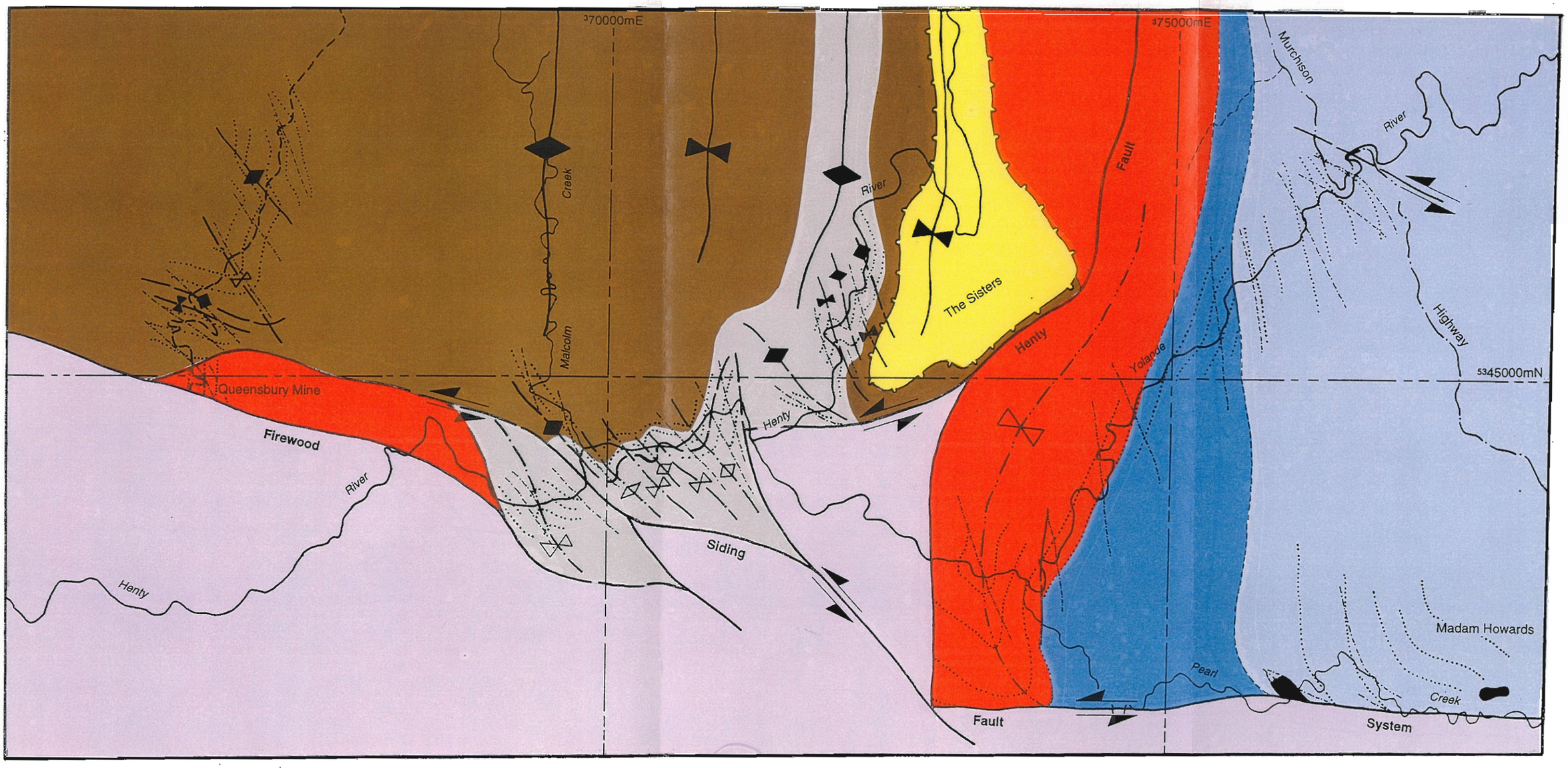

Figure 1 Simplified geological map of the Firewood Siding fault area. Data from Pearl Creek, Yolande River, Henty River and Queensbury Mine track collected during this study. Remaining data compiled from Baillie et al. (1977), Corbett et al. (1989) and Corbett et al. (this report).

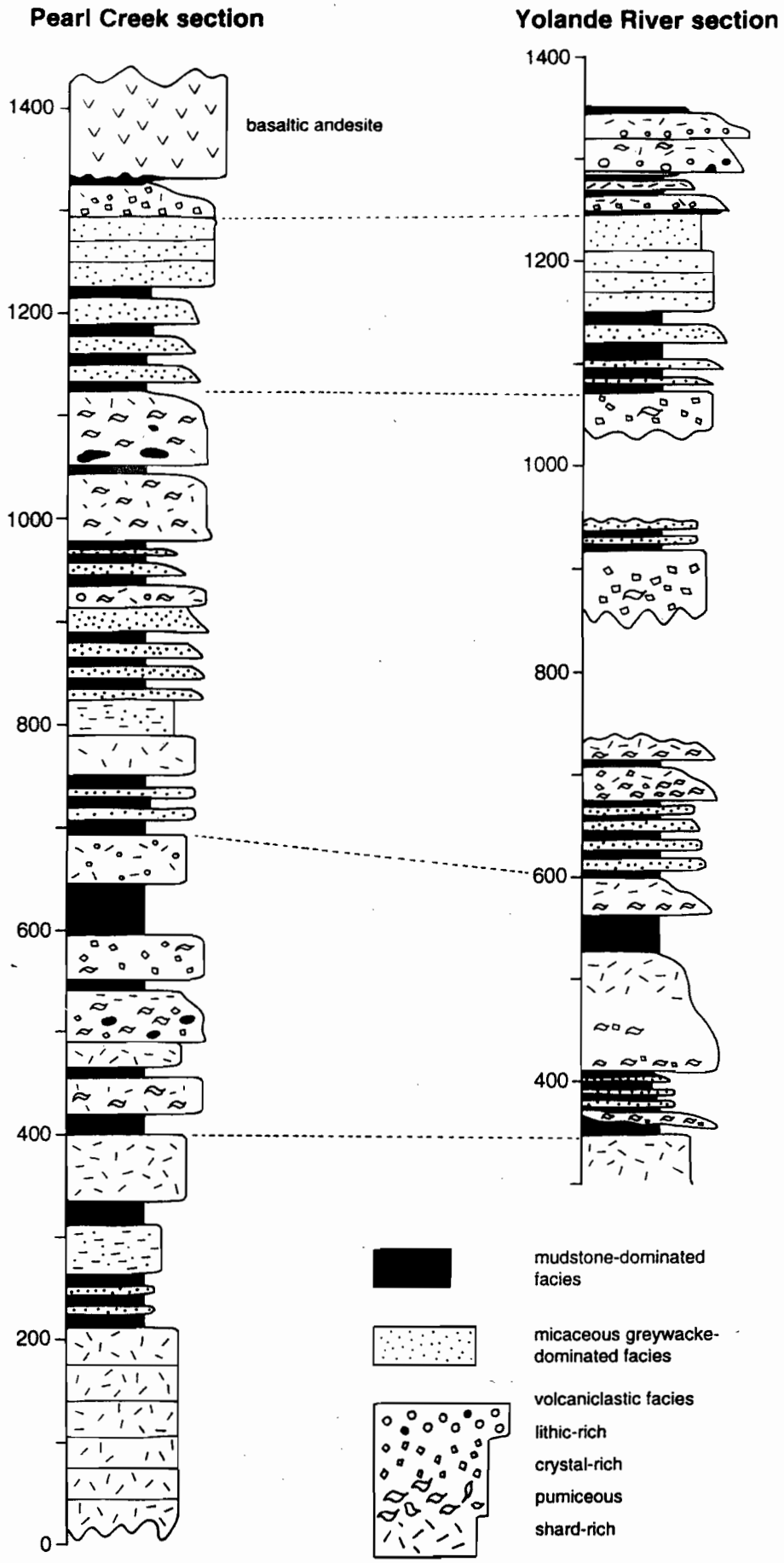

Figure 2 Lithofacies and vertical facies distribution of 'lower' Yolande Cycle correlates from Pearl Creek and the Yolande River.

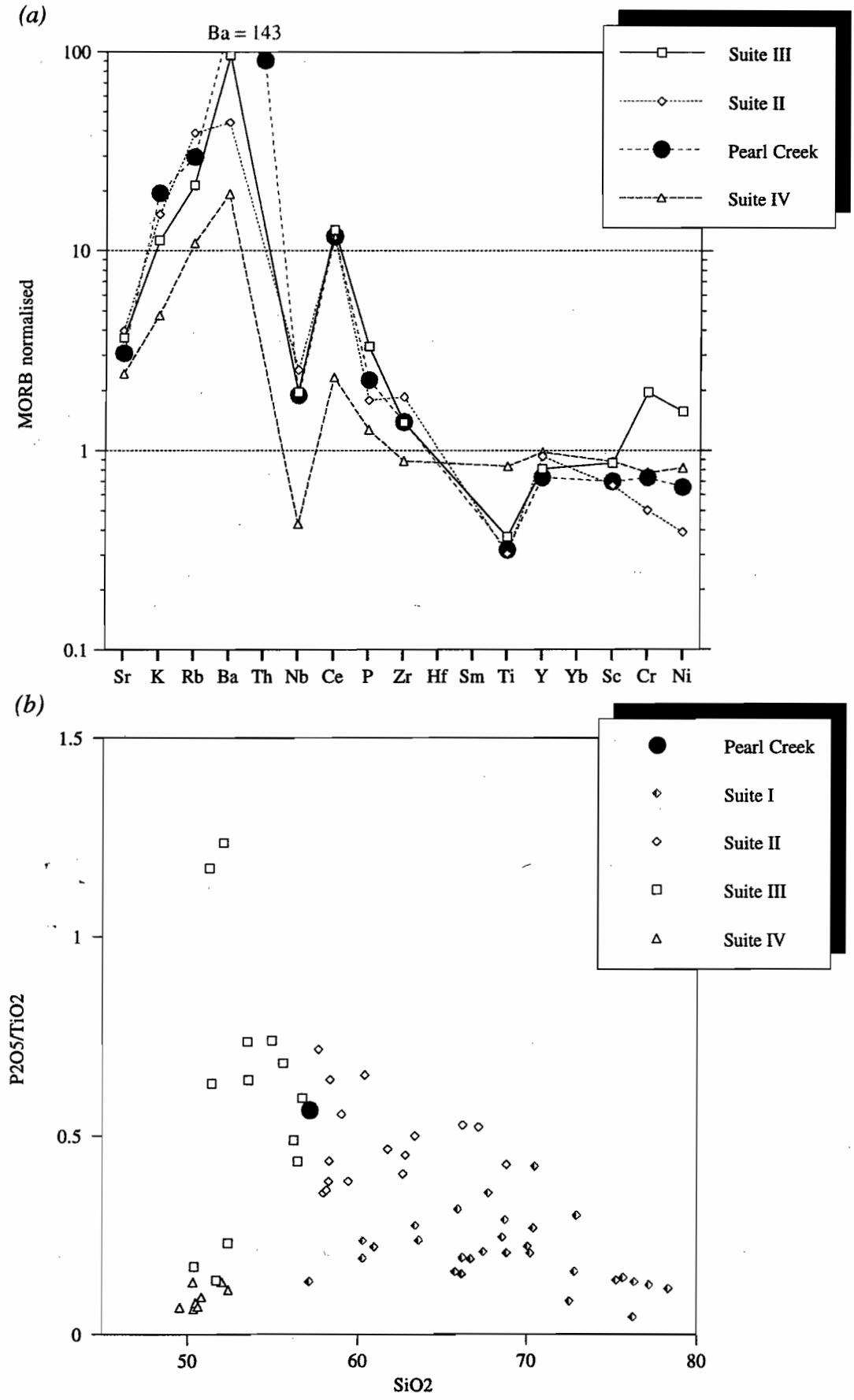

Figure 3. Geochemical affinities of the Pearl Creek basaltic andesite. (a) MORB-normalised plot of Pearl Creek unit, Suite II, Suite III and Suite IV lavas and intrusives of the Mt Read volcanics, (b) SiO_2 vs P_2O_5/TiO_2 discrimination plot for Mt Read volcanics. Mt Read volcanics data from Crawford et al. (1992).

Crawford et al. (1992), but has slightly depleted Ni and Cr implying a more evolved composition than typical Suite III rocks. A composition which is transitional between Suite II and Suite III volcanics is also shown in the SiO_2 vs P_2O_5/TiO_2 plot of Crawford et al. (op cit.) (Fig. 3b). On this geochemical basis, the Pearl Creek basaltic andesite is correlated with the Anthony Road andesite or the Lynch Creek basalts.

'Upper' Yolande Cycle

In terms of lithofacies, the boundary between the 'lower' and 'upper' Yolande Cycle in the Yolande River section is marked by an abrupt reduction in grainsize and bedding thickness. A sedimentary provenance persists across the boundary with interbedded weakly micaceous and volcanogenic sandstone, conglomerate and silty mudstone comprising the main rock types . Evidence for syn-depositional volcanic activity is lacking throughout much of the 'upper' Yolande Cycle. In particular, thick pumiceous volcaniclastics deposits which occur abundantly within the higher portions of the 'lower' Yolande Cycle were not recognised above the boundary. A thick sill-like felsic volcanic unit positioned towards the top of the cycle is the only representation of volcanism in the stratigraphy.

The mapped thickness of the 'upper' Yolande Cycle section is 450 m (Fig. 4), however considering the change in bedding orientation at the lower contact (see below), the potential exists for substantial thickening towards the south. The basal 270 m comprises a distinct coarsening and thickening upward cycle of compositionally and texturally immature siliciclastics. In contrast, the interval from 270 m to 370 m marks an abrupt return to fine-grained lithotypes and is dominated by mudstone facies. This section from 0–370 m is the main focus for the description of lithofacies and discussion presented below. Throughout much of the package, there is abundant evidence for soft sediment deformation in the form of load casts and mud injections along the base of sandstone layers, chaotically mixed intervals of sandstone and mudstone, intrafolial folds with slump-like morphologies, rolled-up sandstone 'inclusions' contained in mudstone and discontinuous, lensoidal sandstone layers. Coherent packages of thinly bedded strata up to 70 m in thickness also occur in the lower and uppermost portions of the section.

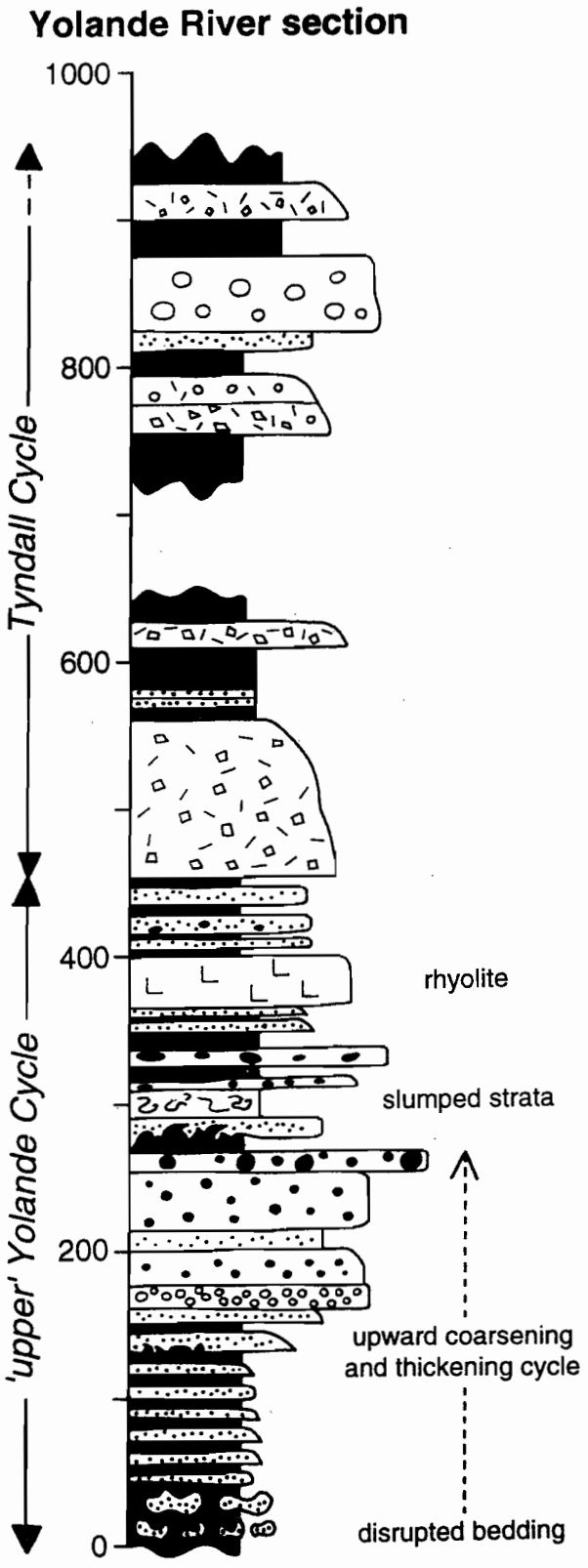

Figure 4 Lithofacies and vertical facies distribution of 'upper' Yolande and Tyndall Cycle correlates from the Yolande River.

The lowermost 150 m consists predominantly of thinly bedded mudstone and fine- to medium-grained sandstone. Sandstone beds are generally less than 10cm thick and possess turbiditic characteristics such as normal grading. T_a Bouma divisions are rare and locally attain coarse-sand grades. Parallel- and ripple-laminated sandstone intervals were most commonly recognised (T_b and T_c Bouma divisions) and are indicative of deposition from tractional currents. The fine-grained and thinly bedded character of this facies is consistent with deposition in lobes on the lower or middle portions of a fan system. Palaeocurrent directions determined from ripple cross laminated intervals are consistently towards the SSW (Fig. 5).

A slump fold measured from the lower part of the sequence indicates a palaeoslope towards the SSW (Fig. 5) and is consistent with palaeocurrent data. Significant contortion of layering occurs at the base of the package, some of which is clearly associated with cleavage-related (ie. Devonian) deformation, however the chaotic nature of many structures implies that at least some of the deformation occurred prior to lithification. Although traction current activity is ubiquitous, there is no evidence for shallow water reworking of sandstones such as wave ripples or bi-directional palaeocurrents and hence a relatively deep water, sub-wave base environment of deposition is interpreted.

The middle portion of the section coarsens and thickens upward rapidly through intercalated thickly bedded sandstone and mudstone to granule- and ultimately cobble-grade conglomerate. Turbiditic characteristics become absent up section, where coarse-grained lithologies form massive beds with tabular to lensoidal (channellised) geometries. Conglomerates possess both clast- and matrix supported textures and low degrees of internal organisation. The upward change in the basal and middle portions of the 'upper' Yolande Cycle from normally graded sandstones with well-preserved internal sedimentary structures to disorganised facies is interpreted to reflect a transition from low to medium density turbidite sedimentation to deposition from high density debris flows.Sandstones and conglomerates from the middle portion of the 'upper' Yolande Cycle are compositionally immature and contain a significant proportion of reworked

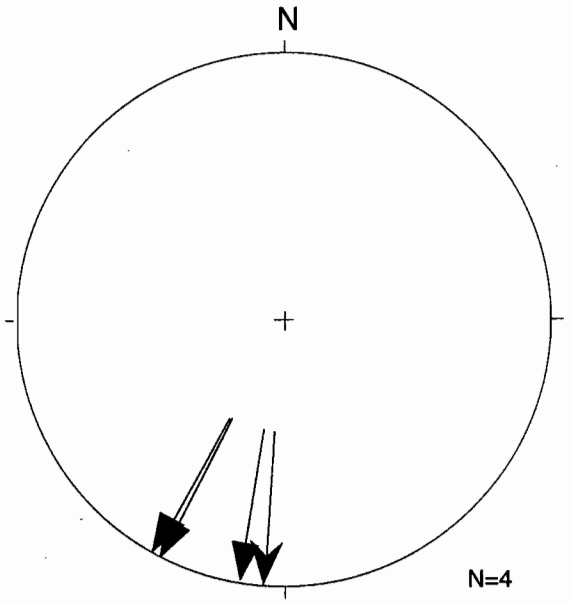

Figure 5 Palaeocurrent/palaeoslope measurements from basal 'upper' Yolande Cycle.
ripples
slump fold

volcanogenic debris and subordinate contribution from Precambrian basement sources. Angular to sub-rounded quartz crystals are common as are "cherty" volcanogenic mudstone lithic fragments and quartz-porphyritic volcanic clasts, particularly in conglomerate units. Coarser-grained sedimentary lithic clasts include quartzose sandstones, but are much less abundant that fine-grained lithics. Clast shapes are generally angular with irregular forms suggestive of incomplete lithification at the time of deposition. It should be noted however that irregular clast habits may also be the result of deformation during Devonian orogenesis. The uppermost conglomerate unit is approximately 5 m in thickness and contains sub-rounded cobbles and boulders of fine- to medium-porphyritic rhyolitic and andesitic volcanic clasts. A significant component of these units is interpreted to be intrabasinally-derived.

The section from 270 m to 370 m of the 'upper' Yolande Cycle section consists of mudstone with subordinate massive sandstone and debris flow conglomerate intervals up to 1m in thickness. With the exception of the uppermost 30 m, strata are contorted with structural morphology consistent with pre-lithification deformation. Plastically deformed mudstone intraclasts are common in both sandstones and conglomerates.

The types and vertical distribution of lithofacies contained in the 'upper' Yolande Cycle are similar to those described associated with slope systems (e.g. Shanmugam et al 1995). The package from 0–370 m is interpreted as an intrabasinally-sourced prograding slope fan, with the oldest, thinly bedded mudstone-dominated interval representing most distal low energy deposits formed at the base or lower portions of the slope. The upward coarsening sandstone and conglomerate in the middle portion of the succession represents the coarse grained load that bypassed the upper levels of the basin slope and was debauched from a major ?canyon feeder system to form volumetrically significant middle to lower slope sandy mounds. The uppermost mudstone-dominated interval, with abundant evidence for soft sediment deformation and only minor coarse-grained facies closely resembles pro-delta, upper slope deposits and canyon-fill deposits described in the literature. Contortion probably resulted from en masse sliding of mud-sheets either along gravitationally unstable slopes or into major channel systems.

Nature of the boundary between 'lower' and 'upper' Yolande Cycle

As indicated earlier in this section, there is a marked contrast in structural geometry above and below the boundary between the 'lower' and 'upper' Yolande Cycle. Bedding in 'upper' Yolande Cycle rocks striking approximately 30° clockwise of the lower package. Although strata contained in both packages dip steeply and young towards the west, those within the 'lower' Yolande Cycle strike consistently NNW whereas 'upper' Yolande Cycle beds strike NNE to NE. This orientation of bedding identified within the younger package persists throughout overlying Tyndall Cycle rocks. As the contact between the 'upper' and 'lower' parts of the Yolande Cycle is unexposed and traversed at only one point, interpretation of its original nature is ambiguous.

There is undoubtably evidence for localised strain along the contact as manifest by numerous small scale brittle faults, narrow domains in which layering is intensely boudinaged or mesoscopically buckled and strong associated cleavage development. However, it is unlikely that the abrupt change in bedding orientation is solely attributable to Devonian faulting as the principal Devonian cleavage possesses a consistent NNW strike, both east and west of the contact. Thus if it were argued that the contact marks the position of a major fault, it must predate the major phase of Devonian compression and folding. A Devonian structural history of this type is a atypical of that documented from other areas in the Dundas Trough, where brittle faulting postdates major folding episodes. An alternative explanation is that the change in bedding strike reflects the interference of two major non-coaxial folds: i.e. refolding of a NE-trending pre-Devonian cleavage (?Cambrian) closure by a major NNW-trending Devonian structure. This interpretation must be given consideration as a N-S trending Cambrian fold generation has been previously documented in this region (Berry, 1996; Keele, 1995). Discussion of potential fold geometries will be given further consideration below.

In view of the change in lithofacies across the boundary between the 'lower' and 'upper' Yolande Cycle, in particular the evidence for cessation of active volcanism, it could also be argued that the variation in bedding orientation reflects a fundamental change in basin geometry that was coeval with sedimentation. Deposition of the 'upper' Yolande Cycle

on an irregular basin topography resulting from fault block rotation is one model that could explain the present structural geometry. A similar argument has been put forward to explain non-cylindrical fold geometries and apparent unconformities in Denison Cycle strata from the Dundas region (Selley, 1996). There is no evidence for significant erosion of the 'lower' Yolande Cycle along the boundary however, and if the explanation offered above is correct, the boundary would represent a Middle Cambrian onlapping surface, with 'upper' Yolande Cycle strata abutting or ponding against a tilted package of 'lower' Yolande Cycle strata. The development of an intrabasinally-sourcing prograding slope fan, as was interpreted for the 'upper' Yolande Cycle, would not be an unexpected depositional response to block tilting and provides support for such a basin history.

In summary, evidence exists for a pre-cleavage (?Cambrian) phase of deformation, however there is insufficient data at present to distinguish between the a Late Cambrian fold or Middle Cambrian onlap surface model. The latter is perhaps worthy of further investigation as it indicates a phase of extension at the time of massive sulphide development. Sections mapped south and north of the Yolande River would help in defining the nature of the contact. If the onlap model is correct, slumping would be expected to continue south along the contact with associated thickening of the 'upper' Yolande Cycle.

Tyndall Cycle

Lithostratigraphic correlates of the Tyndall Cycle were mapped in the region east of the Henty Fault (Fig. 1). Most of the data presented below were collected from the Yolande River, however similar lithologies along strike were mapped and sampled for petrographic and geochemical analysis (results presented in Berry et al., this report) from a track located approximately 2.5 km NNE of the Yolande River section. Correlation of these rocks with the Tyndall Group was first proposed by workers from the Tasmanian Mines Dept on the basis of their high magnetic response. Previous mapping by Poltock (1992) (as interpreted by Berry,1996) in the region 5 km to the NW of the present study area has demonstrated that probable correlates of the Lynchford Member (basal Tyndall Group) crop out along the western side of the Henty Fault. These rocks have not be investigated during this study.

Tyndall Cycle rocks overlie interbedded mudstone and volcanogenic sandstone of the 'upper' Yolande Cycle with apparent conformity (Fig. 4). Strata are dominantly west-facing except adjacent to the Henty Fault, where they are folded about a NW- to NE-trending syncline. The thickness of the section from the base to the core of the syncline is approximately 500 m. Thickly-bedded crystal rich volcaniclastic sandstone is the most conspicuous facies, however mudstone divisions and packages of thinly interbedded turbiditic sandstone and mudstone also form a significant proportion of the rocks in this sequence. Volcaniclastic lithic breccia units occur rarely. Much of the section is poorly exposed, with most recessive units comprising fine-grained lithotypes.

The basal part of the Tyndall Cycle consists of very thick bedded, normally graded to massive crystal rich volcaniclastic sandstone units, with rare, discontinuous lenses of mudstone. Petrographically, these sandstones contain large albitised monocrystalline plagioclase crystals (35%), fresh clinopyroxene (10%), Fe-Ti oxides (5%), volcanic quartz (3%), rare brown hornblende and minor lithic clasts of volcanic origins. The groundmass consists of intergrown irregular albite crystals with minor chlorite and actinolite needles. Abundance of magnetite is responsible for this unit's high magnetic response and is a characteristic feature of the Tyndall Group. Geochemical analyses of the crystal rich sandstone facies indicate tholeiitic affinities for the parental magma and correlation with the Lynchford Member (Berry et al., this report).

Finer grained lithotypes involve a mixed volcanic-sedimentary provenance. Rhythmically interbedded dark grey mudstone and pale grey quartz dominated sandstone beds are composed of Precambrian derived material, whereas green chloritic mudstone and silty mudstone are likely to have a significant volcanogenic input. Massive cobble-grade conglomerates occur near the top of the section and contain well-rounded clasts of aphyric to coarsely porphyritic rhyolitic to dacitic volcanic clasts set within a coarse sand-grade matrix of crystals and lithic fragments. The high degree of clast rounding in these conglomerates indicates shallow water to sub-aerial exposure and erosion of volcanic terrains prior to deposition.

Denison Cycle

Denison Cycle correlates are restricted in their distribution to the western side of the Henty Fault (Fig. 1). Strata are closely to tightly folded about WNW- to N-trending closures, however there is an overall younging of the succession towards the west. Keele (1995) estimated a total thickness of 2000 m for the Denison Cycle in this region.

Henty River section

The oldest rocks in this cycle closely resemble Stitt Quartzite and comprise interbedded mature quartzose sandstone and black mudstone. Exposures of this facies were mapped along the Henty River between 372250E–5345800N and 369750E–5344000N (Fig. 1). Strain in these rocks is anomalously high due to their proximity to the FSF and as such, construction of stratigraphic sections was not attempted. Berry (1996) mapped what he considered to be Stitt Quartzite facies approximately 6km north of the Henty River section and proposed a possible correlation with the thick NNE trending belt of Stitt Quartzite in the Farrell Rivulet area. Although exposure is patchy, it now appears valid to extend this belt of rocks southward to the Firewood Siding Fault. Exposures of the Stitt Quartzite correlate in the region mapped are dominated by black mudstone and thinly bedded micaceous sandstone and siltstone. At least one 100 m thick sandstone-dominated interval occurs however, with beds ranging 1–100 cm in thickness (average 25 cm) and possessing well-preserved turbiditic and less commonly mass-flow characteristics. Where thickly bedded, sandstone beds are usually amalgamated. T_{adb} Bouma divisions are common in beds with turbiditic affinites, whereas the T_c ripple laminated division is usually absent. SW-directed palaeocurrent measurements (Fig. 6) determined from inclined longitudinal flame structures were collected in a sandstone dominated interval situated approximately 2 km west of The Sisters.

Sandstone dominated turbiditic intervals closely resemble *medium/thin-bedded* and *thick-bedded sandstone facies* of Bull (1994) from west of the Rosebery Mine area. Bull interpreted these facies to indicate deposition in a predominantly deep water setting, probably in association with a turbidite fan system.

Mass-flow sandstone facies was recognised in complexly folded rocks cropping out in the Henty River adjacent to the FSF near. This facies is manifest as a succession of massive, 1m thick sandstone beds which occur near the top of a turbidite-dominated coarsening upward cycle. Slumps and mudstone

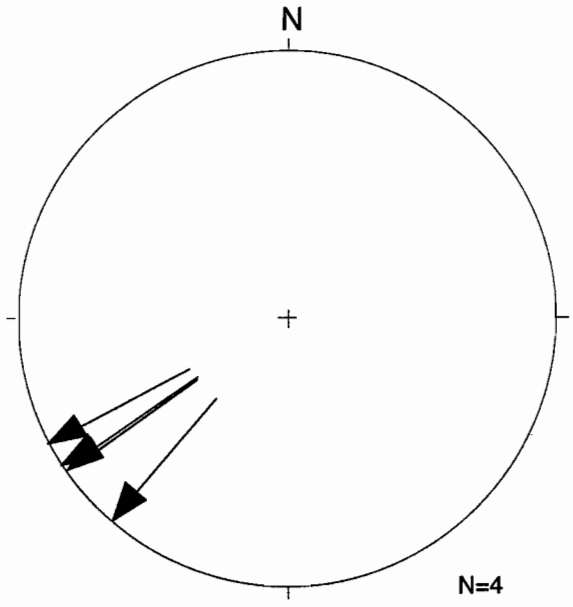

Figure 6 Palaeocurrent measurements from Stitt Quartzite correlate in the Henty River.
inclined longitudinal mud flames

flames are commonly associated with the massive sandstone succession as are mudstone intraclasts, which were observed to dispersed throughout entire beds in some cases. The association of massive structure, lack of normal grading and the presence of "floating" intraclasts in these sandstones argues against deposition from turbulent flows. These textures and the association of soft sediment deformation features are typical of non-turbulent plastic flows (ie. debris flows) which deposit sediment by frictional freezing.

Queensbury Mine track

A 1000 m section of Denison Cycle correlates was mapped along the Queensbury Mine track between 367185E–5347300N and 366500E and 5345200N. An Iverian fossil locality near the base of the section places these rocks towards the top of the Upper Cambrian. The succession faces mainly towards the east, but is folded about tight to open WNW to N trending closures.

A stratigraphic log showing the types and distribution of lithofacies is shown in Figure 7. The most conspicuous feature of this diagram is the predominance of coarse-grained lithofacies, which comprise more than 70 % of the total section. Coarse-grained lithofacies include thick intervals of granule to pebble conglomerate, massive to crudely bedded sandstone and more organised intervals of medium to thick bedded graded sandstone. Two distinct styles of conglomerate facies can be distinguished on the bases of internal structure and provenance. The first of these form crudely organised clast-supported beds up to 3 m in thickness. Normal grading is developed throughout a few beds, however massive internal structure is more common. Reverse-graded bases were recognised in a few cases. Some conglomerate beds appear lensoidal, with channellised bases. The mode of deposition of this conglomerate type is interpreted as being from high density turbidity currents, which were probably confined to major channel systems. They commonly occur in association with massive and normally graded clean quartzose sandstone and are best represented towards the lower parts of the section. Clast types in this first conglomerate type are mainly extrabasinally-derived and include quartzite fragments, pink and white chert and vein quartz. Fragments are set in a sand-sized

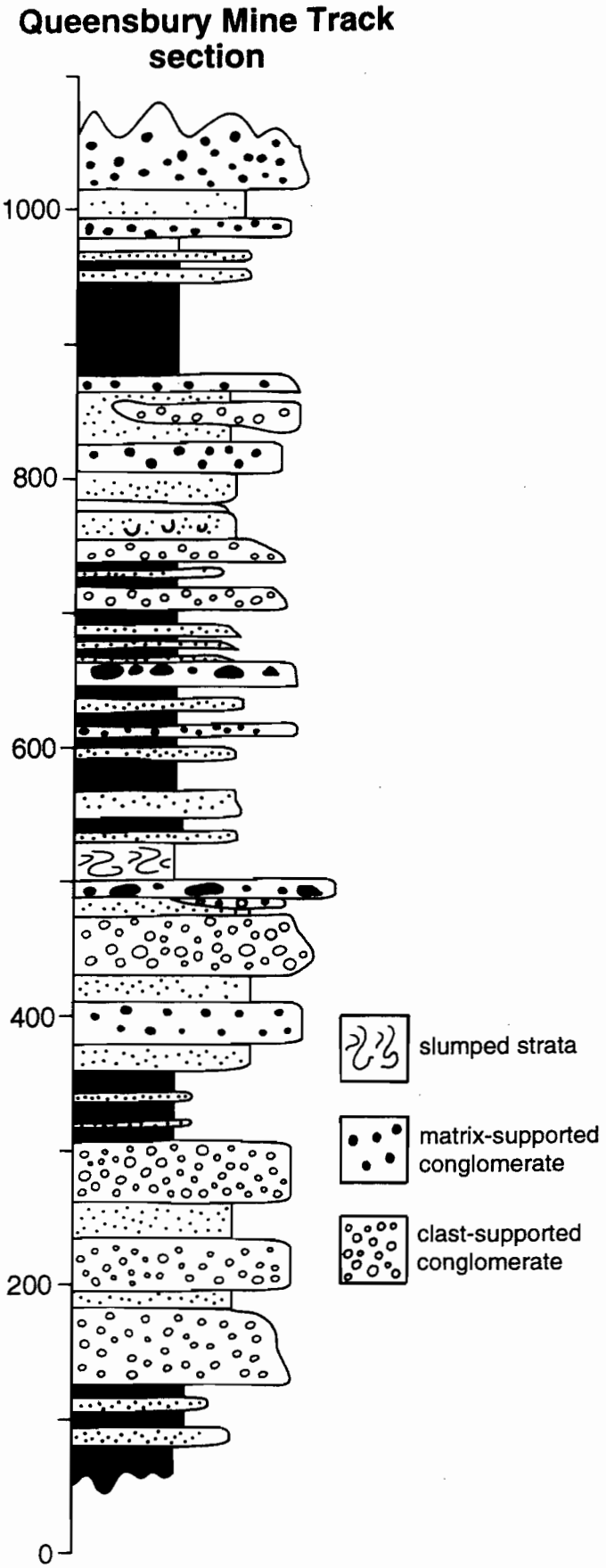

Figure 7 Lithofacies of Denison Cycle correlates exposed along the Queensbury Mine track.

matrix of rounded quartz and subordinate lithic fragments, giving the rock an overall pale pink to cream colour. This provenance resembles that of many other Precambrian-derived conglomerates such as the Zeehan, Misery Hill and Owen Conglomerates, the last two at least being probable time equivalents. The second conglomerate-type generally lacks any coherent internal structure and form tabular thick to very thick massive deposits. It is usually matrix-supported, with clasts set in fine sand or mud. Large mudstone rafts are dispersed throughout some beds. This conglomerate type is generally associated with massive sandstone and slumped intervals. The provenance of this conglomerate type is similar to that of the first, however an additional intrabasinal component is apparent. Clasts considered to have had an intrabasinal origin includes plastically deformed green mudstone and partially dismembered inclusions of fine sand. The mud and fine sand which form most of the matrix component are probably also intrabasinally derived. This second facies association is characteristic of sediments deposited from large, laterally unconfined debris flows.

Finer-grained facies include thin to medium bedded sandstone and mudstone, delicately laminated mudstone and structureless mudstone. Sandstone beds included within these facies show well-preserved turbidite characteristics. Complete Bouma cycles were observed at a number of localities. The overall stratigraphy of the upper Denison Cycle represents a package of rapidly accumulated sediment which was introduced from both turbulent and non-turbulent plastic flows.

Discussion of sedimentology and its record of Cambrian basin development

Potential evidence for syn-depositional tectonic activity and basin development in the sedimentological record include: chaotic facies (eg. slumped or liquefied strata, debris flow associations), sudden influx of coarse-grained debris, rapid change from deep to shallow water depositional environments, rapid lateral facies variation and disconformity surfaces resulting from periods of uplift and erosion/non-sedimentation or pooling of sediment against older tilted strata. From the work undertaken in this study, those stratigraphic sections containing facies associations which best meet some of these criteria include the section of 'upper' Yolande Cycle strata mapped in the Yolande River and upper part of the Denison Group exposed along the Queensbury Mine track. The entire Middle and Upper Cambrian succession is interpreted to represent relatively deep water, below wave base sedimentation as no evidence was found in support of shallow water deposition or erosional disconformities resulting from localised uplift and emergence. This argument becomes less convincing in the Denison Cycle wherein much of the stratigraphy was unexposed (ie. basal boundary with the Tyndall Cycle and transition from Stitt Quartzite to the Iverian sequence), however on the basis of available data, the Cambrian stratigraphy north of the FSF is considered to record essentially continuous sediment accumulation in sub-wave base depocentres. Thus if the FSF was active as a transfer fault during Middle and/or Late Cambrian sedimentation, it was down-thrown to the north.

The identification of a prograding slope fan system within the 'upper' Yolande Cycle provides the best evidence for basin activity during the Middle Cambrian. The texturally and compositionally immature detritus contained within the middle and upper parts of this sequence, coupled with a facies association of coarse-grained crudely stratified units, point towards a proximal intrabasinal source during this period of sedimentation. SSW directed palaeocurrent measurements from the basal fine-grained turbiditic portion of the sequence are consistent with roughly axial drainage patterns developed in a major N–S trending basin, but potentially differ significantly from those supplying detritus contained in immediately overlying coarser-grained strata. In rift systems comprising linked half-grabens, only a small proportion of coarse-grained debris is supplied directly from footwall blocks, with the greatest volume being introduced along drainage patterns transverse from the tilted hangingwall (ie. back towards the footwall block) or from topographically elevated accommodation zones which connect half graben segments (eg. transfer structures). Hangingwall-derived debris would be expected to be largely intrabasinal, whereas that sourced from transfer zones is more likely to be "basement" or extrabasinally derived. Once debris reaches the base of slope in small half graben systems, drainage patterns

potentially swing towards basin axial orientations. Thus base of slope drainage patterns can deviate by up to 90° from middle and upper slope channels developed within the same major feeder system.

Although convincing evidence for major stratigraphic break within the Yolande Cycle has not been documented from the Dundas Trough, there is some evidence for basin activity and slope instability at this time. For instance, the chemical composition of detritus contained in the Murrays Road Greywacke in the Que–Hellyer region potentially records input from an intrabasinal source which contrasts significantly from the dominantly extrabasinally derived material contained in the underlying Animal Creek Greywacke(Berry et al., this report). Furthermore, the presence of upper-most Yolande Cycle/ lower Tyndall Cycle debris flows containing reworked mineralised debris in the Newton Dam Spillway (Gibson, 1991) indicates that middle Yolande Cycle massive sulphide deposits were locally becoming eroded at this point in time. In terms of the magmatic evolution of the Mt Read volcanics, the upper part of the Yolande Cycle records the transition from shoshonitic magmatism (eg. upper Que–Hellyer Volcanics; Pearl Creek) to the tholeiitic signature of the Sock Creek basalts and the overlying Tyndall Cycle (Crawford et al., 1992; Berry et al., op cit.). If the tholeiitic magmatic signature is considered to represent the period of maximum extension in the evolution of the Dundas Trough, then is must have occurred during the upper Yolande and/or early Tyndall Cycles. Although the evidence presented above is very circumstantial, it is consistent with a period of extension and change in basin geometry during the later part of the Yolande Cycle.

Little or no evidence has been found to indicate that the FSF was actively controlling sedimentation during the Middle Cambrian. No significant facies variation was recognised between the Yolande River and Pearl Creek sections of the 'lower' Yolande Cycle, and perhaps more importantly no slumping or chaotic sedimentary breccias were identified immediately adjacent to the FSF. As the sedimentology of the 'upper' Yolande Cycle was not investigated near the FSF however, the potential still exists for further work in this succession south of the Yolande River to reveal evidence of fault activity. Weak evidence for Middle Cambrian fault activity along the FSF is indicated from the Tasmanian Dept of Mines Queenstown 1:25,000 sheet, which shows a string of elongate mafic volcanic bodies following the trace of the FSF. The eastern-most of these volcanic units is that mapped during this study at Pearl Creek. If it can be shown that these units are comagmatic, it may be argued that their present distribution resulted from localisation along Middle Cambrian fracture zone.

Sedimentation during the Tyndall Cycle and lower part of the Denison Cycle (ie. Stitt Quartzite correlate) marks a return to more stable basin conditions. With the exception of volcanic debris introduced during the Tyndall Cycle, most detritus was sourced from Precambrian "basement" terrains. Heavy mineral populations in support of this interpretation come from Stitt Quartzite sandstones from the Rosebery area, in which the ratio of euhedral to rounded zircons is 1:16 (Berry et al. this report). Most facies of the Stitt Quartzite correlate closely resemble those described from the type area near Rosebery, which Bull (1996) interpreted to represent deposition in a basin axial position controlled by N–S striking growth faults. This interpretation is supported by the distribution of Stitt Quartzite correlates, which appear to form a semi-continuous belt extending southward from the Rosebery Mine area. The only 'anomalous' facies recognised in the lower Denison Cycle is the massive sandstone interval positioned adjacent to the FSF and considered indicative of sedimentation from sandy debris flows. The proximity of this facies to the FSF and its position near the top of an upward coarsening and thickening turbiditic cycle may indicate that a topographic high providing sediment input existed at this time near the present position of the FSF.

The rapid and sustained influx of coarse-grained debris recorded in the Late Cambrian Queensbury Mine track section indicates a period of vigorous basin activity. Chaotic facies associations and the lack of obvious coarsening or fining upward cycles contrasts with older successions mapped in this region but is typical of Dundas Group facies associations developed to the north (Selley, 1996). The lack of the coherent vertical stratigraphy envisaged for classical turbidite fan models is interpreted to indicate that upper Denison Cycle basin slopes were too narrow to allow the development of a typical prograding system. Sedimentation in a small,

laterally confined basin with proximal input from both intrabasinal and extrabasinal sources best accounts for the character of the upper Denison Cycle facies associations. The common Precambrian provenance of clast-supported conglomerate facies and the overlying Zeehan Conglomerate indicates a potential transitional relationship from the upper Denison Cycle to the Ordovician succession, an interpretation which is supported by the para-conformable contact between these two packages west of the Professor Plateau. This inferred transitional at the top of the Denison Cycle, coupled with the confined nature of the depocentre may indicate that at this location, the uppermost Mt Read volcanic was beginning to accumulate in the cores of synclines generated during Late Cambrian closure of the Dundas Trough. If this is the case, evidence of erosional unconformities would be expected within the Denison Cycle. Although no such surfaces have been identified during this study, partly due to the lack of exposure, a pre-Iverian unconformity has been interpreted by Selley (1996) within the type section of the Dundas Group 15km to the north.

Structural Geology

Regional structural geometry and previous work

Berry (1996) and Keele (1995) have convincingly demonstrated that a Late Cambrian phase of folding has deformed rocks north of the FSF. Their evidence comes mainly from the region between the Professor Range and the Murchison Highway where contrasts in bedding dips of Cambrian strata and those of the unconformably overlying Pioneer Sandstone are greatest. Moreover, the N–S structural grain defined by folding in the Cambrian succession contrasts with the NW to NNW fold trends within the Ordovician rocks, with some N–S folds dying out under the Ordovician cover. Both workers have postulated that the change in fold orientation reflects tightening and possibly refolding of pre-existing open Cambrian structures which originally trended clockwise of the regionally developed NW Devonian fold trend. Berry (op cit.) provided further evidence for this fold interference geometry by demonstrating that the principal Devonian cleavage transects major fold axial surfaces, indicating that strata were at least inclined prior to cleavage development. N–S trending Cambrian structures have not been interpreted by these authors towards the west of the area however, where the Pioneer Sandstone overlies the uppermost (Iverian) succession with apparent conformity (Baillie and Corbett, 1985). Structural and stratigraphic relationships in this region indicate that either Cambrian folding did not persist towards the west, or that folding pre-dated or was synchronous with the deposition of the Iverian succession. In other words, Iverian strata was already beginning to accumulate within the synclinal cores of open Cambrian folds.

In the present study area, the influence of Devonian deformation associated with the FSF has effectively obscured much of the Cambrian structural geometry. Only as one moves northward from the deformation zone around the FSF can evidence of a pre-cleavage structural history be identified (eg. the abrupt change of bedding strike in the Yolande River section). With the aim of characterising the Devonian structural geometry in this region I have summarised the work of Baillie and Williams (1975) who documented the variation in deformation style developed in the Siluro-Devonian succession south of the FSF. The most conspicuous geometric feature in the region investigated by these workers is the swing of structural grain (defined by fold and cleavage traces) from NNW to WNW as the FSF is approached from the south. To explain this geometry, Baillie and Williams (op cit.) interpreted a two-phase deformation history in which an initial generation of folds developed with NNW-trending axes were refolded about a second WNW-trending generation of folds with sub-horizontal to shallowly plunging axes. They considered only the later WNW-trending folds and associated axial planar cleavage to be developed in the Bell Shale correlates adjacent to the FSF. A presumed detachment surface at the base of the Bell Shale was invoked to explain the absence of the earlier fold generation in this area. Localised folding of the WNW-striking cleavage by a NNW fold generation was recognised in the vicinity of the FSF and was attributed to late stage movement on this structure.

Within the deformation zone located north of the FSF, Keele (1995) also recognised an early E–W fold generation. He interpreted an isolated synclinal closure immediately north of the FSF and proposed that this structure pre-dated the N–S generation of Cambrian folds.

Mesoscopic structure and domain analysis

Three broad structural domains containing Middle to Late Cambrian strata, each with their own distinctive structural geometries, have been recognised from data collected during field mapping: Yolande River–Pearl Creek, Henty River and Queensbury Mine domains (Fig. 8). They are referred to below as Domains 1, 2 and 3 respectively. Although each domain contains distinct stratigraphic levels, their structural geometries are not necessarily characteristic of these levels in other regions. In all cases, domains are divided into smaller sub-domains in which the geometric associations of structural elements are relatively homogenous.

Evidence for at least two generations of folding has been recognised in many areas. In general however, both the complexity and intensity of folding increases towards the FSF, most notably in Domain 2 where the interference of two fold generations is best displayed. One principal cleavage is developed throughout the study are and a second, more widely-spaced fabric also occurs locally. The principal cleavage has a slaty morphology in fine-grained rocks, but rougher and more widely spaced in volcanic units and coarser grained siliciclastic rocks. In areas where the structure is relatively simple, this cleavage is steeply-dipping and possesses a uniform NNW strike. On the basis of this orientation and the cleavage's morphology, the principal cleavage is correlated with the regionally developed Devonian S_1 fabric.

Domain 1

Domain 1 includes data collected within the triangular block which is bounded to the south by the FSF, to the west by the Henty Fault and to the east by the Murchison Highway (Fig. 8). It contains strata from the Yolande and Tyndall Cycles. The structural geometry of this domain has been briefly described earlier in this report, where special mention was made of the change in strike of bedding between the 'lower' and 'upper' parts of the Yolande Cycle. This change in strike marks the boundary between sub-domains 1a and 1b. A smaller sub-domain (sub-domain 1c) is situated in the south along the FSF.

In general, bedding strikes between 042 and 332, and the principal cleavage strikes anticlockwise of bedding. However, within 500 m of the FSF and also in the north-east corner of the domain, a dramatic rotation of both bedding and cleavage towards the WNW was recognised. Furthermore, at one location adjacent to the southern margin of the domain, cleavage developed within a crystal-rich sandstone was observed to strike clockwise of bedding.

For the most part, both bedding and cleavage contained with sub-domain 1a strikes NNW and dips steeply towards the west (Fig. 9a, b). Vergence is consistently eastward, indicating that strata are situated on the sub-vertical eastern limb of a NNW-trending anticline. At a position near the Murchison Highway bridge over the Yolande River however, both bedding and cleavage are rotated clockwise (up to 80°) about a sub-vertically plunging rotation axis. This folding event unambiguously post-dates the main tightening and cleavage development phase of NNW folding, however as no data was collected north of the second generation hinge, the exact nature of the structure is unclear. Increased density of brittle faults along the WNW-striking limb of the steeply plunging fold suggests that it may be related to fault drag on an as yet unidentified structure. Where the principal cleavage has experienced significant clockwise rotation, a second spaced cleavage striking NW was developed (Fig. 9d). Note that the orientation of this spaced fabric is roughly parallel to that of the unfolded principal cleavage.

Poles to bedding in sub-domain 1b (Fig. 9e) indicate that the major synclinal hinge positioned near the Henty Fault is plunging moderately towards the NNE. There is some degree of point scatter away from the calculated profile plane, which is interpreted to reflect the non-cylindrical nature of the syncline. The orientation of cleavage (Fig. 9f) remains unaltered from that in sub-domain 1a and that it transects the axial surface of the major fold is clearly demonstrated by the opposing plunge of the intersection on eastern and western limbs (Fig. 9g). It has been suggested earlier that the abrupt change in bedding orientation across the sub-domain 1a–1b boundary records a pre-cleavage deformation event. This interpretation is based upon the lack of cleavage variation across the boundary. Two models for this structural geometry have been proposed: (1) Devonian folding of mutually inclined layers formed during Middle Cambrian block tilting and onlap (Fig. 10a), and (2) interference of an early NNE- to NE- trending

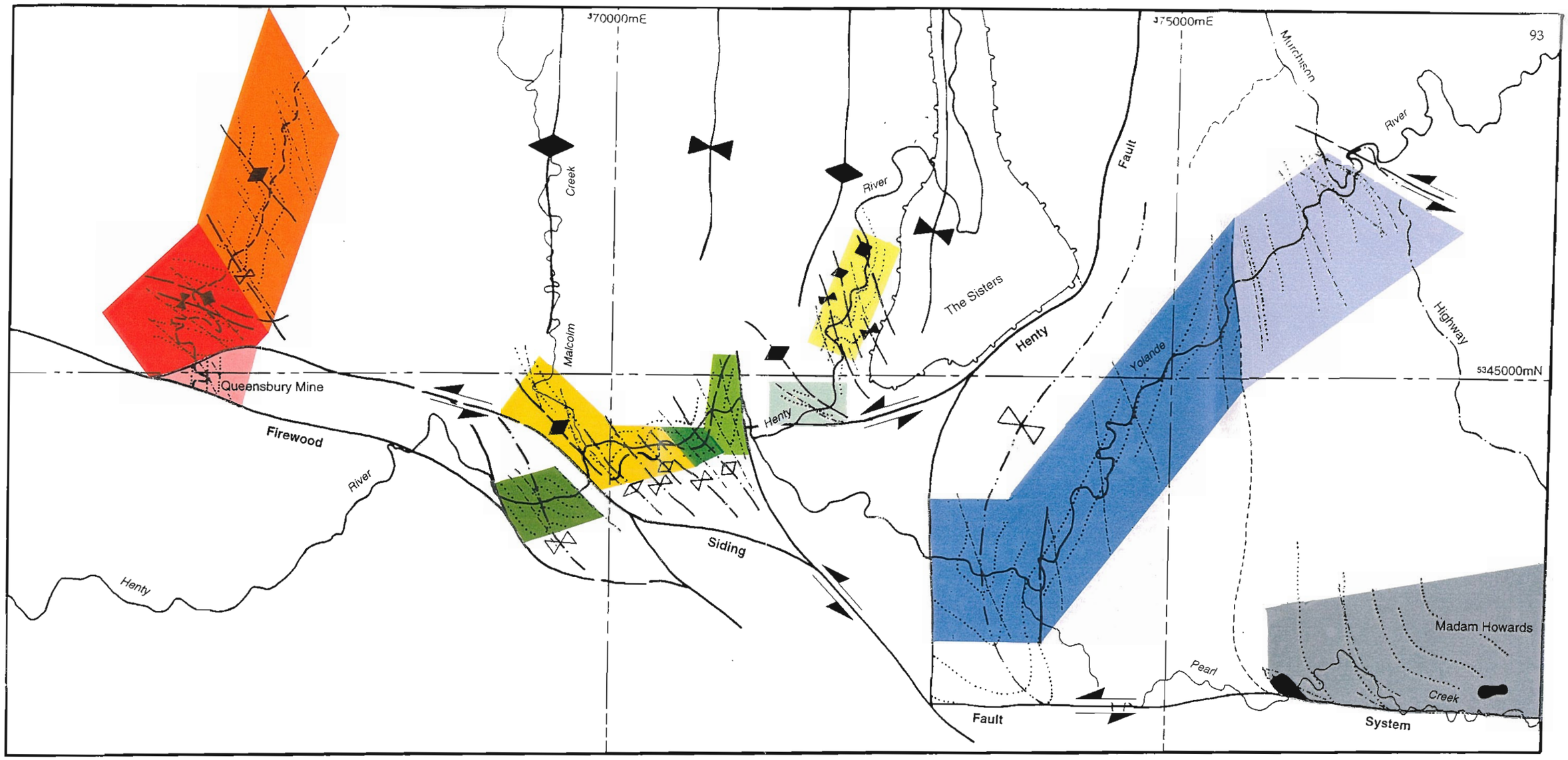

river or creek
road
track
fault
unconformity
trace of bedding
trace of principal Devonian cleavage

Fold axial traces

F_{1-2} (Cambrian fold retightened during Devonian)

F_2 (fold nucleated during Devonian orogenesis)

F_3 (Devonian folds: proximal to the Firewood Siding Fault)

undifferentiated

Domain 1: 1a 1b 1c

Domain 2: 2a 2b 2c 2d 2e 2f

Domain 3: 3a 3b 3c

0 1000m

scale

Figure 8 Structural domain map of Middle and Upper Cambrian strata north of the Firewood Siding Fault system.

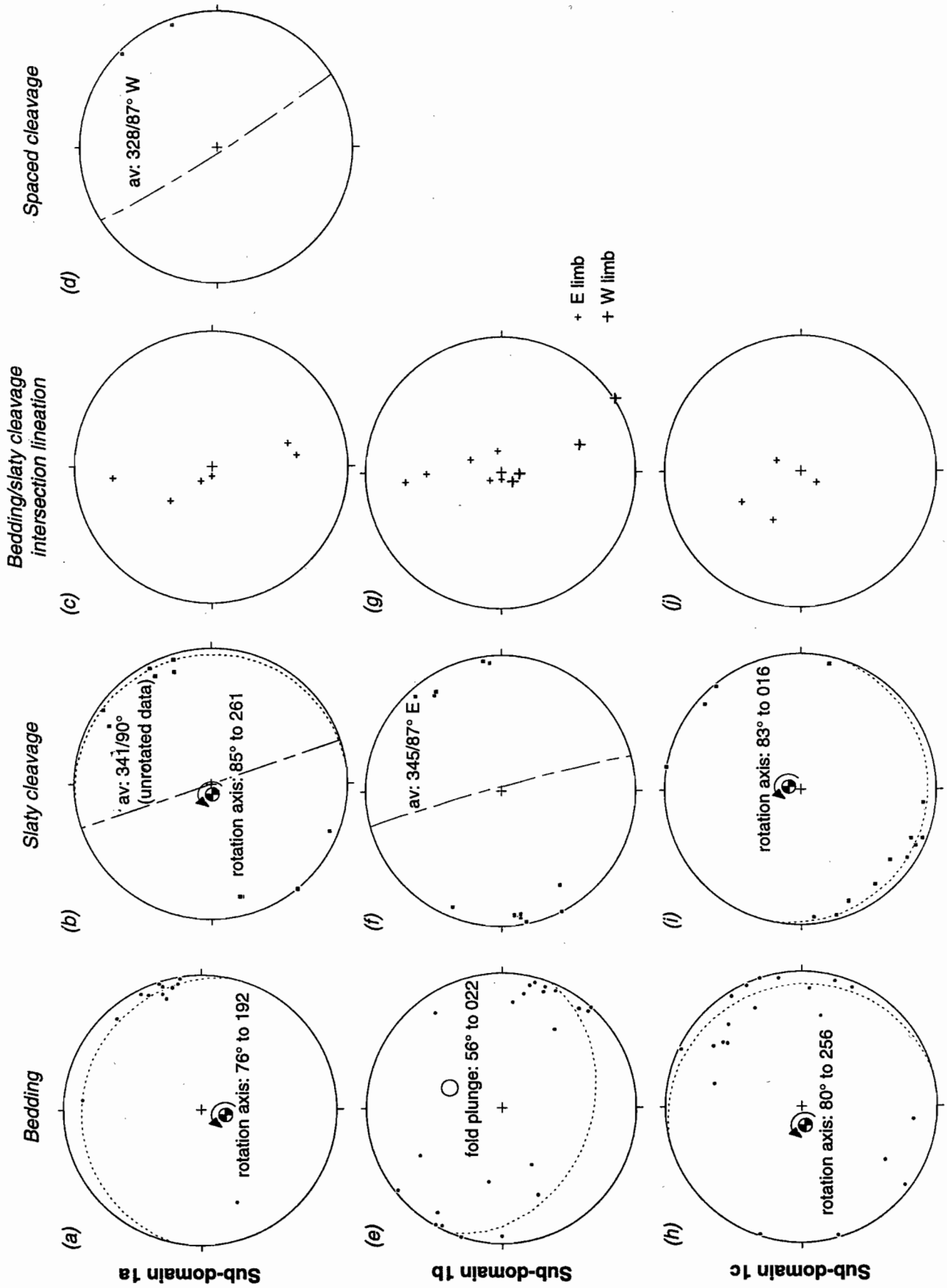

Figure 9 Equal area stereographic projections of mesoscopic data from domain 1.

fold by a NNW-trending Devonian fold . Evidence in favour of the first of these models is based largely on the association of lithofacies within the 'upper' Yolande Cycle and has been discussed in previous sections. In favour of the second model is the documentation of pre-cleavage Late Cambrian folding north of this region (Berry, 1996; Keele, 1995). In the cases described by these workers, Devonian folds have presumably grown 'parasitically', causing tightening and re-orientation of older structures rather than developing independently of the first generation. The potential fold interference pattern for sub-domains 1a and 1b is shown in Figure 10b. That the NNE to NE bedding strike is preserved in sub-domain 1b but not in sub-domain 1a may perhaps be explained by the bend in the Henty Fault acting as a barrier during Devonian compression. The steeply plunging F_2 fold depicted on the western limb of the early structure (Fig. 10b) is shown to explain the strongly non-cylindrical geometry in this region.

Sub-domain 1c contains a sub-vertically plunging open fold that causes both bedding and cleavage to become rotated into parallelism with the FSF (Figs 8, 9h, i). As was the case in the NE corner of domain 2, this steeply plunging structure post-dates both NE- and NNW-trending fold tightening.

Domain 2

Data included in domain 2 are all situated close to the trace of the FSF. The structure is very complex in this region with evidence shown for up to three fold generations. Most intense deformation occurs west of the confluence of the Henty and Yolande Rivers to Malcolm Creek. Within this area broad cataclasite zones are developed in incompetent lithotypes (one up to 400 m in width), bedding is isoclinally folded and downward facing fold geometries are common. The dominant structural grain varies throughout the domain from WNW–ESE to N–S. In general, where strain is intense the structural grain trends WNW and swings clockwise moving northward from the FSF.

Six sub-domains have been defined along this 6km section (Figs 8, 11), however no attempt here will be made to discuss the detail of each individually. The earliest generation of folds were identified in the sub-domain located west of The Sisters (sub-domain 2a). The dominant structural grain in this sub-domain is roughly N–S and with easterly facing strata situated on the eastern limb of a large wavelength, N- to NNE-trending anticline. Cleavage strikes anti-clockwise of the gross bedding trend and is axial planar to a series of open to close folds with wavelengths of less than 10 m. These small scale folds have consistent "Z"-vergences and an *en echelon* distribution on the limb of the larger structure with highly variable steep to moderate plunges towards SE or SSE. As the principal cleavage is axial planar to minor folds which plunge variably on a single limb of a larger wavelength fold, it cannot be axial planar to the major structure. That the F_2 folds trend anticlockwise of the N–S bedding strike (indicated by "Z"-vergences) indicates that the cleavage must also anticlockwise-axially transect the larger scale fold. The most logical explanation for these fold-cleavage relationships is re-tightening, rotation and cleavage transection of a large wavelength pre-cleavage (?Cambrian), N- to NNE-trending fold during WSW–ENE directed Devonian compression. For the purposes of the following discussion, the early fold generation is defined as F_{1-2} (i.e. F_1 fold re-tightened during D_2) and the smaller wavelength structures with axial planar cleavage are termed F_2.

F_{1-2} folds die out rapidly towards the trace of the FSF, where high amplitude tight to isoclinal F_2 folds become the dominant structural elements. In this region (notably sub-domain 2e) F_2 folds have rotated anticlockwise to SE and ESE trends. A cleavage developed roughly axial planar to the ESE-plunging folds has been identified in a sub-domains 2b and locally within 2f, however in general the principal fabric transects these folds in a clockwise sense and strikes NW . There is considerable spread of cleavage data in some domains (eg. sub-domains 2e and 2f) with poles plotting around a large segment of the primitive circle. Although there is little variation in cleavage morphology between those data that strike WNW and those striking NW, the latter were commonly observed to be axial planar to a third generation of open to close SE-plunging folds (F_3 :sub-domains 2d, 2e and 2f) and thus clearly post-date development of the ESE-trending F_2 folds. At only two localities however, was I able to clearly demonstrate two distinct cleavage generations via overprinting relationships.

As the principal cleavage transects the major structures in a clockwise sense where the latter trend WNW and in an anticlockwise sense where folds

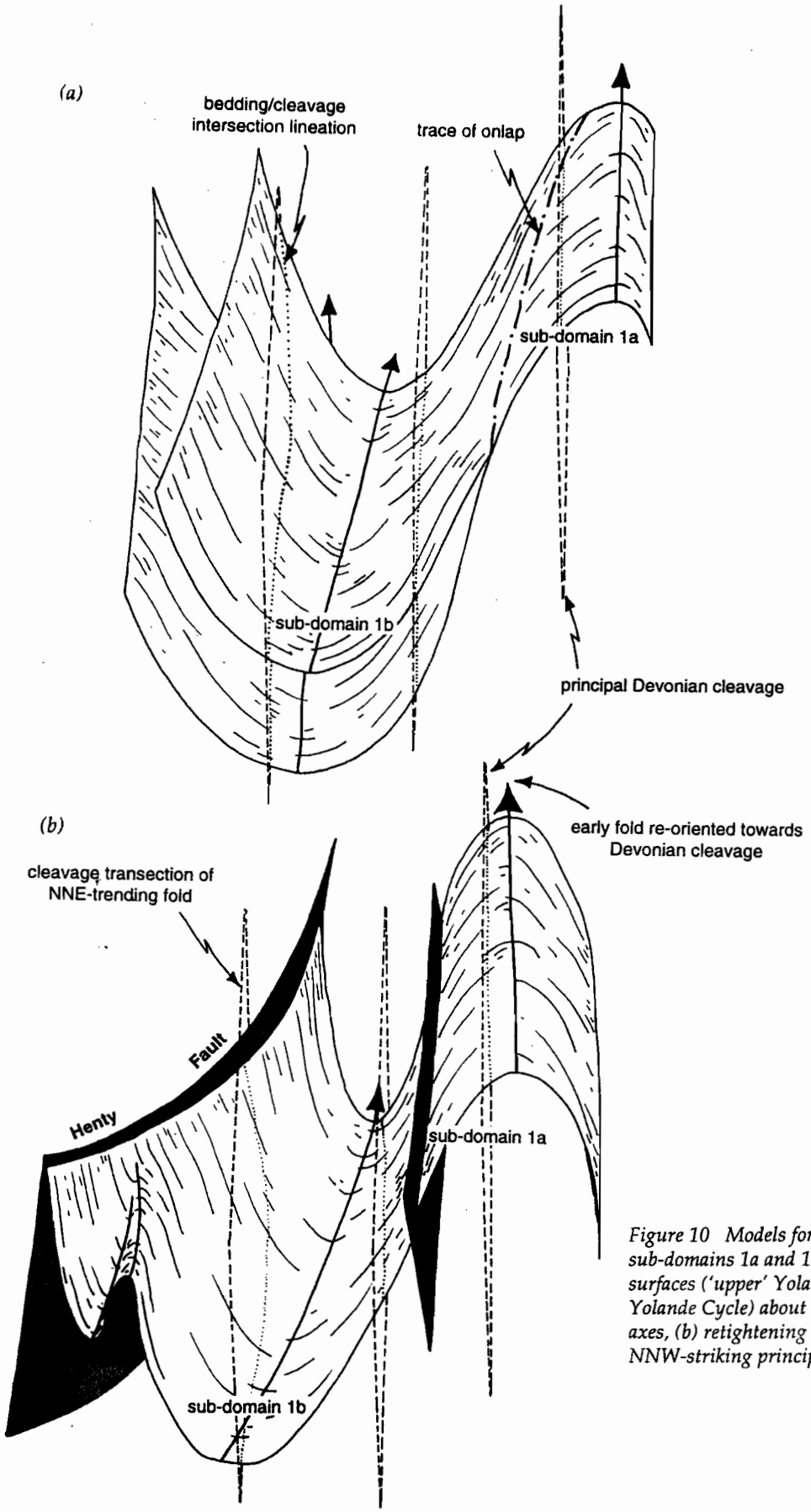

Figure 10 Models for bedding strike variation between sub-domains 1a and 1b: (a) folding of mutually inclined surfaces ('upper' Yolande Cycle lapping onto 'lower' Yolande Cycle) about NNW- and NNE-trending fold axes, (b) retightening of early NNE-trending folds by the NNW-striking principal Devonian cleavage.

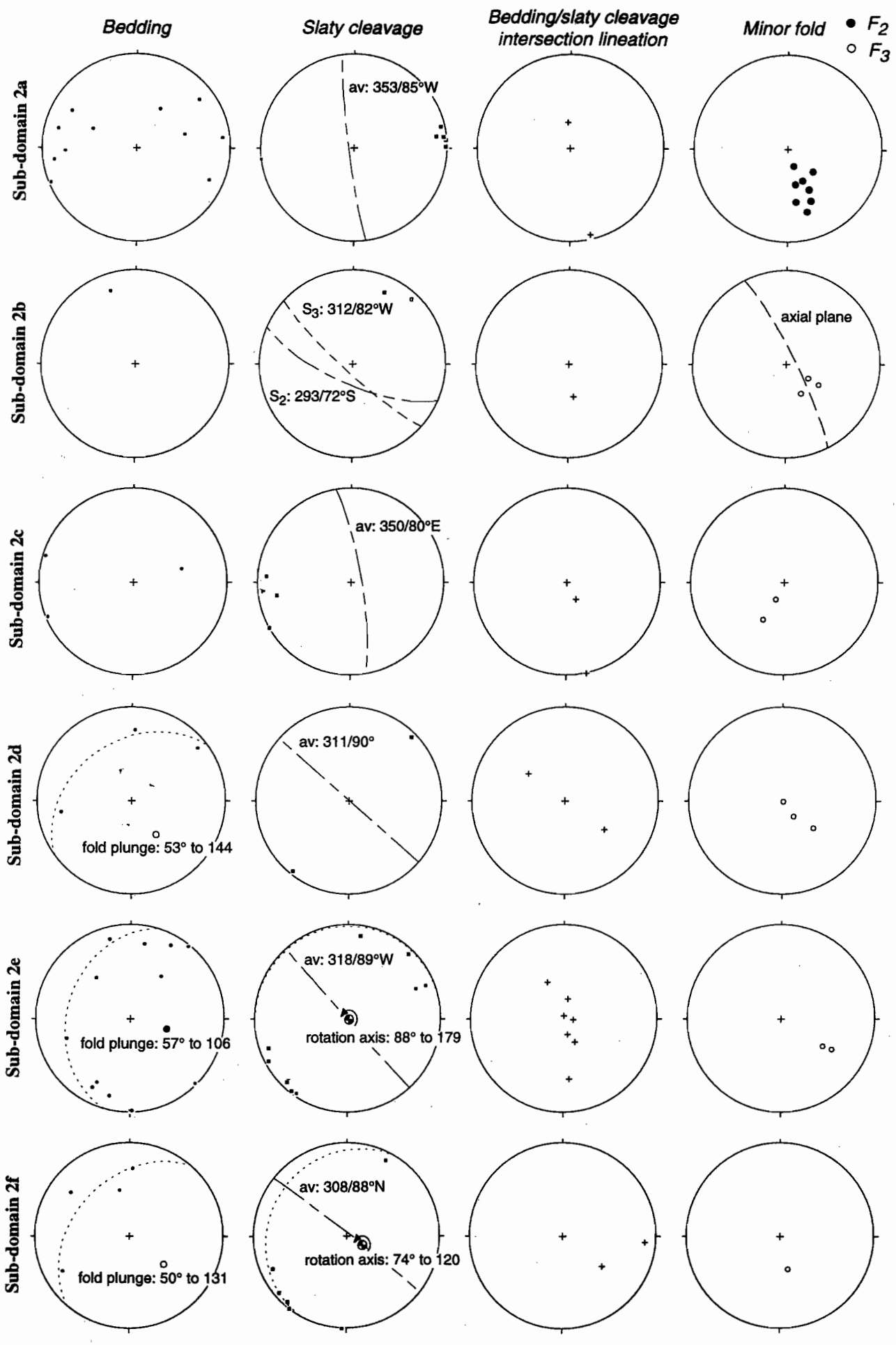

Figure 11 Equal area stereographic projections of mesoscopic data from domain 2.

trend N–S, it would appear that the phase of deformation which resulted in rotation of major folds towards the FSF also predated regional cleavage development. However, other evidence conflicts with this apparent timing relationship. This evidence is manifest in the progressive anticlockwise rotation of the principal cleavage towards the FSF in sub-domains 2e and 2f.

Domain 3

Data from domain 3 (Fig. 12) was collected from the Professor Plateau along the track to Queensbury Mine (Fig. 8). Upper Cambrian strata contained in this domain are deformed by moderately to subvertically plunging open to tight closures (F_2) positioned on the western limb of a large wavelength pre-cleavage NNE-trending anticline (F_{1-2}). In the northern part of the domain, a NW-striking cleavage is roughly axial planar to open steeply-plunging folds with strongly non-cylindrical, probable conical geometries (sub-domain 3a). F_2 folds tighten southward towards a WNW striking splay off the FSF and swing anticlockwise to form structures which plunge less steeply towards the ESE (sub-domain 3b). Adjacent to the splay off the FSF, ESE-plunging folds have become the dominant structures, effectively replacing the hinges of the earlier NNE-trending fold generation. F_2 folds in this region however, are clockwise-axially transected by the principal NW striking cleavage, which is in turn axial planar to a third generation of small-scale, subvertically plunging folds (F_3).

Although deformation is less intense in domain 3 compared to that observed in domain 2, the overall structural history and geometry interpreted for each domain is compatible. Curiously however, there is a marked contrast between the structural geometry described above and that within the fault-bounded block of Tyndall Cycle correlates adjacent to the FSF. Although insufficient data was collected from this fault block to undertake any detailed structural analysis, both the strike of bedding and cleavage atypically possess high angles to the trace of the FSF. The cause of this change in structural geometry between the Tyndall and Denison Cycle stratal packages has not been resolved.

Discussion

Evidence for pre-Devonian cleavage deformation has been identified within each structural domain. In domains 2 and 3, the interpretation of early structures as relating to a N- to NNE-trending generation of fold of probable Late Cambrian age concurs with that of previous workers in this region (Berry, 1996; Keele, 1995). In terms of geometric relationships, it is also valid to interpret the structural history in domain 1 to record oblique tightening of an early NNE- to NE-oriented folding event (ie. development of F_{1-2} folds). I have found no evidence, however, to support the interpretation of Keele (op cit.) that a Middle Cambrian syncline occurs adjacent to the FSF. In consideration of the very high strains typified in rocks from this area, any early structures would be expected to be so heavily obscured by the effects of the Devonian deformation to preserve unequivocal proof of their existence.

The geometries of folds which nucleated during the Devonian deformation (i.e. F_2 and F_3 fold generations from domains 2 and 3) have an overall close similarity with those described by Baillie and Williams (1975) from the Siluro-Devonian succession situated south of the FSF. However, in contrast to the two distinct phases of deformation interpreted by these workers to account for the variation in fold orientation (ie. from NW to WNW), I consider the moderately ESE-plunging F_2 fold generation developed adjacent to the FSF to be temporally related with the SE- to SSE-plunging F_2 structures recognised further northward of the FSF. This interpretation is based primarily on the concomitant swing of the principal cleavage towards FSF about a sub-vertical rotation axis, a feature also recognised in domain 1, but not directly related to the development of F_2 folds. As the cleavage was frequently observed to clockwise-axially transect ESE-trending F_2 folds however, the onset of pervasive cleavage development must post-date the initial clockwise rotation and tightening of these structures. The only explanation for these timing relationships is that cleavage development, tightening of early F_2 folds and rotation of these structural elements towards the FSF all occurred coevally during a single progressive deformation event. It is also probable that F_3 folds and their associated NW striking axial planar

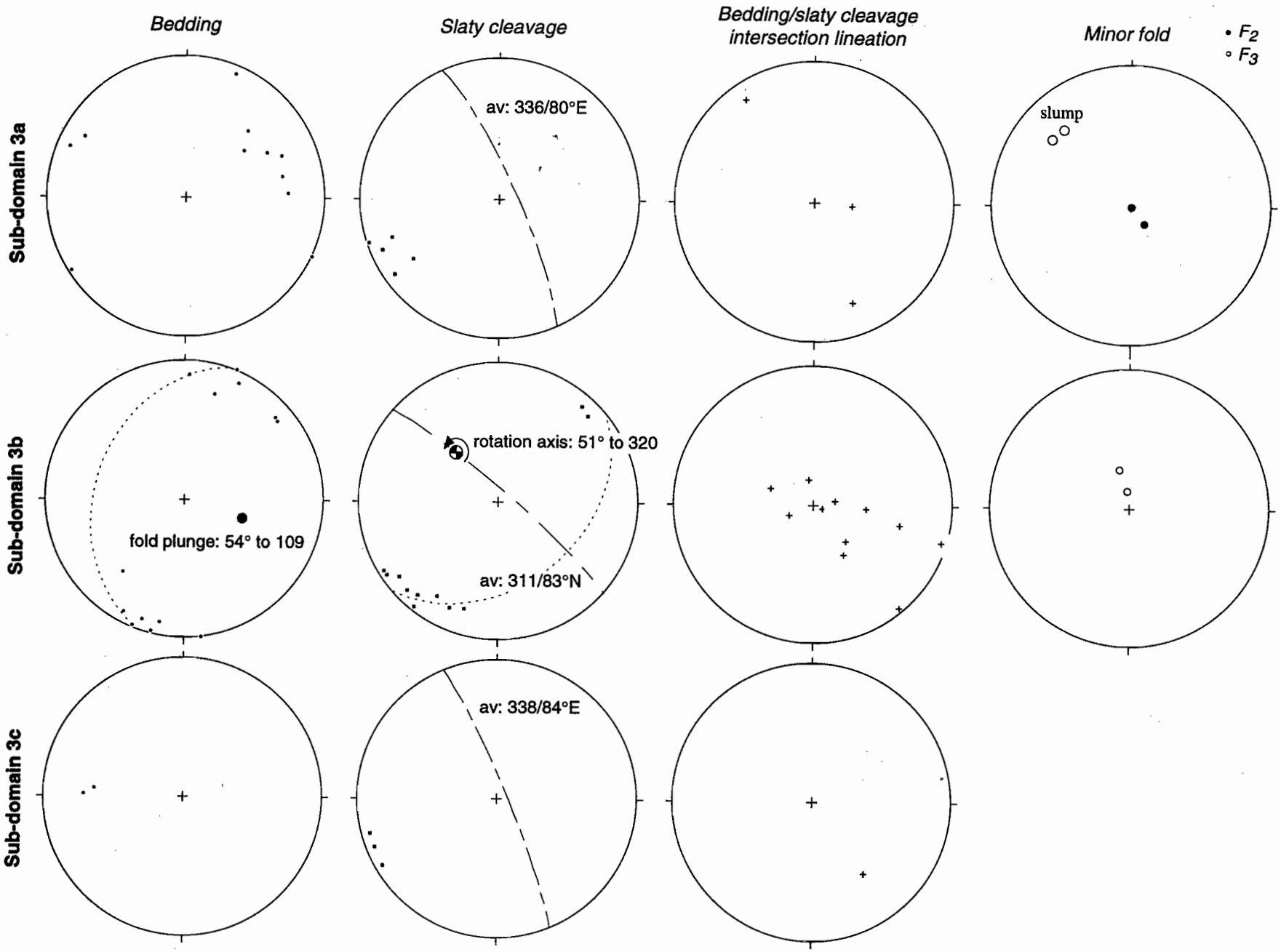

Figure 12 Equal area stereographic projections of mesoscopic data from domain 3.

cleavage developed in the later stages of this deformation event once F_2 became so tight that they could no longer accommodate strain. Williams and Baillie (1975) also documented the NW generation of folds which I correlate with F_3 and considered this these structures to reflect movement on the FSF. The fact that F_3 folds were only mapped adjacent to the FSF supports their proposition.

The structural history outlined above accounts for the variation in structural geometry north of the FSF. At distances greater than approximately 1km north of the FSF, fold geometries record the oblique shortening of mutually inclined layers or pre-existing folds during Devonian ENE–WSW compression. In domains 2 and 3, this has resulted in the development of both F_{1-2} and F_2 folds, whereas evidence of discrete F_2 in domain 1 is lacking, or ia at least weak. This structural geometry contrasts markedly with that localised around the trace of the FSF. In this area, F_2 folds have effectively replaced the hinges of larger wavelength F_{1-2} folds and an additional very strong component of non-coaxial strain is required to progressively rotate structures towards parallelism (ie. anticlockwise) with the FSF. The progressive clockwise younging of structures (ie. from F_2 to F_3) indicates that non-coaxial strain was associated with a significant component of sinistral wrench movement on the FSF. As cleavage morphology and orientation associated with F_3 folds is very similar to the axial planar fabric to F_2 folds in the north, it is probable that rotation and tightening of F_2 folds adjacent to the FSF was synchronous with the development of F_{1-2} and F_2 folds further to the north.

Conclusions

1. Yolande Cycle strata exposed north of the FSF can be divided into two packages on the bases of lithofacies associations and provenance characteristics. The 'lower' Yolande Cycle comprises intercalated acidic to intermediate shard-rich and pumiceous volcaniclastic units as well as a significant volume of medium-grained Precambrian/MUC-derived micaceous greywacke towards the top. A basaltic-andesite unit with transitional high-K to shoshonitic affinities marks the top of the 'lower' Yolande Cycle in Pearl Creek. The 'upper' Yolande Cycle exposed in the Yolande River is mostly lacking in volcaniclastic material and contains an upward coarsening and thickening cycle of intrabasinally-derived debris representing a prograding slope fan. The development of this fan system marks a change in basin geometry which potentially relates to a phase of extension and block tilting.

2. No sedimentological evidence has been identified which supports the development of the FSF as a transfer structure during the deposition of the Yolande Cycle. The distribution of Middle Cambrian mafic volcanic units along the present trace of the FSF may provide evidence of an ancient syn-magmatic fracture system.

3. Correlates of the Stitt Quartzite crop out in the Henty River immediately north of the FSF. They most likely form part of a N- to NNE-trending belt of mature sandstones which extends to the Rosebery Mine area. For the most part, coarse-grained Stitt Quartzite correlates represent deposits from turbidity currents which were probably introduced to the basin along axial channel systems. The association of sandy debris flow facies adjacent to the FSF potentially indicates that a syn-depositional topographic high existed nearby providing a source of reworked Precambrian-derived material.

4. The upper part of the Denison Cycle records a period of vigorous sedimentation and basin activity. Depocentres for dominantly coarse-grained detritus were small and laterally restricted and may have been controlled by the development of large-scale folds during the Late Cambrian.

5. Fold and cleavage relationships north of the FSF reflect superposition of Devonian structures on a pre-existing Cambrian structural geometry. In the Yolande River area a marked change in bedding strike between the 'lower' and 'upper' Yolande Cycle has been interpreted as the effects of Cambrian tectonism. Insufficient data exists at present to unequivocally determine the cause of this geometry however and both folding of a Middle Cambrian onlap surface and re-tightening of a NNE-trending Late Cambrian fold during ENE–WSW directed Devonian compression are

valid structural models. In the area west of the Henty Fault, fold geometries change dramatically as the FSF is approached from the north. North of the FSF, N- to NNE-trending pre-cleavage (?Cambrian) folds are re-tightening during Devonian compression to form large wavelength N–S trending F_{1-2} folds. Smaller-scale non-cylindrical and *en echelon* F_2 folds are coevally developed anticlockwise of the major F_{1-2} structures and have steep to moderate plunges and axial planar cleavage. In the vicinity of the FSF, high amplitude F_2 folds replaced the hinges of F_{1-2} structures and have rotated anticlockwise towards the WNW and the trace of the FSF. These F_2 folds sometimes have an axial planar cleavage, but are generally transected in a clockwise sense by the principal Devonian fabric, which becomes axial planar to steeply or moderately plunging F_3 folds. F_{1-2}, F_2 and F_3 folds were probably developed during a single progressive deformation event related to ENE–WSW directed Devonian compression with a localised but significant non-coaxial strain component related to sinistral movement on the FSF.

References

Baillie PW & Williams PR 1975. Sedimentary and structural features of the Bell Shale correlate (Early Devonian), Strahan Quadrangle, western Tasmania. Pap. Proc. Roy. Soc. Tas. 109, 1–13.

Baillie PW & Corbett KD 1985. Geological Survey explanatory report Strahan 1:50,000 sheet. Department of Mines, Tasmania 76 pp.

Baillie PW, Corbett, KD, Cox SF, Corbett EB, Bravo AP, Gee RD, Gulline AB, Legge PJ, Pike GP, Turner NJ, Williams PR, McClenaghan MP & Brown AV 1977. Strahan. 1:50,000 series. Mines Dept Tas.

Berry RF 1996. A structural cross-section of the Mt Read volcanics at 535000N. AMIRA Project P.291A Fifth report 1–12.

Berry RF & Keele RA 1993. Cambrian structure in western Tasmania. AMIRA Project P.291 Final report 55–68.

Berry RF, Meffre S & Fulton R (this report). Heavy minerals, provenance and lithostratigraphy. AMIRA Project P.291A Final report.

Berry RF, Selley D, White MJ & Meffre S (this report). Lithogeochemistry. AMIRA Project P.291A Final report.

Brown AV 1986. Geology of the Dundas–Mt Lindsay–Mt Youngbuck region. Geological Survey Bulletin 62. Department of Mines, Tasmania 221pp.

Bull SW 1994. Preliminary report: Sedimentology of the Dundas Group with reference to a possible syn-depositional growth fault west of Rosebery. AMIRA Project P.291A First report 1–14.

Bull SW 1995. Second report: Sedimentology of the Dundas Group and correlates with reference to a possible syn-depositional growth fault west of Rosebery. AMIRA Project P.291A Third Report 35–44.

Corbett KD 1992. Stratigraphic-volcanic setting of massive sulphide deposits in the Cambrian Mount Read volcanics, Tasmania. Bull. Soc. Econ. Geol. 3, 564–586.

Corbett KD, Berry RF & Selley D (this report). Stratigraphic correlation. AMIRA Project P.291 Final Report.

Corbett KD, Calver CR, Everard JL & Seymour DB 1989. Queenstown. 1:25,000 series. Dept Mines Tas.

Crawford AJ, Corbett KD & Everard JL 1992. Geochemistry of Cambrian volcanic-hosted massive-sulfide-rich Mount Read Volcanics, Tasmania, and some tectonic implications. Econ Geol. 87, 597–619.

Gibson RP 1991. The geology of the Mt Read volcanics in the Anthonly Road–Newton Creek area, western Tasmania. Honours Thesis, Univ. Tasm. (unpubl.) 88pp.

Keele RA 1995. A new structural section between Queenstown and Zeehan: preliminary results on structure and unconformity relationships between the Upper Dundas Group and Zeehan Conglomerates. AMIRA Project P.291 Third report 45–50.

Poltock R 1992. Geology of the Henty Fault wedge, western Tasmania. M Econ Geol Thesis, Univ Tasm (unpubl.) 76pp.

Selley D 1996. Structure and sedimentology of the Dundas Group, western Tasmania. PhD, Univ. Tas. (unpubl.).

Shanmugam G, Block RB, Mitchell SM, Beamish GWJ, Hodgkinson RJ, Damuth JE, Straume T, Syvertsen SE & Shields KE 1995. Basin-floor fans in the North Sea: Sequence stratigraphic models vs. sedimentary facies. AAPG Bull. 79, 477–512.

Sedimentological evidence for Cambrian growth faults on the eastern side of the Dundas Trough, western Tasmania

Matt White
edited by Ron Berry
CODES Special Research Centre, Geology Department, University of Tasmania

Abstract

Four areas on the eastern side of the Dundas Trough were studied to test the model for Middle Cambrian extension proposed in AMIRA project P291. Three areas were along a proposed precursor to the Henty Fault. These areas were the Moxon Saddle–Henty area, the Northern Anthony Road–Murchison Gorge area, and the Hanging Rock area. Another probable Cambrian growth fault structure, to the east of Moxon Saddle, in the Anthony River–Mount Selina area was also studied to test a smaller growth fault.

In the Moxon Saddle area, Tyndall Group rhyolites were probably originally deposited on both sides of the fault, and were subsequently eroded off the northeastern fault block across a fault scarp. In the Henty area, provenance of volcaniclastic units of the upper part of the Tyndall Group, were probably derived from the CVC to the east, being consistent with a west-block-down fault configuration. A normal, west dipping fault orientation is preferred. This fault was active during or after Tyndall deposition. We found no evidence that indicated a pre-Tyndall Group fault in this area. In the Murchison and Hanging Rock areas no new evidence was found for Cambrian movement along the palaeo-Henty Fault. In the Anthony River area, the geometry of the surviving sedimentary package is most consistent with active extensional faulting during Tyndall Group deposition with basin inversion during the Denison Cycle.

Introduction

Four areas on the eastern side of the Dundas Trough within the Mount Read Volcanics were investigated with the aim of finding sedimentological evidence, to confirm the presence of Cambrian growth faults interpreted by Berry & Keele (1993). Cambrian growth faults have been proposed along the western side of the Dundas Trough and also within the trough (Berry & Keele 1993). This version of the report is the result of editing the original report (White 1995) to bring it into line with other aspects of the study not available at the time of the original report. Dr White did not have an opportunity to check these editorial changes and responsibility for introduced errors remains with the editor.

During extension, active growth faults have a significant control on clastic sedimentation. This is most obvious in modern subaerial rift systems (e.g. East African Rift; Baker 1986). In relatively deep subaqueous settings, the effects of growth faults on sedimentation are less obvious due to the quiet sub-wavebase conditions limiting erosion and reworking (cf. Bull 1995). Recognising Cambrian growth faults in the Dundas Trough is difficult and requires detailed structural and sedimentological analysis. The sedimentological methods used to define growth faults were (1) regional lithofacies analysis and (2) identification of distinctive components in clastic facies on the down-thrown side of the fault. Method 2 was the most important technique applied in this project. Due to the massive nature of the deposits in these areas, (where transportation processes were largely by subaqueous high-density sediment gravity flows), no paleocurrent indicators were identified.

The areas studied were the Moxon Saddle–Henty area, the Northern Anthony Road–Murchison Gorge area, the Hanging Rock area and the Anthony River area (Fig. 1). The inferred Cambrian growth-fault structure at Moxon Saddle (which occurs to the east

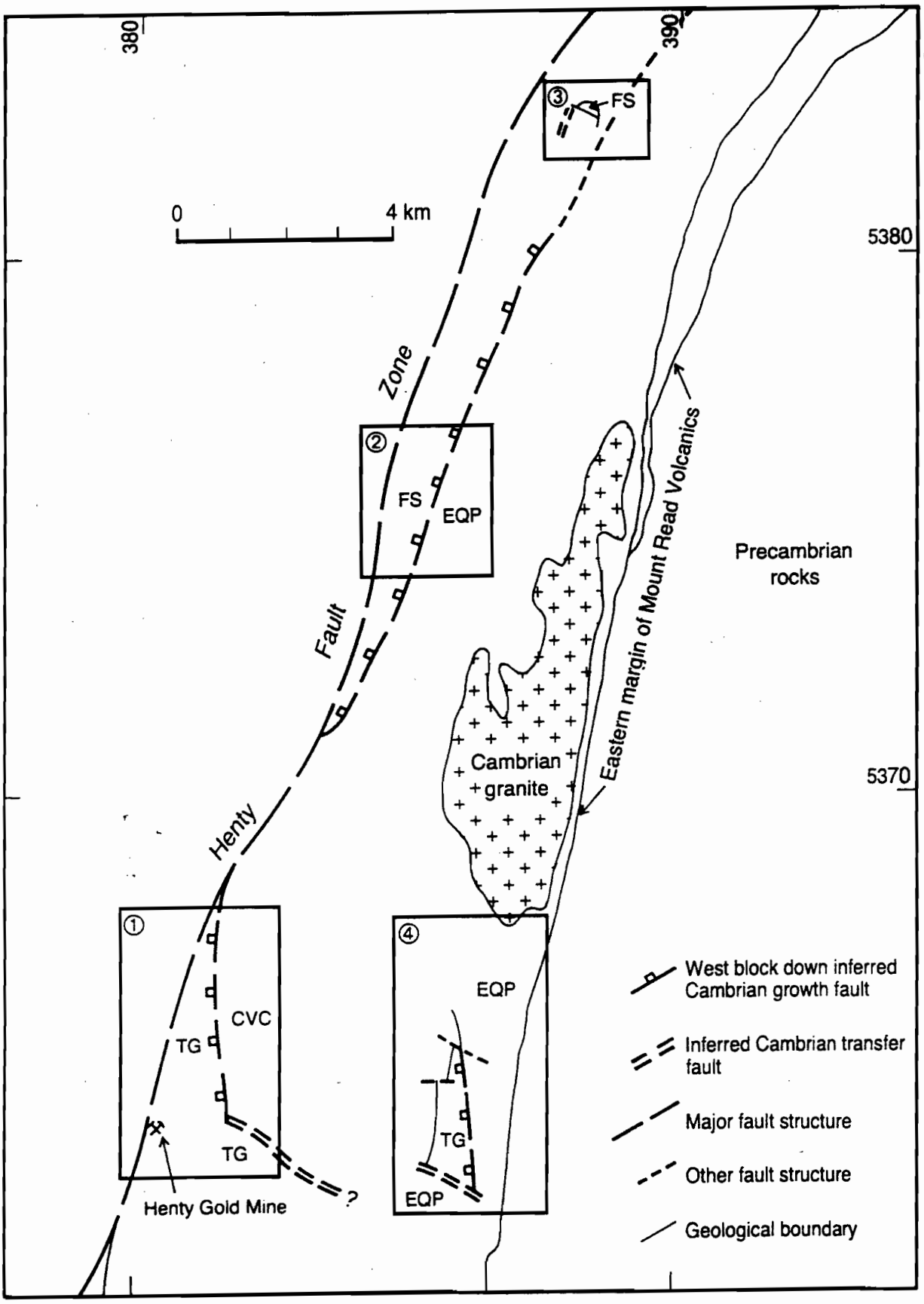

Fig. 1 — Location diagram showing the four areas studied for this project. (1) Moxon Saddle–Henty area; (2) Northern Anthony Road–Murchison area; (3) Hanging Rock area; and (4) Anthony River area. TG = Tyndall Group, CVC = Central Volcanic Complex, EQP = Eastern quartz-phyric sequence, FS = Farrell Slate sequence. Geology from Berry & Keele (1993), Corbett & McNeill (1988).

of the Henty Fault Zone and strikes north–south) merges with the Henty Fault Zone to the north, and then diverges away from it again to the northeast in the Murchison area (Fig. 1). This structure probably extends further north, passing close to the Hanging Rock area (Fig. 1). This fault was interpreted as a growth fault (west block down) active during a Middle Cambrian extension event (Berry & Keele 1993). Areas close to the main Henty Fault Zone were not studied as post-Cambrian activity has largely destroyed evidence for Cambrian activity. Another probable Cambrian growth fault structure occurs to the east of Moxon Saddle around the Anthony River–Mount Selina area. An east–west transfer linking these two major growth faults is possible but unlikely.

Moxon Saddle–Henty Area

Moxon Saddle

The Moxon Saddle area lies approximately 2 km NNE of the Henty Gold Mine (Fig. 2). The Henty Fault Zone (HFZ) in this area, comprises a NNE-trending, steeply west-dipping fault zone containing highly distorted, foliated, sericite-chlorite altered mudstone, sheared Central Volcanic Complex rocks and other fault zone facies which record a complex history of fault movements (Berry 1989). To the east of the HFZ is a wedge-shaped area of Tyndall Group rocks composed dominantly of coherent rhyolite, along with minor lenses of crystal-, lithic-rich volcaniclastic pebbly sandstone (Figs 2, 3). The Tyndall Group 'wedge' is fault bounded to the east by rocks of the CVC (Figs 2, 3) composed mainly of feldspar-phyric volcanic facies (McNeill 1987, Jenkins 1991) including lavas and possible pumice-bearing volcaniclastic units. This east-bounding fault (informally referred to as Moxons fault) merges with the Henty Fault Zone to the north around 5368600N (see Fig. 1). Moxons fault has been interpreted as a Cambrian growth fault structure associated with the Henty Fault system (Berry & Keele 1993) with a west-side-down configuration.

The Tyndall Group in the Moxon Saddle area is dominated by quartz-feldspar porphyritic coherent volcanic rock interpreted as rhyolite lava. Flow banding textures are generally planar with minor occurrences of mesoscopic open flow-folding. The banding orientation varies over the area but is generally steeply dipping to the south and west (see McNeill 1987). Autobrecciation textures are uncommon in these rocks, and patchy chlorite alteration forms pseudobreccia textures in places. The phenocryst content varies from 5% to 25% and phenocryst size also varies (quartz is up to 6 mm in places). These rocks correlate with the rhyolite lavas in the Henty Canal area to the south which are stratigraphically within the Comstock Formation (White & McPhie, 1996).

Moxons fault is a wide (50–100 m), north-trending, steeply west?-dipping shear zone with feldspar-phyric rocks of the CVC to the east. Approaching the fault contact, the NNW-trending, steeply west-dipping cleavage foliation increases in intensity. At the position of the inferred fault the rocks are strongly silica-sericite-pyrite altered, strongly weathered and the foliation is very intense, completely destroying the primary texture of the rock. The foliation is subparallel to the regional cleavage foliation suggesting a Devonian age for the shearing. Jenkins (1991) inferred a Devonian age for the last movement on this fault structure. No structural evidence for Cambrian movement was found.

Thin lenses of pebbly volcaniclastic sandstone occur within the Tyndall Group rhyolite sequence close to Moxons fault (located by Boyd 1994) and may represent redeposited volcaniclastic facies adjacent to a Cambrian fault scarp. One clastic lens (Lens A) occurs well within the lava sequence (Fig. 2) consisting of quartz-feldspar crystal-rich volcaniclastic sandstone with minor amounts of lithic fragments (<5%), and minor magnetite grains (characteristic of the Comstock Formation, White & McPhie, 1996). The lithic clasts are dominantly pebble size and consist of quartz-feldspar porphyry (rhyolite lava) clasts, green sericite altered clasts and fine grained cream coloured siliceous (cherty) aphyric clasts. Two pebbly volcaniclastic sandstone lenses (Lens B, Lens C) occur further north on the eastern limit of the Tyndall Group, up against the fault contact (Fig. 2). These rocks are strongly foliated, strongly silica-sericite-chlorite altered, and moderately weathered making precise interpretation difficult. They consist of crystal-lithic sandstone with 10–20% lithics and abundant quartz, feldspar with minor

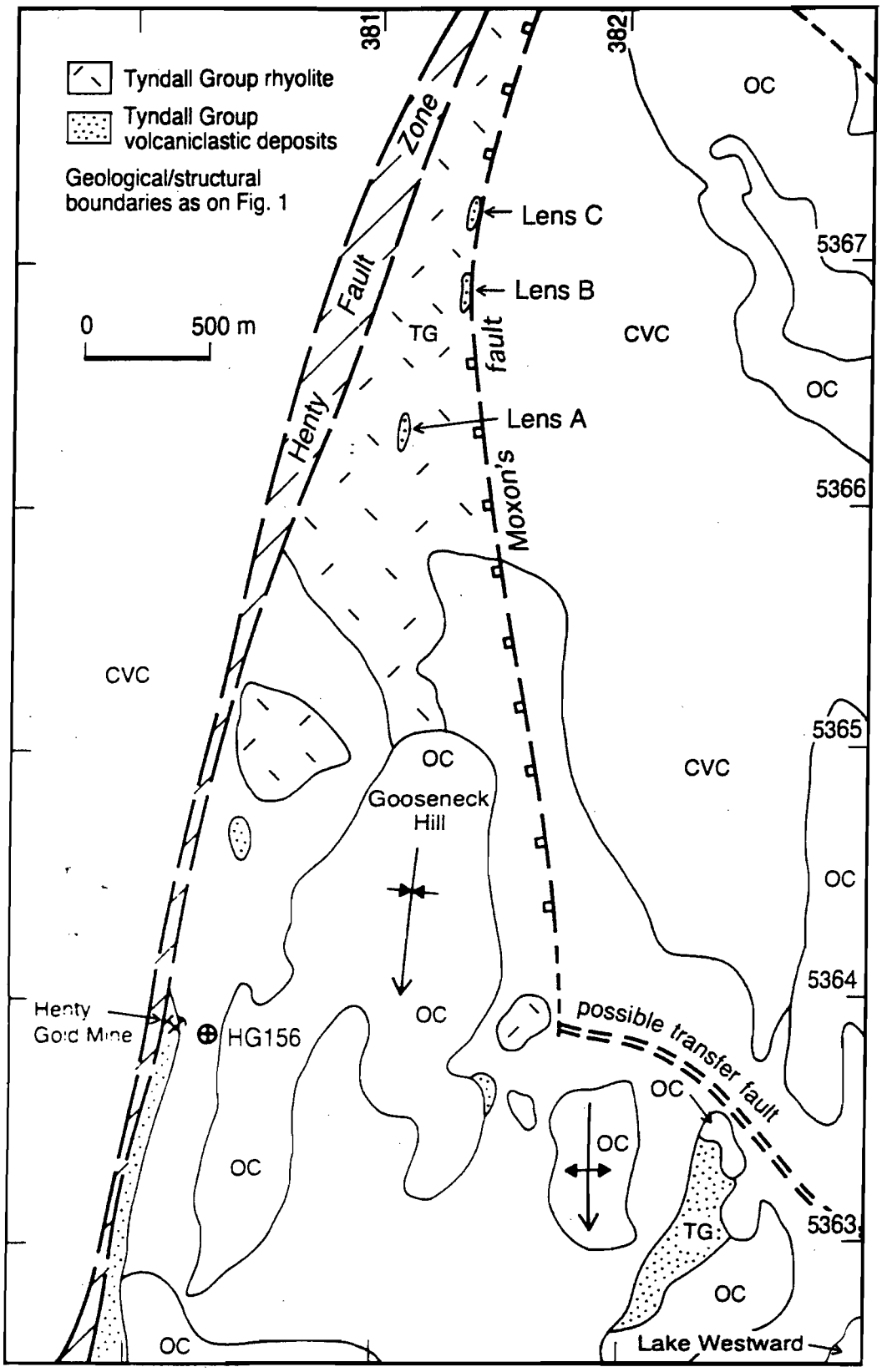

Fig. 2 — Geological sketch map of the Moxon Saddle–Henty area showing the position of the inferred Cambrian growth fault (Moxons fault) and possible associated transfer fault. TG = Tyndall Group, CVC = Central Volcanic Complex, OC = Owen Conglomerate. Geology from McNeill (1987), Berry & Keele (1993), herein.

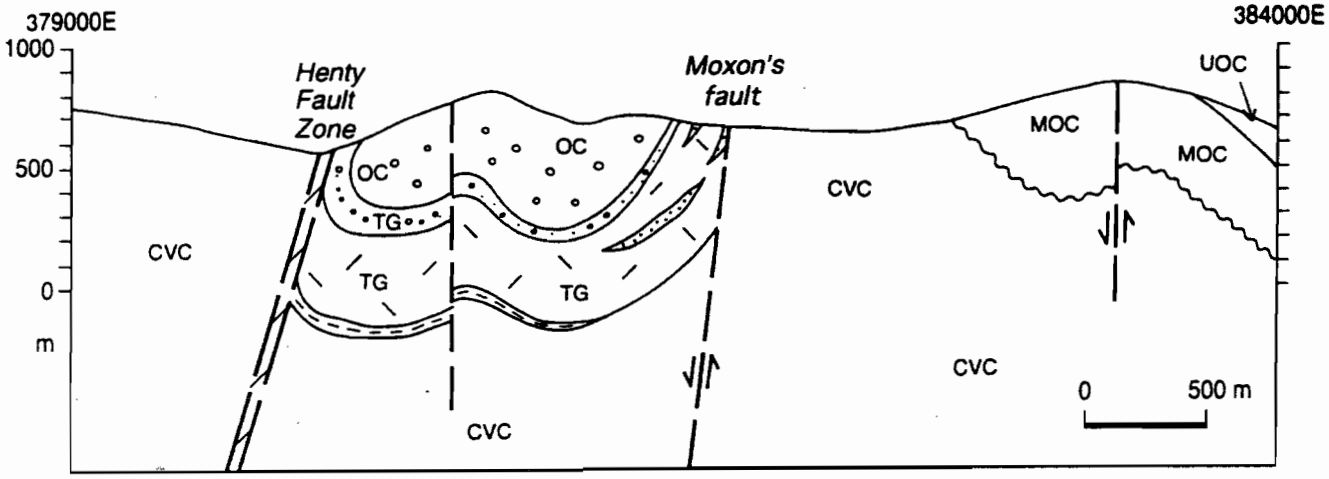

Fig. 3 — East–west cross-section interpretation sketch of the Moxon Saddle–Henty area at 5364000 N. TG = Tyndall Group, CVC = Central Volcanic Complex, OC = Owen Conglomerate, MOC = Middle Owen Conglomerate, UOC = Upper Owen Conglomerate. Geology from McNeill (1987), herein.

magnetite. The lithics comprise angular pebble size quartz-feldspar porphyritic (rhyolite) clasts, silica-sericite-hematite altered clasts, creamy silica altered aphyric clasts and very rare feldspar-phyric hematite altered clasts. The presence of clastic units in the Tyndall Group, adjacent to the fault is consistent with a growth fault interpretation. Some of the aphyric clasts and rare feldspar-phyric clasts may have been sourced from the CVC rocks to the east. However, the lack of diagnostic CVC clast types and the absence of paleocurrent indicators limit the significance of these results.

Lake Westward

Tyndall Group facies also occur 2–3 km SSE of Moxon Saddle, just northwest of Lake Westward and near the south eastern side of Gooseneck Hill (see Fig. 2). These are volcaniclastic breccia/conglomerate and sandstone facies, typical of the upper Tyndall Group. In this area, the Tyndall Group is conformably overlain by the Lower Owen Conglomerate with a thin (1–5 m wide) transitional zone (of mixed Precambrian and volcanic provenance) on the contact (Jukes Conglomerate; see McNeill 1987). The Tyndall Group volcaniclastic conglomerate beds are dominantly massive with planar diffuse stratification in places and are generally several metres thick. Pebbly sandstones associated with the conglomerate beds are diffusely stratified and in places are lensoidal, showing low angle truncations and minor cross-bedding. Planar bedded fine to medium sandstone beds (cm thick) were also observed. The conglomerate beds contain subangular to subrounded pebble to boulder sized clasts in a sandy matrix. The clast type is almost entirely quartz-feldspar porphyritic rhyolite (similar to the Tyndall Group lavas further north) and the matrix is a coarse quartz-lithic sandstone, with sericite ± hematite alteration. The conglomerates also contain rare red hematite-silica clasts and rare creamy-white siliceous clasts. The most likely source of this facies is the Tyndall Group rhyolite lava complexes, which occur lower in the Tyndall Group (Comstock Formation) and are exposed further north at Moxon Saddle. Some of the rhyolite clasts in the conglomerate are subrounded to rounded and have probably been reworked in above-wavebase environments prior to deposition. The eroded lava debris was probably initially deposited in an series of alluvial fans or fan delta systems. Some of the diffusely stratified and cross-stratified volcaniclastic units near Lake Westward may represent this style of deposition. Much of the lava-derived debris was then redeposited down-slope, in subaqueous sediment gravity flows.

Henty Drill Hole

A Henty drill hole (HG156), drilled vertically as the new Henty shaft pilot hole, intersects the Tyndall

Group sequence in the footwall of the Henty Gold Mine, approximately 2 km SSW of Moxon Saddle (see Fig. 2). The sequence in the hole is similar to the Tyndall Group sequence at Moxon Saddle. A number of volcaniclastic conglomerate/breccia and sandstone units occur in the sequence along with rhyolite lavas and associated autoclastic breccias. The hole was logged to check if the volcaniclastic facies contain distinctive components that suggest an easterly provenance. A summary of the drill hole log is given (Fig. 4). The hole passes through an inclined synclinal structure, firstly up-sequence through the Tyndall Group into the Owen Conglomerate (positioned in the core of the syncline), then back down-sequence again into the upper Tyndall Group volcaniclastic units and finally down into the underlying Tyndall Group rhyolite sequence (Fig. 4). A fault slice of Owen Conglomerate occurs in the Tyndall Group sequence near the top of the hole.

Volcaniclastic lithic breccia/conglomerate and sandstone facies occur in the hole stratigraphically underlying the Owen Conglomerate (upper part of the Tyndall Group) (see Fig. 4). The breccia/conglomerate facies are both clast- and matrix-supported and contain angular to subrounded (and minor rounded), pebble to cobble size clasts. The clast population is dominated by rhyolite clasts that have a similar texture to the massive rhyolites at Moxon Saddle. The facies also contains minor proportions of feldspar ± altered-ferromagnesian phyric intermediate volcanic clasts, aphyric chlorite-sericite altered clasts and cherty siliceous clasts. The intermediate volcanic clasts are similar in texture to typical CVC rocks and may have been derived from the CVC to the east. CVC facies are also widespread to the west of the Henty Fault Zone, but their present position is due to significant post-Cambrian movements on the Henty Fault Zone. The provenance direction for the intermediate clasts cannot be directly determined but an easterly source is likely.

Structural Models

1. The erosion of Tyndall Group rhyolite lavas, implied by the abundance of rhyolite-derived clastic units to the south of Moxon Saddle, may be due to erosion of lavas originally deposited on the eastern side of Moxons fault, (up-thrown side of normal fault). The east–west transfer (proposed by Berry & Keele 1993) at the south end of Moxons fault may also have controlled deposition. In other words, the northeast block which once contained Tyndall Group lava facies, probably shed eroded lava debris to the south and west, depositing the rhyolite-derived volcaniclastic deposits in a basin on the downthrow side of the two faults (Fig. 5). This interpretation is consistent with the regional distribution of facies observed in the Anthony Road/Henty area further south (data collected previously from PhD project work). In these areas, rhyolite lava and lava-derived clastic units thin out southward, but the Tyndall Group stratigraphy actually thickens to the south, possibly indicating deepening of the basin to the south away from the proposed growth fault.

2. An alternative interpretation is that Moxons fault was originally an east-dipping reverse fault that underwent movement during late Tyndall Group time (Middle Cambrian to Late Cambrian). In this model, rhyolite lava on the eastern side of the fault was uplifted during late Tyndall Group time and shed rhyolite lava debris and some CVC clasts into a depocentre to the west and south. Like model 1), this model requires relative uplift of the eastern block. The reverse movement may have occurred during the Delamerian compressional deformation events proposed by Berry & Keele (1993). However, the Delamerian events are thought to have occurred after Tyndall Group time.

3. Models proposing only Devonian deformation are not capable of explaining the rapid stratigraphic changes that occur across the Moxons fault.

Models 1 and 2 are possible, however the first model is most favoured, because it also explains why the eastern block is upthrown during Tyndall deposition but is the centre of thickest Owen Conglomerate deposition in the Late Cambrian.

Northern Anthony Road–Murchison Area

Volcanic and volcaniclastic units in the Farrell Slate sequence along the northern part of the Anthony Road, approximately 1–2 km south of the Murchison Highway junction, and along the Murchison Dam Road were also assessed for this study (Fig. 1). The contact between the Eastern-quartz phyric sequence

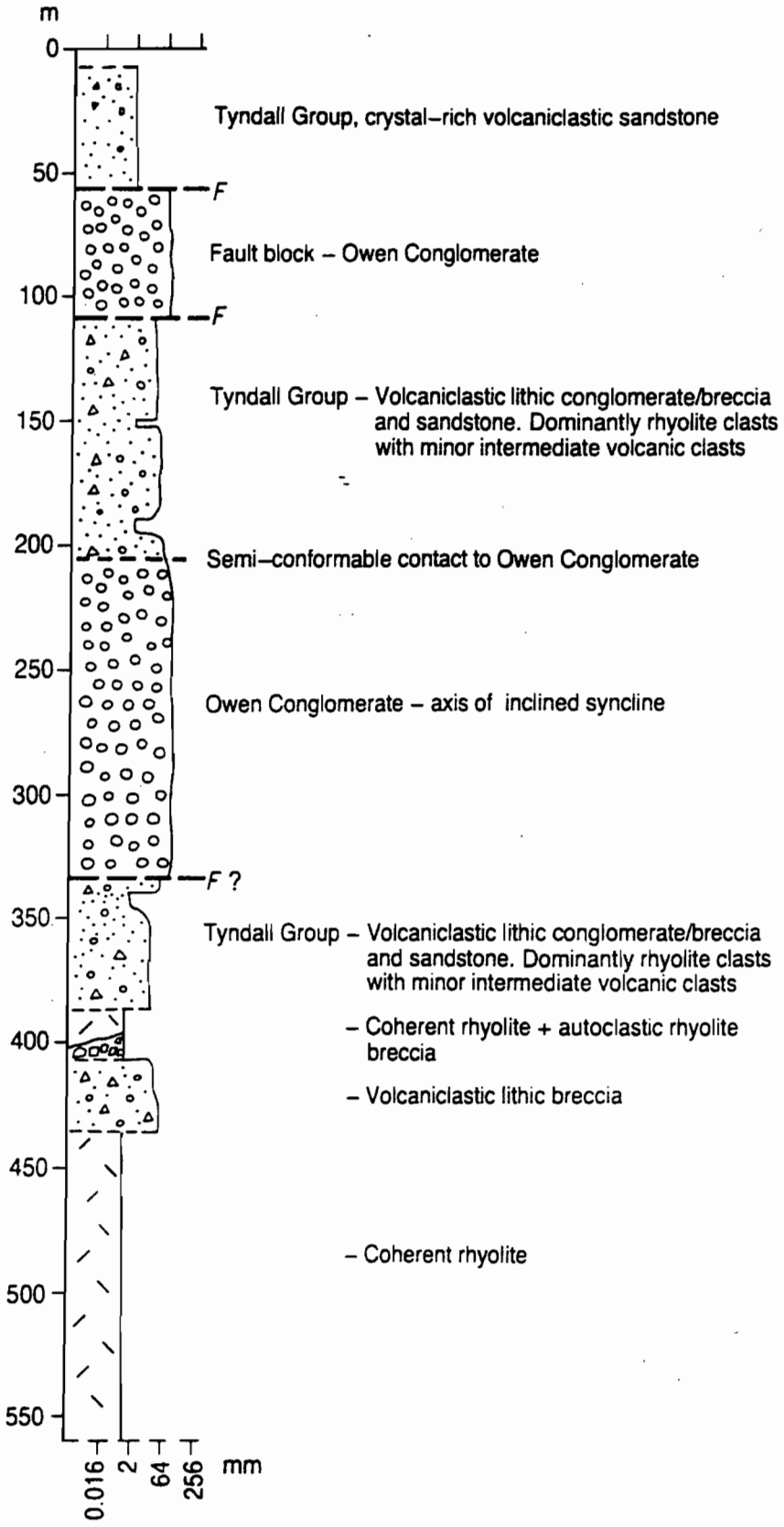

Fig. 4 — Diamond drill log summary of the Henty shaft pilot hole HG156. See Figure 2 for collar location.

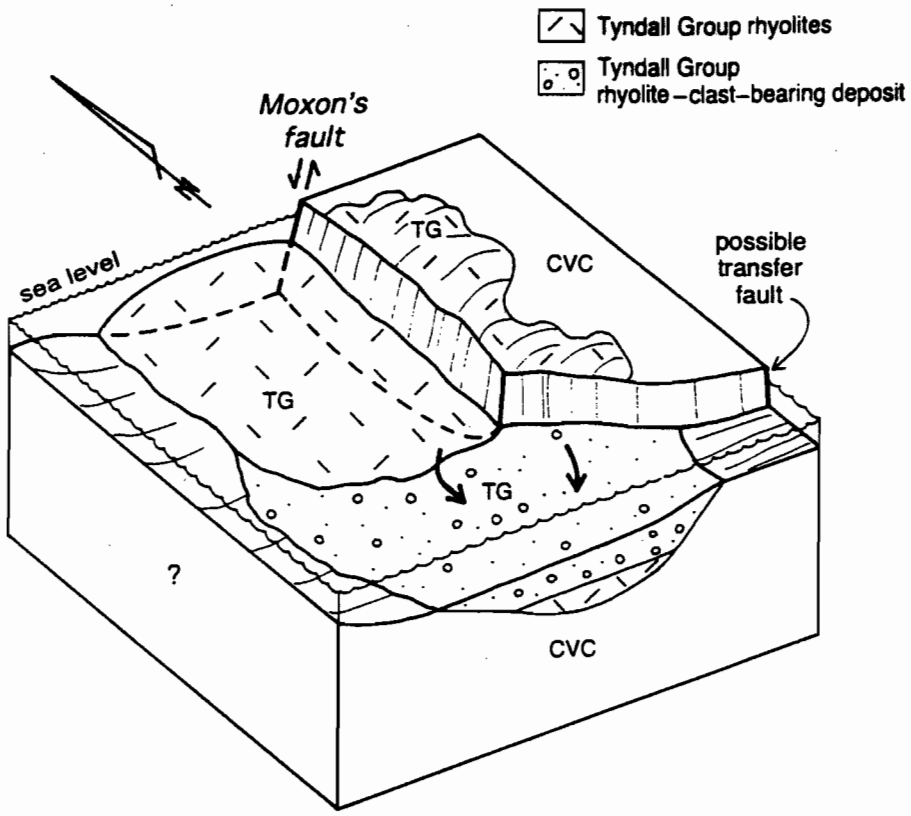

Fig. 5 — Schematic block diagram depicting the preferred model for Tyndall Group deposition in the Moxon Saddle–Henty area. The diagram shows a normal growth fault (Moxons fault) and possible transfer fault controlling deposition of the rhyolite-clast-bearing volcaniclastic units of the Tyndall Group. TG = Tyndall Group, CVC = Central Volcanic Complex.

(EQPS) (or Murchison Volcanics, Polya 1981) and the Farrell sequence is interpreted as a west-dipping inverted Cambrian normal growth fault (Berry & Keele 1993), which records Cambrian movement associated with the Henty Fault system. The Farrell volcaniclastic units were investigated for components that indicate an easterly provenance. The provenance of these clasts is undefined and provide no constraints on the basin model proposed.

Hanging Rock

The Hanging Rock area is located about 500 m east of Mackintosh Dam and was accessed by canoe from the western shore of Lake Mackintosh. At Hanging Rock, undifferentiated units of the Farrell Slate sequence (which includes slate, non-volcanic sandstone and volcaniclastic sandstone/breccia facies) were identified by Corbett & McNeill (1986).

The sequence at Hanging Rock contains three lithofacies:

- a sequence of turbiditic graded sandstone and mudstone,
- a large area of porphyritic textured intermediate to mafic volcanic rock (probably andesite or basalt) and overlying polymict volcaniclastic pebble/cobble conglomerate and sandstone, and
- a pebbly sandstone with quartz-feldspar phyric volcanic clasts dominant

These units are unconformably overlain by siliciclastic conglomerate and sandstone of the Owen Conglomerate. The contact is very sharp, with no evidence of faulting and an angular discordance of 47°. No evidence for an eastern source was identified. The truncation of the Farrell Slate against an unconformity indicates that any basin bounding fault is further east at the level of this Animal Creek Greywacke correlate.

Anthony River Area

The Anthony River area, around Lake Plimsoll and Mount Selina contains a wedge-shaped body of Tyndall Group volcaniclastic conglomerate and sandstone facies (Fig. 6). The area was briefly investigated two years ago (White 1996). During that time, the Anthony Power Tunnel was briefly assessed and the Mount Selina–Anthony River area was mapped, mainly to investigate the types of facies present in the Tyndall Group rocks. The Tyndall Group facies in this area correlate with the upper Tyndall Group (White 1994). The area was re-visited to establish the nature of the eastern boundary of the Tyndall Group (to the Eastern quartz-phyric sequence) and to investigate clast types in the Tyndall Group conglomerates in order to establish their provenance.

The wedge-shaped body of Tyndall Group is fault bounded to the south. This fault boundary comprises a cross-cutting, ESE-striking (sub-vertical?) contact, at a high angle to bedding in the Tyndall Group, with older Eastern quartz-phyric sequence rocks exposed to the south (Fig. 6). This is probably a Devonian fault as it trends subparallel to other Devonian structures in the area. However, a Cambrian normal/transfer fault may have existed at this location prior to Devonian reactivation (see below).

The western contact of the Tyndall Group 'wedge' passes into siliciclastic units of the Middle Owen Conglomerate with possible lenses of Jukes Conglomerate in places at the contact (McNeill 1987). Bedding attitudes are similar across this boundary suggesting a semi-conformable to disconformable contact. A few kilometres north, in the Anthony Power Tunnel, the same contact is highly irregular and sharp, and represents an irregular erosional contact. Units of the Middle Owen Conglomerate lie directly on the Tyndall Group, and the Lower Owen Conglomerate is missing, implying some time break between these units. The contact is therefore interpreted as a disconformity.

The eastern contact of the Tyndall Group with the EQPS is interpreted as a fault contact (herein referred to as Selina fault) (Figs 6, 7) as strong shearing and intense chlorite-pyrite alteration is present at the contact in exposures in the Anthony River. A few kilometres further north in the Anthony Tunnel, this contact consists of a strong shear zone (approximately 5–10 m wide) that required concrete lining for tunnel support. This fault probably represents a Cambrian growth fault with a west side down configuration. It was active in the Devonian, as the regional cleavage associated with Devonian folding is intense and subparallel to the fault attitude. The Tyndall Group facies wedge out or thin to the north (Fig. 6), due to (1) primary lateral thickness changes controlled by basin architecture; (2) erosional disconformity; or (3) an east-bounding fault (Selina fault) displacing part of the Tyndall Group during Devonian reactivation. Number 1 above is the most likely option as the overlying Middle Owen Conglomerate also thins to the north (see McNeill 1987).

The Tyndall Group is composed of polymict volcaniclastic conglomerate and pebbly sandstone, typical of the upper Tyndall Group (White 1994). Grainsize ranges from cobble/boulder clast-supported conglomerate to coarse sandstone, with sandy matrix-supported pebble/cobble volcaniclastic sandstone being the most common facies. The beds are generally thick to very thick and massive (m to 10's m thick) showing diffuse planar stratification in places. The deposits are poorly sorted and clasts vary considerably in size and shape. Well rounded clasts are common indicating reworking above wave base prior to deposition, with some additions of subrounded to subangular and lesser angular types. The clast population is diverse, comprising dominantly quartz-feldspar (felsic) porphyritic volcanic clasts, granite clasts, and undifferentiated hematite altered clasts, with minor sedimentary intraclasts, metamorphic Precambrian basement-derived quartzite, feldspar-ferromagnesian (intermediate) porphyritic clasts, and other undifferentiated altered clasts. The matrix is medium to very coarse sand largely composed of quartz crystals and lithic fragments. The strong Devonian strain has flattened the clasts in places and modified the primary clast shapes. Within 100 m of the east bounding fault (Selina fault), the foliation is intense and clasts have been very strongly flattened.

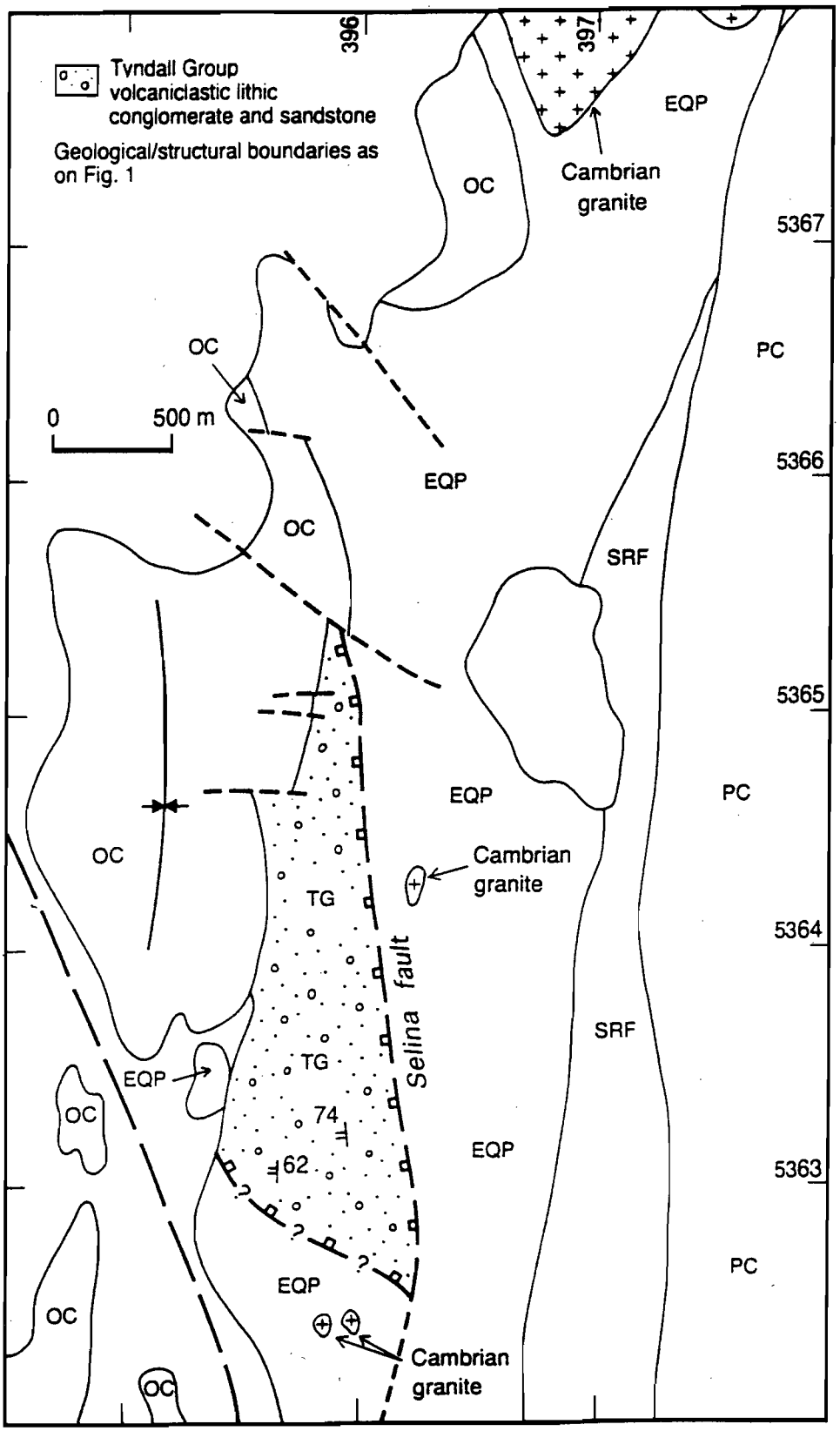

Fig. 6 — Geological sketch map of the Anthony River area showing the position of the inferred Cambrian growth fault (Selina fault). TG = Tyndall Group, EQP = Eastern quartz-phyric sequence, SRF = Stitch Range Formation, PC = Precambrian rocks, OC = Owen Conglomerate. Geology from McNeill (1987), herein.

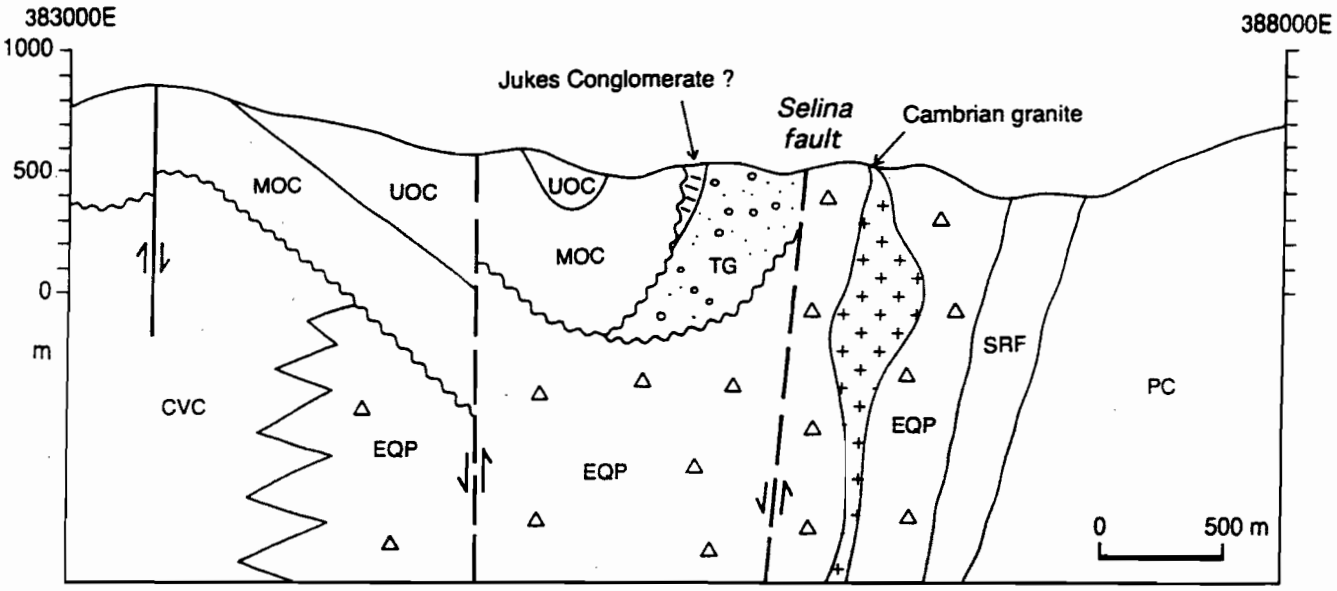

Fig. 7 — East–west cross-section interpretation sketch of the Anthony River area at 5364000 N. TG = Tyndall Group, CVC = Central Volcanic Complex, EQP = Eastern quartz-phyric sequence, SRF = Stitch Range Formation, MOC = Middle Owen Conglomerate, UOC = Upper Owen Conglomerate. Geology from McNeill (1987), herein.

Provenance of the Tyndall Group and structural model

The most interesting and obvious lithics in the Tyndall Group conglomerates are the large granite boulder clasts, which are well exposed around the Anthony Saddle Dam. The granite clasts are up to 1 m across and are, on average, larger than the other clasts implying proximity to source. The clasts are subrounded to moderately rounded and have a typical granite to microgranite texture, very similar the Murchison Granite exposed to the north and east. The Murchison Granite intruded the EQPS (exposed to the east of the Tyndall Group) prior to deposition of the Tyndall Group. Granite clasts are also found in the Tyndall Group around Mount Darwin suggesting post-granite age for the Tyndall Group (Corbett 1979). The presence of large granite clasts in the Tyndall Group in the Anthony River area, close to the position of the inferred Cambrian fault is good evidence to suggest that the granite was eroded, shedding debris, into a basin to the west across a normal-fault-scarp margin (Figs 7, 8). Although the southern extent of the Tyndall Group is probably marked by a Devonian fault, a Cambrian east–west transfer may have existed near this southern margin of the Tyndall Group and also controlling deposition into the basin (Fig. 8).

An alternative explanation is that Selina fault was originally a reverse fault involving substantial upward movement of the eastern block. This model solves the problem of uplift, however, the bedding attitudes in the Tyndall Group rocks dip steeply to the west, and when restored to horizontal, the fault is west-dipping, consistent with the normal fault model.

Summary

The geological evidence in the Anthony River area suggests that Cambrian movement was apparent on what is referred to as the Selina fault, during upper Tyndall Group (Boomerangian) time. This is consistent with observations of Keele (1991) and Berry & Keele (1993), who interpreted a normal fault on the contact of the Tyndall Group and the Eastern

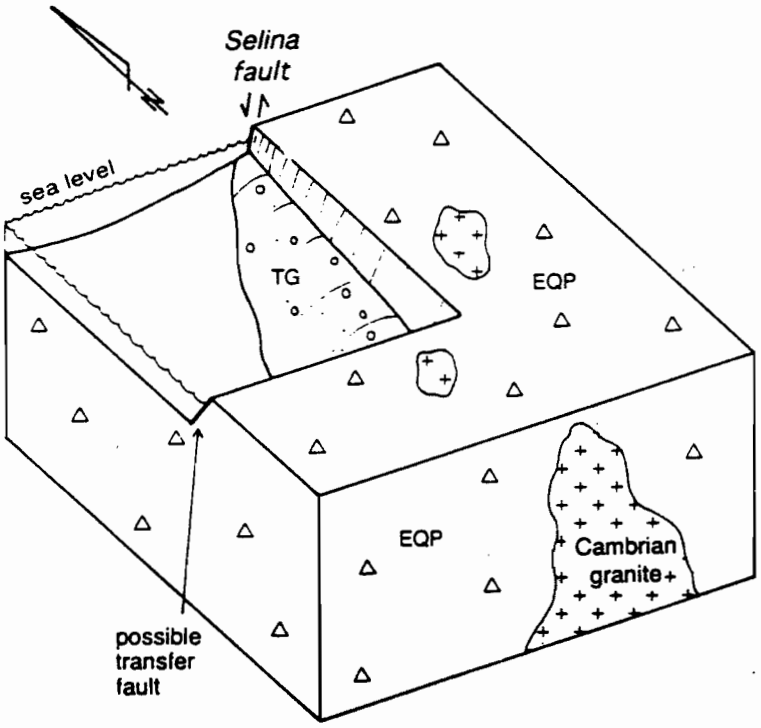

Fig. 8 — Schematic block diagram depicting the preferred model for Tyndall Group deposition in the Anthony River area. The diagram shows the normal growth fault (Selina fault) and a possible transfer fault or growth fault to the south controlling deposition of the Tyndall Group volcaniclastic units. TG = Tyndall Group, EQP = Eastern quartz-phyric sequence.

Quartz-phyric sequence in this area. A southern bounding possible transfer fault may have constrained Tyndall Group deposition into a small fault-bounded basin. Reverse movement on the fault involving east-block upward movement is another possibility.

Conclusions

The possible Cambrian growth fault that lies to the east of the Henty Fault Zone (proposed by Berry & Keele, 1993) was assessed at three locations (Moxon Saddle–Henty area, Northern Anthony Road–Murchison area, Hanging Rock).

- In the Moxon Saddle area, crystal-, lithic-bearing volcaniclastic units rich in rhyolite clasts occur in the Tyndall Group, adjacent to the proposed Cambrian growth fault, suggesting that the Tyndall Group rhyolites were probably originally deposited on both sides of the fault, and were subsequently eroded off the northeastern fault block across a fault scarp (Fig. 5). In the Henty area, feldspar-altered ferromagnesian phyric intermediate volcanic clasts in volcaniclastic units of the upper part of the Tyndall Group, were probably derived from the CVC to the east, being consistent with a west-block-down fault configuration. Reconstruction of the fault dip is difficult but a normal, west dipping fault orientation is preferred.
- In the Murchison area, crystal-, lithic-bearing volcaniclastic facies were located in the Farrell sequence, on the western (down-thrown) side of the proposed growth fault, consistent with the interpretation of Berry & Keele (1993). However, the provenance of the clasts could not be confidently determined and no new evidence for normal faulting was found.
- No sedimentological evidence was found to suggest a Cambrian growth fault to the east of Hanging Rock. A major angular unconformity in this area is consistent with a fold control on Owen Conglomerate deposition.

The Anthony River area contains Tyndall Group volcaniclastic conglomerate and sandstone, in fault

contact with the EQPS to the east. The Tyndall Group contains abundant felsic volcanic clasts and granite clasts. The geometry of the surviving sedimentary package is most consistent with active extensional faulting during Tyndall Group deposition with basin inversion during the Denison Cycle.

References

Baker, B.H., 1986. Tectonics and volcanism of the southern Kenya Rift Valley and its influence on rift sedimentation. In Frostick L. E. et al. (eds): Sedimentation in the African Rifts. Geol. Soc. Spec. Publ. 25: 45–57.

Berry, R.F., 1989. The history of movement on the Henty Fault Zone, western Tasmania: an analysis of fault striations. Aust. J. Earth Sci. 36: 189–205.

Berry, R.F., 1993. Rosebery section. Structure and mineralisation of western Tasmania, AMIRA Project P.291 Final Report: 1–15.

Berry, R.F. & Keele, R.A., 1993. Cambrian structure in western Tasmania. Structure and mineralisation of western Tasmania, AMIRA Project P.291 Final Report: 55–68.

Boyd, D., 1994. Geology of the Moxon Saddle prospect, western Tasmania. RCG Exploration Pty Ltd unpubl. report.

Bull, S.W., 1994. Preliminary report: Sedimentology of the Dundas Group with reference to a possible syn-depositional growth fault west of Rosebery. Structure and mineralisation of western Tasmania, AMIRA Project P.291A Report No. 1: 1–14.

Bull, S.W., 1995. Second report: Sedimentology of the Dundas Group and correlates with reference to a possible syn-depositional growth fault west of Rosebery. Structure and mineralisation of western Tasmania, AMIRA Project P.291A Report No. 3: 35–43.

Corbett, K.D., 1979. Stratigraphy, correlation and evolution of the Mt Read Volcanics in the Queenstown, Jukes–Darwin and Mt Sedgwick areas. Tasmania Department of Mines, Geological Survey Bulletin 58: 1–74.

Corbett, K. D. & McNeill, A. W., 1986. Map 2. Geology of Rosebery–Mt Block area. 1:25,000 Geological Map. Geological Survey of Tasmania, Department of Mines, Hobart.

Corbett, K.D. & McNeill, A.W., 1988. Map 6. Geological compilation map of the Mount Read Volcanicsand associated rocks, Hellyer to South Darwin Peak. 1:100,000 Geological Map. Geological Survey of Tasmania, Department of Mines, Hobart.

Davidson, G.J. & Kitto, P., 1995. Progress Report 3: Detecting Cambrian structures in the Mount Read Volcanic Belt using sulfur isotopes – on-going work at Rosebery. Structure and mineralisation of western Tasmania, AMIRA Project P.291A Report No. 3: 51–61.

Jenkins, D.R., 1991. Volcanology, mineralisation and alteration of the Red Hills, western Tasmania. Unpubl. BSc (Hons) thesis, University of Tasmania, Hobart.

Keele, R.A., 1991. The Zeehan–Red Hills–Lake Selina Traverse — A domain approach to the analysis of structural data. Structure and mineralisation of western Tasmania, AMIRA Project P.291 Report No. 3: 40–56.

McNeill, A.W., 1987. Geology of the Mount Murchison area. 1:25 000 map sheet 4. Geological Survey of Tasmania-Department of Mines, Hobart.

McNeill, A.W. & Corbett, K.D., 1992. Geology and mineralisation of the Mt Murchison area. Mt Read Volcanics project Geological Report 3. Division of Mines and Mineral Resources.

Polya, D.A., 1981. The geology of the Murchison Gorge. Unpubl. BSc (Hons) thesis, University of Tasmania, Hobart.

White, M.J., 1994. Stratigraphy and palaeovolcanology of the Cambrian Tyndall Group, Mount Read Volcanics, western Tasmania. Structure and mineralisation of western Tasmania, AMIRA Project P.291A, second report, October 1994: 37–40.

White, M.J. & McPhie, J. (1996). Stratigraphy and palaeovolcanology of the Cambrian Tyndall Group, Mount Read Volcanics, western Tasmania. Australian Journal of Earth Sciences 43, 147-160.

Middle and early Late Cambrian growth structures along the western margin of the Dundas Trough

Stuart Bull and David Selley
CODES Special Research Centre, Geology Department, University of Tasmania

A fundamental aim of the AMIRA P.291A project was to place constraints on Middle and Late Cambrian basin geometry and in particular define the position and geometry of growth structures which potentially controlled drainage systems and sites of deposition. A number of prospective growth structures have been investigated (eg. growth faults and transfer structures east of the Henty Fault; White, 1995: potential growth faults west of Rosebery; Bull, 1994; 1995: Mt Cripps Fault; Berry and Corbett, 1996: Firewood Siding Fault; Keele, 1995; Selley and Meffre, this report), their locations being based on the structural model of Berry and Keele (1993), which postulated a basin geometry consisting of a series of N-S striking growth faults linked by E-W trending accommodation zones or transfer faults. The purpose of this report is to summarise the results from studies near Rosebery (ie. Bull, 1994; 1995) and to clarify stratigraphic nomenclature employed in these studies in terms of the revised three-fold stratigraphic subdivision of Corbett et al. (this report).

The present distribution of Dundas Group correlates to the north and west of Rosebery led Berry and Keele (1993) to propose segmentation of an inferred Middle to Late Cambrian western boundary growth fault at the "Rosebery transfer system". This latter structure was inferred to link a N-S striking growth fault which coincided with the western limits of Dundas Group sedimentation at the southern end of the Huskisson Syncline, and second N-S trending structure to the northeast which terminated just west of Rosebery or along the eastern margin of the "Dundas inlier". In an attempt to provide evidence for the existence of the inferred growth structure immediately west of Rosebery, Bull (1994) focussed on lithofacies associations from the belt of Stitt Quartzite in the Rosebery area. At the time of this study, the Stitt Quartzite and its correlates were included within the Yolande Cycle and were considered to pre-date deposition of the latest Middle and Late Cambrian strata of the Dundas Group. In the stratigraphy of Corbett et al. (this report) however, the Stitt Quartzite has been re-assigned to the basal part of the Denison Cycle, with the felsic to intermediate volcaniclastics of the White Spur Formation forming the uppermost part of the Yolande Cycle in this region. The intervening mudstone-dominated Chamberlain Shale is a probable chronostratigraphic equivalent of the Tyndall Cycle. The work of Bull (op cit.) indicated deposition of the Stitt Quartzite in a turbiditic fan system which was just below wave base. No evidence was found to suggest that the inferred N-S structure was actively shedding debris eastward, however the lack of relevant palaeocurrent data prevented accurate determination of major drainage patterns and potential source terrains. Conglomerate units positioned at higher stratigraphic levels, within the upper part of the Westcott Argillite and Salisbury Conglomerate, were considered as deposits which potentially recorded erosion of a fault scarp.

Examination of Dundas Group correlates positioned immediately southward of the inferred "Rosebery transfer system" revealed a very different lithofacies association from that to the west of Rosebery. Bull (1995) proposed a three-fold subdivision of the Middle to earliest Late Cambrian succession exposed in the Huskisson River (Fig. 1) on the bases of lithofacies and provenance characteristics: (i) a basal non-volcanogenic division containing an Undillan faunal assemblage towards it base and comprising a thick chert clast conglomerate

interval, thinly bedded siltstone, sandstone and mudstone (data sourced entirely from Brown (1986)), (ii) a middle division of ?syn-eruptive immature intermediate to felsic volcaniclastic units, and (iii) an upper division consisting of siltstone, sandstone and conglomerate, all of which possess a mixed metasedimentary-basic volcanic provenance. Recognition of a distinctive volcaniclastic unit from the middle volcanogenic portion of the Huskisson River section provided a potential time-line with the succession exposed west of Rosebery. The volcaniclastic unit in question contained large (up to 5mm) quartz phenocrysts, abundant feldspar crystals and relict pumice fragments. Bull (1995) considered this facies to represent a lithostratigraphic correlate of compositionally and texturally similar units described by McPhie and Allen (1992) from the Southwell Subgroup and White Spur Formation. On the basis of this correlation and the presence of Undillan fossils, we have now included the lower non-volcanogenic division and the overlying volcaniclastic division of the Huskisson River section within the upper part of the Yolande Cycle. Chrono-stratigraphic correlates of this succession in the Dundas region to the south include the Hodge Slate, Razorback Conglomerate and 'lower' Brewery Junction Formation. The upper mixed provenance, partly conglomeratic division of the Huskisson River section was considered by Bull (op cit.) to represent a time equivalent of the relatively thinly-bedded and fine-grained succession comprising Chamberlain Shale, Stitt Quartzite and Westcott Argillite, and is therefore now included as chrono-stratigraphic correlates of the Tyndall and Denison Cycles (Fig. 1).

Bull (1995) interpreted the lithological variation between the Denison Cycle correlates contained in the Huskisson River section and those positioned immediately west of Rosebery to reflect fundamental differences in the drainage patterns for each region (refer to Fig. 3 *in* Bull, op cit.). The coarse-grained and texturally immature lithofacies of the Huskisson River section were thought to be principally derived from Precambrian siliciclastics and Crimson Creek Formation correlates located immediately north from the "Rosebery transfer system" and accumulated on or near a topographically uplifted transfer ramp. In contrast, the compositionally and texturally mature character of the Stitt Quartzite demands a more distal provenance, with sediment pathways probably occupying a basin-axial position. The principal function of N-S trending growth faults in terms of sediment dispersal patterns was to provide a corridor for major drainage systems rather than to actively supply and direct detritus into the basin. In support of this interpretation is the recognition of the Stitt Quartzite as forming a semi-continuous narrow belt extending southward from the Que River to the Firewood Siding Fault.

Provenance analysis using heavy mineral population techniques have also demonstrated significant differences in the source signatures of Denison Cycle correlates from the Huskisson River and Rosebery areas (Berry et al. this report). Samples collected from the Huskisson River area contain a chromite population derived entirely from a local Crimson Creek tholeiitic source, whereas those from the Rosebery area contain a more complex chromite provenance that is dominated by MUC-derived material but locally includes a significant contribution from a high-Ti tholeiitic source.

In summary, in terms of lithofacies and provenance characteristics, there are fundamental differences between Denison Cycle strata positioned close to the western limits of the Dundas Tough and in the area near Rosebery. These differences are interpreted to reflect contrasts in sediment dispersal patterns and basin geometry between these regions.

References

Berry RF & Corbett KD 1996. Mt Cripps Fault: Evidence for Cambrian movement: provisional results. AMIRA Project P.291A Fifth Report 35-46.

Berry RF & Keele RA 1993. Cambrian structure in western Tasmania. AMIRA Project P.291 Final report 55-68.

Berry RF, Meffre S & Fulton R (this report). Heavy minerals, provenance and lithostratigraphy. AMIRA Report P.291A Final report.

Brown AV 1986. Geology of the Dundas-Mt Lindsay-Mt Youngbuck region. Geological Survey Bulletin 62. Department of Mines, Tasmania 221pp.

Bull SW 1994. Preliminary report: Sedimentology of the Dundas Group with reference to a possible syn-depositional growth fault west of Rosebery. AMIRA Project P.291A First report 1-14.

Bull SW 1995. Second report: Sedimentology of the Dundas Group and correlates with reference to a possible syn-depositional growth fault west of Rosebery. AMIRA Project P.291A Third Report 35-44.

Corbett KD, Berry RF & Selley D (this report). Stratigraphic correlation. AMIRA Project P.291 Final Report.

Keele RA 1995. A new structural section between Queenstown and

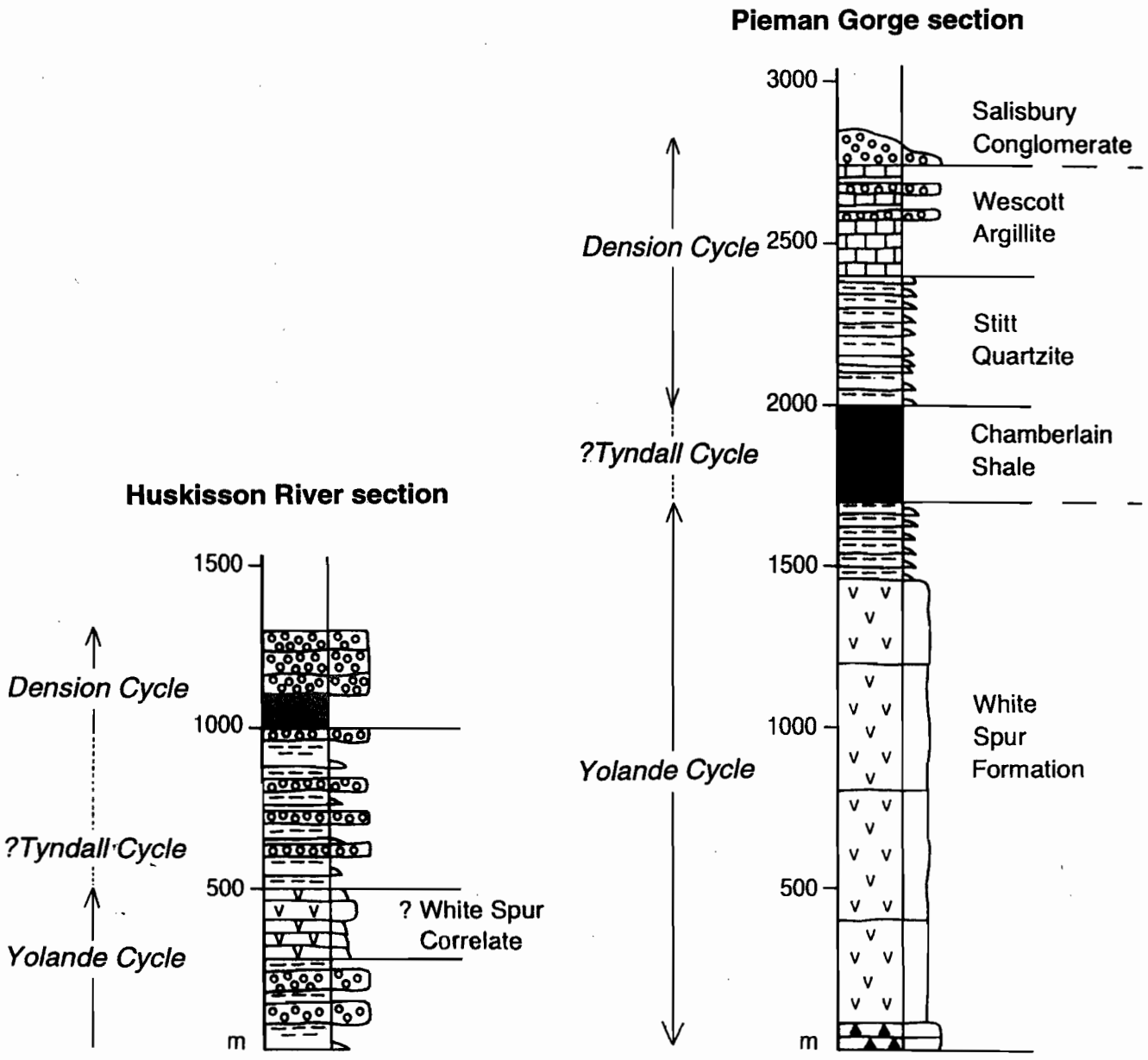

Figure 1 Sketch logs showing facies variation within Middle and Upper Cambrian strata from the Pieman River gorge (Rosebery area) and the Huskisson River. Modified from Bull (1995).

Zeehan: preliminary results on structure and unconformity relationships between the Upper Dundas Group and Zeehan Conglomerates. AMIRA Project P.291 Third report 45-50.

McPhie J & Allen RL 1992. Facies architecture of mineralised submarine volcanic sequences: Cambrian Mount Read volcanics, western Tasmania. Bull. Soc. Econ. Geol. 3, 587-596.

Selley D & Meffre S (this report). Structure and sedimentology of Middle and Upper Cambrian strata adjacent to the Firewood Siding Fault. AMIRA Project P.291A Final report.

White MJ 1995. Sedimentological evidence for Cambrian growth faults on the eastern side of the Dundas Trough, western Tasmania. AMIRA Project P.291A Fourth report 23-38.

The sulfur isotope signature of Cambrian faults in the Mt Read Volcanic Belt, and their implications for sulfur enrichment in submarine volcanosedimentary rift basins

Garry J. Davidson and Paul Kitto
CODES Special Research Centre, Geology Department, University of Tasmania

Abstract

Sulfur isotopic results from Cambrian growth faults in the Mount Read Volcanics can in some circumstances constrain their timing. Those containing base-metal sulfides, with S- and Pb-isotope values similar to the large Mount Read Volcanic Belt VHMS deposits ($\delta^{34}S$ 5–18‰), are likely to represent fault-controlled upflow zones in Cambrian hydrothermal cells. Unmineralised faults with normal or strike-slip fault offsets, can contain pockets of heavy sulfur isotope values ($\delta^{34}S$ > ~18‰), as finely disseminated pyrite, within 50 m of the recognisable fault trace. The same range of heavy values is recognised at the margins of large base metal deposits, such as Rosebery and Hellyer, where it is interpreted to represent shallow sub-surface reduction of Cambrian seawater sulfate. The heavy values in the faults are interpreted to have been emplaced into fault traces either by sulfate reduction of fault anhydrite during the evolution of the fault, or by mixing of seawater sulfate with reduced hot porewaters on the fault margins during initial fluid recharge. The mechanism of continuous anhydrite burial on growth fault hangingwalls is regarded as a fundamental mechanism of delivery of seawater sulfate-derived sulfur into hydrothermal reservoirs, and may account for the strong sulfur enrichment of altered back-arc basin crust compared to its mid-ocean ridge counterpart.

Growth faults are dynamic structures. As time passes, every portion of the downthrown fault trace experiences the full range of fluid and thermal conditions available on the fault, because each segment initiates at surface and is progressively buried by deposition and fault movement. It is consequently expected that a wide range of sulfur isotope signaures should be recorded in growth faults, and this is added to if the fault has a complex later history. Where faults have been examined in detail in this study, their isotopic composition is very variable, and this is accounted for by a complex retainment pattern of the isotopic signature of multiple fluid batches passing through each fault, rather than by isotopic heterogeneity in a single event.

However, only sulfur isotope values >18‰ and <~–5‰ are diagnostic of Cambrian fluids in the Mount Read Volcanic Belt (MRVB), because of overlaps with the isotopic range of Devonian magmatic and deformational fluids. Values less than –5‰ have only been identified in background oxidised Cambrian aquifers to date—particularly associated with albitisation—but it is very likely that this fluid facies was widespread, but possibly poorly preserved, in early Cambrian faults. Background rocks in the MRVB contain a very wide isotopic range with no definite mode, including the very light values of oxidised aquifers (0 to –14.5‰), light to intermediate values consistent with an original igneous signature (0 to ~6‰), and intermediate values overlapping the range of Cambrian massive sulfide deposits (5–18‰), which are interpreted as products of low W/R reaction with high temperature hydrothermal fluids during the Cambrian.

The recommended strategy to determine fault parentage is to sample at <20 m spacing across fault traces and their margins, incorporating all alteration styles and sulfide generations, and analysing using wholerock sulfur isotope methods. The near-surface history of growth faults is likely to be preserved on their margins, because of greater lateral permeability, and proliferation of small fault traces, whereas the isotopic record of the deep history of the same fault

is likely to be preserved in focussed thin zones of movement. Sampling strategies should take account of this.

Introduction

Sulfur isotopes have been extremely useful in the Mount Read Volcanic Belt for determining the fluid history of hydrothermal events. Their use is enhanced for the Cambrian, because of the extreme fractionation of seawater sulfate at this time (Claypool et al., 1980), allowing greater resolution of sulfur sources. The use of sulfur isotopes as fluid tracers is extended here to determining the age of faults in submarine volcanic sequences. However, to carry out this aim, it has been necessary to first characterise background variation in volcanic rocks of the MRVB (Fig. 1), including the margins of Cambrian massive sulfide deposits.

Methods and techniques

Three sulfur extraction methods were employed in this study, with sulfur isotopes being determined on a VG Sira series II mass spectrometer, under the supervision of M. Power Sr. at the Central Science Laboratory of the University of Tasmania. This machine delivers isotopic precisions of $1\sigma = 0.2‰$, using an internal laboratory gas standard to correct for machine drift. The three extraction methods are:

1. **Conventional hand-drilling and cuprous oxide extraction**. The method was applied when sulfides were coarser than ~2 mm, after the preparation of a polished surface to inspect for contaminant sulfide inclusions. A hand-held microdrill was used to powder the pyrite grains to obtain ~12 mg of sample. The sample was then reacted with cuprous oxide under vaccuum in a furnace , using the method of Robinson and Kusabe (1975), to obtain SO_2 (g) for analysis in the mass spectrometer. The method is most applicable where the total isotopic value of a sulfide is required.

2. **Laser ablation microprobe extraction.** Doubly polished thin-sections were prepared at ~100 μm thickness. Because the method is destructive, photographs of grains of interest were taken prior to the analysis. The rock-chips were then dissolved from their glass mounts, and cleaned with solvent. Individual sulfide grains down to ~100 μm diameter were analysed by torching with a Nd-YAG laser in the presence of O_2, using the method of Huston et al. (1995). Results systematically vary by ~6‰ from the cuprous oxide combustion method, and are corrected accordingly, depending on the sulfide type. The method is most applicable for determining the isotopic composition of several fine-grained sulfide generations, or delineating isotopic zonation within grains. It is not as reliable as hand-drilled samples for determining the bulk sulfur isotopic composition of sulfide phases.

3. **Heavy mineral separation and cuprous oxide extraction.** This method was refined during the project using advice from CSL technician Christine Cook. It was employed to determine the isotopic combined value of monosulfides and polysulfides, in rocks containing fine-grained sulfides (<~100 μm). These values could be interpreted as "background" for the Mt Read Volcanics. Samples were crushed to 2mm mesh, and the –2mm fraction was retained, amounting to ~150 g of sample. Heavy mineral separates were obtained commercially through Analabs (Perth) for $17/sample using heavy liquids (Method MT831). A superpanner was also used in-house on a second sample batch with the assistance of student technician Daniel van der Aa, which also produced treatable heavy mineral separates. The objective of the separation was to remove hydrous silicates, and also carbonate phases, that interfere with sulfur analysis in the mass spectrometer. The samples were washed and dried, then treated with weak HCl to remove remaining carbonate. After removing a small reference sample, the residue of resistate heavy minerals (including sulfide grains) was crushed to a fine powder using a steel mortar and pestle, to ensure homogeneity.The reduction to a fine powder after acid treatment and before Cu_2O reaction enhanced the reaction of the disseminated sulfide particles. The heavy mineral powder was combined with 150–800 mg of Cu_2O (an excess is required to avoid production of SO_3) and analysed according to the method of Robinson & Kusabe (1975).

Figure 1 Location and geology of regional samples (red dots) used to establish the background sulfur isotope composition of the MRVB. Yellow stars are the locations of Cambrian faults used for detailed studies; 1. Tullabadine Dam; 2. Pieman River; 3. Dalmeny st., Rosebery; 4. Moxons Fault; 5. Zig Zag Hill/Comstock. Back Peak sampling area is ~ 10 km east of 400000mE, 5390000mN (see also Fig. 15).

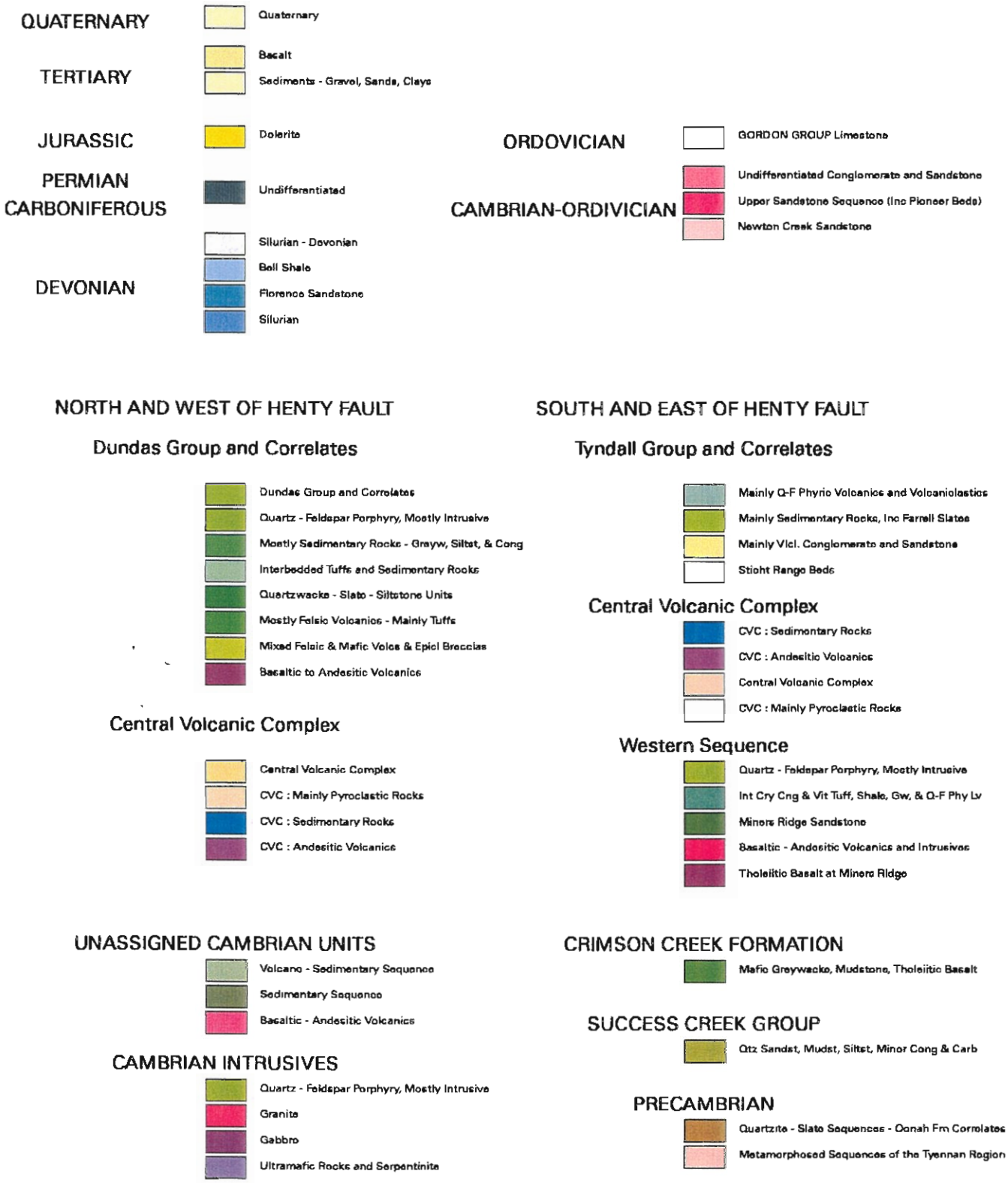

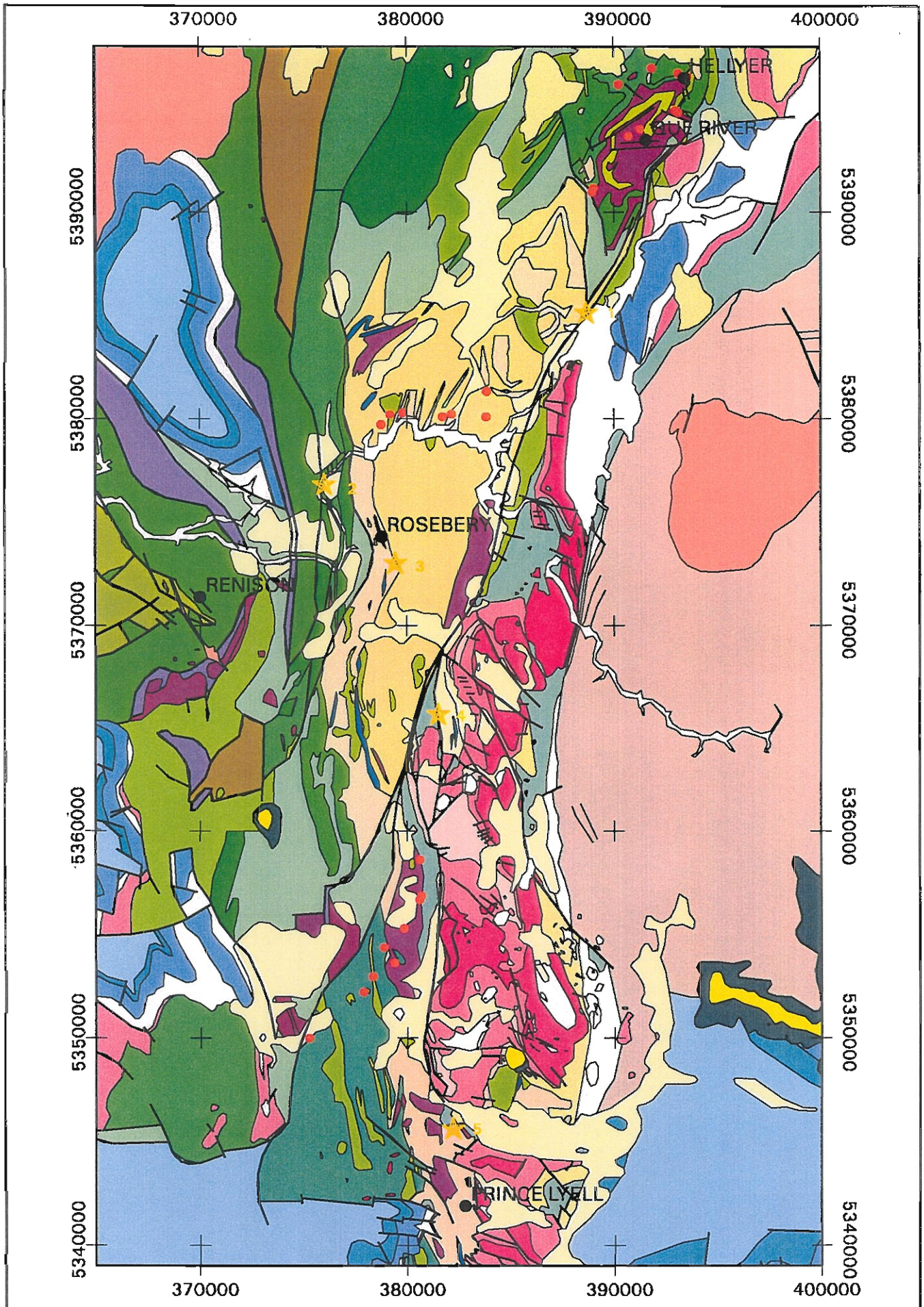

Regional Sulphur Sample Locations

SCALE 1:250000

CODES: AMIRA Project P.291A — Structure and Mineralisation of Western Tasmania. March 1997

Table 1. Repeat analyses by different sulfur isotope methods. KIBA and Tas. whlrock are wholerock analytical methods.

Sample no.	Analysis Type	anal. no.	Sulfur ‰	Sample no.	Analysis Type	anal. no.	Sulfur ‰
49R-984.0'	laser	1553	7.58	**mox4**	KIBA	XRAL	7.02
	laser	1554	4.46		Tas. whlrock	4093	2.69
	KIBA	XRAL	20.18	**PKGD10**	Tas. whlrock	3957	8.6
	KIBA	XRAL	21.04		KIBA	XRAL	9.42
	KIBA	XRAL	21.42	**PKGD13**	conventional	3808	-3.18
	KIBA	XRAL	21.04		laser		-2.6
57R-2250.0'	laser	1513	-4.47		laser		-3.26
	Tas. whlrock	3955	4.27	**PKGD14**	conventional	3807	2.18
	KIBA	XRAL	-0.58		laser		-0.06
	KIBA	XRAL	0.26		laser		1.1
	KIBA	XRAL	-0.01	**PKGD15A**	conventional	3798	-2.46
	KIBA	XRAL	-1.60		laser		-4.14
109R-559.5m	laser	1562	6.13		laser		-1.32
	laser	1563	2.74	**PKGD22a**	conventional	3809	12.33
	laser	1564	6.84		laser		14.42
	KIBA	XRAL	6.69		laser		13.52
	KIBA	XRAL	7.29	**PKGD22b**	conventional	3810	16.21
	KIBA	XRAL	7.89		laser		11.87
	KIBA	XRAL	8.78		laser		15.61
109R-591.2m	laser	1531	33.09	mox3	Tas. whlrock	4367	11.6
	laser	1532	36.71		KIBA	XRAL	12.13
	KIBA	XRAL	33.24		KIBA	XRAL	12.49
	KIBA	XRAL	34.29				
	KIBA	XRAL	34.45				
	KIBA	XRAL	34.57				
	Tas. whlrock	3961	30.18				
109R-620.5m	laser	1507	17.52				
	laser	1509	22.81				
	Tas. whlrock	3959	18.65				
	KIBA	XRAL	16.62				
	KIBA	XRAL	16.76				
	KIBA	XRAL	16.92				
109R-649.6m	laser	1474	6.12				
	KIBA	XRAL	14.27				
	KIBA	XRAL	14.12				
	KIBA	XRAL	15.93				
	KIBA	XRAL	16.03				
109R-892.0m	laser	1555	25.34				
	KIBA	XRAL	9.19				
	KIBA	XRAL	9.22				
	KIBA	XRAL	9.41				
	Tas. whlrock	4372	13.60				
PKGD2	Tas. whlrock	3956	2.66				
	laser		5.71				
	laser		4.26				
	KIBA	XRAL	3.38				
	KIBA	XRAL	4.85				
	KIBA	XRAL	4.25				
	KIBA	XRAL	3.82				

An ideal sample volume of 200 mg is indicated by analysis of results (see below).

Repeat analyses and errors

Results of repeat analyses by different methods are shown in Table 1. The bulk sulfur method outlined above was tested using the KIBA extraction method (Ueda & Sakai 1983) available commercially through XRAL laboratories in Canada (US$147/sample; discounted in this project, and discounted for bulk sample numbers). In the KIBA method, after treatment with HNO_3 and stanniferous "KIBA" reagent, S is concentrated as silver sulfide prior to hot reaction with cuprous oxide to obtain SO_2. XRAL required 2 gm of wholerock sample, although 100–200 mg is sufficient for normal sulfur contents. A 2σ error of 0.3‰ was quoted. The procedure produced good agreement by comparison with laser ablation values from the same samples in most instances, but was very time-consuming, with the test batch taking ~7 months to be returned.

The wholerock and KIBA results differed markedly for two samples, 109R-892 and Mox 4 (Table 1). Given the close results for most of the repeated samples, large differences between the the two methods for these two are considered to reflect differences in composition of fine compared to coarser sulfide. The KIBA method measures total sulfur, whereas the heavy mineral separation method does not analyse the very fine-grained sulfide fraction, because it does not accumulate in the extraction. It is possible that in some instances the composition of this sulfide differs from the bulk value. In addition, samples with low sulfur contents (<100 ppm S) and high hydrous mineral abundances, repeated poorly using the heavy mineral separate technique (Table 2), although samples with >200 ppm S repeated well. Samples with high water contents (as indicated by the mass spectrometer) and S contents < 100 ppm have been removed from the data base discussed here. These samples mainly produced low SO_2 gas volumes (Fig. 2).

The other important area of variance amongst the repeat samples was between some laser results and either wholerock method. This was the case for 49-984', 109R-649.6 m and 109R-892.0 m (Table 1). These differences are attributed to the fine-scale of sampling using the laser method, which will not always reflect the bulk value if only 1–3 laser analyses are obtained. A large difference between laser and wholerock results is taken to indicate inhomogeneity at the sampling scale for these particular samples, given the good agreement in most instances. The finding raises the issue that anomalous laser isotope values should be treated cautiously and followed up with a more comprehensive sampling technique, if the aim is to determine the bulk value of sulfur. They may be evidence of complex sulfide overgrowths caused by changes in fluid composition with time in a fault (see later).

A plot of extracted S gas volume versus the known total sulfur content of the rock, shows that high S samples do broadly produce high yields as expected, but with many exceptions (Fig. 2). Adjustment for

Table 2 A comparison of repeat analyses for the background data set, obtained using the heavy mineral separation method with cuprous oxide extraction.

Sample	S ppm	^{34}S-repeat 1	^{34}S-repeat 2	comment
71424	100	-1.8	22.6	high H_2O
71426	100	-19	-1.9	massive H_2O
71442	1100	3.2	7.3	good
71443	200	5.1	7.7	massive H_2O
PKGD2	visible py	2.7	6.3	
PKGD10	visible py	8.6	8.6	
71531	1800	6.4	7.9	massive H_2O

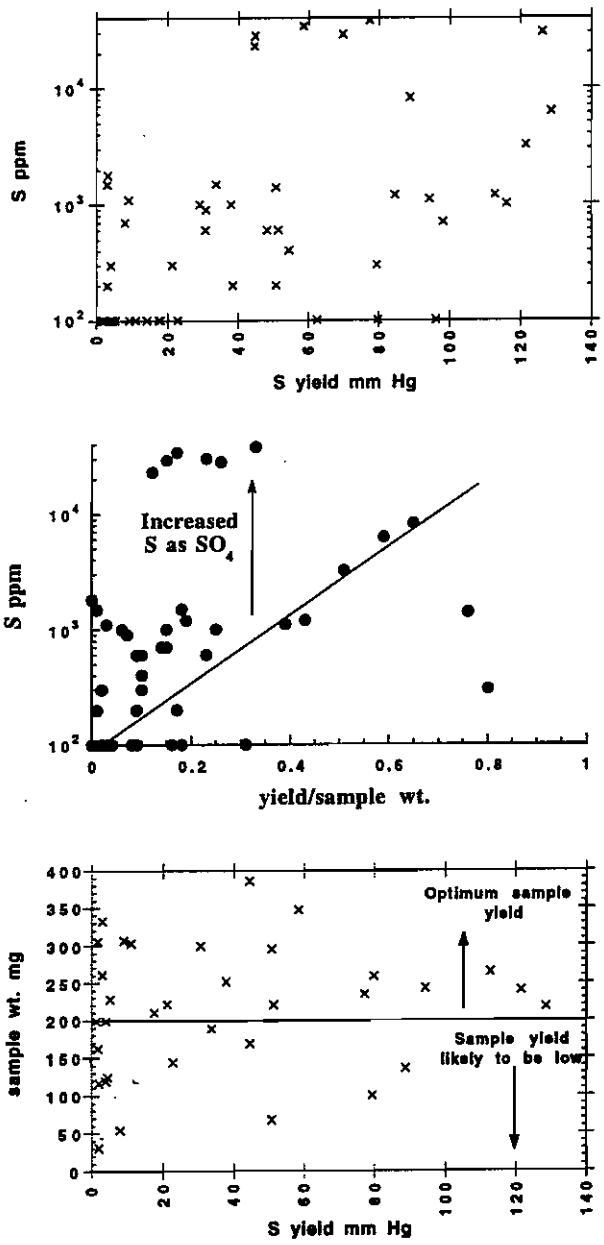

Figure 2 Relationships between S ppm of wholerock samples in the background data set, and the S yield and sample weight determined during the measurement of sulfur isotopes using the heavy mineral separation wholerock technique.

sample weight by ratioing it with the yield does not remove the anomalies, which mainly consist of samples with high S contents providing low yields (Fig. 2). These samples probably contain significant sulfate as barite, which would not be removed by the Cu_2O oxidation method. A review of this data also has provided better constraints on the ideal sample weight to be used for the heavy mineral extraction method (Fig. 2). 54% of samples less than 200 mg had yields of < 20 mm Hg, whereas this was the case for only 38% of samples > 200 mg. The 38% is inflated by the inclusion of samples with low S contents, for which sample weights of 600–1000 mg were employed to try to evolve sufficient gas for analysis; only 28% of 32 samples with 200–600 mg weights had yields of < 20 mm Hg. This analysis is applicable to general wholerock sulfur isotope analysis in which the sulfide S content is unknown. A standard 200 mg sample is recommended. The use of large sample weights for samples with known low ΣS was not successful and is not recommended.

Summary of Findings

- The three methods employed in the study show reasonable agreement using the same samples, with some important exceptions. Significant differences between some laser S values and wholerock values indicate inhomogeneous sulfur distribution.
- A heavy mineral separation combined with a weak acid treatment, together removing most micas and carbonate, is suitable for concentrating the sulfide component of altered volcanic rocks with ΣS > 100 ppm, to the point that it can be treated using a standard Cu_2O analysis. The commercially available KIBA extraction technique is recommended for rocks with ΣS <100 ppm at this stage.
- A plot of sample S yield/sample weight versus S ppm indicates that for most samples higher primary S contents resulted in higher yields as expected. However, a significant number with high ΣS had low yields, consistent with the presence of sulfate rather than sulfide.
- For samples with unknown S contents, a standard 200 mg sample weight is recommended for the heavy mineral separation technique.

Background variation of sulfur isotopes in the Mt Read Volcanic Belt

Introduction

Background variation of sulfur isotopes in the Mt Read Volcanics has never been established, although it has commonly been central to interpretation of sulfur sources for deposits. The isotopic composition of the host- and source-rocks is generally assumed using modern values, with most previous studies

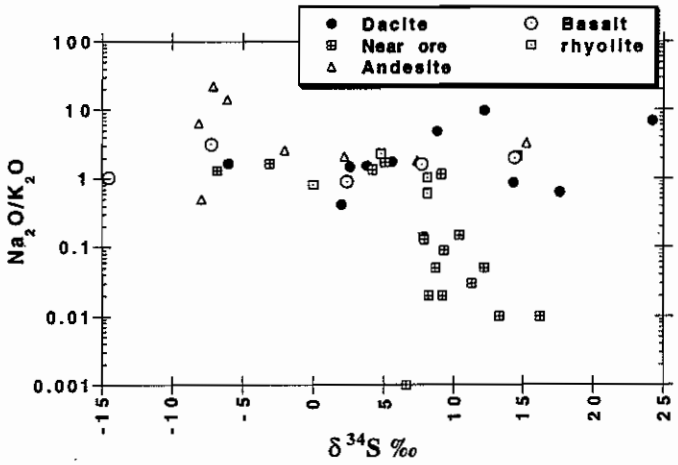

Figure 3 Background $\delta^{34}S$ values for the Mt Read Volcanics, versus the wholerock ratio Na_2O/K_2O, an index of competing albite and sericite alteration.

adopting 0 ± 2‰ for meta-volcanic rocks and their source intrusions. Given a post-collisional back-arc setting for the Mt Read volcanics, even this assumption of the unaltered felsic composition needs to be corrected to $\delta^{34}S$ = 4–5‰ (Japanese and Marianas Quaternary arc felsic volcanics; Ueda & Sakai, 1984; Woodhead et al., 1987)). Modern back-arc basic volcanics average $\delta^{34}S$ = 0.3 ± 1‰ (Kusakabe et al., 1990; Alt, 1994), which is appropriate for primitive lavas such as the Hellyer Basalt. An estimate of the current background variation of the Mt Read Volcanics was obtained in this study using the heavy mineral separation technique. The sample set was taken from Stolz & Large(1992), stored at the University of Tasmania, which used fresh and altered volcanics from a variety of typical Mt Read units to establish background gold abundances. It is biased towards the Que-Hellyer sequence. With the removal of suspect data points, and near-ore alteration samples, the background is represented by 27 samples, and hence is definitely only a pilot study of the overall variation.

Results

Results are summarised in Appendix 1 and Figure 3, with locations in Figure 1. Rather than the narrow variation predicted from modern primary igneous values, the results are extremely variable, $\delta^{34}S$ = –14.5 to +24.2‰. The mode is very broad (–7.5 to 10‰), and the mean is 3.8 ± 9.3‰. This range indicates that most rocks have experienced major changes in their primary sulfur isotope composition, despite having been selected in the Stolz & Large (1992) study as least altered samples on the basis of their mineralogy and geochemistry. These authors determined that the sample set contained no weathered material, so that the sulfur geochemistry must relate to post-depositional fluid circulation. Most of the sample set has Na_2O/K_2O ratios of 0.5–3.0, which overlaps the primary igneous range. The exceptions are:

(1) very sodic andesites and basalts which preferentially display isotopic values between –10 and –5‰, in samples that have 400–3000 ppm S. In this group albitisation coincides with strong isotopic depletion;

(2) very potassic near-ore alteration, which mainly exhibits a restricted isotopic range of $\delta^{34}S$ = 6 to 16‰, very similar to the general isotopic range of sulfur in Cambrian massive sulfide deposits. The four sample points that are lighter than this range (Fig. 3) provide an insight into the spatial relationship between very light sulfur and ore signature sulfur, at least at Que River (Fig. 4). The downhole variation indicates that light sulfur occurs in rhyolites and andesites furtherest from the stringer zone, separated from the ore signature stringer material by a zone of heavier sulfur (14.6‰).

In terms of correlations between hostrock type and sulfur isotope signature, there is weak evidence that mafic units (basalts and andesites) contain a higher proportion of isotopically light samples than do felsic lithologies (Fig. 3). However, this assertion

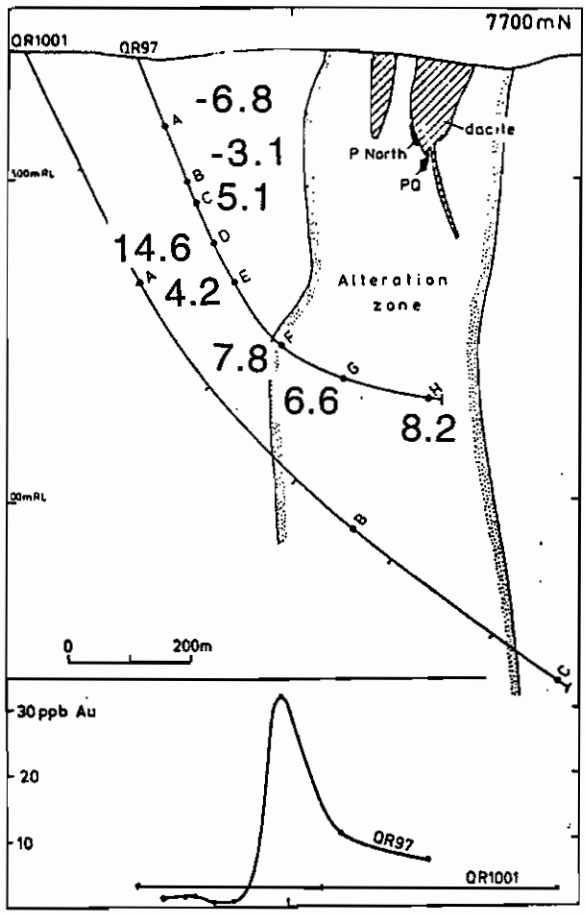

Figure 4 Spatial distribution of sulfur isotopes in the Que River footwall, using hole QR97 on section 7700 mN, modified after Stolz & Large (1992).

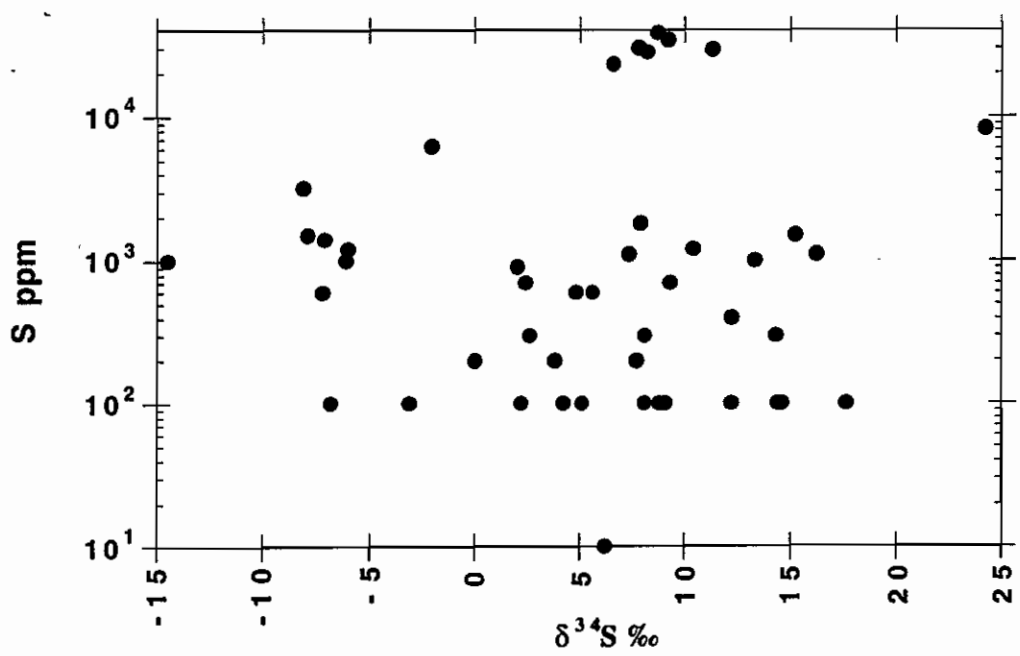

Figure 5 S ppm versus $\delta^{34}S$ for the background Mt Read Volcanic Belt lithologies. No association is evident between these parameters.

requires further testing given the small sample numbers of each sub-group. There is no evidence for a relationship between ΣS and sulfur isotope ratio (Fig. 5).

Interpretation

Sulfur in modern and ancient altered submarine volcanic sections

The disadvantage of using the Stolz & Large (1992) sample set (grateful though I am Joe!) for the background sulfur isotope survey is that the physical relationship of samples to fossil Cambrian or Devonian structures cannot be established, although in their study Stolz & Large avoided obvious sheared zones. The interpretation of values must consequently be made relative to known modern variation, and to theory. It is reasonable to assume that the background values represent mixes of primary igneous sulfur and secondary hydrothermally introduced sulfur. However, no indication of the end-member isotopic value of the primary igneous sulfur can be determined from this data set.

Very heterogeneous sulfur distributions have been discovered in Mid Ocean Ridge Basalt sections on the seafloor (Alt 1995), and in several sections through primitive back-arc oceanic crust on the Troodos Massif (Alt, 1994). No one has yet obtained a section or a three dimensional view of the variability of sulfur isotopes in felsic volcanic terrains. Alt (1995) combined ODP holes 504B and 735B into a single composite core penetrating 1.7 km into oceanic crust. On the basis of the ODP drilling, he developed a concept of sulphur cycling in off-ridge oceanic crust. This involves the penetration of oxidised low temperature sulphate-rich seawater hundreds of metres down into permeable seafloor pillow basalts, where some sulphate is lost by anhydrite deposition during mild heating. The rest of the sulphate interacts with deeper high temperature reduced waters along an interface, resulting in sulphide deposition (Andrews, 1979; Alt ,1995). This zone contains heavier sulfur ($\delta^{34}S$ = 3–5 ‰) indicating a contribution from seawater sulphate. Here Alt defined a potential major new sulphur sink in the Earth's crust. Below the hydrological interface, which generally comes to equilibrium at a decrease in rock permeability, hot reduced waters leach sulphide from the dykes and underlying gabbros. Above it, low temperature alteration by the oxidised waters also leach igneous sulphide sulphur and partially convert it to sulphate, leaving a residuum of light sulphide ($\delta^{34}S$ = –18 to +1 ‰) (Figs 6, 7). Closer to the high heat flow zone of the mid-ocean ridge axis, the lower hot reduced fluids ascend along faults to the seafloor and deposit their sulphur as massive sulphide bodies (Fig. 7). Alt (1995) concluded that the estimate of stored hydrothermal sulphur in ocean crust is much smaller than previously thought, because sulphur deposited as anhydrite in basalt aquifers is redissolved by cool oxidised seawater, without ever exiting from seafloor vents. The results from the back-arc sections were very similar, with the exception that the amount of water-rock reaction, and consequently the amount of added new sulfur for the back-arc, was ~2X that of altered oceanic crust. Alt (1995) calculated that ~35% of the back-arc sulfur came from seawater.

Application to the Mt Read Volcanic Belt

Isotopically light zones — The overall $\delta^{34}S$ variation discovered within the Mt Read Volcanics is ~40‰, which is similar to that of the Troodos back-arc section. Unlike this section, most of the sampled Mt Read Volcanic Belt are coherent volcanics, pyroclastic and volcaniclastic rocks, rather than minor volcanics, and major abundances of dykes, gabbros and ultramafics. Consequently there were far more permeable rocks in the Mt Read belt than in the Troodos back-arc, and this should have produced an increase in the abundance of low temperature, oxidised, values. With 18 samples < 5‰, this appears to be the case. A second possible interpretation of the light values is that they reflect deposition of biologically-derived sulfur, since this is also dominated by light isotopic values. This explanation is not currently favoured, because of the similarity of setting between the back-arc/oceanic examples and the Mt Read examples. Values less than 5‰, and certainly those less than ~–2‰ for basic rocks, earmark regions of low temperature oxidised seawater circulation in the Mt Read Volcanics. The Que River section indicates that these regions may extend virtually all the way to high temperature upflow zones along Cambrian faults, suggesting that

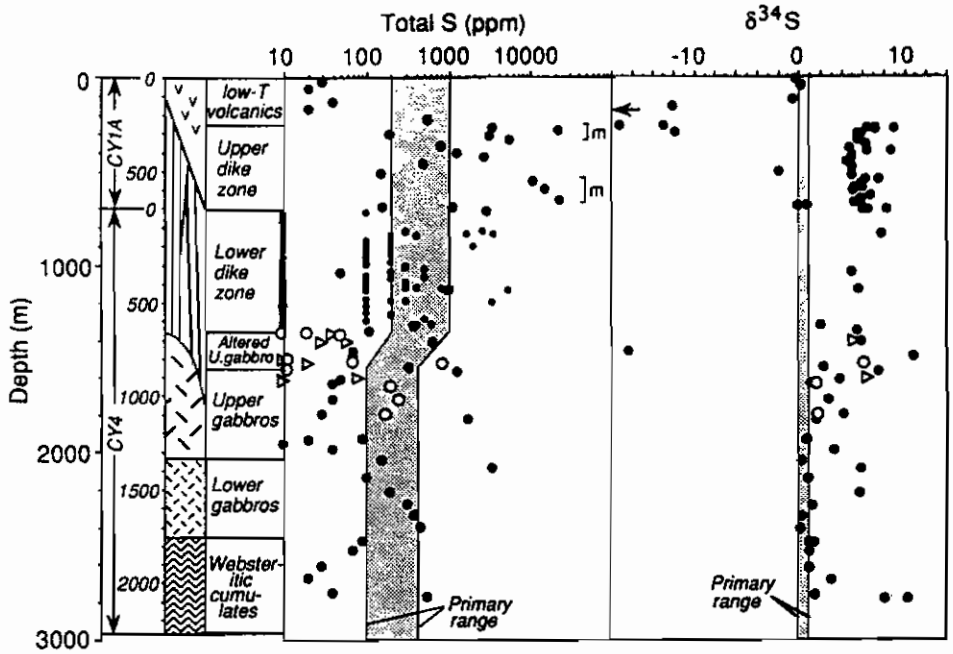

Sulfur data for a section through the Troodos ophiolite as represented by holes CY1A and CY4. Lithology and alteration zones are shown at left. Data for drillcore from Table 1 plotted as large solid circles, epidosites plotted as open triangles, and other outcrop samples from Table 2 plotted as open circles. Data plotted as small solid circles from BARAGAR et al. (1989). Shaded areas represent inferred range of primary sulfur contents and $\delta^{34}S$ values. "m" indicates mineralized zones in the upper dikes. Arrow indicates sample that plots off scale (−26.1‰). See text for discussion.

Figure 6 Sulfur isotope profiles through altered back-arc (top) and mid-ocean (off-axis) crust (bottom), after Alt (1994, 1995).

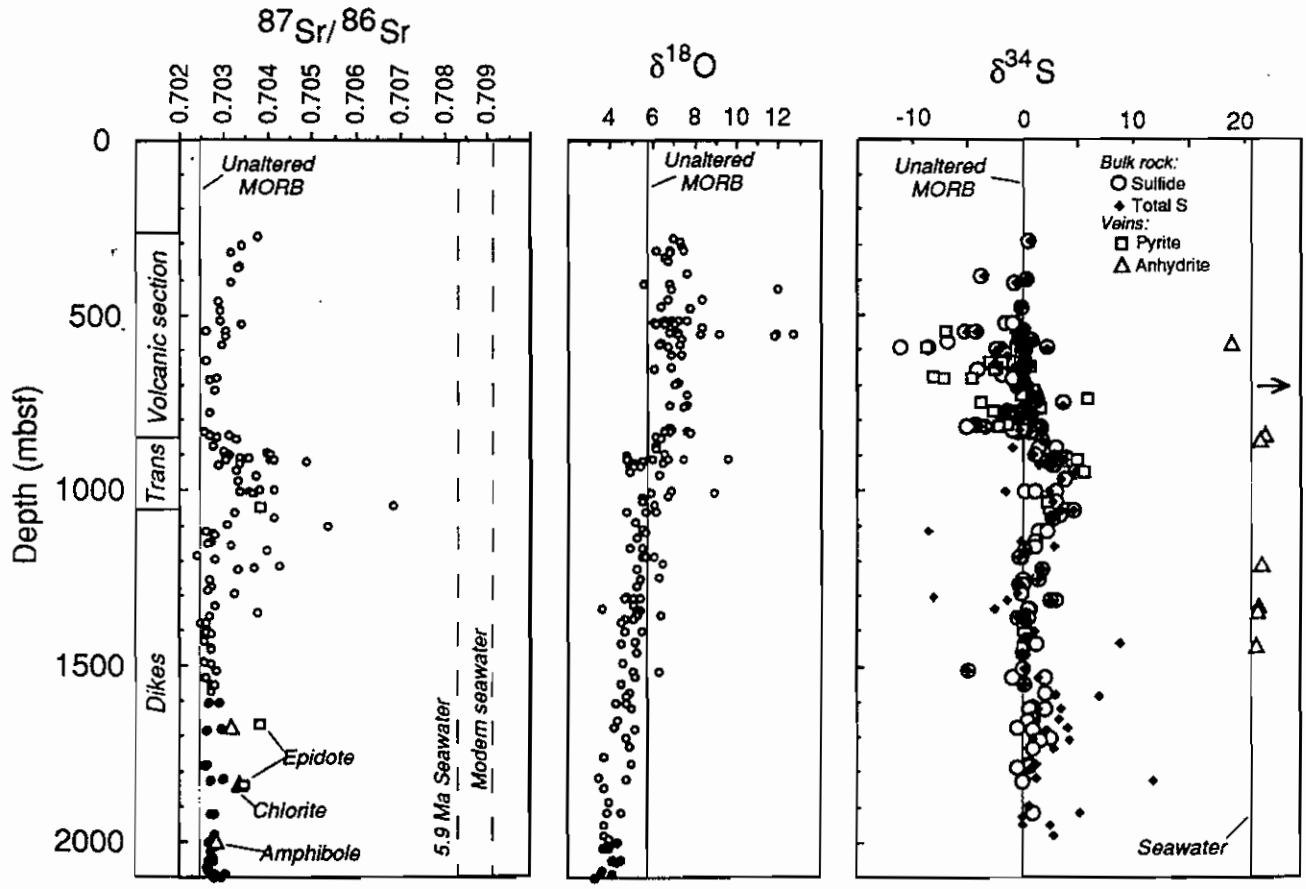

Strontium, oxygen, and sulfur isotopic compositions for whole-rock samples and selected secondary minerals with depth for Hole 504B. Trans = transition zone. Strontium data from Table 1 (whole rocks = solid circles; secondary minerals are labeled) and various sources (Barrett and Friedrichsen, 1982, 1987; Barrett, 1983; Hart and Mottl, 1983; Friedrichsen, 1985; Staudigel and Hart, 1985; Kawahata et al., 1987; Kusakabe et al., 1989; Shimizu et al., 1989). Oxygen data from Table 1 (solid circles), Alt et al. (1986b, 1989b, 1995), and Nesbitt et al. (1987). S data from Alt et al. (1989a, 1995), Zuleger et al. (1995), and Bach et al. (this volume).

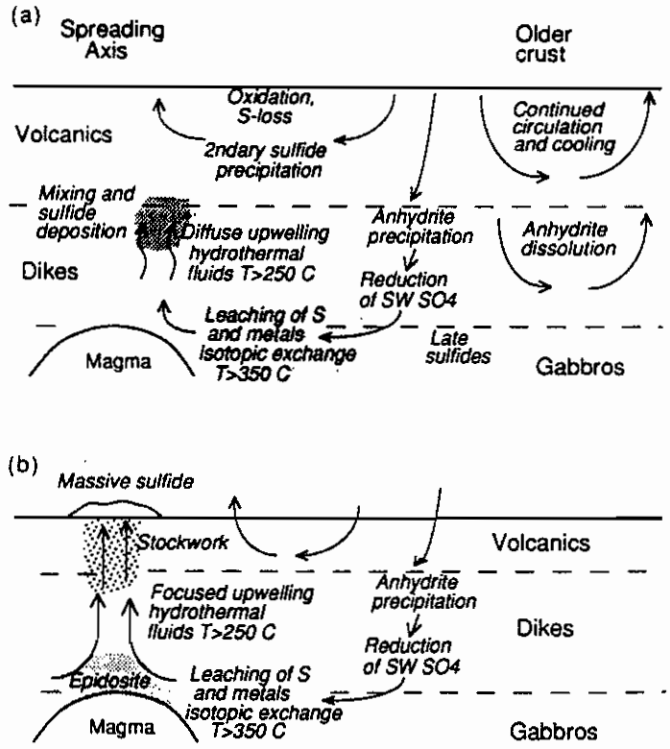

Figure 7 Processes of sulfur deposition and consequent isotopic fractionation, after Alt (1994). In (a) the volcanic section is open to seawater circulation, leading to oxidation of sulfides at T<100° C, and loss of sulfur to seawater. Anhydrite precipitates locally with values heavier than seawater, but is later dissolved by cold seawater. Sulfate reduction occurs deeper in the crust at T>250° C, but sulfur is also leached from this area by the hot fluids, and redeposited along the mixing interface between cool and hot water. In (b) the same principles operate areound a massive sulfide deposit of the Troodos massif, but high temperature fluid flow dominates close to the intrusion, resulting in S-leached "epidosite" alteration, and focussed upwelling of fluids with T>250° C. In scenario (b), low temperature leaching is comparitively unimportant.

the low temperature signature was established, then was followed by high temperature upflow along the Que-Hellyer Fault system. In terms of implications for Cambrian faults, it seems likely that low temperature oxidised fluids should have penetrated faulted zones more deeply than in regional volcanic aquifers, although the light isotopic signature was not discovered in any of the Cambrian faults examined in this study.

Ore signature samples — The isotopic signature of ore zones in the Mt Read Volcanic Belt varies between 5 and 18‰, with the lightest values characterising mineralisation in basic rocks, compared to heavier values in felsic terrains. Solomon et al. (1988) suggest that this difference is caused by greater abundances of rock sulfur being furnished by high S basic rocks, compared to lower S felsic rocks. During high temperature leaching, comparatively greater reduction of seawater sulfate occurs in the felsic terrains. An additional factor not considered by Solomon et al. (1988) is that it is likely (but not proven) that felsic rocks in the Mt Read Volcanics had primary igneous values of 4–8‰ similar to modern arcs, whereas the basic rocks probably retained a primitive mantle signature 0 ± 1‰.

By comparison, values of 5–18‰ in the background sample set must have experienced deposition from higher temperature fluids, and by analogy with the back-arc/oceanic circulation model, lay below the oxidised seawater aquifers. However, only those samples with Na_2O/K_2O ratios < ~0.5 are considered to have been part of focussed high temperature alteration systems. Similarly in the Troodos back-arc section, it is common to find ore signature regions of sulfur isotopes, with elevated S contents, that are interpreted as mixing zones between low and high temperature fluid regimes (Alt, 1994), but are not

considered to be products of focussed fluid flow that would have been capable of forming ore bodies (Fig. 6).

High $\delta^{34}S$ samples — Samples isotopically greater than "ore signature" sulfur, approaching the value of Cambrian seawater sulfate (~30‰), are considered to be "high $\delta^{34}S$" samples. Only one background sample (24.2 ‰ in dacite) was in this category. It is considered to result from near-complete reduction of seawater sulfate, and will be further discussed with the Cambrian Faults data set.

Summary of Findings

- Background variation in the Mt Read Volcanic Belt volcanics and pyroclastic rocks is –14.5 to 24.2‰, with an uneven mode from –7.5 to +10‰, overlapping the expected igneous background of 0–6‰.

- By comparison with findings in ancient and modern submarine volcanic belts, values <5‰ in felsic rocks, and <–2‰ in mafic rocks, are interpreted as the signature of low temperature (<100°C) oxidised fluid reaction. In the Mt Read Volcanics, areas with such values were low temperature porous aquifers, or lay in the upper zones of recharging faults. Some of these zones coincided with significant albitisation identified by $Na_2O/K_2O > 2$.

- Samples with "ore signature" isotopic values of $\delta^{34}S = 5–18$‰ experienced interaction with reduced high temperature ore fluids (in which the sulfur value was a combination of reduced seawater sulfate and leached rock sulfur) within high temperature aquifers, or along mixing zones with low temperature oxidised aquifers. Where deposition occurred at high W/R, such as stringer systems to mineralisation, Na_2O/K_2O ratios were lowered below 0.5.

The isotopic signature of shallow sulfate reduction around massive sulfide deposits — Rosebery case study

Introduction

As a first step to determining whether lower temperature Cambrian fluid circulation could be detected using sulfur isotopes, the periphery of a massive sulfide deposit that was associated with subtle Cambrian faulting was examined on the premise that variable degrees of sulfate reduction would be present and might be detectable. Support for this approach came from Alt & Chaussidon (1989), who document a modern seafloor example of this phenomenon, but the best characterised ancient example comes from Hellyer (Gemmell & Large, 1993). Here, a zone of heavy disseminated sulfide occurs in footwall veins adjacent to the main ore zone. A similar but smaller enrichment was found in regularly spaced samples at Que River in this study. The Hellyer isotopically enriched zone extends at least 200m from ore, and consequently is an important component of the ore halo. There is no evidence that this sulfur made a significant contribution to the footwall high temperature stringer zone. Gemmell & Large (1993) attribute the incomplete reduction in the ore periphery to near-exhaustion of the mineral reductants in this area, but a second option is that the temperature of circulation was such that the reduction was sluggish; i.e. Sakai & Dickson (1978) measured the half-time of exchange between sulfate and sulfide as a few minutes at 350°C, whereas at 200°C it is a few years. Thus lower temperatures would ensure only partial reduction in mixing zones.

The north end of the Rosebery ore bodies (Fig. 8a,b) was selected for this study because (1) pyrite is definitely present; (2) the potential overprint of Devonian fluids is minimal; (3) drill samples are available up to 1.7 km north at the same stratigraphic level as the mineralisation, (4) good stratigraphic control is available; and (5) Rosebery probably occurs on a major Cambrian structure or structures. Previous structural work indicates that Cambrian structures in this area dip steeply north in the plane of the steeply east-dipping north-south striking stratigraphic sequence. The area contained enough drillholes along strike from the most northerly 'B-lens' mineralisation to potentially construct a sulfur

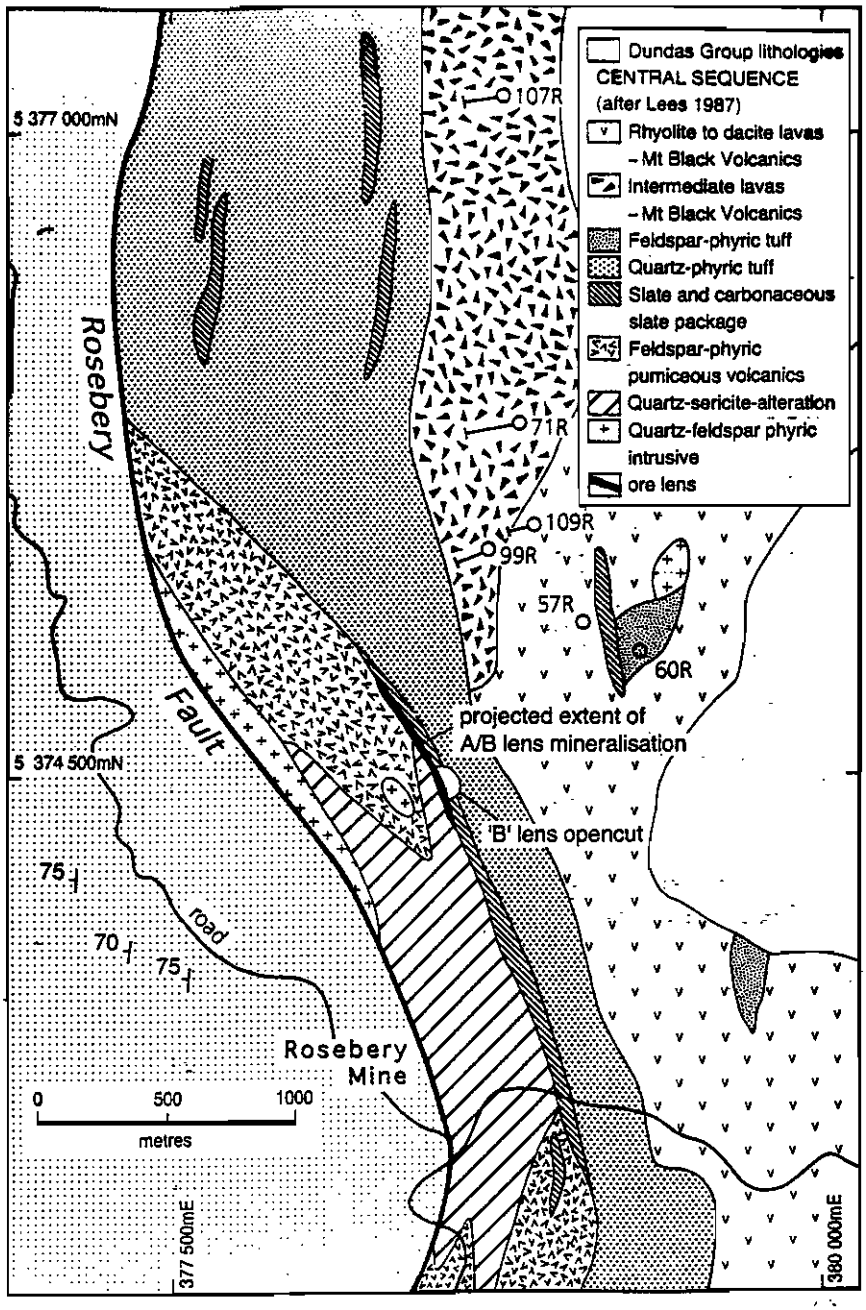

Figure 8a Geology of the B-lens area at Rosebery, after Lees (1987).

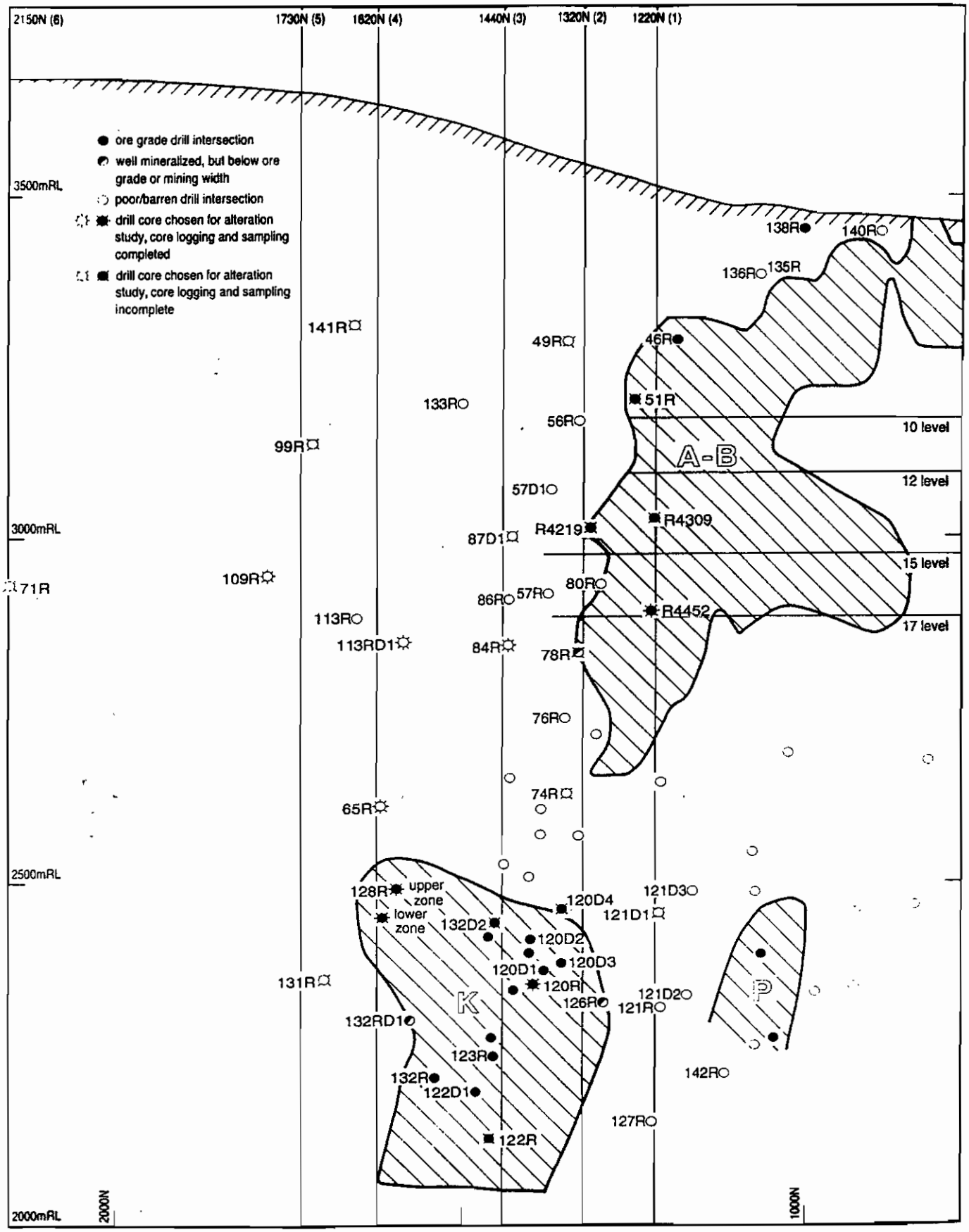

Figure 8b Long section with 1996 drilling locations and the known geometry of ore lenses from the north end of Rosebery after Allen et al. (1996); comments on drillholes in the legend do not relate to this study.

isotope profile which was transverse to known Cambrian structures.

Methods

Samples and results are listed in Appendix 2. Profile locations are shown in Table 3. Ten-metre interval samples of six holes were obtained through the Rosebery footwall and ore position north of B-lens, but sulfides were not visible in all samples. Most sulfur isotope analyses were obtained using a laser ablation instrument at the University of Tasmania, but check wholerock analyses (KIBA technique) were made on seven samples (Table 1). Laser-ablation extraction generated sample pit diameters of 100–300 μm. However, the very small size of most grains necessitated the common practice of amalgamating the sulfur from 2–8 grains visible in one section, within 0.5 cm of one another, to obtain enough sulfur to measure in the mass spectrometer. Only pyrite grains were analysed in this study. Further attempts to obtain a representative sample involved averaging up to five individual analyses from the same sample. However, in three of the wholerock replicates, the wholerock and laser estimates were still significantly different, suggesting that in some areas sulfur isotope values vary widely at hand-specimen scale. Wholerock values are considered a more reliable indicator of overall variation. Consequently the laser results must be interpreted with care, and anomalous results are only significant at drillhole scale when supported by surrounding results.

Results

143 analyses were obtained, including seven KIBA technique samples, and three heavy mineral wholerock estimates. Results are summarised in Figure 8, with ranges and averages annotated in Figure 11.

Table 3 Holes sampled at the north end of Rosebery for sulfur isotope variation. Locations are in mine coordinates and are shown on Fig. 8.

Hole	Collar northing & dist. (m) from ore	Collar easting	Collar RL	Section intersected
60R	1210N 0	657E	3651RL	Intersects B-lens ore. Includes H'wall black shale, upper footwall
49R	1385N 175m	51E	3548RL	B-lens periphery Includes H'wall black shale, upper footwall
57R	1394N 184m	521E	3594RL	B-lens periphery Includes H'wall black shale, upper footwall
109R	1782N 572m	350E	3563RL	Deep hole from black shale through the ore position, footwall pumiceous volcanics to the Rosebery Fault.
71R	2178N 968m	398E	3530RL	H'wall black shale, transitional host sequence, upper footwall
107R	2991N 1781m	612E	3399RL	H'wall black shale, transitional host sequence, upper footwall

Footwall variation — Footwall pyrite immediately below B-lens (range: $\delta^{34}S$ = 7.3–17.3‰; mean $\delta^{34}S$ = 11.5‰, n = 19) is isotopically similar to sulfur from B-lens itself (9.6–10.9‰, n = 2), mirroring the findings of Green (1983), for the southern Rosebery zone. The same 'ore' signature is present in hole 71R (970 m north of B-lens), although the number of samples was small (n=11 analyses; Fig. 9), because sufficient sulfur was not always present.

The footwall between B-lens and hole 71R contains zones of heavy near-surface sulfur in the top 70 m of the sequence, overlying a region at least 310m thick of ore-signature pyrite (Figs 9, 10), as determined in holes 49R and 109R. In detail, the range and averages in 49R and 109R are similar (–3 to ~+45‰), av. 16.57‰ (n = 3) and 16.17‰ (n = 13) respectively. The data in hole 109R, the most comprehensive sulfur isotope section obtained, are better viewed in their spatial context (Fig. 10). The ore position and the underlying 70 m of stratigraphy contain both very isotopically heavy ***and*** ore-signature pyrite, giving a range here of 5–46‰, with a mean of 23.5‰ (n = 13 analyses from six samples). Where available, the wholerock value has been used instead of the laser estimate. Given that Cambrian $\delta^{34}S$ is ~30‰ (Claypool et al. 1980), much of this data is actually heavier than the likely contemporary seawater sulfate. The underlying 310 m of stratigraphy through to the Rosebery Fault is characterised by B-lens to lower-than-B-lens values (–7 to +11‰).

The variation in hole 107R is distinctly heavier than the next-nearest hole 71R. The data ranges between 11.8 and 20.2‰, with a mean of 15.1‰ (n = 13).

Black slate — Disseminated black slate pyrite is isotopically very variable, with an average $\delta^{34}S$ value of 10.4‰ (range $\delta^{34}S$= –6.5 to +26.0‰, n=36), whereas vein pyrite varies from 4.6–15.9‰ (n = 10). Where both pyrite nodules (up to 1cm diameter) and dispersed fine pyrite euhedra were present in slate, the dispersed pyrite was ~ 20‰ lighter than the nodular variety. A smaller variation was obtained within the nodules, with the margins being~2‰ heavier than the cores. Where it was possible to compare the variation of vein and disseminated pyrite in the same sample (60R-2827, 60R-2890), the vein pyrite was up to 4‰ lighter (Fig. 11), suggesting some mixing with lighter sulfur during vein formation. However, given that the veins display the same total isotopic variation as the disseminated pyrite, they are regarded mainly as the product of local remobilisation. This was not a systematic part of our study, so that further work is warranted to confirm the result. The result must be viewed cautiously, given that vein pyrite can vary 5‰ in a single grain (71R-1707; Appendix 2).

Devonian? pyrite — Post-cleavage disseminated pyrite varied isotopically from 1.1‰ to 3.8‰ (n = 4). These values are marginal to the range of Cambrian variation at Rosebery. Given the association of the pyrite with carbonate and pyrrhotite, these values may represent the value of Devonian granite-related sulfur at Rosebery.

Interpretation

Previous sulfur isotopic work at Rosebery — It is important to examine the isotopic variation at Rosebery, as context for the values that have been obtained in this study. The research prior to this study has established a detailed picture of sulfur isotope variation in (1) the main mineralised lenses; (2) the Devonian granite-overprint on these lenses; and (3) sulfides and sulfates of the overlying barite zone. Limited data has also been obtained from footwall sulfide veins/disseminations immediately below high grade mineralisation, and from disseminated sulfides in the hangingwall black slates.

Base-metal sulfides and barite — The main sulfide lenses at Rosebery vary from $\delta^{34}S$= ~7–18‰ (Solomon et al., 1969; Green, 1983; Solomon et al., 1988), generally heavier than deposits in the northern Mount Read Volcanic Belt, which average ~7‰. Massive pyrite-chalcopyrite ores at Rosebery are distinctly lighter than the base-metal ores, with a mode at 9‰. This is also the case at Hercules to the south (Khin Zaw, 1991). In addition, Green (1983) showed that there are distinct and systematic isotopic variations in the base metal ores, with the overall $\delta^{34}S$ value increasing (1) in the higher lenses; (2) in the upper portions of single lenses, and; (3) as a general trend southwards. Green's conclusions are based on an unfolded model of the Rosebery orebody.

Sulfide that is associated with the barite-rich ores

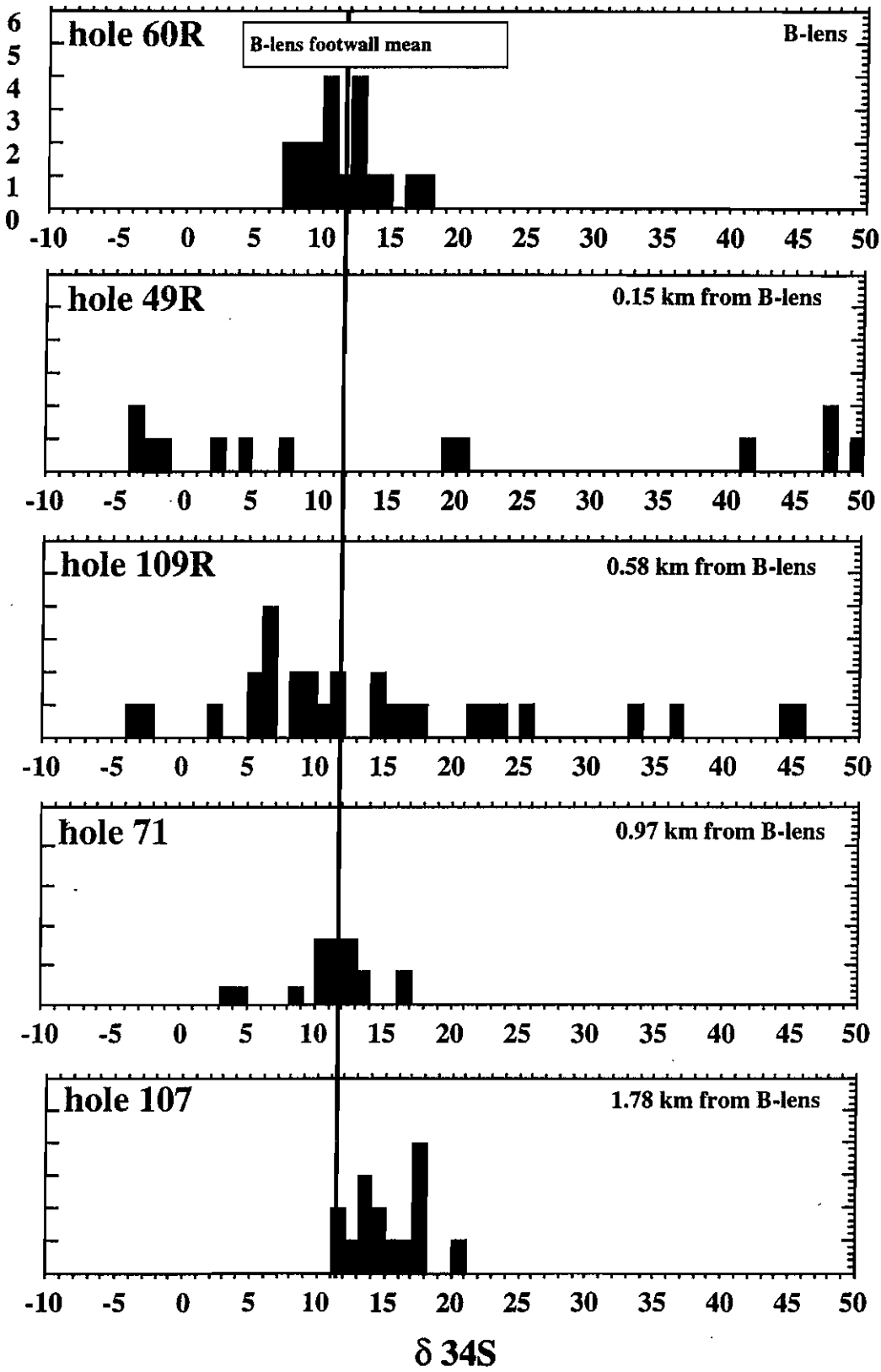

Figure 9 A frequency histogram summary of the sulfur isotope variation in five holes north of Rosebery B-lens. Data include footwall, hostrock and ore pyrites, but specifically exclude hangingwall and Devonian sulfides, where they were clearly identifiable. Each frequency point is the average of up to 5 individual laser ablation analyses.

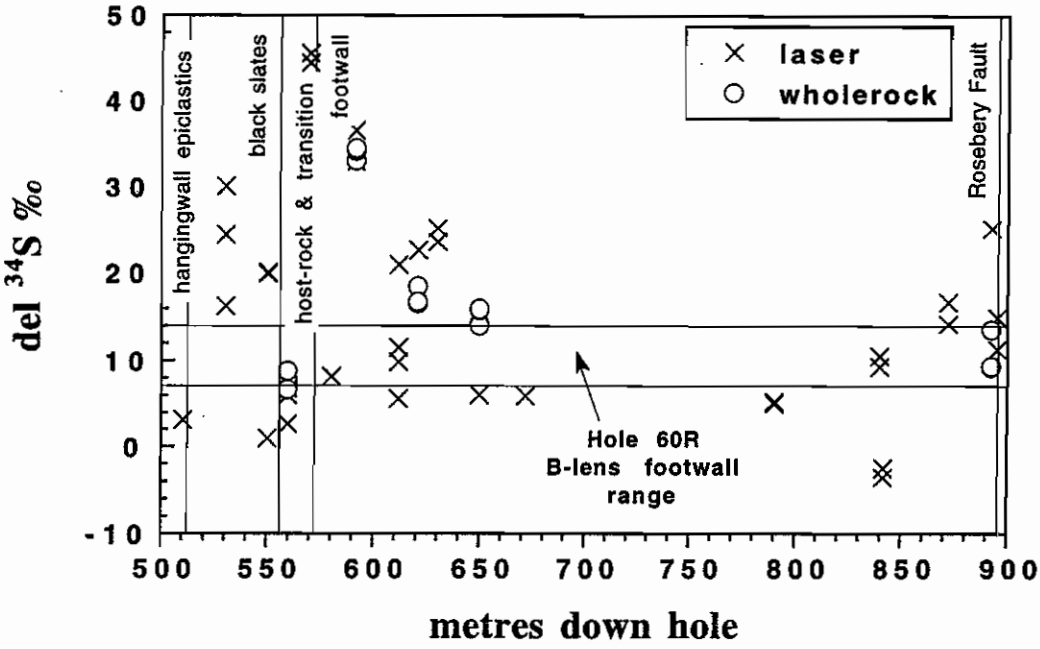

Figure 10 Total downhole sulfur isotope variation in hole 109R.

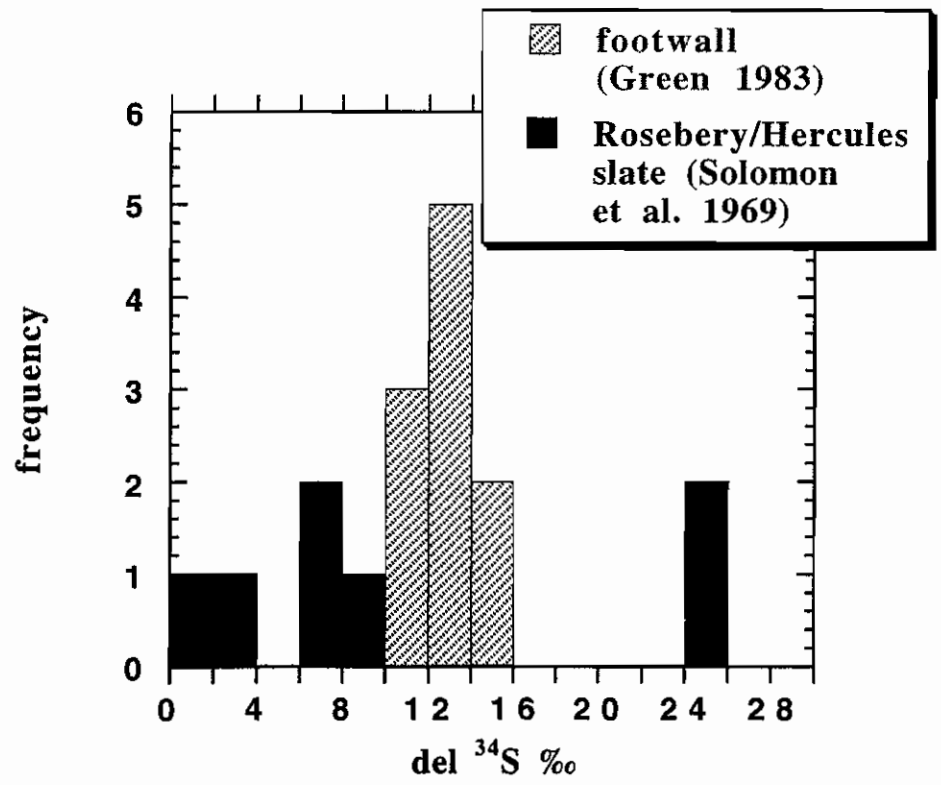

***Figure** 11 A compilation of sulfur isotope values from pyrite in Rosebery footwall alteration and carbonaceous slates.*

at Rosebery have the heaviest sulfur (13–20‰), but are considered by Solomon et al. (1988) to be in equilibrium with barite (deposited at 300° C) ranging from $\delta^{34}S$ = 33–41‰, slightly above the late Cambrian seawater sulfate value (30‰).

Solomon et al. (1988) emphasise that Rosebery "is the only example in the Mount Read Volcanic Belt displaying stratigraphic zoning of $\delta^{34}S$ values (increasing with time)", which they interpret as the result of an increase in the reduced seawater sulfate component, principally caused by exhaustion of available leachable rock sulfur in the deep footwall as hydrothermal circulation continued, and particularly as it began to wane.

Footwall alteration — Green (1983) and Solomon et al. (1969) analysed eight pyrite-bearing veins from footwall alteration in the southern zone at Rosebery. The values varied from $\delta^{34}S$ = 10.6–14.9‰, average 12.5‰ (Fig. 11). These values were very similar to those of directly overlying massive sulphides at this locality (Green 1983). Solomon et al. (1988), in considering these data, concluded that they indicated that shallow seawater convection within the Rosebery footwall was not likely, because there was no isotopic support for a change in oxidation state.

Carbonaceous slate-hosted pyrite: hangingwall variation — Only three samples of hangingwall carbonaceous slate have been sampled at Rosebery previously (Solomon et al., 1969). At these sites the material analysed is referred to as "pyrite-quartz lenses parallel to cleavage", and hence is likely to represent at least locally remobilised sulfide. Repeat analysis of two samples suggested that intra-sample variation is <2‰. The isotopic range is very great, from 2.3–25.3‰. Two samples from Hercules (described as "pyrite nodules") lie within this variation, bringing the total number of analyses of this lithology to seven (Fig. 11).

Devonian sulfur — It has been demonstrated by several workers that no isotopic change occurred as a result of the Devonian replacement of base metal sulfides by pyrrhotite during granite intrusion in the southern lodes at Rosebery (Green, 1983; Solomon et al., 1988; Khin Zaw, 1991). Khin Zaw found that pre-existing Cambrian variation was only homogenised at a hand-specimen scale by this process, not changed. This work suggests either that the value of Devonian sulfur was identical to the Rosebery Cambrian value, or that the general sulfur content of Devonian fluid was low, with the result that its signature was overwhelmed by Cambrian sulfur in the ore environment.

Integrated interpretation — Within the footwall north of B-lens, the top 70 m for 500 m to the north is characterised by isotopically heavy sulfur, indicating a local zone of direct and near-complete seawater sulfate reduction. In terms of Cambrian structures and seawater circulation, this area must be considered an area of shallow downflow, possibly imposed on high temperature alteration, evidenced by the wide band of 5–12‰ sulfur below 70 m, and by sporadic "ore signature" values within the heavy zone (Fig. 10).

By the same logic, the area around hole 71R, 968 m north of B-lens, is a separate hydrothermal upflow zone. The top 60 m of footwall here has an average of $\delta^{34}S$ = 11.5‰, and a range of 3.6–13.2‰ (n=6 samples, with 11analyses total), which is identical to the B-lens variation (Fig. 12).

There are still several unknowns, shown with question marks on Figure 12. Firstly, how extensive is the heavy sulfur facies which occurs between B-lens and the upflow in hole 71R? Hole 109R has clearly shown that the zone has a distinct depth limit, but its lateral extent is uncertain with the current extent of drilling. What is the relationship between the upflow zone of hole 71R and the adjacent downflow in hole 109R? This question awaits further infill sampling. Lastly, what is the real significance of higher $\delta^{34}S$ values in hole 107R 1.8 km from B-lens, compared to other zones of heavy sulfur? The $\delta^{34}S$ range in 107R is far more restricted than in holes 109R and 49R, and unlike these, has less overlap with "ore signature" values. On this basis fluid circulation may have been better mixed, with mixing occurring between deep upwelling reduced sulfur, and pure reduced seawater sulfate, as might occur towards the edge of a regional upflow cell.

The Rosebery Fault data represents an interesting variation on this theme. Hole 109R finishes in the fault, and the passage of Devonian fluids is recognised by abundant carbonate-tourmaline-pyrite/pyrrhotite veins. Our early work recognised a Devonian signature in some texturally distinct areas of $\delta^{34}S$ = 1–4‰, whereas Khin Zaw (1991) has shown that where Devonian fluids contact Cambrian sulfides, their

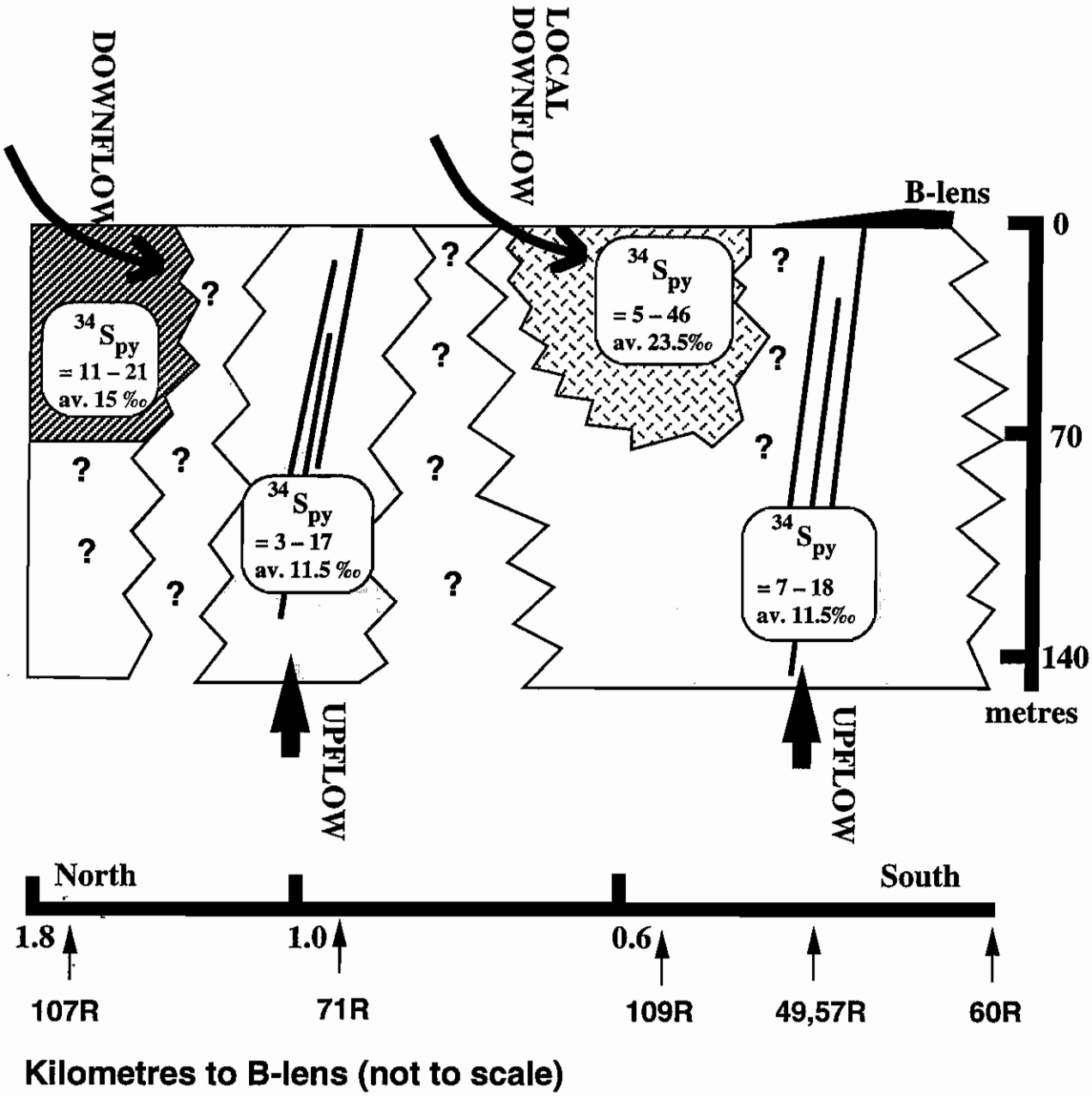

Figure 12 Sulfur isotope facies of the Rosebery footwall, a schematic section. Question marks indicate where the relationship between sulfur isotope domains is not well established.

innate sulfur content is so low that there is no net isotopic change, and a homogenised Cambrian signature remains. It is yet to be demonstrated that Devonian fluids scavenge and transport Cambrian sulfur to new sites, although this is possible, given that they clearly scavenge large quantities of Pb and Zn. Carbonate-tourmaline-bearing veins in and near to the Rosebery fault in hole 109R contain $\delta^{34}S = -3.5$ to 14.5‰ (Fig. 10). This consists of a discrete vein zone 54 m from the fault with a narrow range of $\delta^{34}S = -3.5$ to −2.4‰, grains of pyrite 3 m from the main trace with $\delta^{34}S = 14.5$‰, and pyrite in the main fault with $\delta^{34}S = 11.3$–15.0‰. Hence some carbonate-tourmaline zones contain the Devonian light S signature, whereas the main fault trace contains ore signature sulfur, which either originated by Cambrian seawater reduction, or by Devonian scavenging of Cambrian sulfur.

Summary of Findings

- Areas of $\delta^{34}S > 18$‰ in the Rosebery footwall are the signature of shallow Cambrian seawater inflow and partial sulfate reduction, occurring within 500 m of major focussed hydrothermal upflow zones. 70 m is the maximum depth extent of heavy sulfur isotope values in hole 109R, and may delineate the sub-surface boundary of partial sulfate reduction.

- The region 1 km north of B-lens (hole 71R) is characterised by the upflow ore signature of B-lens alteration ($\delta^{34}S = 11.5$‰ on average), and is likely to underlie massive sulfide mineralization at the footwall contact.

- The expectation that sulfate reduction zones could be detected at the edge of massive sulfide deposits has been confirmed, although the extent of such zones in the Rosebery footwall appears to be far greater than for the focussed alteration at Hellyer (Gemmell & Large, 1993).

Cambrian faults

Fault selection

Cambrian faults from six locations, as outlined in Table 4, were identified by Project P291, on the criteria of unit juxtaposition, and thickness changes across faults. Faults with obvious Devonian movements were avoided to minimise the complexity of the geochemical signature. The sampling strategy was to surface-sample the faults wherever possible along and across strike, to determine the distribution of sulfur isotopes associated with them. In practice it was not always possible to find the exact location of the fault trace, resulting in samples being taken from as close as possible to the suspected position.

The samples were divided into two groups for the purposes of analysing isotopic compositions; (1) those with no visible sulfides, which were analysed using the heavy mineral separation technique, and (2) those with visible sulfides, which were analysed by conventional methods, and if necessary, by laser ablation.

Results

Although six faults were initially selected in this study, and sampled in the first reconnaissance phase, only three regions supplied statistically useful data, because of outcrop limitations. These regions became priority targets in the follow-up sampling phase; they were the Back Peak area including the Carters Prospect, the Zig Zag Hill/Comstock area, and the Moxons Saddle area.

A compilation of all results from the unmineralised sampled Cambrian Faults (Figs 13, 14; Appendix 3), in which the average of results from individual samples is plotted in a frequency histogram, indicates that the unmineralised Cambrian faults are enriched in heavy sulfur (av. = 16.8‰, n = 25). This is significantly heavier than much of the background distribution, and the range of individual Cambrian Pb-Zn deposits, but comparable to the range of sulfur isotopes in the deposit peripheries (Gemmell & Large 1993, this study).

Back Peak area/Carters Prospect — The Back Peak area contains mineralised and unmineralised faults which were active at the onset of rifting of the Mt Read

Table 4 Sampling details of regional Cambrian Faults.

Fault	Location	Sampling Details	Sulfur Isotopes (‰)	Nature of samples
Carters Prospect 406500mE 5394400mN	2km NW of Back Peak, vein-systems transecting the Precamb/Camb Back Peak Beds contact	Fault not directly sampled. Samples mainly 30 m east of probable fault trace.	2.7–6.8, av. py =4.7 (n=11)	Some visible disseminated py and galena in silicified areas; Pb-isotopes indicate Cambrian age
"Moxons" Fault (a Henty Fault splay) 381500mE 5365850mN	2km NW of Henty mine, on the Tyndall-CVC contact	100m wide shear zone with strong chlorite and sericite alteration	2.7–32.0, av. =15.6(n=7)	Samples taken at ~20 m intervals across the shear on 2 sections 800m apart.
"Dalmeny St" Fault 379400mE 5373200mN	Rosebery township	A brittle fault dipping 80°/076° was sampled, likely to be Devonian, but this corresponds to the Cambrian location	11.9–15.6, av. 13.5‰ (n=4).	No visible sulphides; Sample intervals: 0, 1, 5m; weathered.
Pieman River 375900mE 5377100mN	1.5 km SW of Bastyan Dam	Juxtaposes Crimson Ck Fm with Dundas Group sediments N-S growth fault	15.9–33.6, (n=3)	Disseminated pyrite in sediments
"ZigZag Hill" Fault 382200mE 5345800mN	Comstock Valley, 6 km north of Queenstown	Fault not exposed. Separates Tyndall Group andesites from volcaniclastics. Associated with strong red-K-feldspar alteration	8.6–23.9, av. 18.6 (n=8)	Minor visible py, most abund-ant in the andesite.

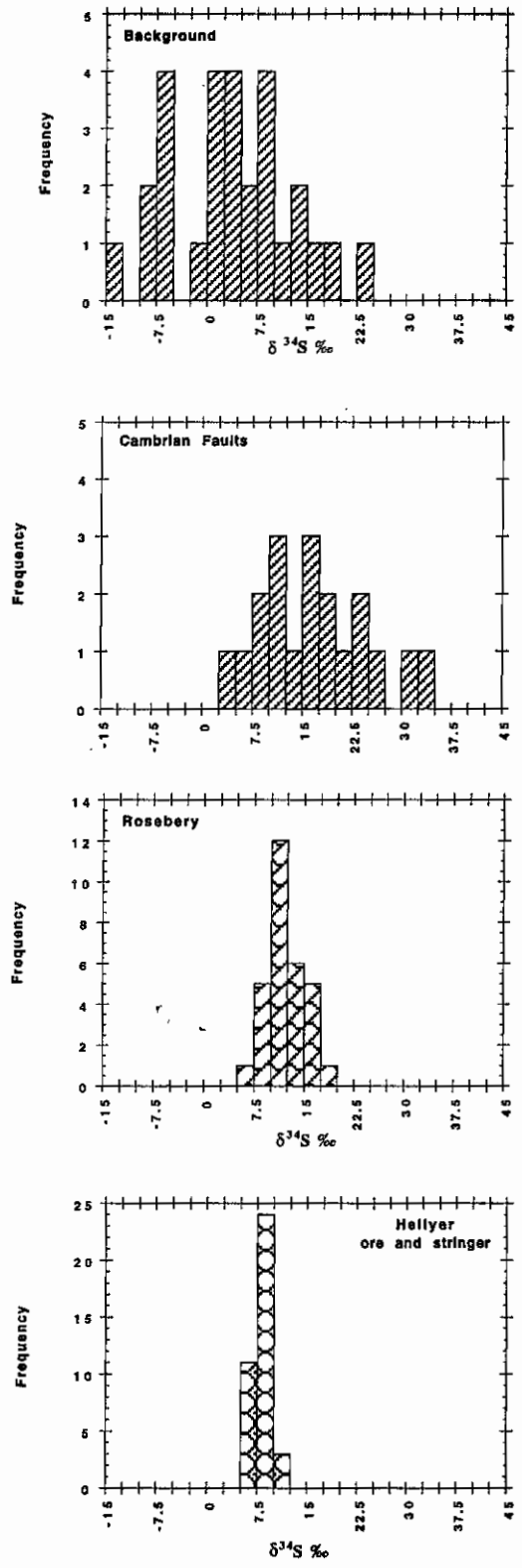

Figure 13 Frequency histograms comparing the ranges of deposit sulfur with the background variation and the range of sulfur isotope values known from Cambrian faults.

Volcanic Belt depocentre. Five un-named faults occur (Fig. 15) with syn-sedimentary movements implied by variations in thickness of the Sticht Range Bed-correlate conglomerates, volcaniclastic sandstones, vitric tuff and siltstones at the base of the sequence. Post-Denison Group movements are also indicated by unit offsets. This sequence is intruded by the large Cambrian Bond Range porphyry sill, which is also transected by the growth faults (Fig. 15). Carters Prospect consists of Pb-Zn veins and disseminated base-metals within and immediately above Precambrian basement, associated with silicification, and localised on one of the larger growth faults.

Twenty-three sulfur isotope analyses have been completed to obtain an overview of sulfur isotope variation around three faults in the area. Sulfur isotopes were mainly obtained by the wholerock method, with some conventional and laser ablation analyses at the Carters Prospect (Fig. 18).The data indicate that the main mineralised fault, at the Carters Prospect, is characterised by the lightest sulfur, $\delta^{34}S$ = ~5‰ for pyrite and galena, with a greater sulfur isotope range occurring on the other two faults (7.5–14.2‰). Visible sulfides and silicification occur on all faults. Carters Prospect is close to the value of other Cambrian massive sulfides in the Southwell Subgroup, such as Hellyer ($\delta^{34}S$ = ~ 7‰). Pb-isotope analyses indicate that the Carters galena has a Cambrian parentage (Table 5), disproving a Devonian parentage suspected from earlier MRT survey work on the nearby Anio Creek anomaly.

It is surprising that the hydrothermal value is so similar to other Southwell subgroup hydrothermal systems, if a model is applied of hydrothermal circulation largely driven through Precambrian metasedimentary basement during early rifting. This

Table 5 *Pb-isotope analyses of pure galenas from Carter's Prospect, Back Peak area.The data is slightly less radiogenic than the Hellyer Pb-isotope field.*

Sample	206/204	207/204	208/204
PKGD1a	18.284	15.608	38.148
PKGD1b	18.272	15.606	38.144
PKGD1c	18.274	15.601	38.147

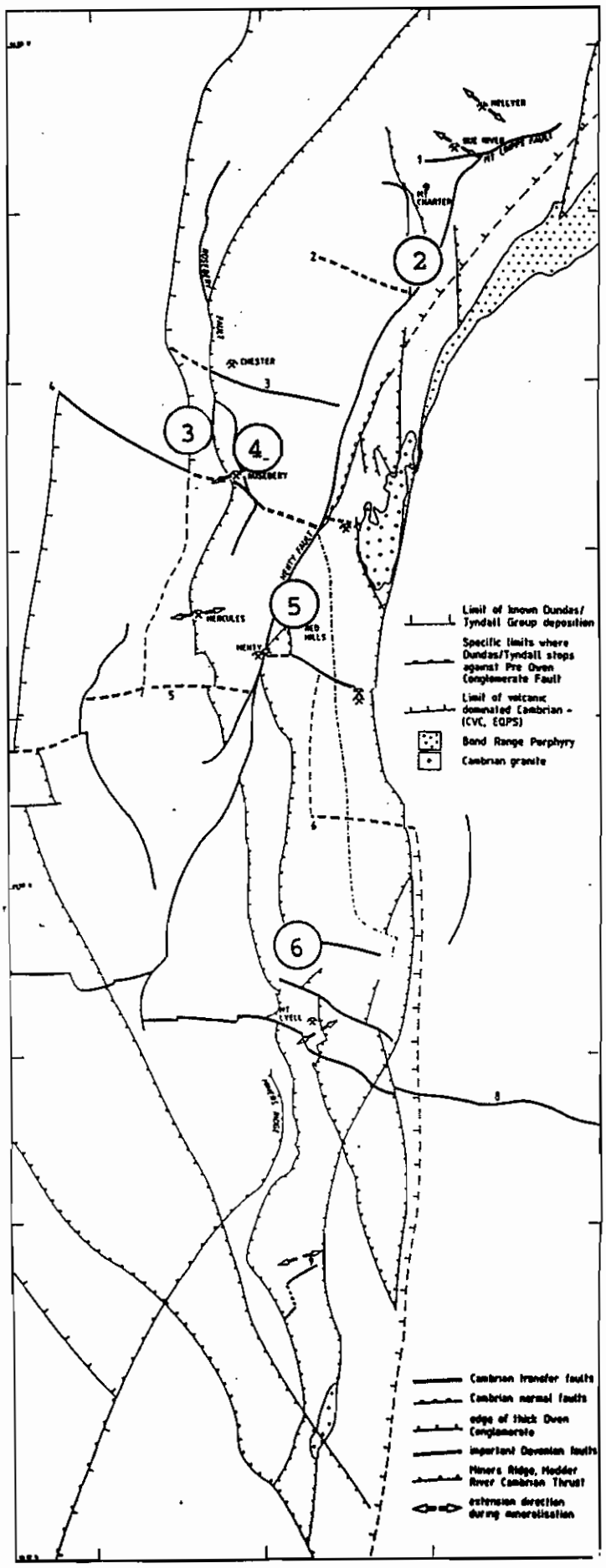

Figure 14 Location of faults examined in this study, with reference to the Cambrian faults identified by Project P291. 1. Back Peak-Carters area; 2. Tullabardine Dam; 3. Pieman River; 4. Dalmeny St, Rosebery; 5. Moxons Fault; and 6. Zig Zag Hill/ Comstock.

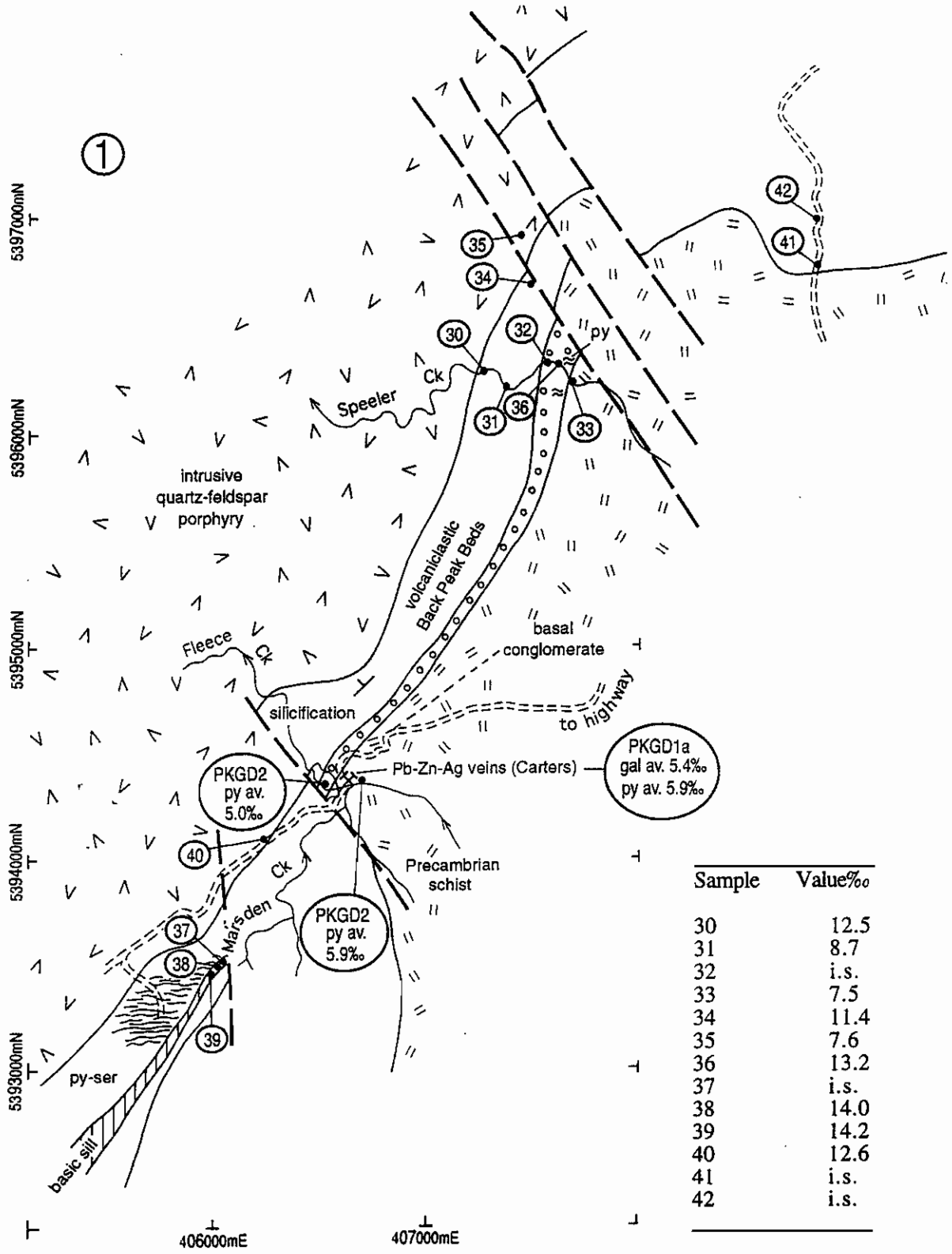

Sample	Value‰
30	12.5
31	8.7
32	i.s.
33	7.5
34	11.4
35	7.6
36	13.2
37	i.s.
38	14.0
39	14.2
40	12.6
41	i.s.
42	i.s.

Figure 15 Geology and sample locations for the Back Peak sampling area, northern Tasmanian Mt Read Volcanic Belt. i.s.— insufficient sulfur for analysis. Sample details are provided in Appendix 3. Large numeral refers to the location on Fig. 14.

model would predict the inheritance of metasedimentary sulfur isotope values (likely to be highly variable, between –40 and +20‰). A second option to account for the value at Carters, and the comparitively low values of sulfur isotopes in the adjacent faults, is that all hydrothermal circulation was driven post-depositionally by the intrusion of the Bond Range porphyry, with sulfur being derived from the Cambrian volcaniclastic rocks in the Back Peak Beds, from the porphyry itself, and from minor seawater sulfate reduction. In this model only minor circulation would have occurred through the deformed Precambrian basement. The implication of this second hypothesis is that the very heavy values which typify most Cambrian faults elsewhere in the MRVB may not be present beneath the Bond Range porphyry. Instead the values could reflect a more homogenised system with respect to sulfur, similar to sub-surface reaction zones hypothesised as the source regions of massive sulfide deposits by many workers, although heavier zones might be expected if growth faults continued to allow ingress of seawater sulfate. In terms of metals exploration, the second hypothesis should target replacement base metals deposits at the permeability barrier of the Bond Range porphyry, as well as sites of high fluid flow, such as growth faults in the underlying substrate.

Whichever hypothesis is relevant, it is important to identify the signature of mineralising hydrothermal activity in areas of interest, in order to assess the significance of sulfur values in the nearby faults. At the main fluid focus (Carters) the sulfur isotope range is 2.6–6.8‰, whereas the adjacent faults contain values nearly 10‰ heavier (7.5–14.2‰), indicating that reduced seawater sulfate was preferentially incorporated into these. This alone suggests a Cambrian age for sulfides on the basis of the sulfur isotopes. However, if the isotopic range of mineralised systems in the entire MRVB was applied as the main discriminant, all values in the Back Peak area would be considered high temperature Pb-Zn-related. This does not appear to be the case.

"Moxons" Fault — "Moxons" Fault is the largest fault sampled in this program. The fault was described by White (1995) as a west-block-down normal fault between Tyndall Group and CVC at Moxons Saddle (Fig. 16a, b, c), and the growth fault interpretation of Berry & Keele (1993) was supported by the presence of pebbly volcaniclastic sandstone lenses along the fault in the Tyndall Group. The main fabric in the fault is suggested to be Devonian, although two cleavages were present in parts of the two sections examined. Strong chlorite ± sericite alteration is present, as is incipient K-feldspar alteration, which is not surprising given the close proximity to the Red Hills K-feldspar alteration zone.

The distribution of sulfur isotopes was determined by sampling along two transects of the existing fault at ~20 m intervals, 800 m apart. Good outcrop in the saddle permitted sampling of fresh rock along each transect. Wholerock sulfur isotope values of 2.7–32.0‰ were obtained, with no visible sulfides being identified; Davidson & Kitto (1995) erroneously quoted an isotopic range of 3–6‰ for this fault, but these values actually relate to chalcopyrite prospects in the Henty Fault to the west, and to an unmapped strongly altered shear west of the Henty Fault (Fig.16). Sulfur in Moxons Fault is distinctly heavier than that from either of these structures. The heavy sulfur (26.1–32.0‰, n = 2) is distributed in a 30 m wide zone towards the eastern side of the fault, associated with chlorite ± K-feldspar alteration. Samples in the centre of the shear have $\delta^{34}S$ = 2.7–12.2‰, indicating that the sulfur isotope distribution is overall very variable; on the geological evidence, it is extremely likely that both Cambrian and Devonian sulfur is present within the shear, or that sulfur from different Cambrian sources is present. However, values of ~30‰ are likely to be derived from Cambrian seawater sulfate reduction, since heavy sulfur fluids are not known from the Devonian of Tasmania.

Comstock — The "Zig Zag Hill" Fault, identified by M. White, is a small scale normal fault in the Tyndall Group, with no obvious associated shear fabric in its wallrocks, and only a mild east-west Devonian deformational overprint (the structure itself is covered by alluvium for at least 20 m to either side). Pyrite is disseminated up to 200 m away from the structure, associated with chlorite alteration, in both volcaniclastic sandstones and coherent to autobrecciated andesites. Strong pink K-feldspar-chlorite alteration occurs lower in the stratigraphy. Sulfur isotope values from this alteration are from samples PKGD7 and PKGD45–48 on Fig.17a, with $\delta^{34}S$ = 11.1–

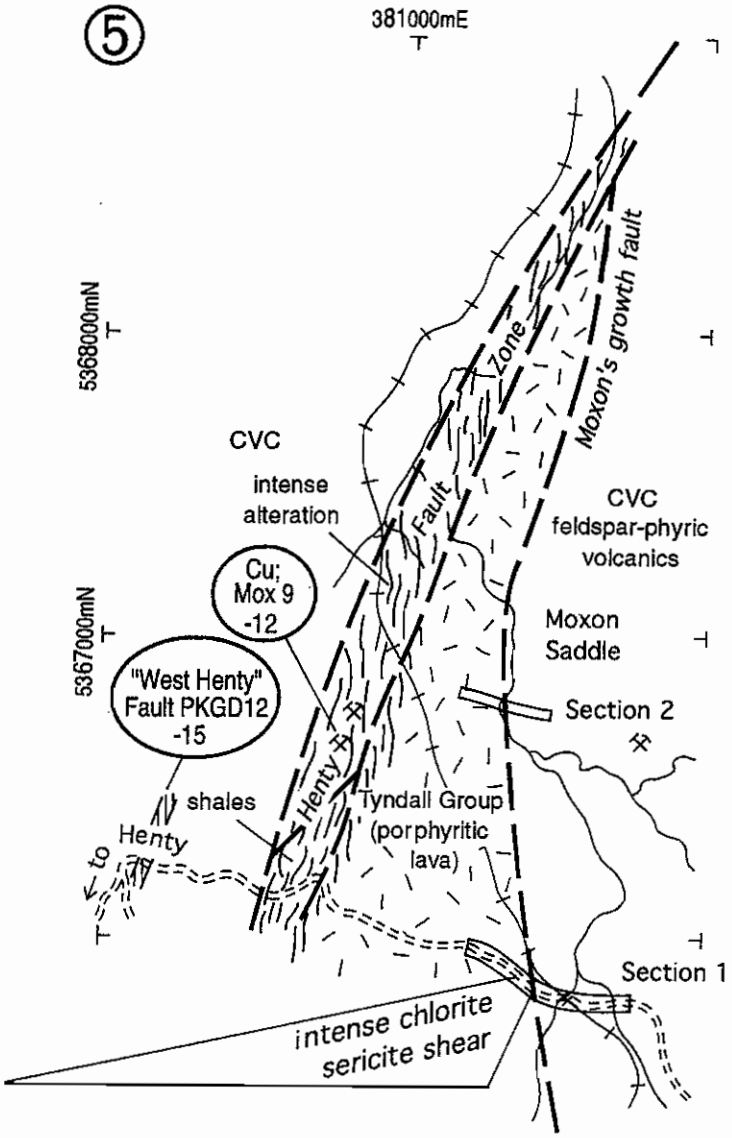

Figure 16 (a) Geology (and sample locations) of the Moxons Fault area, on the Tyndall Group Central Volcanic Complex contact. (b) Sampling details along section 1 (see Fig. 15a), a road section on the Red Hills track, with power-lines shown by a line and crossed box. (c) Sampling details along section 2, in which precise location is given by AMG coordinates on a pegged grid.

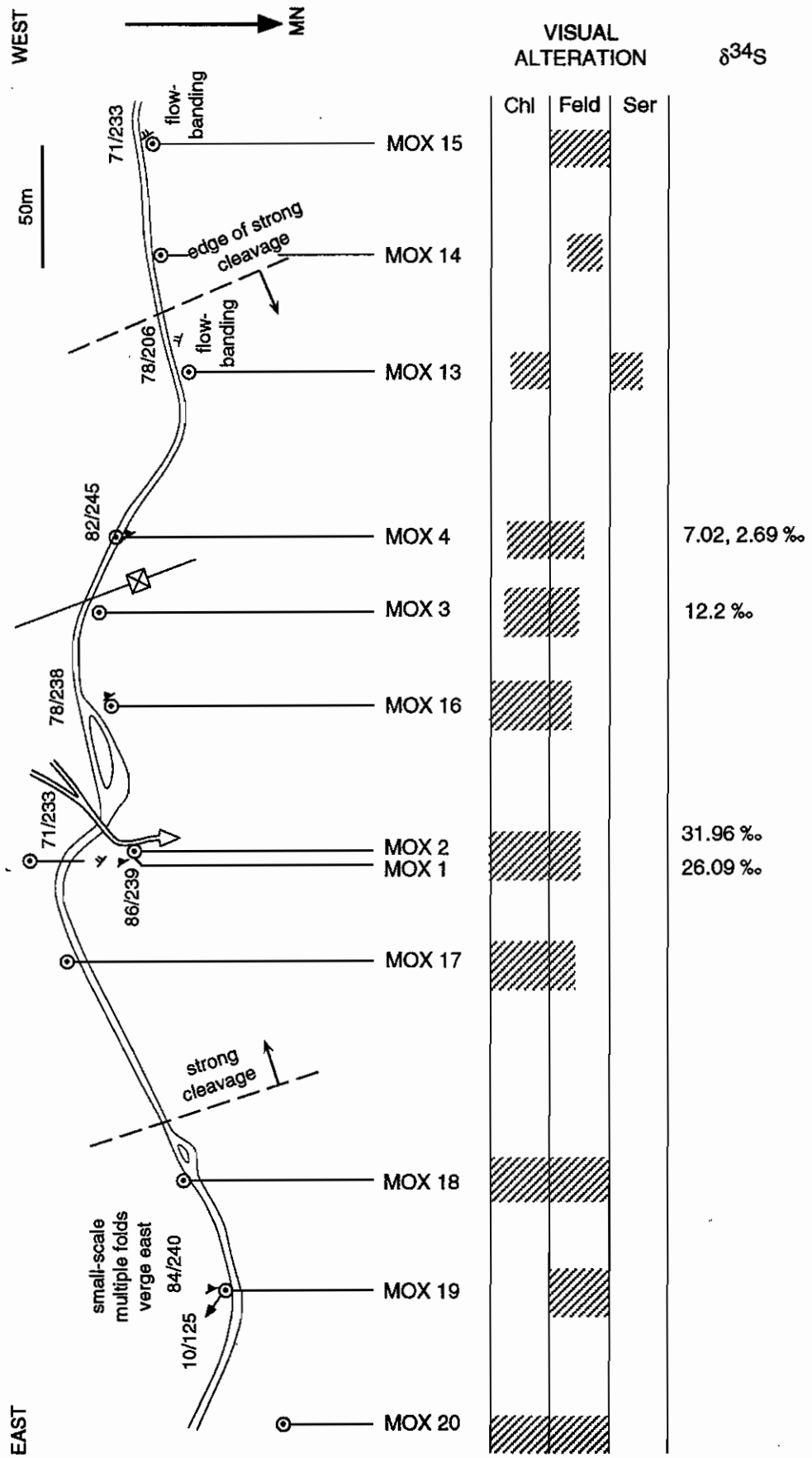
WEST
MN
EAST
50m
VISUAL ALTERATION
Chl
Feld
Ser
δ34S
71/233
flow-banding
MOX 15
edge of strong cleavage
MOX 14
78/206
flow-banding
MOX 13
82/245
MOX 4
7.02, 2.69 ‰
MOX 3
12.2 ‰
78/238
MOX 16
71/233
MOX 2
31.96 ‰
MOX 1
26.09 ‰
86/239
MOX 17
strong cleavage
MOX 18
small-scale multiple folds verge east
84/240
MOX 19
10/125
MOX 20

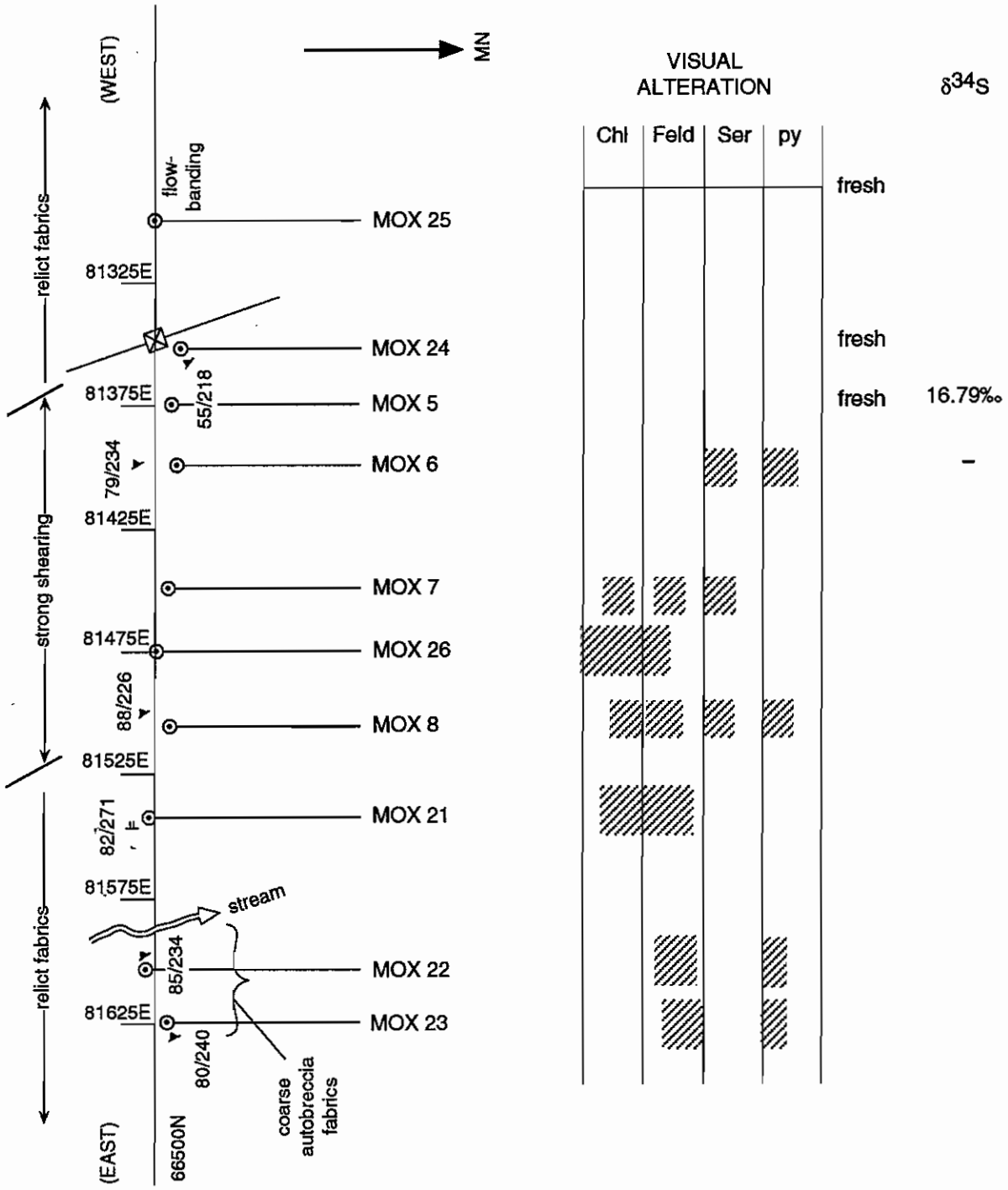
(WEST)
MN
flow-banding
MOX 25
81325E
MOX 24
81375E
55/218
MOX 5
79/234
MOX 6
81425E
MOX 7
81475E
MOX 26
88/226
MOX 8
81525E
82/271
MOX 21
81575E
stream
85/234
MOX 22
81625E
MOX 23
80/240
66500N
(EAST)
coarse autobreccia fabrics
relict fabrics
strong shearing
relict fabrics
VISUAL ALTERATION
Chl
Feld
Ser
py
fresh
fresh
fresh
δ34S
16.79‰
–

17.1‰ (n = 5). Sulfur isotope values in the disseminated pyrite of the Comstock tuff (PKGD10, 10a, 10b, 11) contain visible pyrite that is distinctly isotopically heavier ($\delta^{34}S$ =~ 18.1–24.7‰, n = 4) using the laser, but rwholerock analyses indicate the overall value is ~10–11‰, consistent with the presence of significant isotopically light sulfide as well as the coarse heavy grains. Further analyses will be available at the meeting for discussion. However, a significant contribution from Cambrian seawater is suggested by the isotopically heavy coarse grains, supporting a Cambrian age for the structure, in view of the lack of Devonian fluid overprint. It is important to note that these would not have been discovered without using the laser ablation technique. K-feldspar alteration may represent a deeper alteration style. Its relationship to the chlorite alteration is not known due to outcrop constraints. Samples PKGD7, 45 and 46 probably derive from slightly upslope, since all material up to PKGD47 on the transect consisted of very large boulders of K-feldspar-chlorite alteration.

Pieman River — The proposed Cambrian growth fault of Bull (1995) and Berry & Keele (1993), 1.5 km west of (and parallel to) the Rosebery Fault was sampled (Fig. 17b), using disseminated pyrite in siltstones adjacent to vein and faults that showed evidence of Devonian reverse movement. This fault juxtaposes Crimson Creek Formation with Stitt Quartzite, although the exposed outcrop is mainly Crimson Creek Formation (Bull, 1995). Sulfur isotope values are $\delta^{34}S$ = 15.9–33.6‰, (n = 3), consistent either with the direct precipitation of sulfides from Cambrian fluids, or the scavenging of Cambrian sulfides by Devonian fluids. However, very heavy values have only been found in shallow Cambrian convection systems elsewhere in the Mt Read Volcanics, favouring an original growth fault or Cambrian aquifer origin.

"Dalmeny" Street fault, Rosebery hangingwall — Several thin veins and faults occur at a position corresponding to a probable low-angle Cambrian fault separating feldspar-quartz phyric tuff from feldspar-phyric volcanics of the Mt Black Volcanics, ~400 m east of the Rosebery lodes (Fig. 17c). The brittle character, undeformed state, and association with minor reverse faults all suggest that pyrite in these veins was deposited during Devonian deformation. The sulfides were sampled on the premise that the Devonian features would nevertheless have preserved a Cambrian signature from the pre-existing structure. Values of $\delta^{34}S$ = 11.9–15.6, av. 13.5‰ (n = 4) were obtained. These values are similar to normal Rosebery base metal sulfides, and hence most likely derive directly by the remobilisation of sulfur away from the main Cambrian sulfide body during the Devonian. They do not support local remobilisation of heavy sulfur from a Cambrian growth fault that originally contained heavy sulfur. They do indicate an ultimate Cambrian source for sulfur in these veins, with a Devonian timing of introduction.

Interpretation

The primary aim of analysing the sulfur isotope character of faults was to determine if those with Cambrian histories have any distinguishing isotopic features. The values can be compared with those of (1) the regional background (Fig. 3); (2) Cambrian deposits (Fig. 13); (3) "Barren" Cambrian alteration systems (see below); and (4) Devonian Pb-Zn vein deposits (Fig. 19).

It has been demonstrated that background sulfur has an extremely wide isotopic variation, which includes unusually light sulfur values (to –14.5‰). Cambrian deposits have a very restricted range for each deposit, but overall they vary from 5–18‰, with the lighter end characterising deposits in basaltic piles (Que River, Hellyer), and heavier values found in deposits from felsic piles (Rosebery, Hercules) (Solomon et al., 1988). A small group of "barren" alteration systems, dominated by chloritic footwall alteration and stratiform pyrite, have a distinctly lighter signature, and include Boco (–1.2 to 4.7‰; Green & Taheri, 1992), Chester (–3–0.4‰; Solomon et al., 1988), Specimen Creek (–2.9 to 1.8‰; Jackson, 1996), Basin Lake and Cattleys Grid (values not quoted; Green & Taheri, 1992). The light values of these Cambrian systems are attributed by Solomon et al. (1988) and Green & Taheri (1992) to wallrock reaction at < 200°C, preventing the reduction of seawater sulfate, but permiting local leaching of igneous rock sulfur. In this respect they resemble the background sulfur isotope population, and are best explained as thermal anomalies within oxidised aquifers during Cambrian alteration. Unfortunately

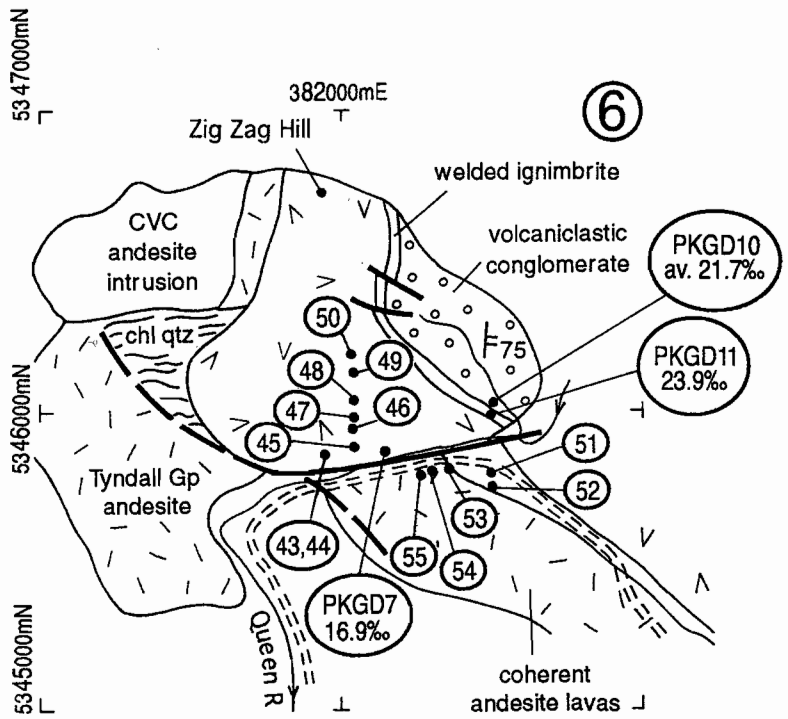

Sample	Value‰
43	10.2
44	17.1
45	13.2
46	16.0
47	11.1
48	i.s.
49	17.1
50	v.a.
51	v.a.
52	v.a.
53	v.a.
54	v.a.
55	v.a.

Figure 17 (a) Geology and sample locations for the Zig Zag Hill area, Tyndall Group. i.s.— insufficient sulfur for analysis; v.a.— value awaited. Sample details are provided in Appendix 3. (b) Sampling details for the Pieman River site. (c) Sampling details for the Dalmeny St Fault site near Rosebery. The Murchison Highway is shown, whereas by oversight, Dalmeny St does not appear.

these values overlap with Devonian magmatic sulfur isotope values, although the latter are associated with a distinctive trace element suite.

Devonian epigenetic vein deposits (Farrell field, Sterling Valley, Langdons, Lynch Creek goldfield, Lakeside), thought to relate to distal Devonian magmatic activiity, have a restricted sulfur isotope range (5–17‰; Fig. 19), virtually identical to the field of Cambrian massive sulfide deposits. Green & Taheri (1992) interpret this overlap to indicate that Devonian fluids obtained most of their sulfur from leaching Cambrian crust, with the lighter values resulting from mixing with Devonian magmatic sulfur, for instance accounting for values of 7–10‰ for Sn-Au deposits at Lakeside. This argument assumes that Cambrian massive sulfide deposits in some way represent the value of average Cambrian crust. In fact the background study indicates that Cambrian background values have a far wider spread than the massive sulfide deposits, and it is probably fortuitous that Devonian fluid circulation averaged the Cambrian + Precambrian crust to produce a similar isotopic range.

None of the above sulfur populations is capable of producing $\delta^{34}S$ values approaching the Cambrian seawater sulfate value (30‰). Consequently faults with $\delta^{34}S$ > 18‰ are considered to have had a Cambrian history. This is supported by the heavy isotopic values characterising the margins of Cambrian massive sulfides, that are attributed to in situ reduction of seawater sulfate. Additionally, where careful analysis suggests that unmineralised faults in a fault array have heavier sulfur than nearby Pb-Zn mineralised faults, such as in the Back Peak area, a Cambrian history for the unmineralised faults is also likely but not proven. Transects across and around Cambrian faults has shown that the heavy values are not present throughout, but instead occur

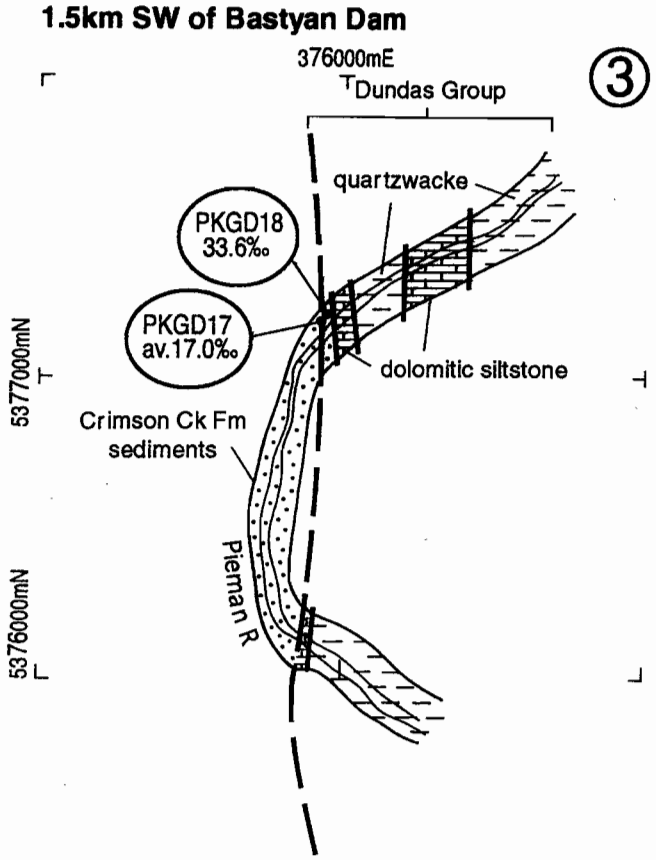
1.5km SW of Bastyan Dam
376000mE
Dundas Group
③
quartzwacke
PKGD18
33.6‰
PKGD17
av.17.0‰
dolomitic siltstone
5377000mN
Crimson Ck Fm
sediments
Pieman R
5376000mN

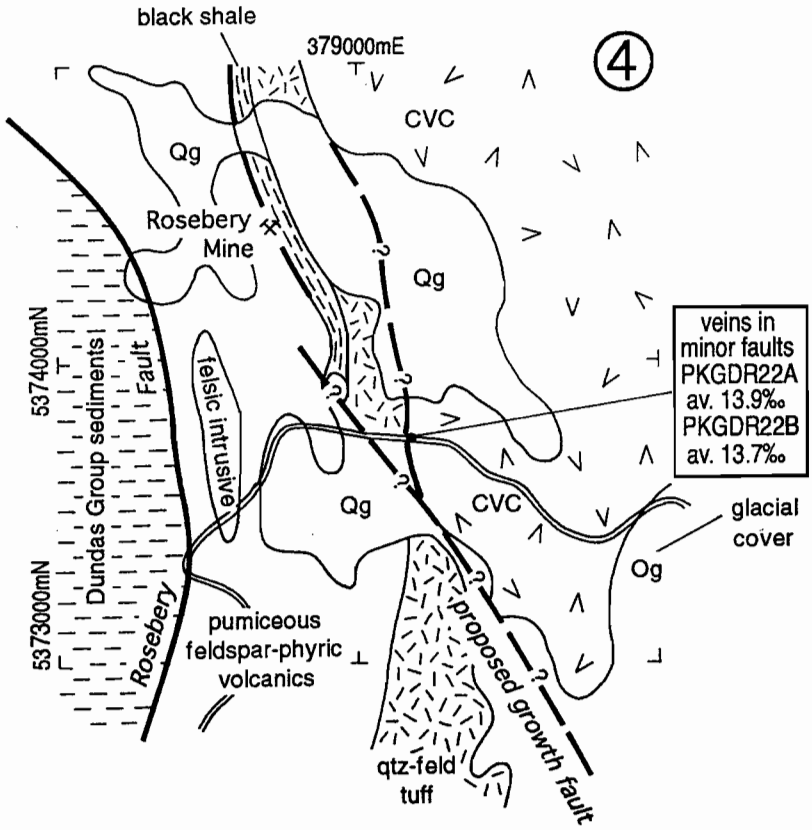
black shale
379000mE
④
CVC
Qg
Rosebery
Mine
Qg
veins in
minor faults
PKGDR22A
av. 13.9‰
PKGDR22B
av. 13.7‰
5374000mN
Dundas Group sediments
Fault
felsic intrusive
Qg
CVC
glacial
cover
Og
5373000mN
Rosebery
pumiceous
feldspar-phyric
volcanics
proposed growth fault
qtz-feld
tuff

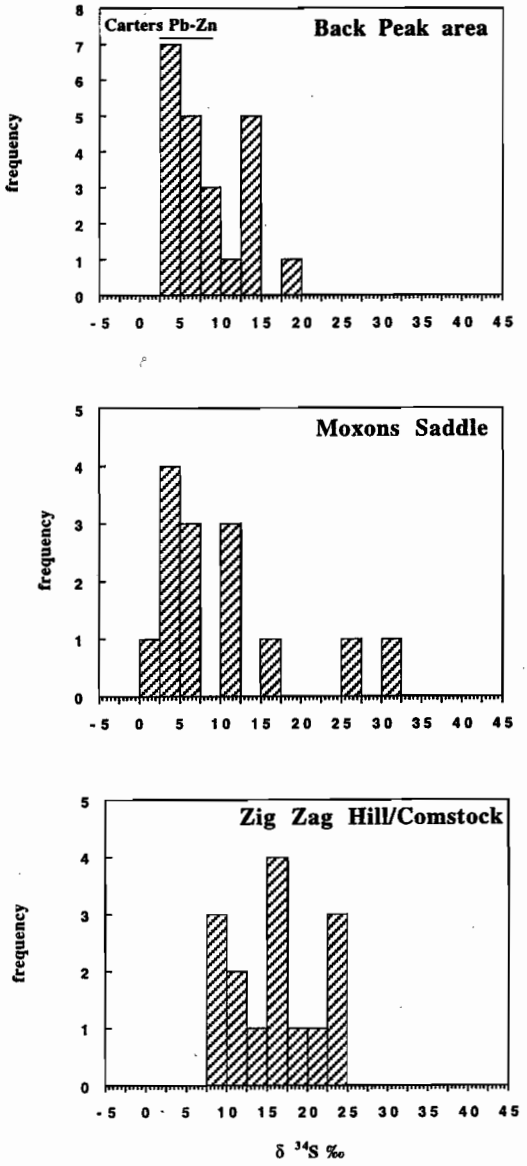

Figure 18 Frequency histograms for the Back Peak area, Moxons fault, and the Zig Zag Hill fault. Further data will be available at the March meeting.

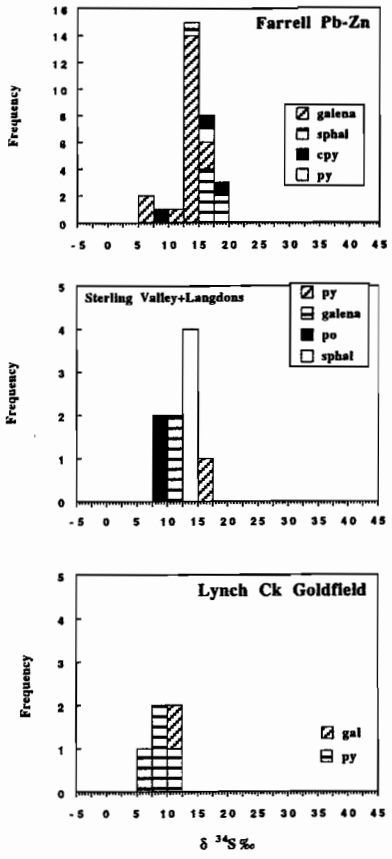

Figure 19 Frequency histograms of Devonian epigenetic mineralisation from the Mt Read Volcanics. Data from Green & Taheri (1992), Jackson (1996) and references therein, Solomon et al.(1969), Mawdesley (1996) and Solomon et al. (1988).

in pockets towards their margins. This is consistent with long histories of movement, in which different fluids have been present at different times. Even during the Cambrian, changing thermal regimes and position within the crust are likely to have altered the composition of sulfur passing with time through faults. With this in mind, the occurrence of minor pockets of rock with $\delta^{34}S > 18‰$ indicates the former presence of Cambrian fluids. Sampling to determine the fault parentage should therefore be undertaken systematically across the trace at less than 20 m intervals, analysing all possible sulfide generations as well as the wholerock composition.

Mechanisms of incorporation of sulfur into Cambrian fault traces and basins — The sulfur isotopic variation in the Cambrian volcanic package provides a hint that more variation should be expected in Cambrian faults than is currently recognised from this study.Very simplistically, faults are likely to have had discontinuous traces in the top 500 m of unconsolidated sediment and volcaniclastics, connecting at depth with better defined brittle zones, in turn connecting with shear zones in zones of deep burial. The upper fault portions helped to connect shallow oxidised aquifers and promote downflow of oxidised seawater into the crust. Consequently the

light isotopic values of oxidised aquifers should also have extended some way down recharging Cambrian faults. To date however, light values have not been found in unmineralised faults.

As the descending seawater was heated deeper in the fault, it deposited much of its sulfate and calcium as anhydrite (e.g. Shanks et al., 1981). Once heated above ~200°C, reduction of the remaining sulfate to H_2S was rapid. However, at this temperature and above, in situ rock sulfur would have been leached, resulting in a typical Cambrian VHMS-forming fluid with $\delta^{34}S$ = 5–18‰, which is likely to have circulated into deep hydrothermal aquifers. The incorporation of heavy sulfur into the fault trace must consequently have occurred above the level of rock sulfur leaching, probably at and above the zone of anhydrite deposition. Two possible mechanisms are envisaged:

1. During movement into the fault, oxidised cool seawater in the fault was juxtaposed with hotter reduced porewaters adjacent to the fault. Fault waters were drawn by pressure changes during seismic event into the fault walls, resulting in heating and rapid reduction of seawater sulfate. This provides a mechanism for depositing heavy sulfur in pockets towards the fault margins. A second mechanism to achieve this result is reduction mainly in the near-surface parts of growth faults, where it is consequently distributed over a larger area due to greater lateral permeability, and proliferation of small fault traces. In the deeper parts of growth faults below the main level of sulfate reduction, fluid circulation would have been more confined to central zones of fault movement (Fig. 20).

2. Anhydrite that was deposited by heating waters in the fault was reduced by organic matter and ferrous minerals in the adjacent volcaniclastic sediments, either immediately after deposition, or during deep burial, or even during Cambrian metamorphism. The great advantage of this mechanism is that the growth fault hangingwall is continuously moving anhydrite into the burial environment, so that rather than being dissolved by later cold fluids as is common on the modern seafloor (Alt et al., 1985), the anhydrite is available for reduction by aqueous ferrous iron in equilibrium with hot reduced fluids (Fig. 20). Footwall anhydrite, on the other hand, is removed continuously because it is uplifted and leached away in the oxidised zone on the shoulder of the listric fault.

This is a powerful mechanism to account for the sulfur enriched character of back-arc and rift basins compared to mid-ocean ridges; Alt (1994) estimates that back-arc basins contain ~twice the amount of sulfur in alteration zones as do mid-ocean ridge systems. Additionally, sulfur in the Cyprus ophiolite complex is estimated to consist of 35% seawater sulfate, compared to less than 10% for MOR systems. This is attributed here to the efficacy of growth faults in conveying seawater sulfate deeper into the crust for wholescale reduction and storage. At mid-ocean ridges there is no continuous accumulation of a thick volcanosedimentary pile, and additionally the hydrothermal alteration cells are continuously drifting away from their thermal sources, resulting in cooling and incursion of cold seawater, which leaches and removes anhydrite.

The unique character of growth faulting provides a reason to expect that the heavy sulfur signature should be present at all structural levels in the fault. It also provides a reason to expect that such isotopic evidence will only occur in isolated pockets. This is because every segment of the downthrown side of a growth fault experiences the fault-fluid history during burial, so for instance, every fault segment was initially propagated in the oxidised seawater zone, but during burial and further deposition within the basin, moves to deeper levels, in equilibrium with reduced hotter fluids. During its history in the deeper environment, younger sulfides may be leached, and new grains deposited. In addition, many growth faults experience new fault movements during inversion and later deformation, as has occurred during the Devonian Tabberaberan Orogeny, which further removes evidence of old events, and deposits new assemblages. Given this interpretation, large faults should contain very disparate sulfur signatures, unless the last event produced pervasive metasomatism.

Summary of Findings

- Cambrian faults contain pockets of heavy sulfur ($\delta^{34}S$ >18‰), similar to the range observed at the margins of Cambrian massive sulfide deposits and attributed to in situ seawater sulfate reduction.

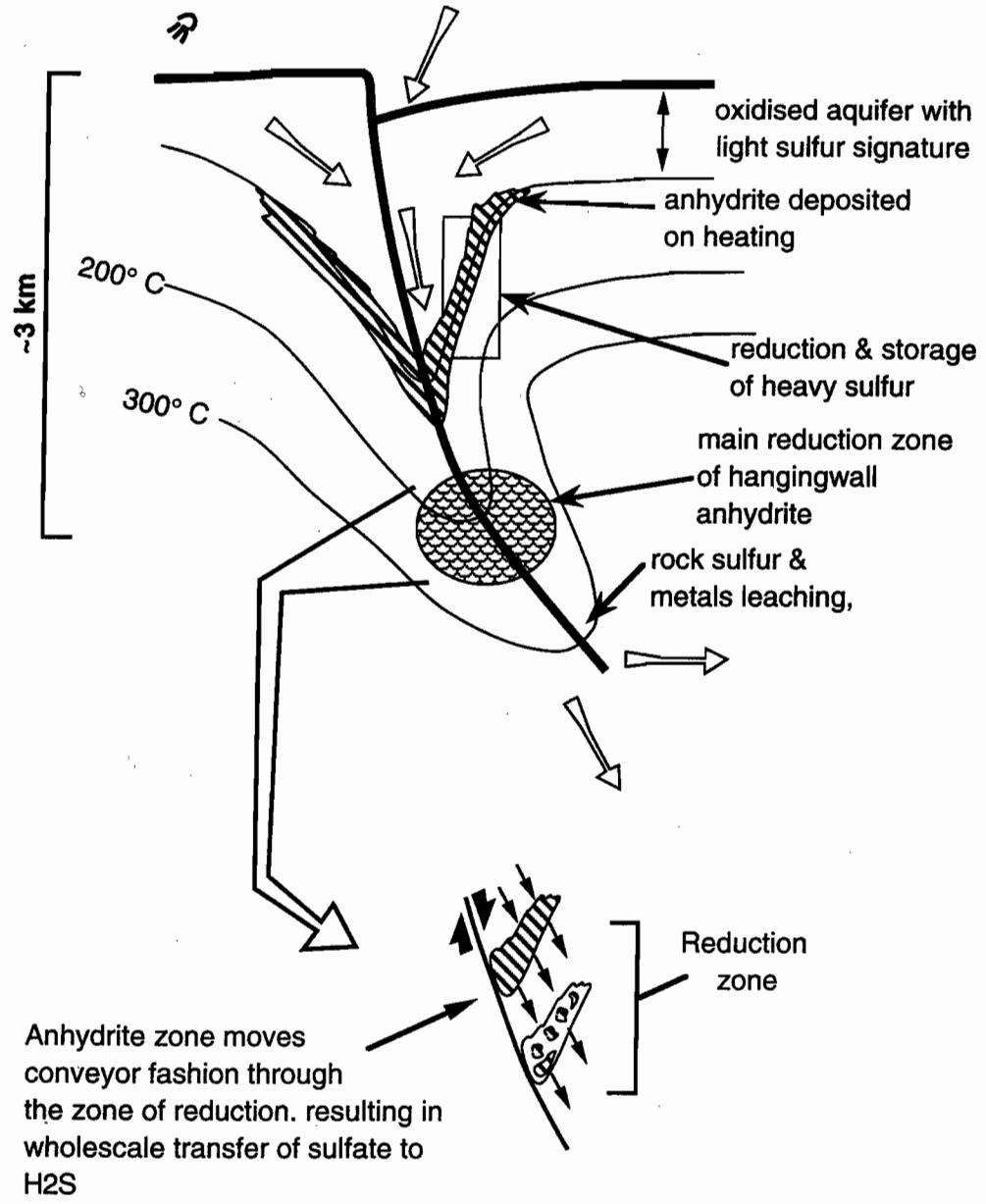

Speculative anatomy of a Cambrian growth fault, and a conveyor model for the movement of anhydrite (=seawater sulfate) into rift basin depths

Figure 20 A speculative anatomy of a large Cambrian growth fault, showing the zonation in sulfur isotope character from oxidised reservoirs, through an anhydrite deposition zone, narrowing to an aqueous sulfate+anhydrite reduction zone between 200 and 300° C. The final evolved fluid moves away into a deep hydrothermal aquifer where it incorporates further rock sulfur by leaching. The dynamic aspects of the model include (1) conveyance of upper fault portions down into the deep burial environment where they experience new fluid conditions, and (2) continuous movement of hangingwall anhydrite down hrough the zone of sulfate reduction, where it is reduced to aqueous H_2S.

The presence of even a few samples with this signature indicates a Cambrian fault history, because with burial, and subsequent deep metamorphism and orogeny, faults are subject to new fluid fluxes, which leach or modify the evidence of previous fluid movements, and deposit new sulfides.

- Growth faults may be extremely important mechanisms for delivering seawater sulfate deep into back-arc basins for reduction, and could account for why back-arc basins are sulfur-rich compared to Mid-ocean Ridge environments. The dynamic burial of the fault hangingwall as a long-lived phenomenon is the main process involved, together with the key deposition of anhydrite along a reverse solubility gradient during the descent and heating of oxidised seawater across a thermal gradient. This fluid descent should occur at a far greater rate along permeable faults than in the general volcanosedimentary basin.

- Devonian mineral deposits occur over a restricted $\delta^{34}S$ range (5–18‰) which is identical to the range of Cambrian massive sulfide deposits, but probably results from averaging of inhomogeneous Cambrian sulfur during hydrothermal circulation.

- Sampling to determine the parentage of faults using sulfur isotopes should occur by establishing a detailed transect across a fault trace, and sampling all available alteration types and any sulfide generations. Very variable isotopic results should be expected given the dynamic history of growth faults.

Acknowledgements

Rosebery mine personel and the Pasminco Exploration Company are thanked for allowing access to Rosebery mine drillcore for this project. Joe Stolz kindly provided the samples for the background sulfur isotope study. Debbie Harding is thanked for her dedicated professionalism in getting figures completed for absurd deadlines. Michael Blake is thanked for compiling the location figure for the regional samples. Christine Cook, Mike Power Snr. and Daniel van de Aa toiled to provide the wholerock sulfur isotope values, with helpful advice on methods from Dr Jeff Alt. Ron Berry provided enormous support and many thoughtful suggestions during the planning and interpretation.

References

Allen R., Duhig N. & Large R. (1996) Rosebery alteration study. CODES AMIRA Project P439— Studies of VHMS-related alteration: geochemical and mineralogical vectors to ore, May 1996. 95–117.

Alt J.C. & Chaussidon M. (1989) Ion microprobe analyses of the sulfur isotopic composition of sulfides in hydrothermally altered rocks, DSDP/ODP hole 504B. Proc. of the Ocean Drilling Program., scientific results 111: 41–45.

Alt J.C., Saltzman E.S. & Price D. (1985) Anhydrite in hydrothermally altered basalts: DSDP Hole 504B. In Anderson, R.N, Honnoroez J., Becker K. et al. (eds.), Init. Repts. DSDP, 83: Washington (US Govts. Printing Office): 283–288.

Alt J.C. (1994) A sulphur isotopic profile through the Troodos ophiolite, Cyprus: primary composition and the effects of seawater hydrothermal alteration. *Geochim. Cosmochim. Acta* 58: 1825–1840.

Alt J.C. (1995) Sulphur isotopic profile through the oceanic crust: sulphur mobility and seawater-crustal sulphur exchange during hydrothermal alteration. *Geology* 23: 585–588.

Andrews A.J. (1979) On the effect of low temperature seawater-basalt interaction on the distribution of sulphur in oceanic crust. *Earth Plan. Sci. Letts.* 46: 68–80.

Berry R.F. & Keele, R.A. (1993) Cambrian structure in western Tasmania. AMIRA Project P.291— Structure and mineralisation of Western Tasmania, Final Report: 55–68.

Bull, S.W (1995) Second Report: sedimentology of the Dundas Group and correlates with refernce to a possible syn-depositional growth fault west of Rosebery. AMIRA project P.291A Third Report March 1995: 35–44.

Claypool G.E., Holser W.T., Kaplan I.R., Sakai H. & Zak I. (1980) The age curves of sulfur and oxygen isotopes in marine sulfate and their mutual interpretation. Chem. Geol. 28: 199–260.

Davidson G.J. & Kitto P. (1995) Progress report 4: Detecting Cambrian structures in the Mount Read Volcanic Belt using sulfur isotopes— sulfur isotopes of growth faults. AMIRA Project P.291A— Structure and mineralisation of Western Tasmania, October 1995: 39–50.

Gemmell J.B. & Large R.R. (1993) Evolution of a VHMS hydrothermal sytstem, Hellyer deposit, Tasmania, Australia: sulphur isotope evidence. Resource Geology Special Issue 17: 108–119.

Green G.R.(1983) The geological setting and formation of the Rosebery volcanic-hosted massive sulphide orebody, Tasmania. Ph.D thesis, University of Tasmania (unpublished). 288 p.

Green G.R. & Taheri J. (1992) Stable isotopes and geochemistry as exploration indicators. Bull. Geol. Surv. Tasmania 70: 84–91.

Huston, D.L., Power M., Gemmell J.B. & Large R.R. (in press) Design, calibration and geological application of the first operational Australian laser ablation sulphur isotope microprobe. Aust. J. Earth Sci.

Jackson M. (1996) The genesis of auriferous quartz veins at Lynch Creek, western Tasmania. Unpubl. hons. thesis, University of Tasmania, 122 p.

Khin Zaw (1991) The effect of Devonian metamorphism and metasomatism on the mineralogy and geochemsitry of the Cambrian VMS deposits in the Rosebery-Hercules district, western Tasmania. Ph.D thesis, University of Tasmania (unpublished).

Kusakabe M., Mayeda S. & Nakamura E. (1990) S, O, and Sr isotope systematics of active vent material from the Mariana backarc basin spreading axis at 18° N. Earth Plan. Sci. Letts. 100: 275–282.

Lees T. (1987) Geology and mineralisation of the Rosebery-Hercules area, Tasmania. M.Sc thesis, University of Tasmania (unpublished). 184 p.

Mawdesley A. (1996) Structural and geochemical controls on Pb-Zn-Ag mineralisation in the Farrell field, Tasmania. Unpubl. hons. thesis, University of Tasmania, 125 p.

Robinson, B.W. & Kusabe, M. (1975) Quantitative preparation of SO_2, for $^{34}S/^{32}S$ analyses from sulfides by combustion with cuprous oxide. Anal. Chem., 47: 1179–1181.

Sakai H. & Dickson F.W. (1978) Experimental determination of the rate and equilibrium fractionation factors of sulfur isotope exchange between sulfate and sulfide in slightly acid solutions at 300° C and 1000 bars. Earth Plan. Sci. Letts. 39: 151–161.

Shanks W.C., Bischoff J.L. & Rosenbauer R.J. (1981) Seawater sulfate reduction and sulfur isotope fractionation in basaltic systems: interaction of seawater with fayalite and magnetite at 200–350° C. Geochimica et Cosmochim. 45: 1977–1995.

Solomon M., Rafter T.A. & Jensen M.L. (1969) Isotope studies on the Rosebery, Mount Farrell and Mount Lyell ores, Tasmania. Minera. Deposita 4: 172–199.

Solomon M., Eastoe C.J., Walshe J.L. & Green G.R. 1988 Mineral deposits and sulfur isotope abundances in the Mount Read Volcanics between Que River and Mt Darwin, Tasmania. Econ. Geol. 83: 1307–1328.

Stolz & Large (1992) Evaluation of the source-rock control on precious metal grades in volcanic-hosted massive sulfide deposits of western Tasmania. Econ. Geol. 87: 720–738.

Ueda A. & Sakai H (1983) Simultaneous determinations of the concentration and isotope ratio of sulphate- and sulphide-sulphur and carbonate-carbon in geological samples. Geochem. J. 17: 185–196.

Ueda A. & Sakai H. (1984) Sulfur isotope study of Quaternary volcanic rocks from the Japanese Islands arc. Geochimica et Cosmochim. 48: 1837–1848.

White M. (1995) Sedimentological evidence for Cambrian growth faults on the eastern side of the Dundas Trough, western Tasmania. AMIRA Project P.291A— Structure and mineralisation of Western Tasmania, October 1995: 23–38.

Woodhead J.D., Harmon R.S. & Fraser D.G. (1987) O, S, Sr and Pb isotope variations in volcanic rocks from the Northern Mariana Islands: implications for crustal recycling in intra-oceanic arcs. Earth Plan Sc. Letts. 83: 39–52.

Appendix 1. Background sulfur isotope variation in the Mt Read Volcanic Belt.

SAMPLE	CAT. NO.	STATUS	DESCRIPTION	anal. no.	∂34S	CO2 mmHg	S yield mmHg	sample wt. mg	S ppm	Na2O	K2O	Na2O/K2O	Location
BACKGROUND DACITES													
PRR/C	71425	Background	dacite	4374	2.6	61.6	21.3	221	300	3.73	2.52	1.48	CVC— Pieman Rd (outcrop)
PRR/E	71427	Background	dacite	4376	17.6	41.8	5.2	228	<100	2.64	4.19	0.63	CVC— Pieman Rd (outcrop)
PRR/I	71431	Background	dacite	4380	3.8	75.7	50.8	295.3	200	4.06	2.65	1.53	CVC— Pieman Rd (outcrop)
MAC10/B	71436	Background	dacite	4385	8.8	19	2	116.6	<100	6.28	1.29	4.87	Hellyer area (core)
HAT6/A	71441	Background	dacite	4389	12.2	17.6	4	118.9	<100	6.53	0.67	9.75	Hellyer area (core)
HL30/A	71444	Background	dacite	4392	24.2	94.2	88.8	135.9	8200	6.12	0.88	6.95	Hellyer area (core)
AR10	71523	Background	dacite	4406	-6	128.3	112.8	264.1	1200	4.55	2.78	1.64	Tyndall+Yolande R Sequ. (outcrop)
AR15	71526	Background	dacite	4409	2	52.9	30.9	416.6	900	1.73	4.09	0.42	Tyndall+Yolande R Sequ. (outcrop)
AR17	71527	Background	dacite	4410	5.6	78.6	48.2	514.7	600	4.93	2.8	1.76	Tyndall+Yolande R Sequ. (outcrop)
AR19	71529	Background	dacitic tuff	4412	14.3	88.4	79.4	99.6	300	3.36	3.86	0.87	Tyndall+Yolande R Sequ. (outcrop)
BACKGROUND RHYODACITES & RHYOLITES													
PRR/G	71429	Background	rhyodacite	4378	8.1	33.1	4	199	300	3.56	3.44	1.03	CVC— Pieman Rd (outcrop)
PRR/H	71430	Background	rhyodacite	4379	8.1	17.5	1.8	162.3	100	2.12	3.45	0.61	CVC— Pieman Rd (outcrop)
MC1/C	71447	Background	rhyolite	4394	4.8	85	51.4	220.1	600	5.09	2.2	2.31	Mt Charter area
AR18	71528	Background	rhyolitic epicla	4411	0	71.1	38.5	419	200	3.18	3.88	0.82	Tyndall+Yolande R Sequ. (outcrop)
BACKGROUND BASALTS													
MAC1/A	71432	Background	basalt	4381	2.4	34.2	8	54.3	700	0.93	1.04	0.89	Hellyer Basalt (core)
MAC10/A	71435	Background	basalt	4384	-14.5	50.6	38	251.5	1000	2.11	2.05	1.03	Hellyer Basalt (core)
MAC10/C	71437	Background	basalt	4386	-7.2	78.9	30.7	299.2	600	3.92	1.24	3.16	Hellyer Basalt (core)
HL55/B	71443	Background	basalt	4391	7.7	16.8	3	332.6	200	1.52	0.95	1.6	Hellyer Basalt (core)
MC1/B	71446	Background	basalt	4393	14.4	33.3	5.3	574.1	100	2.8	1.39	2.01	Mt Charter area (core)
BACKGROUND ANDESITES													
MAC5/A	71433	Background	andesite	4382	-8.1	176.8	121.6	240	3200	4.34	0.68	6.38	Hellyer Basalt (core)
MAC5/B	71434	Background	basaltic andesi	4383	-7.9	261.4	3	260.6	1500	0.98	1.95	0.5	Hellyer Basalt (core)
MAC10/D	71438	Background	andesite	4387	-2.06	178.4	128.6	217.4	6200	5.05	1.94	2.6	Hellyer Basalt (core)
HAT5/A	71440	Background	andesite	4388	-7.1	59.6	50.8	67.2	1400	4.18	0.19	22	Hellyer Basalt (core)
HL55/A	71442	Background	andesite	4390	7.35	38.1	9	306.9	1100	2.9	1.59	1.82	Hellyer Basalt (core)
MC1/D	71448	Background	andesite	4395	2.2	21.3	2.3	692.6	100	3.57	1.7	2.1	Hellyer Basalt (core)
MC2A/A	71449	Background	andesite	4396	15.2	56.6	33.8	188.4	1500	3.57	1.08	3.31	Mt Charter area (core)
AR13	71525			4408	-6.1	58.5	29.1	496.1	1000	4.22	0.3	14.07	Tyndall+Yolande R Sequ. (outcrop)
NEAR ORE SAMPLES													
QR97A	71451	Background	rhyolite	4397	-6.8	46.8	22.9	143.6	<100	3.07	2.43	1.26	Que River (core)
QR97B	71452	Background	andesite brecc	4398	-3.1	27	4.5	124.2	<100	3.36	2.02	1.66	Que River (core)
SAMPLE	CAT. NO.	STATUS	DESCRIPTION	anal. no.	∂34S	CO2 mmHg	S yield mmHg	sample wt. mg	S ppm	Na2O	K2O	Na2O/K2O	Que River (core)
QR97C	71453	Background	andesite	4399	5.1	49.6	1.7	305.2	<100	3.16	1.84	1.72	Que River (core)
QR97D	71454	Background	andesite	4400	14.6	59.8	1.7	774.6	<100	2.67	1.24	2.15	Que River (core)
QR97E	71455	Background	andesite	4401	4.2	53.4	9.2	787.8	<100	3.27	2.42	1.35	Que River (core)
QR97F	71456	altered	andesite	4402	7.8	168.5	126.1	541	30000	0.58	4.25	0.14	Que River (core)
QR97G	71457	altered	andesite	4403	6.6	58.8	44.5	385.8	23000	0.01	4.13	0.002	Que River (core)
QR97H	71458	altered	andesite	4404	8.2	56.5	44.7	168.8	28000	0.06	3.41	0.02	Que River (core)

Appendix 1. Background sulfur isotope variation in the Mt Read Volcanic Belt.

QR97	71459	altered	andesite	4405	6.2	254.7	11	302.9	?				Que River (core)		
LH1/B	71531	altered	rhyolite	4414	7.9	781.6	3.2	881.5	1800	0.46	3.64	0.13	Leech Hill		
LH1/C	71532	altered	rhyolite	4415	9.3	353.5	98.1	703.8	700	0.28	2.96	0.09	Leech Hill		
LH1/D	71533	altered	rhyolite	4416	9.2	98.4	58.4	347.4	34000	0.05	3.26	0.02	Leech Hill		
HA8/A	71534	altered	rhyolite	4417	11.3	79.7	69.7	455	29000	0.17	6.76	0.03	Howards Anomaly, Tyndall Group		
HA8/B	71535	altered	rhyolite	4418	8.7	83.2	77.2	235	38000	0.3	5.72	0.05	Howards Anomaly, Tyndall Group		
JD2001/A	71536	altered	rhyolite	4419	9.1	38.6	14.2	527.1	100	3.49	3.02	1.16	Jukes-Darwin-Lyell		
JD2001/C	71538	altered	rhyolite	4421	10.4	235.7	84.6	437.5	1200	0.63	4.16	0.15	Jukes-Darwin-Lyell		
JD2001/D	71539	altered	rhyolite	4422	13.3	297.1	116.1	466.6	1000	0.05	8.13	0.01	Jukes-Darwin-Lyell		
JD2002/B	71541	altered	rhyolite	4424	12.2	487.5	54.4	525	400	0.23	4.49	0.05	Jukes-Darwin-Lyell		
JD2002/C	71542	altered	rhyolite	4425	16.2	126.4	94.3	242.6	1100	0.05	7.22	0.01	Jukes-Darwin-Lyell		
SEDIMENT															
LD86-1/B	71544	background	argillite	4426	4	133.6	96.1	547.7	100	2.33	2.62	0.89			

Appendix 2. Rosebery footwall sulfur isotope data.

DDH/METRES	MINE SEQUENCE	SAMPLE DESCRIPTION	anal. no.	Machine ∂34S	Corrected value	Corr'd value (laser)	Sample mean ‰	Comment	hole diam µ
DDH 107R									
107R-546.6m	Black Shale	Py in 2mm veinlet	1048	2.70	0.51	6.26	7.60	Vein py edge	300
			1049	5.20	3.19	8.94		Vein py centre	300
107R-558.5m	Black Shale	Disseminated Py in epiclastic sandstone							
107R-601.1m	HW epiclastics	Disseminated Py in Qz-Fels phyric volcanoclastics							
107R-621.0m	HW epiclastics	Disseminated Py in Qz-phyric volcanoclastics							
107R-639.7m	HW epiclastics	Disseminated Py in Qz-Fels phyric volcanoclastics							
107R-651.4m	Host rock	Laminated Fels-phyric shales	1052					Too small	
			1053	11.77	10.26	16.01	16.64	1mm py vein, Cambrian	250x3
			1054	12.95	11.52	17.27		Same vein; 1cm to 1053	400x2
107R-652.5m	Host rock	Disseminated Py in Qz-Fels phyric volcanoclastics	1069	0.46	-1.91	3.84	3.84	Anhedral clot 2mmx3mm: Dev.?	400
107R-661.1m	FW volcanics (Pumiceous Breccia)	Disseminated Py in semi-massive Fels-phyric sandstone	1070	10.90	9.32	15.07	15.07	Recryst. Cambrian py; 200µ av.	300x2
107R-669.9m	FW volcanics (Pumiceous Breccia)	Disseminated Py in siliceous Fels-phyric volcanoclastic/epiclastic	1082	8.64	6.88	12.63	12.63	Recryst. Cambrian py; 70µ av.	250X7
			1083					Too small	
107R-677.3m	FW volcanics	Disseminated Py veined by late carbonate	1064	12.71	11.26	17.01	17.01	Recryst'd py; 400µ av.	300
			1065	12.70	11.25	17.00		Recryst'd py; 400µ av.	300
107R-688.3m	FW volcanics (Pumiceous Breccia)	Disseminated Py in massive pumiceous breccia	1073	7.83	6.02	11.77	12.42	Recryst'd py; 400µ av.	250x2
			1074	9.04	7.32	13.07		Recryst'd py; 100µ av.	250x5
107R-711.1m	FW volcanics (Pumiceous Breccia)	Disseminated Py in massive pumiceous breccia	1071	10.82	9.24	14.99	14.15	Recryst'd py; 400µ av.	400
			1072	9.25	7.55	13.30		Recryst'd py; 400µ av.	250
107R-722.3m	FW volcanics (Pumiceous Breccia)	Disseminated Py in massive pumiceous breccia & 5cm siderite	1066	15.65	14.43	20.18	15.41	Recryst'd py; 700µ av.	300
		alteration zones	1067	7.82	6.01	11.76		Recryst'd py; 700µ av.	250
			1068	10.18	8.54	14.29		Recryst'd py; 100µ av.	250x5
107R-728.0m	FW volcanics (Pumiceous Breccia)	Disseminated Py in massive pumiceous breccia with silicified Fels	1051	9.49	7.80	13.55	15.75	Recryst'd py; 500µ av.	300X2
		phyric texture	1050	13.58	12.20	17.95		Recryst'd py; 300µ av.	300
DDH 49R									
49R-800.0'	HW epiclastics	Disseminated Py in turbiditic mass flows?	1540	4.68	5.45	11.20	11.20	Large std. dev. One piece of anhedral py	
49R-815.0'	Black Shale	Black shales with Py-nodules	1552	12.32	14.65	20.40	20.40	Large std. dev.-UNCERTAIN SAMPLE NO.	
49R-840.0'	Black Shale	Black shales with abundant Carb-Py veining	1524	18.15	20.23	25.98	25.98	3 mm long py veinlet	
49R-898.0'	Black Shale	Black shales with abundant Carb-Py veining	1544	10.96	13.02	18.77	8.97	2-4 mm wide massive py & qutz	
			1545	-5.11	-6.33	-0.58		as again, 0.5 cm along	
			1546	2.62	2.98	8.73		as again, midway between the others	
49R-925.0'	Black Shale	Py-black shales	1505	3.71	4.06	9.81	10.41	Py in black shale concretion	
			1506	5.24	5.26	11.01		concretion margin	
49R-935.0'	Host rock (split)	Thin epiclastic layers interbedded with Py-black shales	1500	-14.24	-17.84	-12.09	-4.86	high std. dev.	
			1502	-2.39	-3.39	2.36		high std. dev.	
49R-954.0'	FW volcanics (Pumiceous Breccia)	Disseminated Py in pumiceous breccia	1503	-6.85	-8.83	-3.08	-2.50	subhed. py extending from straight vein	
	(pyrite adjacent to straight vein)		1504	-7.10	-9.13	-3.38		anhedral: Dev.?	
			1529	-6.10	-7.89	-2.14		py vein	
			1530	-5.45	-7.14	-1.39		py euhedra: 7 grains in all	
49R-956.0'	FW volcanics (Pumiceous Breccia)	Disseminated Py in pumiceous breccia							
49R-984.0'	FW volcanics (Pumiceous Breccia)	Disseminated Py in pumiceous volcanoclastic	1553	1.67	1.83	7.58	6.02	high std. dev. Fine anhedral py/po in vein	
			1554	-0.92	-1.29	4.46		high std. dev. A.a.	
XRAL CHECK			XRAL			20.18			
XRAL CHECK			XRAL			21.04			
XRAL CHECK			XRAL			21.42			
XRAL CHECK			XRAL			21.04			
49R-998.0'	FW volcanics (Pumiceous Breccia)	Disseminated Py-Po in pumiceous breccia	1483	29.42	35.42	41.17	46.19	po?	
			1486	35.92	43.35	49.10		300µ blebs of po?	
			1487	34.28	41.35	47.10		200µ blebs of po?	
			1499	34.51	41.63	47.38		200µ blebs of po?	

Appendix 2. Rosebery footwall sulfur isotope data.

DDH/METRES	MINE SEQUENCE	SAMPLE DESCRIPTION	anal. no.	Machine ∂34S	Corrected	Corr'd value	Sample	Comment	hole diam μ
DDH 57R									
57R-2250.0'	Black Shale	Black shales with thin laminated turbidite layers containing	1513	-8.10	-10.22	-4.47	-4.47	Large Std. dev. Massive region+carb.Dev?	
		**wholerock determination	3955			4.27			
XRAL CHECK			XRAL			-0.58			
XRAL CHECK			XRAL			0.26			
XRAL CHECK			XRAL			-0.01			
XRAL CHECK			XRAL			-1.60			
57R-2273.0'	Black Shale	Black shales with disseminated Py cubes	1479	6.98	8.05	13.80	13.60	Coarse 2–3 mm py; dissem cpy also	
			1480	6.64	7.63	13.38		a.a.	
57R-2290.0'	Black Shale	Disseminated Py in laminated epiclastics	1551	-5.36	-6.64	-0.89	-3.68	Schistose py	
			1569	-9.97	-12.18	-6.48		anhedral py within chlorite alteration	
57R-2301.0'	Mineralised Black Shales	Graphitic?-Py black shales cut by 15cm wide Qz-Rhod vein	1471	7.05	8.13	13.88	13.94	meta-vein of py	
			1473	7.14	8.24	13.99		meta-vein of py, 1 cm from last	
57R-2325.0'	Host Rock	Disseminated Py±Sph±Qz in fine grained epiclastic	1541	-7.43	-9.12	-3.37	0.64	X-cutting late? vein with ab. fine py	
			1542	3.93	4.55	10.30		X-cutting late? vein with ab. fine py	
			1543	-8.79	-10.77	-5.02		Large Std. dev. A.a	
57R-2362.0'	FW Volcanics?	Siliceous epiclastic with Py-Sph-Chl veinlets							
57R-2437.0'	FW Epiclastics	Disseminated Py in Qz-Fels phyric sequence							
57R-2437.0'	FW Epiclastics	Disseminated Py in Qz-Fels phyric sequence							
N.B. THE EARLY SAMPLES FROM THIS HOLE MAY BE FROM A DEFLECTION									
57R-2391.0'	Ore Zone	Disseminated Py-Sph-Gal in chloritised host							
57R-2424.0'	FW Volcanics	Disseminated Py in fels-phyric chloritised volcanics							
57R-2460.0'	FW Volcanics	Disseminated Py in epiclastics							
57R-2495.0'	FW Volcanics	Disseminated Py(±Po) in volcanoclastics							
57R-2535.0'	FW Volcanics	Disseminated Py-Sph in volcanoclastics							
57R-2546.0'	FW Volcanics	Disseminated Py-Sph in volcanoclastics							
DDH 109R									
109R-510.0m	Black Shale	Disseminated Py in turbiditic-conglomeric mass flow with black	1547	-2.01	-2.60	3.15	3.16	800μ patch of anhedral py	
		shale clasts	1548	-1.99	-2.57	3.18			
109R-530.0m	Black Shale	Disseminated Py in calcite veined black shale	1565	8.98	10.64	16.39	23.75	schistose py 2mm across in black shale	
				15.86	18.92	24.67		high std. dev. Background fine py	
				20.45	24.45	30.20		high std. dev. 3 gns in a thin veinlet	
109R-550.0m	Black Shale	Disseminated Py in laminated Black shale with minor calcite veinlet	1537	12.07	14.35	20.10	13.80	coarse strained pyrite	
			1538	-3.75	-4.69	1.06		fine background pyrite: 8 blasts	
			1539	12.19	14.50	20.25		coarse strained pyrite	
109R-559.5m	Host Rock	Disseminated Py in a pumiceous Fels-phyric epiclastic with	1562	0.47	0.38	6.13	5.24	A single 200μ py in a clump of gns.	
		chloritic-calcite veins	1563	-2.35	-3.01	2.74		high std. dev.	
			1564	1.05	1.09	6.84		a.a.	
XRAL CHECK	XRAL CHECK		XRAL			6.69			
XRAL CHECK	XRAL CHECK		XRAL			7.29			
XRAL CHECK	XRAL CHECK		XRAL			7.89			
XRAL CHECK	XRAL CHECK		XRAL			8.78			
109R-569.6m	Transition Zone	Disseminatd Py in pumiceous mass flow	1514	34.17	38.81	44.56	45.09	a 2-3mm cluster of fine py-cpy	
			1515	35.08	39.87	45.62			
		**wholerock determination-h.m.sep	4369				40.50		
109R-580.0m	Transition Zone	Disseminatd Py in pumiceous mass flow with chloritic veinlets	1517	2.81	2.44	8.19	8.19	high std. dev. anhedral py in thin vein	
109R-591.2m	FW Volcanics	Disseminatd Py in pumiceous mass flow with prolific Qz-Chl	1531	24.28	27.34	33.09	34.90	internally intricate py-po: Dev?	
		crack-seal veins	1532	27.40	30.96	36.71		internally intricate py-po: Dev?	
XRAL CHECK			XRAL			33.24			
XRAL CHECK			XRAL			34.29			
XRAL CHECK			XRAL			34.45			

Appendix 2. Rosebery footwall sulfur isotope data.

DDH/METRES	MINE SEQUENCE	SAMPLE DESCRIPTION	anal. no.	Machine ∂34S	Corrected	Corr'd value	Sample	Comment	hole diam µ
XRAL CHECK			XRAL			34.57			
		**wholerock determination	3961			30.18			
109R-599.2m	FW Volcanics	Disseminatd Py in pumiceous mass flow with both chloritic veinlets and Qz-Carb veins							
109R-611.3m	FW Volcanics	Fels-phyric mass flow with minor Py in a chloritic interval	1519	4.31	4.18	9.93	12.06	high std. dev. Massive py in 1mm x 2mm zone	
			1520	0.57	-0.16	5.59		high std. dev.	
			1521	5.69	5.78	11.53		euhedral 200µ pyrite	
			1523	14.01	15.43	21.18		anhedral pyrite	
109R-620.5m	FW Volcanics	Fels-phyric mass flow with Py disseminated along fractures	1507	10.86	11.77	17.52	20.17	Large anhedral clot	
			1509	15.41	17.06	22.81		Other end of same	
		**wholerock determination-h.m.separate	4370			30.20			
		**wholerock determination	3959			18.65			
XRAL CHECK			XRAL			16.62			
XRAL CHECK			XRAL			16.76			
XRAL CHECK			XRAL			16.92			
109R-629.4m	FW Volcanics	Fels-phyric mass flow with minor disseminated Py	1477	15.18	18.05	23.80	24.58	euhedral py x 2, 0.4 cm apart	
			1478	16.45	19.60	25.35		euhedral py x 3, 0.5 cm apart	
109R-642.0m	FW Volcanics	Fels-phyric mass flow with Py disseminated along fractures							
109R-649.6m	FW Volcanics	Disseminated Py in Fels-phyric mass flow with Chl-Qz veining	1474	0.69	0.37	6.12	6.12	2 mm long collection of subhedra: Dev?	
		**wholerock determination	4371				9.20		
XRAL CHECK			XRAL			14.27			
XRAL CHECK			XRAL			14.12			
XRAL CHECK			XRAL			15.93			
XRAL CHECK			XRAL			16.03			
109R-671.5m	FW Volcanics	Disseminated Py in Fels-phyric mass flow with chloritic alteration	1516	0.93	0.26	6.01	6.01	high standard dev. Late? X-cutting py	
109R-738.7m	FW Volcanics	Chloritic-Kfels alteration of Qz-Kfels phyric mass flow similar to Anthony Rd.							
109R-790.1m	FW Volcanics	Disseminated Py in siliceous Fels-phyric mass flow	1533	0.33	-0.43	5.32	5.17	Veins and strings of py as euhedra	
			1534	0.08	-0.72	5.03		Veins and strings of py as euhedra	
109R-839.5m	FW Volcanics	Disseminated Py in Fels-phyric mass flow	1535	3.80	3.58	9.33	9.93	Recryst'd py in high strain zone	
				4.82	4.77	10.52		Recryst'd py in high strain zone	
109R-841.4m	FW Volcanics	Tour-Qz veining and brecciation together with Py veinlets (Dev.)	1527	-7.24	-9.22	-3.47	-2.96	Vein 2 mm wide	
			1528	-6.35	-8.19	-2.44			
109R-871.5m	FW Volcanics	Fels-phyric mass flow with disseminated Py	1475	9.48	11.09	16.84	15.57	Large Cambrian py xtal	
			1476	7.39	8.54	14.29		Same grain, other end	
109R-892.0m	FW Volcanics-5m from Rosebery Fault	Pumiceous Fels-phyric mass flow with carbonate overprint	1555	16.42	19.59	25.34	25.34	high standard dev. 7 subhedral grains	
XRAL CHECK			XRAL			9.19	9.19		
XRAL CHECK			XRAL			9.22	9.22		
XRAL CHECK			XRAL			9.41	9.41		
	**wholerock determination		4372			13.60	13.60		
109R-895.0m	Rosebery Fault	Siliceous brecciation zone with Carb(±Tour) overprint	1549	7.87	9.29	15.04	13.18	strongly fractured, py on cracks	
			1550	4.77	5.56	11.31			
DDH 60R									
60R-2827.0'	Black Shale	Disseminated Py in laminated black shale with carbonate veinlets	1035	1.16	-1.15	4.60	5.64	Vein in black shale: 3 large grns.	300X3
		parallel to schistocity	1036	3.10	0.93	6.68		8 disseminated grns, 50–100µ	300X8
60R-2850.0'	Black Shale	Disseminated Py in laminated black shale with carbonate veinlets	1032					Too small	
		parallel to schistocity	1033	13.97	12.62	18.37	18.80	Recryst'd & dissem'd;large grains	300X3
			1034	14.77	13.48	19.23		Recryst'd & dissem'd;large grains	300x4
60R-2890.0'	Black Shale	Disseminated Py at the contact between black shales and minor	013, 15, 17					Too small	

Appendix 2. Rosebery footwall sulfur isotope data.

DDH/METRES	MINE SEQUENCE	SAMPLE DESCRIPTION	anal. no.	Machine ∂34S	Corrected	Corr'd value	Sample	Comment	hole diam µ
DDH/METRES	MINE SEQUENCE	SAMPLE DESCRIPTION	anal. no.	Machine ∂34S	Corrected	Corr'd value	Sample	Comment	hole diam µ
		mass flow unit	1014	2.45	0.23	5.98	5.05	Vein pyrite in black shale	400
			1016	5.02	3.00	8.75	8.75	Recrystallised euhedra; 100µ av.	300
			1018	5.07	3.05	8.80		Recrystallised euhedra; 500µ av.	300X5
			1019	0.71	-1.63	4.12		Vein py, 2 grains	300X2
60R-3001.0'	Porphyry????	Disseminated Py in Fels-phyric(Porphyry?) unit with Qz-Carb	1024	-7.18	-10.12	-4.37	-4.01	Recryst'd;100µ av.	6x250
			1025-1027					Too small	
			1028	-6.52	-9.41	-3.66		Big euhedra in deformed vein	250X2
60R-3095.0'	Ore Zone	Massive Py-Sph Gal	1031	5.85	3.89	9.64	9.64	Massive pyrite; analysed one gn	400
60R-3106.0'	Ore Zone	Py-Sph vein	1039	7.02	5.15	10.90	10.90	Abundant pyrite, recrystallised	300x3
60R-3154.5'	FW Volcanics	Disseminated sulphides and stringer veins	1058	12.60	11.14	16.89	17.25	Recrystallised;150µ	300x3
			1059	13.12	11.71	17.46		Recrystallised;150µ	300x3
60R-3197.0'	FW Volcanics	Disseminated Py and Qz-Carb veining	1010	5.24	3.23	8.98	10.56	Recrystallised, single gn; 300µ	400
			1009					Too small	
			1011	8.06	6.26	12.01		Recrystallised, single gn; 300µ	300
			1012	6.84	4.95	10.70		Recrystallised, single gn; 200µ	300x2
60R-3213.0'	FW Volcanics	Disseminated Py in chloritic volcanoclastic	1029	3.57	1.44	7.19	7.25	Recrystallised, single gn; 500µ	300
			1030	3.66	1.54	7.29		Recryst'd; 800µ; 1cm from 1029	300
60R-3253.0'	FW Volcanics	Disseminated Py in chloritic volcanoclastic	1022	8.92	7.19	12.94	12.29	Recrystallised, single gn; 1000µ	300
			1023	7.72	5.90	11.65		Recrystallised, two gn;400µ	300X2
60R-3290.0'	FW Volcanics	Disseminated Py in chloritic volcanoclastic	1007	9.71	8.04	13.79	14.09	Recrystallised, single gn;200µ	150
			1008	10.27	8.64	14.39		Recrystallised, single gn;200µ	350
60R-3325.0'	FW Volcanics	Disseminated Py in sericitised Qz matrix	1020	6.64	4.74	10.49	9.56	Recrystallised, two gn;400µ	250X2
			1021	4.91	2.88	8.63		Recrystallised, single gn;400µ	300
60R-3346.0'	FW Volcanics	Disseminated Py in siliceous volcanoclastic							
60R-3368.0'	FW Volcanics	Disseminated Py in siliceous volcanoclastic	1037	5.46	3.48	9.23	10.06	Recrystallised, 5 gns;150µ	300x3
			1038	7.02	5.15	10.90		Recrystallised, 3 gns;150µ	300X5
60R-3385.0'	FW Volcanics	Disseminated Py in volcanoclastic	1046	8.56	6.80	12.55	12.28	Recrystallised;150µ	300X2
			1047	8.06	6.26	12.01		Recrystallised;200µ	300X2
DDH 71R									
71R-1648.0'	Black Shale	Disseminated Py in carbonate veinlets	1003	12.79	11.35	17.10	16.21	Primary 4mm grain	300
			1004	11.13	9.57	15.32		Primary 0.5mm grain	320
71R-1707.0'	Black Shale	Laminated Black shale with Py veinlets. Po disseminated through-	995	11.71	10.19	15.94	14.15	Gape-fill: single crystal	300
		out core but not in this piece	996	7.01	5.13	10.88		500 µ from 995; same crystal	300
			997	11.28	9.73	15.48		thin short vein; 0.5cm from 995	300
			998	9.03	7.31	13.06		thin short vein; 1 cm from 995	200
			999	11.20	9.64	15.39		same vein as 998; 300µ away	200
71R-2096.5'	HW epiclastics	Disseminated Py in Qz-Fels phyric pumiceous breccia							
71R-2107.0'	HW epiclastics	Disseminated Py in Qz-phyric pumiceous breccia	1005	-2.07	-4.62	1.13	1.13	2mm grain	200
			1006					Sample too small	
71R-2133.0'	Host Rock	Disseminated Py in cherty siltstone	1042	0.19	-2.19	3.56	3.35	Filagree pyrite....Devonian?	250x3
			1043	-0.37	-2.79	2.96		Filagree pyrite....Devonian?	250x2
71R-2174.0'	Host Sequence	Disseminated Py in Fels-phyric pumiceous breccia	1075	4.93	2.90	8.65	10.74	recrystallised py;250µ av.	250X2
			1076					Sample too small	
			1079					Sample too small	
			1080	8.24	6.45	12.20		recrystallised py;250µ av.	200X4
			1081	6.59	4.68	10.43		recrystallised py;250µ av.	200X4
71R-2210.0'	FW Volcanics	Disseminated Py in chloritic Fels-phyric pumiceous breccia	1040-1041					Sample too small	
71R-2210			1481	5.04	5.68	11.43	12.30	450µ euhedral py	
			1482	6.47	7.42	13.17		450µ euhedral py	
71R-2245.0'	FW Volcanics	Disseminated Py nodules in chloritic Fels-phyric pseudo	1056	8.72	6.97	12.72	12.72	recrystallised py xtal; 50µ av.	250x8
		pumiceous breccia							

Appendix 2. Rosebery footwall sulfur isotope data.

DDH/METRES	MINE SEQUENCE	SAMPLE DESCRIPTION	anal. no.	Machine ∂34S	Corrected	Corr'd value	Sample	Comment	hole diam μ
DDH/METRES	MINE SEQUENCE	SAMPLE DESCRIPTION	anal. no.	Machine ∂34S	Corrected	Corr'd value	Sample	Comment	hole diam μ
71R-2286.0'	FW Volcanics	Disseminated Py in pumiceous breccia	1044	6.34	4.42	10.17	10.60	recrystallised py xtal; 2–300μ	250x2
			1045	7.15	5.28	11.03		recrystallised py xtal; 2–300μ	200x5
71R-2325.0'	FW Volcanics	Disseminated Py nodules in chloritic Fels-phyric pseudo	1057	12.67	11.22	16.97	16.97	recrystallised py xtal; 50μ av.	250x8
		pumiceous breccia with Qz-Chl crack-seal veins in core of zone							
71R-2351.0'	FW Volcanics	Disseminated Py in Kfels-Chl altered fels-phyric pseudo	1000-1002					Sample too small	
71R-2351			1526	-0.40	-1.29	4.46	4.03	anhedral pyrite	
			1526	-1.14	-2.14	3.61		euhedral pyrite	

Appendix 3. Cambrian fault sulfur isotope analyses and sample details. Locations on accompanying figures.

Sample	Method	Type	anal. no.	del 34S	HOST
MOXONS SADDLE FAULT					
mox1	wholerock	outcrop	4045	26.09	CVC
mox2	wholerock	outcrop	4048	31.96	CVC
mox3	XRAL	outcrop	XRAL	12.13	CVC
	XRAL	outcrop	XRAL	12.49	CVC
	wholerock	outcrop	4090	12.26	CVC
mox4	wholerock	outcrop	XRAL	7.02	CVC
	wholerock	outcrop	4093	2.69	CVC
mox5	XRAL	outcrop	XRAL	16.79	CVC
mox6	XRAL	outcrop	XRAL	no sulfur	CVC
mox13		outcrop			CVC-foliated pumiceous lava/mass fl
mox14		outcrop			CVC-flow-banded felsic lava.low alt
mox15		outcrop			CVC-flow-banded felsic lava-feld alt
mox16		outcrop			CVC-feld-chl-alt'd schist
mox17		outcrop			CVC-feld-chl-alt'd schist
mox18		outcrop			CVC-feld-chl-alt'd schist. Cu-st'g
mox19		outcrop			CVC-feld-alt'd schist
mox20		outcrop			CVC- feld-alt'd pumiceous breccia
mox21		outcrop			CVC-chl-alt'd banded metavolcanic
mox22		outcrop			CVC-sheared pumiceous? bx
mox23		outcrop			CVC-sheared pumiceous? bx-pyritic
mox24		outcrop			CVC-even grained foliated f-phyr int
mox25		outcrop			CVC-flow banded rhyodacite
mox26		outcrop			CVC-chl-feld alt'd sheared metavolc.
HENTY FAULT ZONE PROSPECTS					
mox9	py-Conv.	outcrop	4109	4.28	CVC
	cpy-conv.	outcrop	4110	3.78	CVC
mox10	py-Conv.	outcrop	4111	3.75	CVC
mox11	cpy-conv.	outcrop	4112	5.32	CVC
mox12	cpy-conv.	outcrop	4113	6.21	CVC
BACK PEAK AREA					
PKGD1a	galena-conv.	outcrop	3795	4.32	Back Peak Beds
	galena-conv.	outcrop	3797	6.46	Back Peak Beds
PKGD1	py-laser	outcrop		6.78	Back Peak Beds
	py-laser	outcrop		5.02	Back Peak Beds
PKGD2	wholerock	outcrop	3956	2.66	Back Peak Beds
	wholerock	outcrop	4480	6.33	Back Peak Beds
	py-laser	outcrop		5.71	Back Peak Beds
	py-laser	outcrop		4.26	Back Peak Beds
XRAL check	XRAL	outcrop	XRAL	3.38	Back Peak Beds
XRAL check	XRAL	outcrop	XRAL	4.85	Back Peak Beds
XRAL check	XRAL	outcrop	XRAL	4.25	Back Peak Beds
XRAL check	XRAL	outcrop	XRAL	3.82	Back Peak Beds
PKGD6	wholerock	outcrop	4106	18.04	Back Peak Beds
PKGD30	wholerock	outcrop	4482	12.52	Back Peak Beds–cs. xtal-rich s/s
PKGD31	wholerock	outcrop	4483	8.67	Back Peak Beds–f.g'd sil'd sltst
PKGD32	wholerock	outcrop	4484		Back Peak Beds-c.g'd p'ly st'd s/s
PKGD33	wholerock	outcrop	4485	7.52	Back Peak B'ds-py'tic sil'd volc cong
PKGD34	wholerock	outcrop	4486	11.38	Porphyry-pink felds-alt'd
PKGD35	wholerock	outcrop	4487	7.56	Porphyry-pink felds-alt'd
PKGD36	wholerock	outcrop	4488	13.17	Sticht Range Beds correlate
PKGD37	wholerock	outcrop	4489		silicic dyke in Back Pk B'ds
PKGD38	wholerock	outcrop	4490	14.01	silicic dyke in Back Pk B'ds+gal vns
PKGD39	wholerock	outcrop	4491	14.2	silicic dyke in Back Pk B'ds +gal vns
PKGD40	wholerock	outcrop	4492	12.58	Q-f-porphyry-bckgr'd
PKGD41	wholerock	outcrop	4493		backg'd- Back Pk Bds; Sil'dslts
PKGD42	wholerock	outcrop	4494		backg'd- Back Pk Bds; Sil'dslts
ZIG ZAG HILL FAULT/COMSTOCK PROSPECT AREA					
PKGD7	wholerock	outcrop	4108	16.89	Comstock Tuff

Appendix 3. Cambrian fault sulfur isotope analyses and sample details. Locations on accompanying figures.

Sample	Method	Type	anal. no.	del 34S	HOST
PKGD10	wholerock	outcrop	3957	8.6	Comstock Tuff
	XRAL	outcrop	XRAL	9.42	Comstock Tuff
	wholerock	outcrop	4481	8.62	
PKGD10a	py-laser	outcrop		24.7	Comstock Tuff
	py-laser	outcrop		18.05	Comstock Tuff
	py-laser	outcrop		23.45	Comstock Tuff
PKGD10b	py-laser	outcrop		20.87	Comstock Tuff
PKGD11	py-laser	outcrop		23.93	Comstock Tuff
PKGD43	wholerock	outcrop	4496	10.18	Comstock Tuff
PKGD44	wholerock	outcrop	4497	17.14	Comstock Tuff
PKGD45	wholerock	outcrop	4498	13.21	Comstock Tuff
PKGD46	wholerock	outcrop	4499	15.98	Comstock Tuff
PKGD47	wholerock	outcrop	4500	11.11	Comstock Tuff
PKGD48	wholerock	outcrop	4501		Comstock Tuff
PKGD49	wholerock	outcrop	4502	17.07	siltst in Comstk Tuff
PKGD50	wholerock	outcrop			conglom in " "
PKGD51	wholerock	outcrop			Comstock Tuff
PKGD52	wholerock	outcrop			Comstock Tuff
PKGD53	wholerock	outcrop			Pyritic andesite
PKGD54	wholerock	outcrop			Pyritic andesite
PKGD55	wholerock	outcrop			Pyritic andesite
WEST HENTY/ FAULT— NOT DEFINITELY CAMBRIAN					
PKGD13	py-conv	outcrop	3808	-3.18	CVC
	py-laser	outcrop		-2.6	CVC
	py-laser	outcrop		-3.26	CVC
PKGD14	py-conv	outcrop	3807	2.18	CVC
PKGD14	py-laser	outcrop		-0.06	CVC
PKGD14	py-laser	outcrop		1.1	CVC
PKGD15A	py-conv	outcrop	3798	-2.46	CVC
	py-laser	outcrop		-4.14	CVC
	py-laser	outcrop		-1.32	CVC
PKGD15B	py-laser	outcrop		-3.91	CVC
PKGD15B	py-laser	outcrop		-2.61	CVC
PKGD15C	py-conv	outcrop	3799	-4.78	CVC
	py-laser	outcrop		3.15	CVC
	py-laser	outcrop		2.86	CVC
PIEMAN RIVER— BASIN EDGE FAULT					
PKGD17	py-laser	outcrop	4132	17	Crimson Creek Fm
PKGD18	py-laser	outcrop		33.59	Crimson Creek Fm
"DALMENY ST"—SMALL DEVONIAN FAULT 200M EAST OF ROSEBERY DEPOSIT					
PKGD22a	py-conv	outcrop	3809	12.33	CVC
	py-laser	outcrop		14.42	CVC
	py-laser	outcrop		13.52	CVC
PKGD22b	py-conv	outcrop	3810	16.21	CVC
	py-laser	outcrop		11.87	CVC
	py-laser	outcrop		15.61	CVC

Trace element investigation of pyrite: a possible discriminator for Cambrian and Devonian fault structures

Paul A. Kitto
CODES Special Research Centre, Geology Department, University of Tasmania

Summary

A major aim of AMIRA P.291A - Structural Controls on Mineralisation in Western Tasmania, was to geochemically characterise and identify potential Cambrian transfer faults. Until now, no one single geochemical technique (e.g. $\delta^{18}O_{qz}$, $\delta^{13}C/\delta^{18}O_{carb}$, $\delta^{34}S$, $^{204/206}Pb$, fluid inclusions, FeS/Cd/Mn ratio sphalerite), be it expensive or inexpensive, exists to discriminate between Cambrian and Devonian faults and related mineralisation in western Tasmania.

Previously described geochemical techniques have been dependent on a specific mineral assemblage that may or may not be present at each location. Pyrite, abundant or in minute concentrations, is ubiquitous in western Tasmania. As such, its trace element concentrations could prove diagnostic in differentiating the nature of hydrothermal fluid flow within a fault zone and therefore the likely Cambrian and/or Devonian origin and/or reactivation of the fault.

Kitto (1995) reported that a new multi-trace element ratio Pyrite Discriminator Index (PDI), base on electron microprobe analyses of pyrite (Co, Ni, Cu, Zn, Pb, As, Se, Ag, Au), provided for the first time a low cost method to differentiate between Cambrian VHMS mineralisation and Devonian granite related hydrothermal mineralisation. The PDI was based on the ratio of trace elements most common to Cambrian pyrite mineralisation (i.e. Co, Zn, As, Se, and Pb) compared to those elements more commonly associated with Devonian granite related pyrite mineralisation (i.e. Ni, Cu, Ag, and Au). The proposed PDI equation was:

Based on the available pyrite trace element data, a PDI value greater than 50 was indicative of a Cambrian VHMS style of mineralisation, and a PDI value less than 50 was indicative of a Devonian granite related style of mineralisation.

Since the last report an effort has been made to:

- lower the microprobe analysis count times from 70 minutes to 10 minutes and still maintain the resolution of differentiation between Cambrian and Devonian systems.
- expand the pyrite data base to additional deposit styles (e.g. Henty Au-style and Devonian base metal deposits).
- explore additional micro-beam techniques capable of performing similar trace element analyses.

The breakdown of the Cameca SX-50 microprobe for a number of months since the last AMIRA meeting has limited data collection for this project.

The necessary microprobe count times required to obtain sufficient trace element detection limits have been a major concern to date. Obviously low detection limits are critical to the success of this technique but a trade off between limited data acquisition at over 1 hour per analysis must be considered. The solution being trialled is to lower the count times and raise the detection limits on most elements to approximately 50 ppm on those elements that are typically at or above this level in pyrite. This has decreased the count time to 10 minutes and allowed a five- to six-fold increase in data acquisition. As a result the technique now allows a much lower cost microbeam technique for pyrite trace element analysis than was previously possible.

An attempt is being made to expand the pyrite trace element data base to more deposit types present in western Tasmania. Previously data was presented on Cambrian Cu-rich (Mt Lyell) and Pb/Zn-rich

(Rosebery and Hellyer) deposits together with Devonian Sn-rich (Renison) systems. Further to these results we have added the Cambrian Au-only (Henty style) deposit and the Devonian base metal deposits (Zeehan mineral field). An attempt at the Ordovician MVT-style (Oceana) deposit has also been undertaken. In the future, background sedimentary pyrite trace element analyses will be established to compliment the existing data sets.

Discussions with RSES have been on going to establish quantitative laser ICPMS analyses of trace elements in pyrite. At the present time such analyses are still in the developmental phase and costs are prohibitive at >$100 for the suite of elements under consideration. However, laser ICPMS facilities are also currently being established at the Central Science Laboratory at the University of Tasmania and should be able to provide a much larger suite of elements at substantially lower cost. The advantage of the Laser ICPMS technique is in the fact that analyses can be obtained in under 3 minutes, with greater detection limits than the microprobe technique, and for a much larger suite of trace elements than are currently possible. This laser ICPMS technique will eventually replace the microprobe system for analysing trace elements in sulphides but not in time for the completion of this AMIRA project.

The final results from this investigation will be presented as a supplementary report at the final AMIRA meeting so as to allow the generation of a maximum quantity of data prior to this date.

Geophysical data as a control on geological sections

Ron Berry and Michael Roach
CODES Special Resarch Centre, Geology Department, University of Tasmania

Abstract

Four structural sections across the Mt Read Volcanics were tested by 2D modelling of the gravity and magnetic fields. The structural models are broadly consistent with the geophysical data within the constraints of the publicly available physical properties database. The geophysical data requires addition of Cambrian and Devonian granites for which there is no surface evidence. Some large magnetic anomalies also require addition of ultramafic bodies but these lie below the level of the original sections. Regionally averaged physical properties determined along the line of the each section are required to improve the stringency of this test of the structural models.

Introduction

Project P291A includes a component on the use of geophysical modelling to test the structural interpretations produced in P291. The proposal was to use the modern high resolution magnetic data combined with the regional gravity to test if the general lithological distribution proposed in the section is reasonable. The P291 program included geophysical modelling along two sections. This was not continued to all sections because of the lack of constraints on geophysical properties. It was hoped that this situation could be improved in P291A if data sets on magnetic susceptibility and density data were available from the sponsor companies. Unfortunately we were unable to negotiate the availability of this data.

Seven sections across the Mt Read Volcanics were drawn based on the structural data and interpretation of P291 and P291A. Four of these were selected for testing against the geophysical database. High resolution airborne magnetic data have been provided by the sponsors in 2 km corridors over parts of these sections.

These are:

Line	Range
5396000mN Hellyer	373000mE–377000mE
5392000mN Que River	373000mE–388000mE
5374000mN Rosebery	376500mE–381400mE
	383000mE–389000mE
5363000mN Dundas	360000mE–381000mE
5350000mN Professor Range	372000mE–380500mE
5336000mN Strahan	None
5326000mN Jukes	None

This data was supplied in a wide range of formats which have now all been successfully translated. The initial processing was reported in Berry & Roach (1996).

Spectral Analysis

The corrected magnetic data for the flight line closest to each geological section was plotted in profile form and correlated with the interpreted geology. Spectral analysis was conducted on each line to quantitatively assess the frequency content of the magnetic data as an adjunct to visual inspection of each profile. The aim of spectral analysis was to assess the relative importance to the overall magnetic response of magnetic sources at different depths and in particular to assess the contribution of near-surface sources. The spectral analysis was consistent with a range of depths and sources and no major distortions related to high frequency anomalies were found. On this

basis the data was suitable for upward continuation to allow regional scale interpretation of the data.

Continuity

The structures shown on the sections are based on projection from geology near the section line. They do not include objects with limited extent perpendicular to the section. The analysis of the data sets indicated that some smaller anomalies are one-dimensional but these largely disappear during upward continuation. This emphasises the fact that regionally averaged physical properties of units are required in modelling.

2D modeling

The final section of this program required generation of profile data suitable for two dimensional forward modeling of the magnetic and gravity anomalies. Because of the complexity of matching the various segments of company data and after comparison with the regional survey it was decided to use the older 1981 MRT magnetic data to generate the profiles. At the level of 1000m used for the modelling here the advantage of the higher resolution surveys is largely negated, and did not warrant the extra work involved in matching and patching the modern surveys together. Gravity data was derived from the MRT TASGRAV database with the MANTLE91 regional field removal.

Regional sections

In testing the regional sections against the gravity and magnetic data, the sections were drawn first, essentially independent of the geophysical database. The essential features of these section was transferred to MODEL2D (Roach, 1993) and then a search was made for the nearest geometry that fitted the field. In this modelling the physical properties of density and magnetic susceptibility were allowed to vary in a small range to improve the fit. Where large wavelength features affected the sections, the initial reaction was to match these with bodies lying below the structural sections (usually >5 km). Thus large scale magnetic anomalies were fitted using serpentinite bodies and large gravity lows were fitted to Devonian granites, consistent with most previous modelling of this area. When these efforts were insufficient the sections were modified to reach a reasonable match. The preferred and range of physical properties used is shown in Table 1. These properties are based on a range of previous reports (eg. Leaman, 1986; Leaman & Richardson, 1989; Payne, 1991; LeClerc, 1996) but are not supported by direct measurement along the line of the sections. In all the sections the modelled magnetic field away from the anomalies is below the measured field. This may reflect a systematic error in the regional magnetic field (IGRF model for the Tasmanian region too low by 50–100 nT) or the magnetic susceptibility of units as shown in Table 1 is too low.

Section 5396000mN

The magnetic and gravity data profiles along section 5396000mN has a number of anomalies.

Magnetic

Short wavelength anomalies are:

1. small anomaly at 373000mE Crimson Creek Formation (magnetic susceptibility = 0.0007 cgs) this value may reflect some contact metamorphic effects on the margin of the Meredith Granite.
2. small anomaly at 376000mE Tertiary basalt (magnetic susceptibility=0.005 cgs)
3. small anomaly at 384000mE Tyndall correlate (magnetic susceptibility = 0.001 cgs)
4. small anomaly at 387000mE Tertiary basalt (magnetic susceptibility=0.005 cgs

Long wavelength

The whole section crosses a long wavelength circular magnetic anomaly that shows no correlation with the surface geology. The interpretation is that the source of this anomaly lies below the level drawn in the structural sections. It is modelled here as the result of ultramafic rocks (MUC) at depths of more than 5 km. The depth is poorly constrained but the magnetic unit does not continue under the Meredith Granite which suggests less than 10 km.

Gravity

The major feature is a very large gradient at the contact of the Meredith granite. This requires a sub-vertical boundary to 8 km with the granite given a contrast of –0.07 t/m^3. In addition the large high at the margin of the granite requires the basement to have a positive anomaly of 0.03 t/m^3 which is consistent with the high proportion of phyllites in descriptions of this area but not with quartz dominated low densities often used for the basement. (Leaman & Richardson (1989) used blocks of +0.07 t/m^3 east of the Meredith Granite on their line 8.) The gravity field drops over the thickest CVC/ Southwell Subgroup in the section consistent with a 0.0 t/m^3 contrast for this unit. The negative anomaly occurs over the porphyry bodies and these have been modelled with granite like densities (–0.05 t/m^3)to match this low. This interpretation requires very large porphyries in this area. Alternatively the CVC/ Southwell Subgroup have a lower density.

Section 537400mN

Magnetics

Short wavelength

- The major anomalies in the west are from the Wilson River Complex. These are consistent with a syncline as inferred from the structure.
- The major anomaly in the east is from the Murchison Granite and surrounding magnetite altered Murchison Volcanics. The interpretation here is that there is a large halo of altered volcanics west of the granite (aMV on section). Alternatively the granite is larger than shown on the 537400 section. These alternatives cannot be distinguished here. The halo shown is rather large and a larger granite may be preferred.
- Subtle magnetic anomaly at 383000mE has been arbitrarily related to internal variations in the CVC (shown as the Sterling Valley Andesites (SA) on Fig 2). The whole section requires a CVC magnetic susceptibility of 0.0003 cgs units which is higher than commonly used but probably reflects the patchy alteration in this area.
- The assumptions of 2D modelling are severely violated in this section by the sub-surface ridge of granite which trends along the section but oblique to it, so that off-section materials are contributing to the field in a way not considered by the model.

Gravity

The gravity field is totally dominated by a Devonian granite ridge. The 3D effects are very important and the granite position is probably too high in Fig. 3 across the central and western part of the section because of the large body of granite to the south of the section. The gravity low over Rosebery has been modelled as a granite coming close to the surface but this is partly an artefact of the larger granite-induced anomaly off section to the south and the granite may not come this close to surface. While all units were included in the gravity calculation, virtually all the variation in the gravity field can be explained by the Devonian granite.

Section 5350000mN

Magnetics

This section has a very large magnetic anomaly over the Tyndall Range. This anomaly has long been considered a result of Cambrian granite. The original section (Berry 1996) included a model of the granite position from Payne (1991). A similar model is used here. There is a small magnetic anomaly near the Henty Fault which is the southern edge of a large anomaly over the Ewarts Track sequence of the Henty Fault wedge. This is marked here as Tyndall Group (Corbett et al this volume) but a slightly higher magnetic susceptibility was required to model this anomaly with the shape inferred on the original section (0.002 cgs rather than 0.001). The remainder of the section is very quiet.

Gravity

There are few features on the gravity profile. There is a broad low over the main CVC and Tyndall Range, and a high over the western end of the section. This has been partly fitted by assuming a lower than normal density for the CVC (–0.02 rather than 0.0 t/m^3) but even this is not enough and following the suggestions of Leaman & Richardson 1989) a slab of lower density Precambrian basement has been added (–0.02 t/m^3). This is a very artificial solution. Especially as this low represents a continuous feature

Table 1 Physical properties used in modelling

Unit	Abbrev-iation	Magnetic Susceptibility preferred cgs units	Magnetic Susceptibility range cgs units	Density contrast preferred t/m^3	Density contrast range t/m^3
Tertiary sediments	Tert	0.00001		-0.5	
Tertiary basalt	Tb	0.005		0.1	
Eldon Group	DvS	0.0001	0.0001 to 0.0003	0.02	0.00 to 0.02
Gordon Limestone	GL	0.00001		0.06	
Owen Conglomerate	OC	0.0001	0.0001 to 0.0004	-0.02	-0.01 to -0.03
Other Denison cycle	DC	0.0003	0.0003 to 0.0004	0.01	0.01 to 0.04
Tyndall Group	Ty	0.001	0.001 to 0.002	0.02	0.02 to 0.04
Central Volcanic Complex	CVC	0.0004	0.0004 to 0.0006	0.02	-0.04 to 0.2
Que Hellyer Volcanics	QHv	0.0001		0.05	
Quartz porphyry	Pp	0.00001		-0.05	
altered Murchison volcanics	aMV	0.003		0.01	
Eastern Quartz-phyric sequence	EQ	0.001	0.0004 to 0.001	0.01	0.0 to 0.01
Farrell Slate	FS	0.0001		0	
Sterling Valley andesites	SA	0.0003		0.04	
White Spur Formation	WS				
Husskisson Group	HG	0.0004		0.01	0.01 to 0.02
Sticht Range Fm	SRF	0.0001		-0.01	
Other Yolande cycle	YC	0.0002	0.0002 to 0.0004	0	-0.01 to -0.02
Crimson Creek Formation	CCk	0.0005	0.0005 to 0.0007	0.05	
Precambrian basement	PC	0.00001	0.0002 to 0.00001	0.02	-0.01 to 0.03
Devonian granite	DGr	0	0 to 0.0001	-0.07	
Cambrian granite	CGr	0.003	0.003 to 0.004	0.01	0.01 to 0.08
serpentinite	Sp	0.01		-0.03	
MUC basalt	bas	0.003		0.1	

south to section 5326000mN where it is much larger. In the eastern section the Denison Cycle (but not Owen Conglomerate) has been set at a density contrast of +0.04 t/m^3. Alternatively the basement could have a positive density contrast. Basement on this section (Fig. 3) has a zero density contrast but magnetic susceptibility of 0.0002 to lift the overall field.

Section 5326000mN

This section has a number of very interesting features. Firstly, in the magnetics there is a very large anomaly at 384000mE which is consistent with the Cambrian granite but at this location there is a coincident gravity high whereas Cambrian granites usually produce very small anomalies in the gravity field. In order to match the field using a magnetic susceptibility of 0.0025 cgs units the required density contrast is +0.08 t/m^3 which is higher than normal granodiorite range but may reflect a dense style of alteration. The anomaly lies right over the Hal Jukes/Taylors Reward prospect. (Leaman & Richardson (1989) used +0.02 t/m^3 for the Darwin Granite on line 20) This high lies centred within a very large gravity low. This was modelled by a basement anomaly with a contrast of –0.07 t/m^3. There is no possibility of modelling this anomaly by variations of density of the upper few kilometres of the section. Leaman & Richardson (1989) have previous modelled this anomaly by assuming a very large block of Precambrian basement of low density. This model was used in Keele (1992) but at this point there is very little constraint on the nature of this anomaly.

In the west there is a very large magnetic high which again is ascribed to structures that lie below the stratigraphic intervals included in the structural section. The King River section is modelled here with typical Tyndall Group properties and this helps to broaden the magnetic field but is not required by the data. This anomaly could be matched entirely using basement features.

Physical Properties

The physical properties used within the sections shown are summarised in Table 1. The major test of the structural models used in this way is whether these properties are reasonable. In most cases the values used lie within the range applied in previous reports that are available to us. In addition for most gravity anomalies it is possible to play off densities of Cambrian units against densities of basement units. The major features of the sections that changed as a result of the geophysical modelling is the addition of the Devonian granites to the sections and the addition of Cambrian granites to the sections. Since the former are largely post kinematic it has little effect on the implications of the structural sections. The Cambrian granites may place restrictions on the sections but this would need to be investigated over many sections to see if any large faults pass through the inferred granite position. The inferred shapes on the sections tested are too small to make dramatic effects on the structural interpretation at this stage.

Summary

Geophysical modelling was applied to four regional structural sections across the Dundas "trough". The gravity and magnetic fields along these sections can be matched to the inferred geometry provided the physical properties are allowed to vary within a reasonable range. This range is poorly constrained by the publicly available physical properties database. Regionally averaged physical properties determined along the line of the each section are required to improve the stringency of this test of the structural models.

References

Berry RF 1996. A structural section of the Mt Read Volcanics at 535000N. AMIRA P291A Fifth report 1–12.

Berry RF & Roach M 1996. Geophysical data as a control on geological sections. AMIRA P291A Report 5, 95–100.

Keele RA 1992. The King River regional cross–section: a transect through the Dundas Trough. AMIRA P291 Report No.4, 11–30.

Leaman DE 1986. Mt Read Volcanics Project: Interpretation and evaluation report 1981 west Tasmania aeromagnetic survey. Dept Mines Tasmania, 114pp.

Leaman DE & Richardson RG 1989. The granites of west and north-west Tasmania-a geophysical interpretation. Geol Survey Tasm. Bull 66, 146pp.

LeClerc M, 1996. The geophysics of the Housetop Granite. BSc (hons) thesis, Univ Tasm (unpubl.)

Payne B, 1991. Geophysics of the Mount Sedgwich Red Hills area. BSc (hons) thesis, Univ Tasm (unpubl.)

Roach M 1993. Model2D Version 3.0 Interactive 2D gravity and magnetic modelling for IBM PC compatible computers. CODES, University of Tasmania, 32pp and disk.

Figure 1 **2D GRAVITY AND MAGNETICS MODEL**

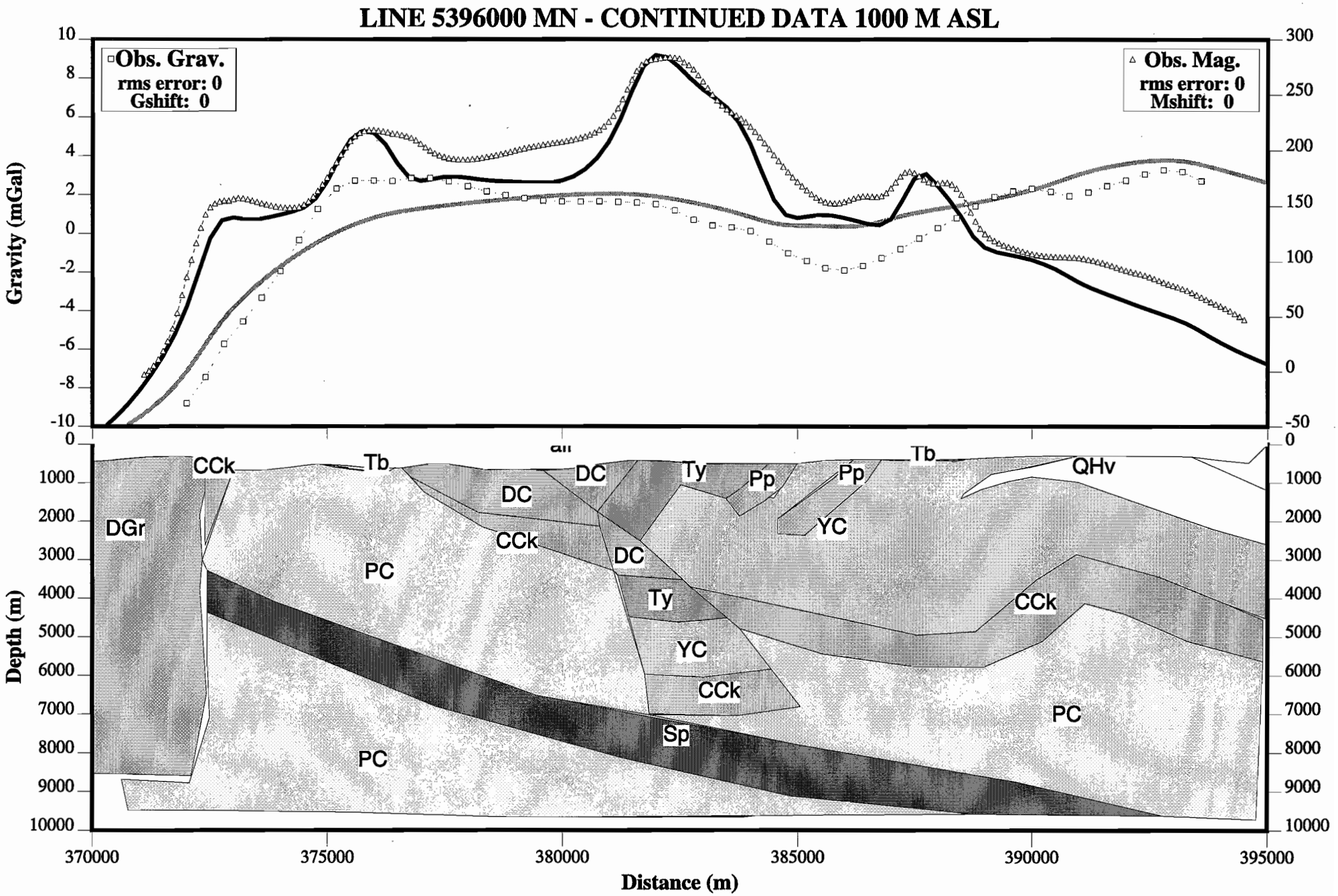

Model File:L96C.MOD Obs. Gravity:G5396000.OBS Obs. Magnetic:M5396000.OBS Date:03-03-1997 Time:12:04:22

Figure 2 **2D GRAVITY AND MAGNETICS MODEL**

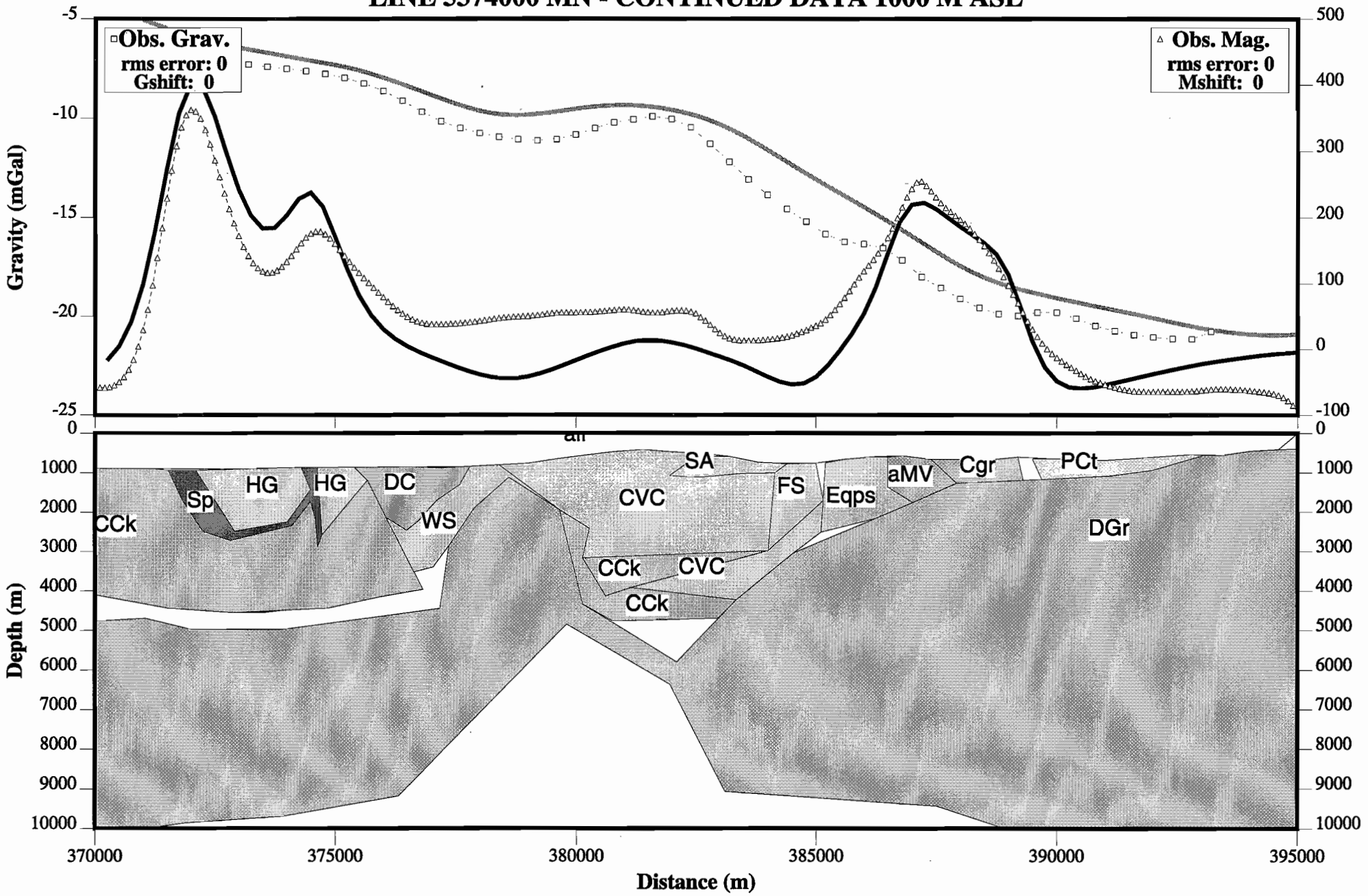

Model File:L74B.MOD Obs. Gravity:G5374000.OBS Obs. Magnetic:M5374000.OBS Date:03-01-1997 Time:19:56:20

Figure 3 **2D GRAVITY AND MAGNETICS MODEL**

LINE 5350000 MN - CONTINUED DATA 1000 M ASL

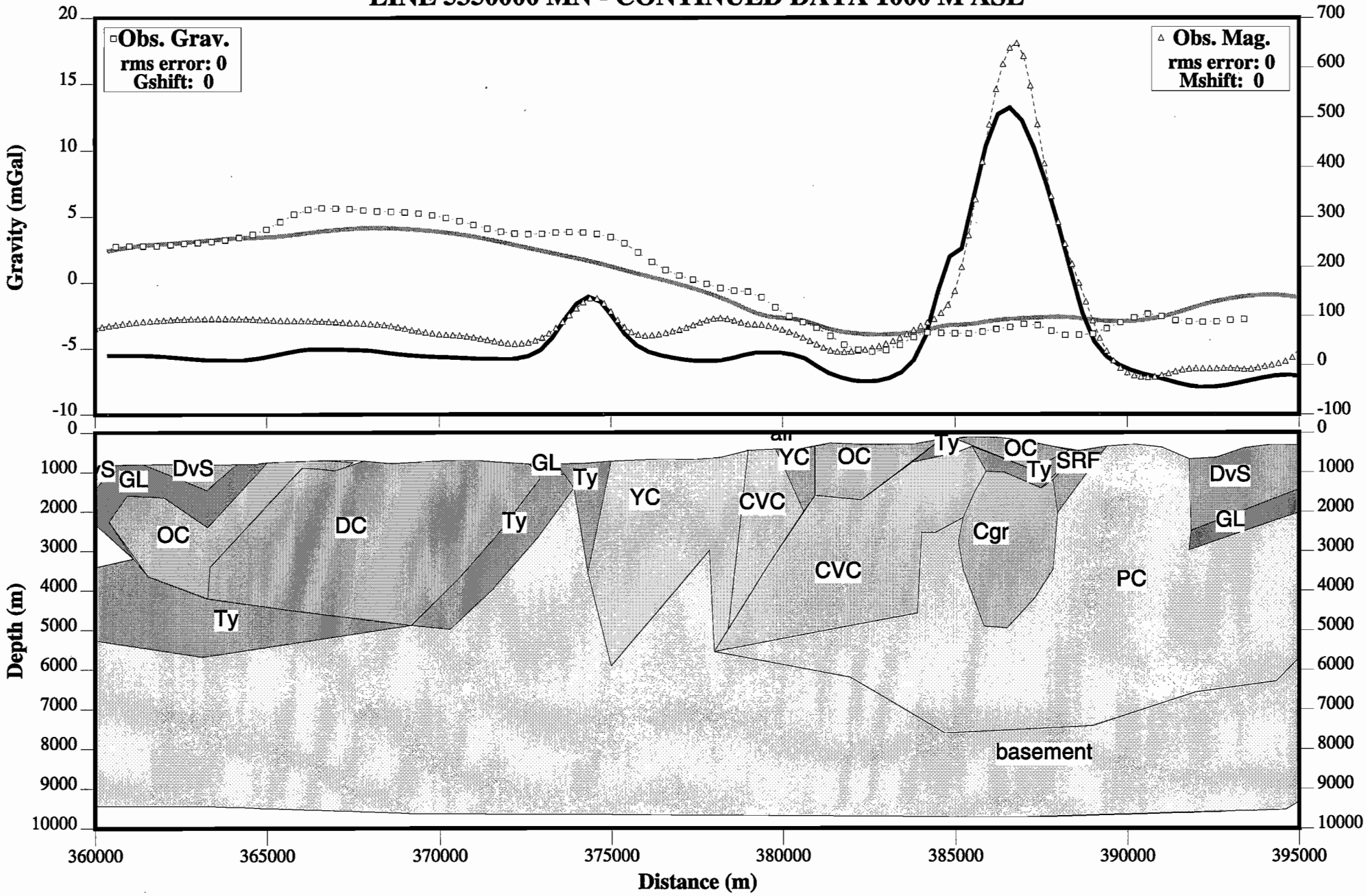

Model File:L50B.MOD Obs. Gravity:G5350000.OBS Obs. Magnetic:M5350000.OBS Date:03-03-1997 Time:16:42:18

Figure 4 **2D GRAVITY AND MAGNETICS MODEL**

LINE 5326000 MN - CONTINUED DATA 1000 M ASL

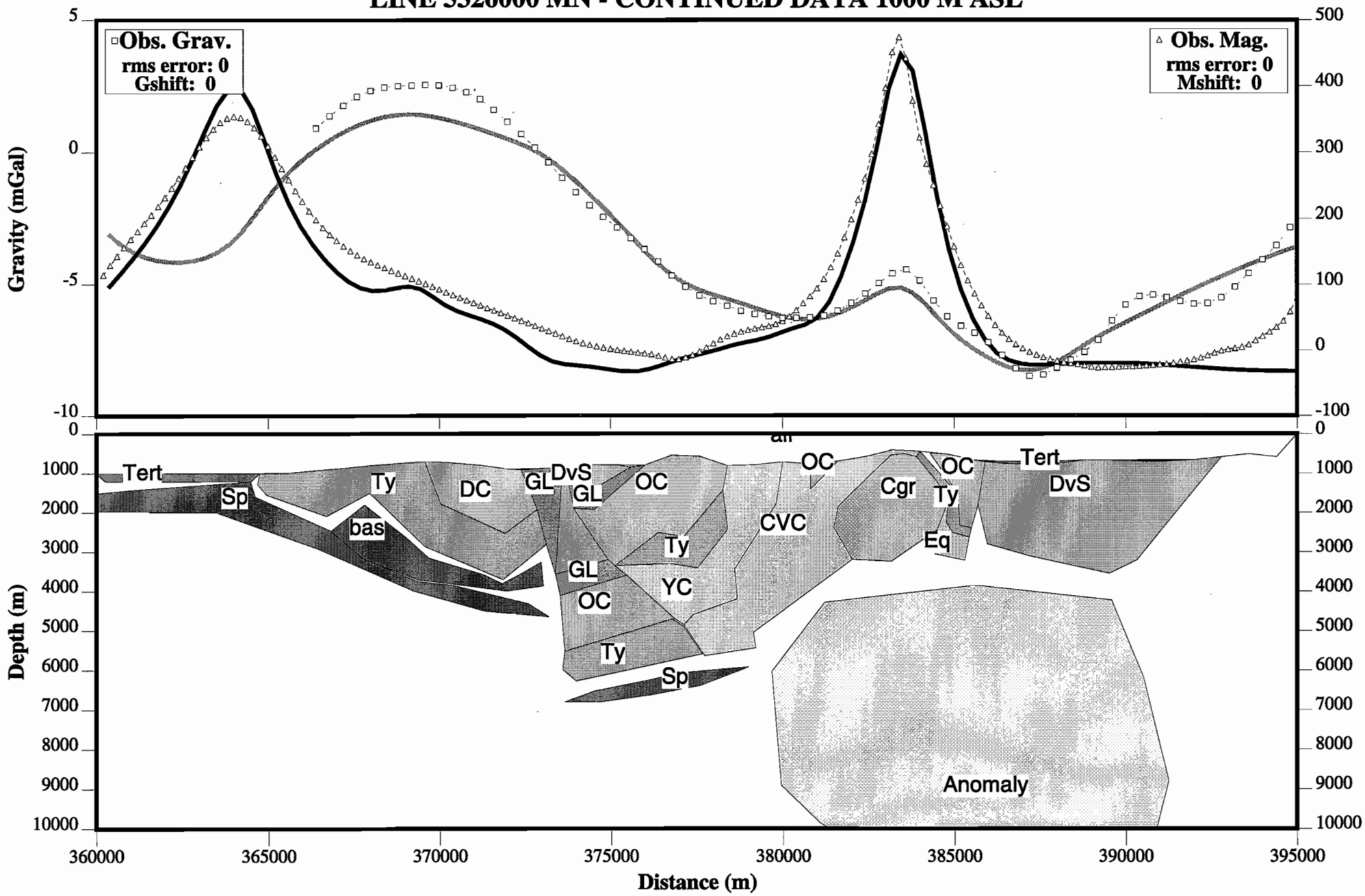

Model File:L26B.MOD Obs. Gravity:G5326000.OBS Obs. Magnetic:M5326000.OBS Date:03-03-1997 Time:16:36:39

Cambrian structure in Western Tasmania: An overview

R.F. Berry
CODES Special Research Centre, Geology Department, University of Tasmania

Abstract

The project tested nine specific aspects of the model for Cambrian fault structure in western Tasmania which were developed in AMIRA P291. The major aims required an ability to separate the tectonic effects of the Undillan from the Boomerangian and to make this distinction despite the obscuring complexities of the Late Cambrian and Devonian deformation. While these investigations were only partially successful, sufficient evidence was found to support the previous interpretation for several structures. In addition a S isotopic fingerprint for Middle Cambrian faults was discovered.

The nature of Middle and Late Cambrian deformation is complex in both time and place. The whole of the Cambrian was a period of very active tectonics in western Tasmania. This can be characterised by a number of stages. A period of extension in the Middle Cambrian reached a thermal and structural maximum in the Undillan and Boomerangian stages of the Middle Cambrian. The major phase of VHMS mineralisation occurred at this time. The transition from a simple deep water basin associated with dacite dominated volcanism to a complex basin with large ranges in water depth and substantial andesitic to basaltic volcanism occurs during the Undillan. Cambrian extensional faults (Henty-Moxons-Cripps zone, Pieman-Rosebery-Husskisson zone) are recognisable at this time but not before. The basin was inverted in the Late Cambrian with active erosion of the older volcanics.

While the Late Cambrian and Devonian deformation have obscured much of the basin geometry during the extensional phase, a few of the larger structures can still be recognised. There is no evidence for wholesale dismemberment of the basin geometry.

Introduction

The principal aim of this project was to test the models of the Cambrian fault structure in western Tasmania which were developed in P291 and to refine these models where appropriate. This was always going to be difficult given the complexity of Cambrian tectonics. It was not sufficient to identify a structure as Cambrian in age but rather to see the Cambrian as five separate structural events. The extensional faulting which has been clearly identified near VHMS deposits is a very short lived event which is restricted to part of the Middle Cambrian (?Undillan). The major aims required an ability to separate the tectonic effects of the Undillan from the Boomerangian and to look through all the complexities of the Late Cambrian and Devonian deformation to make this fine distinction. The evidence provided in P291 supported the existence of these divisions locally but the extension of each to the whole belt was model driven and poorly constrained. The extension project P291A was proposed to test the model at appropriate locations and test these extensions wherever possible..

Summary of component results

Project P291A started with nine discrete aims related to tests of the results of P291. These aims are listed below along with summaries of the conclusions which resulted from this study

1. Use structure and stratigraphic evidence to determine the nature of the Mt Cripps Fault in the Middle Cambrian. Draw structural section north and south of the Mt Cripps Fault and compare the lithological variation from north to south across the fault.

Rationale: To demonstrate the Mt Cripps Fault was active as a transfer structure affecting the depositional environment in the Middle Cambrian.

Result: The final report on this project is Berry, Corbett & Bull (this volume). Sedimentological studies targeted the Murrays Road Greywacke and the Animal Creek Greywacke. The variation in provenance and facies variations indicate the Mt Cripps Fault was present during the deposition of the Southwell Subgroup but no evidence was found for activity on this fault during the deposition of the Animal Creek Greywacke. The structural interpretation suggests that the Mt Cripps Fault was a relatively small feature during the late stage of the Yolande Cycle with an offset less than the thickness of the Southwell Subgroup, but sufficient to lift the southern block into a subaerial position.

Based on this conclusion the Mt Cripps Fault is shown in Fig. 1 as a Middle Cambrian structure and by inference so is the Henty Fault. The extension of the Henty Fault to the north (after Pemberton et al., 1991) is less certain.

2. Examine the structural and stratigraphic evidence for the Cambrian extensional faults along the western boundary of the Dundas Group from Zeehan to the Que River.

Rationale: This boundary was interpreted as a normal fault with a major transfer west of Rosebery. The program here was to study the sedimentology of the Dundas Group along this zone to look for a western source component, and for evidence that the transfer was present during the Middle Cambrian.

Result: The results of this study were reported in Bull (1995) and summarised in Selley & Bull (this volume). The lithological variation between the Denison Cycle correlates contained in the Huskisson River section and those positioned immediately west of Rosebery reflect fundamental differences in the drainage patterns for each region. The lithofacies of the Huskisson River section were principally derived from Precambrian siliciclastics and Crimson Creek Formation. In contrast, the compositionally and texturally mature character of the Stitt Quartzite demands a more distal provenance, with sediment pathways probably occupying a basin-axial position.

Provenance analysis have also demonstrated significant differences in the source signatures of sandstones from the Huskisson River and Rosebery areas. Samples collected from the Huskisson River area contain a chromite population derived entirely from a local Crimson Creek tholeiitic source, whereas those from the Rosebery area contain a more complex chromite provenance that is dominated by MUC-derived material but locally includes a significant contribution from a high-Ti tholeiitic source.

In terms of lithofacies and provenance characteristics, there are fundamental differences between Denison Cycle strata positioned close to the western limits of the Dundas Tough and in the area near Rosebery. These differences are interpreted to reflect contrasts in sediment dispersal patterns and basin geometry between these regions. The Husskisson and Dundas areas are interpreted as a sub-basin which is sheltered from the axial facies (Stitt Quartzite) by the irregularity of the basin geometry. The proposed transfer system is compatible with these geometric requirements. The proposed structures are shown on Fig. 1 as Middle Cambrian faults since the distinctive sedimentology and provenance was present in the Yolande Cycle and continued up to the Denison Cycle.

3. Eastern boundary of Dundas, Tullah to Red Hills: The fault just east of the Henty Fault along this segment was identified as a bounding fault for Tyndall Group deposition. The program aimed to support this interpretation by finding sedimentological evidence for a proximal eastern source in the Tyndall Group and Farrell Slates.

Rationale: This structure is one of the few recognisable Cambrian structures with a west side down movement in the Cambrian. The aim was to demonstrate a syn-depositional origin.

Result: This project was reported in White (1995) and an edited version which is updated to match the results of other projects is included in this volume. Four areas on the eastern side of the Dundas Trough were studied to test the model. Three areas were along a proposed precursor to the Henty Fault. These areas were the Moxon SaddleñHenty area, the Northern Anthony RoadñMurchison Gorge area, and the Hanging Rock area. Another probable Cambrian growth fault structure, to the east of Moxon Saddle, in the Anthony RiverñMount Selina area was also studied to test a smaller growth fault.

In the Moxon Saddle area, Tyndall Group rhyolites were probably originally deposited on both sides of the fault, and were subsequently eroded off the northeastern fault block across a fault scarp. In the Henty area, provenance of volcaniclastic units of the upper part of the Tyndall Group, were probably derived from the CVC to the east, being consistent with a west-block-down fault configuration. A normal, west dipping fault orientation is preferred. This fault was active during or after Tyndall deposition. We found no evidence that required a pre-Tyndall Group fault in this area. In the Murchison and Hanging Rock areas no new evidence was found for Cambrian movement along the palaeo-Henty Fault. In the Anthony River area, the geometry of the surviving sedimentary package is most consistent with active extensional faulting during Tyndall Group deposition with basin inversion during the Denison Cycle.

As a result of this study the Henty Fault and transfers are show on Fig. 1 as Middle Cambrian faults although at they may not be present at the critical Undillan stage.

4. Compare the structure and stratigraphy north and south of the Linda Zone with special emphasis on the Cambrian stratigraphy.

Rationale: We had not demonstrated any pre-Devonian movement on this structure. The aim was to define the history of movement by contrasting structures in each of the Central Volcanic Complex, Tyndall Group and Owen Conglomerate across the transfer.

Result: Reconnaissance surveys in the King River valley indicated that no suitable outcrops were available to test this model in the Tyndall Group. The work in other areas had emphasised the need to concentrate on Middle Cambrian rocks. Thus the emphasis was placed on exposures along the Firewood Siding Fault and the results are reported in Selley & Meffre (this volume).

A near complete section of Middle to Upper Cambrian strata is exposed north of the Firewood Siding Fault. This succession records a prolonged period of below wave base sedimentation sourced primarily from extrabasinal basement sources, but with a locally significant volcanogenic and intra basinally-derived component particularly towards the base. During the upper part of the Yolande Cycle, a change in basin geometry is heralded by the influx of medium to coarse-grained detritus and the development of a slope fan system. Significant basin activity also occurs in the upper part of the Denison Cycle with dominantly coarse-grained debris accumulating in narrow, laterally restricted depo centres which potential mark the onset of Late Cambrian folding in the area.

The structural geometry of the region north of the Firewood Siding Fault reflects the interaction of Cambrian and Devonian structures. N- to NNE-trending Cambrian structures were tightened and rotated during the main Devonian folding episode. Sinistral movement on the Firewood Siding Fault occurred coevally with Devonian folding and has resulted in a complex fold interference pattern that is not evident north of this major fault.

No structural or stratigraphic evidence was found that the Firewood Siding Fault existed during the deposition of the Yolande Cycle sandstones. The primary evidence remains that this structure existed as a late Cambrian transfer zone during the N-S folding. Thus the structure is show on the structural map (Fig. 1) as a Late Cambrian transfer.

5. Investigate lithostratigraphic correlations within the Dundas Group and between the Dundas and CVC.

Rationale: In order to improve the structural interpretation it was necessary to add some extra control lines by tightening up the stratigraphic correlation.

Result: The major results of this program are reported in three reports in this volume (Berry, Meffre, Jenner & Fulton; Berry, Selley, White & Meffre; Corbett, Berry & Selley).

Subdivision of the Cambrian rocks of western Tasmania into three 'cycles' based on pre-Tyndall (Yolande Cycle), Tyndall and post-Tyndall (Denison Cycle) sequences, using biostratigraphic constraints where possible, provides a practical framework for considering basin geometry and geological evolution. The Tyndall Cycle, although occupying only a very short time span (1-2 Myr?) at the end of the Middle Cambrian, is important because it was initiated by a distinctive phase of transitionally tholeiitic volcanism. This compositional signature has been used to correlate the Lynchford member of the Tyndall Group with the Henty Fault wedge basalts and dykes, Native Track Tier volcaniclastics, Lobster Creek intrusives and the lower King River basalts. The distribution of these units supports a widespread volcanic event

which occurred after the main CVC style volcanism and formed at discrete small centres unrelated to the major centres of CVC volcanism. Together these units act as a marker allowing the application of our three fold subdivision across all the Cambrian sequences of western Tasmania.

Cycle 1 opens with deep water sedimentation and dacitic volcanism. Towards the top of Cycle 1 the basin becomes more complex with increased basaltic volcanism and active extensional faulting. This major change in basin geometry occurs at the stratigraphic interval that hosts the major massive sulphide deposits, perhaps reflecting a thermal maximum that also correlates with maximum basaltic volcanism. The Tyndall Cycle was initiated in many areas by explosive basaltic volcanism with a mild but distinct tholeiitic character. Cycle 3 is dominated by clastic sedimentation and is synchronous with east–west compression and basin inversion.

Samples of sandstones have been collected from each of the stratigraphic cycles. The heavy mineral assemblages provide the following source signatures:

- recycled metasedimentary source is characterised by rounded zircon and tourmaline
- MUC source is characterised by low-Ti chromites
- Crimson Creek Formation source contains high-Ti chromite, euhedral zircon and minor recycled metasedimentary components
- Middle Cambrian felsic volcanism contributed euhedral zircon.
- syn-Tyndall andesitic volcanism contributed Fe/Ti oxides.

The older part Yolande Cycle sandstones are dominated by a well mixed component of MUC and recycled metasediments (including at least some Rocky Cape block) and locally a felsic volcanic component, interpreted here as CVC derived. No local fluctuations in provenance were found over the 150 km of strike length investigated except the influx of local felsic volcanic components. The implication is that this is a large deep basin with no local basin margins. Towards the top of the Yolande Cycle , the MUC component becomes less significant in the south. By the top of the Yolande Cycle the basin is complex with many local variations in provenance. The Crimson Creek Formation becomes dominant in the provenance of the Dundas area. These provenance changes reflect similar changes in the sedimentology. A new volcanic phase dominated parts of the basin east of the Rosebery Fault through the Tyndall Cycle but west of the Rosebery fault the stratigraphy was dominated by a western source through this biostratigraphic interval. The Denison Cycle syn-orogenic sediments also show very rapid facies variation with local sources dominant.

The distribution of Tyndall Group correlates in the Native Track Tier and Dial Range Trough was used to support an extension of the Henty fault to the north on Fig. 1.

6. A new transect between Zeehan and Firewood Siding Fault is required to track the change in strain as the Rosebery Fault dies to the south.

Rationale: This section is critical to understanding the changing pattern of Devonian strain south from the Rosebery Fault. The large difference in style between transects to the north of Zeehan with those south of Queenstown requires a test of the reconstructions by placing a detailed transect in the transition zone.

Result: This project was reported in Berry (1996). The section starts west of the Professor Range passes close to the Henty River bridge on the Murchison Highway and along the southern section of the Anthony Road before crossing the southern section of the Tyndall range.

The restored section was drawn for a horizontal Ordovician stratigraphy. The strong out-of-section movement at the Henty Bridge prevents a meaningful reconstruction across this zone, so the restoration is in two sections. This section matches the style of sections to the south, with only moderate total shortening of 14 km. The level of erosion is such that a very good separation of this shortening between Cambrian and Devonian deformation was possible. No obvious dominant transport direction was recognised. A possible position for a major low angle Devonian thrust is west of the section under Permian cover. This could be the continuation of the Rosebery Fault, with the Little Henty Fault acting as a transfer structure but such an interpretation is not supported by the pattern of Devonian folding. The Rosebery section remains a major problem because of the large shortening required by the Rosebery and Mt Black thrusts for which no equivalent has been found on other sections.

The interpretation that the Ewarts Track sequence is a Tyndall correlate made for this section and partly based on the geochemistry section was used to imply

the gabbro complex in the Henty Fault wedge is a basement high during the Tyndall Cycle and this has been shown on Fig. 1.

7. Prepare gravity and magnetics profiles and interpretations over all the existing sections and use them to add constraints to the models.

Rationale: The aim is to test the structural sections against an independent database and see if some additional constraints are obtained.

Result: This project is reported in Berry & Roach (this volume). Four structural sections across the Mt Read Volcanics were tested by 2D modelling of the gravity and magnetic fields. The structural models are broadly consistent with the geophysical data within the constraints of the publicly available physical properties database. The geophysical data requires addition of Cambrian and Devonian granites for which there is no surface evidence. Some large magnetic anomalies also require addition of ultramafic bodies but these lie below the level of the original sections. Regionally averaged physical properties determined along the line of the each section are required to improve the stringency of this test of the structural models.

8. The spatial and temporal relationship between cleavage formation, folding and faulting along the Rosebery Fault from Rosebery Lodes to the Pieman River.

Rationale: To look for evidence that the Rosebery Fault had a Cambrian history. The previous work along this section of the Rosebery Fault had failed to detect any evidence for such and early history.

Result: This project was reported in Berry (1994). There is a close spatial relationship between the Rosebery Fault and a late N-striking cleavage (S_2). This cleavage occurs in the hanging wall at Rosebery but in the footwall in the Pieman River. The variations in morphology of this cleavage reflect the changing circumstances along the fault. At each locality the fault related cleavage occurred in the softer units near the fault but this varied between footwall and hanging wall. The cleavage morphology reflects the strongly varying temperature conditions between those sites which are close to Devonian granitoids and those that are far away. An earlier cleavage was recognised at all localities. This cleavage was not visible in the most intense zones of S_2 cleavage development but overprinting was found on the edge of the zone of S_2 development. The earlier cleavage has a composite origin including both a NNW striking Devonian cleavage and a N striking cleavage of Devonian or Cambrian age. We could not find any way to resolve whether the N-striking cleavage was Cambrian in age.

9. To test the isotopic and chemical signature of faults with known Cambrian and Devonian histories to develop a fingerprint for Cambrian faults. The initial program was targeted at a transect from the Pieman River to the Murchison Dam.

Rationale: Cambrian seawater and ore fluids, and Devonian meteoric, mesothermal and granitic fluids have distinct isotopic signatures which may leave an identifiable trace where there has been large scale circulation, as along zones of enhanced permeability such as faults.

Results: Preliminary results were reported in Kitto (1994, 1995a, b) and the major results are reported in Davidson & Kitto (this volume). A preliminary study of both quartz and carbonate was undertaken. The Devonian quartz bearing veins have oxygen isotopic values related to their distance from the granite. Cambrian and Devonian hydrothermal carbonates have distinctly different carbon and oxygen isotope values. Devonian veins in faults show inherited Cambrian isotopic values where there is no granite contribution. The C and O isotope study failed to give sufficient information because of ambiguity of results and the difficulty in finding a broad spectrum of samples, especially regional carbonate and quartz related to Cambrian fluids. Attempts to overcome these problems included detailed fluid inclusion studies but these did not provide sufficient data to resolve the problems. Pyrite was identified as a better target and the major emphasis since 1995 has been on the S isotope signature of pyrite with lesser effort place on microprobe analysis of pyrite.

Sulfur isotopic results from Cambrian growth faults in the Mount Read Volcanics can in some circumstances constrain their timing. Those containing base-metal sulfides, with S- and Pb-isotope values similar to the large Mount Read Volcanic Belt VHMS deposits (5–18‰), are likely to represent fault-controlled upflow zones in Cambrian hydrothermal cells. Unmineralised faults can contain pockets of

heavy sulfur isotope values ($\delta^{34}S$ > ~18‰), as finely disseminated pyrite, in and within 50 m of the recognisable fault trace. The same range of heavy values is recognised at the margins of large base metal deposits, such as Rosebery and Hellyer, where it is interpreted to represent shallow sub-surface reduction of Cambrian seawater sulfate.

Growth faults are dynamic structures in a fluid history sense. As time passes, every portion of the downthrown fault trace experiences the full range of fluid and thermal conditions available on the fault, because each segment initiates at surface and is progressively buried by deposition and fault movement. It is consequently expected that a wide range of sulfur isotope signatures should be recorded in growth faults. Where faults have been examined in detail in this study, their isotopic composition is very variable, and this is accounted for by a complex retainment pattern of the isotopic signature of multiple fluid batches passing through each fault.

Only sulfur isotope values >18‰ and <-5‰ are diagnostic of Cambrian fluids in the Mount Read Volcanic Belt, because of overlaps with the isotopic range of Devonian magmatic and deformational fluids. Values less than –5‰ have only been identified in background oxidised Cambrian aquifers — particularly associated with albitisation—but it is very likely that this fluid facies was widespread, but possibly poorly preserved, in early Cambrian faults. Cambrian signatures have been recorded from the 'Moxons Fault' and the western boundary fault of the Dundas 'trough' in the Pieman Gorge supporting the interpretation shown on Fig. 1.

Sections review

As a result of the additional work carried out in this project the sections along the Dundas 'trough' have been redrawn into a consistent style and exactly E–W. Five of these sections were redrawn as required by the various project elements and the remaining two were carried out to provide a consistency of style along the belt. These sections are shown in Fig. 2. Minor changes in the sections arise from the correlations of lithology reviewed in Corbett et al (this volume). The original data base for these sections is included in a number of reports from P291 (see Berry & Keele, 1993) and P291A (Berry, Corbett & Bull, this volume; Berry, 1996; Corbett et al., this volume). Additional information comes from Berry & Roach (this volume). The maps all draw heavily on published geological maps (Mt Read Project and Regional Survey maps) but include detailed structural data generated within P291, particularly relevant to the structural style in the Dundas 'trough'. P291A focussed on Cambrian structures and very little new structural data relevant to Devonian effects was added except along the section at 5350000mN.

Implications for Cambrian structure

Middle Cambrian

The only unequivocal evidence of Cambrian extension recognised are syn-volcanic growth faults. The best examples of growth faults are the Mt Charter Fault and minor faults along the eastern margin of the Dundas Trough (e.g. Anio Creek; Marsden Creek, 880776 Sprent River, Comstock Valley/Zig Zag Hill). Growth faults on a much smaller scale have been defined within existing mines (Berry, 1991; Downs, 1993) but these depend on a density of data which is not available in the regional database. The remainder of the volcanic belt has a large number of facies variations which indicate fault control on deposition but it is now very difficult to prove that these were normal faults or that the normal fault movement occurred during the Undillan. We have investigated the localities involved in all the ways we could find that were appropriate. These studies have largely confirmed the accuracy of publicly available data. However they have also indicated that where these structures lie within the basin, with both blocks below storm wave base, they are subtle with small offsets and only very small effects on the local stratigraphy. Most of the stratigraphic evidence that signals a structure does not occur at one point but over a zone. Modern studies of normal faulting (eg. Morley 1995) emphasise the complexity of structures in rift zones and the results here suggest these complexities need to be considered when interpreting the Middle Cambrian sedimentary history of western Tasmania.

The western boundary of the Dundas Group was interpreted as a growth fault especially in the north whee it abuts Precambrian basement, is sharply

truncated against a fault and has Precambrian sourced clasts. The study confirmed the existence of a basin margin in the vicinity of this fault from the Pieman Road and south to the Dundas inlier. The S isotope signature of a Cambrian structure was recorded from the Pieman River near this structure. However to the north of the Que River there is no evidence of Middle Cambrian rocks this far west and our preferred interpretation is that the Middle Cambrian boundary lies under the Rosebery Fault along the sections 5396000mN and 5392000mN (Fig. 2). Thus the boundary is shown as hidden on Fig. 1. The sedimentology supports a transfer zone as shown on Fig. 1 to the west of Rosebery but we have no additional data on its exact position. Further transfer faults are required to explain the structure of the Dundas inlier and these are shown on Fig. 1 but we have not proved these have a Cambrian signature.

Within the trough a normal fault can be detected from the Sharks Fin to Red Hills (Fig. 1) as the eastern margin of lower Yolande Cycle sedimentary rocks. This fault is interpreted as a west-dipping normal fault in the Middle Cambrian and we demonstrated the southern limit was active during the Boomerangian. The southern end terminates east of Henty at a transfer system. The northern end terminates or is offsets at the Mt Cripps fault (Fig. 1).

A number of possible transfer faults or transfer zones were suggested in P291 (Berry & Keele, 1993). Four of these were selected for detailed attention in this project. Of these the Mt Cripps, Rosebery–Pieman and Henty–Selina provided some additional evidence for a Middle Cambrian origin. The Linda Zone was important during Late Cambrian folding but we were unable to prove it existed in the Middle Cambrian. The Comstock Valley structure remains a well define Middle Cambrian structure which we used as one of the test cases for the S isotope signature. The Tyndall Range structure is annotated on Fig. 1 as a possible lateral ramp rather than a discrete fault surface. The other three structure, Tullabardine Creek, Lake Rosebery-Chester and Pyramid Peak– South Jukes, remain possible but have not been shown on Fig. 1 as nothing further was done on them during P291A.

Late Cambrian

The distribution of the Yolande Cycle sediments has a very restricted distribution in western Tasmania (Fig. 1). However most of these limits cannot be ascribed to basin bounding faults. The most common boundary appears to be erosion at the base of the Denison Cycle. Thus the present distribution is more related to the pattern of folding in the Late Cambrian than to the structural control in the Middle Cambrian. The limits of Yolande Cycle which we consider to be related to a Late Cambrian unconformity are shown on Fig. 1 to differentiate them from possible basin bounding structures. Most of the eastern margin as we see it now is limited by this Late Cambrian unconformity. A similar pattern was established by Selley (1997) at Dundas but does not appear to be general along the western margin where the most widespread unconformity limiting the distribution of the Yolande Cycle is at the base of the Pioneer Sandstone (?middle Ordovician). The pattern of Cambrian folds has also shown on Fig. 1. The synclines are outlined by the thick accumulations of Owen Conglomerate and correlates (Berry & Keele 1993). These syn-folding basins reach maximum development late in the Denison cycle.

Summary

The project P291A tackled a range of problems associated with demonstrating the existence of extensional structures within the Cambrian of western Tasmania. While most of these problems are very difficult and for most only partial success can be claimed, sufficient evidence was found to support the previous interpretation of several of these structures. In addition the S isotopic analysis provides a fingerprint to look for more subtle examples in the regional geology.

The nature of Middle and Late Cambrian deformation is complex in both time and place. The whole of the Cambrian was a period of very active tectonics in western Tasmania. This can be characterised by a number of stages. A period of extension in the Middle Cambrian reached a thermal and structural maximum in the Undillan and Boomerangian stages of the Middle Cambrian. The transition from a simple deep water basin associated with dacite dominated volcanism to a complex basin with large ranges in water depth and substantial andesitic to basaltic volcanism occurs during the

Undillan. Cambrian extensional fault patterns are recognisable at this time but not before. The major phase on mineralisation in western Tasmania is restricted to this very brief period of extensional tectonics. The basin was inverted in the Late Cambrian with active erosion of the older volcanics.

While the Late Cambrian and Devonian deformation have obscured much of the basin geometry during the extensional phase, a few of the larger structures can still be recognised. There is no evidence for wholesale dismemberment of the basin geometry.

References

Berry RF 1991. Structure of the Rosebery deposit. AMIRA Project P291 Report 3, 1-16.

Berry RF 1994. Rosebery Fault - cleavage domains. AMIRA Project P291A Report 1,53-66.

Berry RF 1996. A structural section of the Mt Read Volcanics at 535000N. AMIRA P291A Fifth report 1-12.

Berry R.F. & Keele, R.A. 1993. Cambrian structure in western Tasmania. AMIRA Project P.2916 Structure and mineralisation of Western Tasmania, Final Report: 55ñ68.

Bull SW 1995. Second Report: sedimentology of the Dundas Group and correlates with reference to a possible syn-depositional growth fault west of Rosebery. AMIRA project P.291A Third Report March 1995: 35ñ44.

Downs R 1993. Syn-depositional fault controls on the Hellyer volcanic hosted massive sulphide deposit. M. Econ. Geol. thesis, University of Tasmania (unpubl.)

Kitto PA 1994. Isotope studies: preliminary investigations. AMIRA P291A Report 1, 15-52.

Kitto PA, 1995a. Fluid inclusion microthermometry of Cambrian and Devonian fault structures. AMIRA P291A Report 4, 51-72.

Kitto PA, 1995b Geochemical and isotopic signatures associated with Cambrian and Devonian fault structures. AMIRA P291A Report 4, 73-76.

Morley CK 1995. Developments in the structural geology of rifts over the last decade and their impact on hydrocarbon exploration. In Lambiase JJ (ed) Hydrocarbon Habitat in Rift basins, Geological Society London Special Publication 80, 1-32.

Pemberton J., Vicary M.J. & Corbett K.D. 1991. Geology of the Cradle Mountain Link Road-Mt Tor area. Geol. Rep. Mt. Read Volc. Proj. Tasm. 4. Tasm. Dept. Res. & Energy. Div. Min. & Min. Res.

Selley D 1997. Structure and sedimentology of the Dundas area, western Tasmania. PhD Thesis Uni. Tas. (unpubl.).

White M. (1995) Sedimentological evidence for Cambrian growth faults on the eastern side of the Dundas Trough, western Tasmania. AMIRA Project P.291A6 Structure and mineralisation of Western Tasmania, October 1995: 23ñ38